MOHAMMAD MERAJ ALAM

DISTANCE PROTECTION OF NETWORKS SUPPLIED FROM VSC-HVDC



Universidade do Porto

Faculdade de Engenharia

FEUP

DISTANCE PROTECTION OF NETWORKS SUPPLIED FROM VSC-HVDC

MOHAMMAD MERAJ ALAM

Doctoral thesis submitted to the
Faculty of Engineering, University of Porto

Supervisor
Prof. Helder Filipe Duarte Leite Ph.D.

Co-supervisor
Prof. Adriano da Silva Carvalho Ph.D.

Departamento de Engenharia Electrotécnica e de Computadores
Faculdade de Engenharia da Universidade do porto
University of Porto

March 2018

Porto—Portugal

The research leading to these results has received funding from the People Programme (Marie Curie Actions) of the European Union's Seventh Framework Programme FP7/2007-2013/ under REA grant agreement no. 317221, project title MEDOW.

Mohammad Meraj Alam: *Distance Protection of Networks Supplied From VSC-HVDC* , © March 2018

Walidayn means parents.
Parents are the greatest gift I got in my life.

Dedicated to you both. A salute to your hard work.
— Mom & Dad

ABSTRACT

The electrical energy produced in power stations are transported to consumers like industries, factories and residential areas through the use of transmission and distribution networks. This overall structure that includes electrical generators, transmission and distribution lines, transformers, circuit breakers, residential loads is termed as a "Power System".

Power Systems are often exposed to short circuits that lead to either major or minor disturbances in the grid. The large magnitude of fault currents associated with the short circuit can even damage the equipment like generators, transformers, transmission lines, and loads, unless they are protected by the relays and circuit breakers to isolate such short circuit faults from the power system and maintain an overall healthiness of the system. If a fault is not cleared within the prescribed time, it can lead to a heavy damage to the system and its components. Therefore, a need for power system protective devices arises.

In a power system, a transmission line is considered as a highway for electricity supply and thus plays an important role. However, it is subject to high vulnerability as a majority of power system faults take place within. Thus, transmission lines must always be protected by the relays, which should be highly selective, robust and sensitive in nature. Different relays and schemes of protection depending upon the failure scenarios have already been implemented to protect the transmission lines. The differential protection, communication assisted protection like Direct Transfer Trip (DTT), Permissive Over/Under reach Transfer Trip (POTT/PUTT), Directional Comparison Blocking (DCB) and distance protection are some of the main protection schemes employed upon the transmission lines.

Focusing on the distance relay, it provides primary (utilizing communication channels) as well as backup protection that is set to reach a fixed percentage of the transmission line. Transmission of a bulk amount of power over the Extra High Voltage (EHV) lines, which are protected by distance relays, by the use of Voltage Source Converter (VSC) based High Voltage DC (HVDC) network are the recent advancements in a power system. Nonetheless, this scenario also leads to questioning “Whether the distance protection of AC transmission lines connected to VSC based HVDC network perform optimally?” With this question in consideration, the following thesis identifies critical challenges involving impacts of the dynamic behavior of VSC, and its associated fast control actions and grid codes for HVDC connections during faults, upon the performance of distance protection of transmission lines connected to a VSC-HVDC system. This thesis also aims to present the solution to counter problem faced by the distance relay in the presence of VSC-HVDC.

In this thesis, after explaining the research motivation about distance protection, major drawbacks of over-reach of distance zones, and tripping during the overload conditions (that have led to many major blackouts in the history of power system protection, for instance USA 2003 blackout and European blackout in 2006), a comprehensive literature review on distance relay malfunction is presented. The research focus in terms of the research problem and aim of research is presented alongside, further investigating the impacts of dynamic behavior of VSC-HVDC system on the distance protection following the network guidelines of reactive current injection during the fault. Additionally, a study is conducted on the effect of converter current saturation limits, fault resistances, current limitation strategies, and different fault current be-

havior of the converter that are responsible for the malfunction of distance relay by analyzing the apparent impedance trajectory on RX plane.

The state-of-the-art covers a description of VSC technology and its behavior during balanced and unbalanced network conditions. Furthermore, the evolution of HVDC technology is discussed along with the improvements in converter technology for its use in the renewable energy sources. A comparison between the features of an electrical grid with and without VSC interfaced renewable energy sources during the fault is also discussed, which highlights the fact that VSC has limited fault current capability. This current limitation is responsible for the changes in the fault current features, both in terms of magnitude and wave shape.

In continuation, the next chapter elaborates on the grid protection system and the present protection methodologies. Furthermore, by the addition of converter interfaced renewable source of energy in the electrical grid, a state-of the-art is presented regarding the impact of Flexible AC Transmission System (FACTS) devices, Doubly Fed Induction Generator (DFIG) based wind turbines, and Inverter Interfaced Distributed Generation (IIDG), among others, on the distance relays installed in AC transmission lines. The reasons behind the mal-operation of distance relay in the form of relay under-reach and overreach in the presence of VSC are highlighted. Numerous completed and undergoing HVDC projects are discussed in detail along with the implemented technologies.

Subsequently in chapter 4, an investigation on the distance protection of transmission lines in a power system consisting of a point-to-point VSC-HVDC (bipolar) is carried out in PSCAD, taking into account the grid codes for HVDC connections (such as TenneT TSO), and converter current limitation strategies. This chapter describes how the positive and zero sequence currents from the converter side, fault impedance and fault currents from the grid side are responsible for the differences in apparent impedance.

Chapter 5 elaborates on the problem of relay malfunction in the presence of VSC based HVDC system by performing a Control Hardware-in-loop test of a commercial distance protection using Real Time Digital Simulator (RTDS). A commercial distance relay is utilized for this purpose to verify the analytical and simulation work performed in the previous chapter. The analog signals in the form of secondary currents and voltages from CT and PT respectively, are sent to the distance relay through a signal amplifier. The relay responses in terms of the digital trip signals are analyzed by sending them back inside the RTDS to control the circuit breakers.

Correspondingly, an adaptive relaying algorithm to upgrade the distance protection of transmission lines is proposed in chapter 6 of this thesis as a solution. The scheme computes the apparent impedance seen by the relay based on the network conditions, presence of VSC-HVDC, current limitation strategies and reactive current injection magnitude in real-time, as well as continuously updates the protection device with the new reach settings. Many case studies and the results of relay performance are presented in tables that signify the correctness of the algorithm implemented for both the standalone and pilot distance relays. Finally, some points are illustrated as conclusions and recommended topics for the future work.

RESUMO

A energia elétrica é na sua maioria produzida em grandes centrais elétricas, transportada até aos consumidores tais como indústrias, fábricas ou residências, através do recurso a redes de transmissão e distribuição. À produção transporte, distribuição e consumo de energia elétrica dá-se o nome de "Sistemas Elétricos de energia (SEE)".

O SEE é composto de diversos equipamentos elétricos, tais como geradores, linhas de transmissão e distribuição, transformadores, disjuntores, etc que são frequentemente expostos a curtos-circuitos ou defeitos e que levam a perturbações mais ou menos severas da rede elétrica. Uma corrente de curto-circuito ou de defeito de grande magnitude pode vir a danificar qualquer equipamento elétrico, a menos que este seja protegido no tempo relativamente curto.

Uma linha de transmissão tem um papel fulcral no SEE, e podendo ser comparada a uma autoestrada de eletrões. No entanto, esta sujeita igualmente a uma vulnerabilidade quanto a curto-circuitos ou defeitos, já que a maioria dos curto-circuitos na rede de transporte ocorre precisamente nas linhas de transmissão. Assim, as linhas de transmissão devem estar sempre protegidas sistemas de proteção seletivos, robustos e sensíveis. Diferentes relés com funções e esquemas de proteção defirentes, são implementados para proteger as linhas de transmissão. Como por exemplo, a proteção diferencial, a teleproteção com a sua lógica de proteção associada ao relé de distância: "Direct Transfer Trip (DTT)", "Trip Permissível Over/Under Transfer Trip (POTT/PUTT)", "Bloqueio Comparativo Direcional (DCB)".

Tendo como enfoque o relé de distância, este pode atuar quer como relé primário (utilizando canais de comunicação, teleproteção), bem como ser relé de "backup" ou secundário de proteção à linha de proteção. A tendência atual de conversão de energia a partir linhas de transmissão de corrente contínua de alta tensão (CCAT) em corrente alternada de alta tensão (CAAT) é feita por conversores de tensão (VSC, do inglês Voltage Source Converters). Com o aumento das ligações destes conversores em tensão (VSC) à rede elétrica, somo levados a questionar se o relé de distância usado para proteção das linhas de transmissão continua a ter o mesmo desempenho que tinha quando foi parametrizado antes destes conversores estarem ligados às linhas de transmissão? Com essa questão em consideração, o trabalho desenvolvido nesta tese identifica os desafios críticos para as proteções de distância usadas em linhas de transmissão de corrente alternada aquando estas são alimentadas por conversores de tensão, nos seus diferentes modos operação aquando de um curto-circuito. Este trabalho tem igualmente o objetivo de avançar com soluções para mitigar o mau funcionamento do relé de distância na presença dos conversores de tensão (VSC).

No capítulo introdutório é explicado o motivo de investigação sobre a função de proteção de distância em redes alimentadas por conversores de tensão, são revistos os conceitos básicos sobre os relés de distância e os seus problemas de mau funcionamento, tais como problemas de sobrealcance, de operação intempestiva em condições de sobrecarga (que levaram a muitos grandes apagões, por exemplo o apagão Europeu em 2006). É realizado uma revisão de literatura sobre os códigos de rede e a obrigatoriedade de injeção de reactia aquando do curto-circuito na rede elétrica. Assi, poder-se-á entender o comportamento dinâmico dos conversores de tensão numa situação de defeito ou de curto-circuito. Aqui será realizado uma demostração do comportamento dos conversores aquando de curto-circuitos simétricos e assimétricos com diferentes resistências de defeito.

O estado da arte abrange a evolução da tecnologia das linhas de transmissão de corrente contínua ou alternada e é discutida juntamente com as melhorias na tecnologia de conversão para o seu uso nas fontes de energia renováveis. Uma comparação entre as características de uma rede elétrica com e sem fontes de energia renováveis ligadas por conversores de tensão à rede elétrica durante um curto-circuito também é discutida, o que destaca o fato de que o conversor em tensão tem capacidade limitada de corrente de curto-circuito. Essa limitação de corrente é responsável pelas mudanças nas características da corrente de defeito anteriormente antecipadas, tanto em termos de magnitude quanto em forma de onda. Neste trabalho são igualmente estudados e revistos o impacto de dispositivos FACTS (Flexible AC Transmission System), nos relés de distância instalados para proteção das linhas de transmissão. As razões por trás do mau funcionamento do relé de distância, quer por subalcance, quer por sobrealcance na presença de conversores de tensão são destacadas.

No capítulo 4 é investigada a proteção de distância de linhas de transmissão, quando alimentado por uma fonte de tensão. Esta investigação é realizada no software PSCAD/EMTDC. Aquando de um curto-circuito o conversor de tensão injetará na rede elétrica corrente reactiva de acordo com os códigos de rede do operador da rede de transporte TenneT. Neste capítulo é ainda descrito como as correntes de sequência positiva e homopolares do lado do conversor, a impedância de defeito e as correntes de defeito do lado da rede são responsáveis pelas diferenças na impedância aparente vista pelo relé de distância.

O Capítulo 5 demostra sob um teste em malha fechada o problema do mau funcionamento do relé na presença de conversores de tensão. O teste é realizando com recurso a uma proteção comercial de distância e ao Simulador Digital em Tempo Real (RTDS). Um relé de distância comercial é utilizado para este propósito para verificar o trabalho analítico e de simulação realizado no capítulo anterior. Os sinais analógicos na forma de correntes secundárias e tensões secundários, respetivamente, são enviados para o relé de distância através de um amplificador de potência. As respostas do relé em termos dos sinais de trip digitais são analisadas enviando-as de volta para dentro do RTDS para controlar os disjuntores.

No capítulo 6, é analisado a possibilidade de uma função de distância adaptativa como uma solução para mitigar os problemas encontrados anteriormente. O algoritmo desenvolvido calcula a impedância aparente vista pelo relé com base nas condições da rede, presença de conversores de tensão, estratégias de limitação de corrente e magnitude de injeção de corrente reativa em tempo real, bem como atualiza continuamente o dispositivo de proteção com as novas parametrizações. Alguns caso de estudos são efetuados e os resultados do desempenho do relé são apresentados em tabelas que significam a correção do algoritmo implementado para os relés de distância com e sem teleproteção. Finalmente, alguns pontos são ilustrados como conclusões e tópicos recomendados para um possível trabalho futuro.

PUBLICATIONS

Following are the list of publications:

[1] M. M. Alam, H. Leite, and A. S. Carvalho. "Investigating Distance Relay Behaviour on an EHV AC Lines Connected with Voltage Source Converter Based HVDC." In: *Proc. CIGRE Symp., Across Borders - HVDC Systems And Market Integration*.

[2] Mohammad Meraj Alam, Helder Leite, Jun Liang, and Adriano da Silva Carvalho. "Effects of VSC based HVDC system on distance protection of transmission lines." In: *International Journal of Electrical Power & Energy Systems* 92 (2017), pp. 245–260. ISSN: 0142-0615. DOI: https://doi.org/10.1016/j.ijepes.2017.04.012. URL: http://www.sciencedirect.com/science/article/pii/S0142061516320312.

[3] Mohammad Meraj Alam, Helder Leite, Nuno Silva, and Adriano da Silva Carvalho. "Performance evaluation of distance protection of transmission lines connected with VSC-HVDC system using closed-loop test in RTDS." In: *Electric Power Systems Research* 152.Supplement C (2017), pp. 168–183. ISSN: 0378-7796. DOI: https://doi.org/10.1016/j.epsr.2017.06.025. URL: http://www.sciencedirect.com/science/article/pii/S0378779617302742.

[4] Mohammad Meraj Alam, Helder Leite, Dirk Van Hertem, and Adriano da Silva Carvalho. "Adaptive distance relay algorithm for transmission lines connected to VSC based HVDC system." In: *IEEE Transactions on Power Delivery* (2018).

[5] M. M. Alam, H. Leite, and A. S. Carvalho. "Protection of Networks Supplied from Multi-Terminal DC Grids." In: *IEEE Energycon 2016, 4-8 April 2016, Leuven, Belgium (Poster presentation)*.

[6] M. M. Alam, H. Leite, and A. S. Carvalho. "Addressing Challenges to the Distance Protection of Transmission Lines with VSC-HVDC Connection." In: *National Grid Control Center, UK, 5-6 July 2016 (Presentation)*.

[7] M. M. Alam, H. Leite, and A. S. Carvalho. "Grid Vulnerability and Protection Challenges in the era of Renewables and DC Grids." In: *7th HVDC Doctoral Colloquium, 13-15 Sep 2016, Porto, Portugal (Presentation)*.

[8] M. M. Alam, H. Leite, and A. S. Carvalho. "Adaptive Distance Protection of Transmission Lines connected to VSC-HVDC." In: *Energyville, 24 Nov. 2016, Genk, Belgium (Presentation)*.

The woods are lovely, dark and deep.
But I have promises to keep.
And miles to go before I sleep,
And miles to go before I sleep.

— Robert Frost

ACKNOWLEDGMENTS

Believe it or not! No chapters, sections, subsections, and paragraphs are as interesting and exciting as the acknowledgment part while writing a Ph.D. thesis. I am feeling this happiness and satisfaction right now as I am going to achieve another important stage in my life to be called as a *Dr.*. Although I walked alone on this path, the constant support & motivation of few important people in my life was always there walking along with me and that's why I would love to acknowledge them here. I think, this way, I might be able to offer my deepest gratitude to them.

First and foremost, O Almighty Allah! How should I thank your *Rahmat* & *Barkat*, which you constantly showered on me throughout this journey? Many at times, I was helpless, I wasn't able to see any ray of hope, there were no solutions of problems according to me but you pulled me out of all those sorts of difficulties. I don't know how should I thank you, I have no words, I should write *Thank you from the bottom of my heart.*

I would like to thank my *Dad* and *Mom* for being with me and supporting my decisions, pushing me forward, motivating me to run towards the finish line, thank you very much. Your dedication and devotion towards me and my siblings are extreme, which is why you both are my *role model*. I remember those days when you both were constantly keeping the focus on our future. Your effort has paid off today. A big salute to your hard work!

After *Mom* and *Dad*, I don't love anybody else more than my brother *Mohammad Shadab Alam* and my sisters *Mansha Shaheen*, *Zeba Shaheen*, *Arfa Shaheen*, *Tarannum Shaheen*, and *Razia Shaheen*. You are my strength, my dedication, my love, my support. The time we spend together whenever we are at our home is unforgettable. You all are my driving force. Many thanks for being with me and believing in me. You all have great hidden potential. *Family comes first*.

Aligarh Muslim University is my Alma Mater where I studied my senior secondary and Bachelor degree and I consider it my second home. I am feeling glad to thank my Alma Mater and the teachings it imparted among students especially this *"The main purpose of AMU is not just to produce good doctors, engineers, lawyers etc. but to produce good human beings both in attitude and behavior."*

Special thanks to Miss *Shafaq* whose constant support and motivation kept me rowing my boat forward. Thanks for being on my side and padding on my back, highlighting my strengths, believing in me, answering my queries and doubts and suggesting me solutions whenever I was stuck somewhere. you are awesome.

How an acknowledgment can finish without remembering my friends, Noo! It can't. Friends are very important part of one's life. At this moment, I am confused whose name should I put first. Nonetheless, I am starting with my AMU friends who are close to my heart. Many thanks, Mr. *Wasil Jamal* for being with me since the first day of AMU. I still remember our days at AMU when we used to go to the Maulana Azad Library after lunch and you always found

me sleeping, sometimes in the *Dalai Lama* section and many at times upstairs. I will always remember your *tube light* and your confidence in me. I don't know, am I *Lambey race k ghodey* as you used to say?

I would love to show my gratitude to my friend Mr. *Majid Feraz* from whom I learned many things. I always admire you. Your clarity in thoughts, sharp decisions, well-managed work plan and your unconditional support to me are the winning notes. Remembering you, I remember AMU and the old days at NT Hall, Age of Empires, Matri-omelete and what not?

My another friend Mr. *Muhammed Aftab Alam* thank you too. You are superb and fantabulous. our days at AMU mostly on our *BASANTI* "UP 81R 1481" were amazing and can't be forgotten in any sense. I learned to ride. Thanks for showing me the direction when I was moving from India to Portugal. Your support is commendable.

Mr. *Kshitij katiyar*, I want to show my gratefulness to you for the respect you gave since AMU days. You successfully managed to maintain both the relationship with me, one as a senior-junior, giving me the respect and simultaneously as a friend. Extremely awesome. Wish you the success at every step of your life. Many thanks, Mr. *Mobasshir* and your admiration for me and my work. Thanks for the belief. Thanks *Syed Tahseen Raza*, *Salman Bhai*, Obrigado o meu amigo *David Miranda*, many thanks *Hammad*, *Athar*, *Praveen Yadav*, *Divya Kumar Sharma*-you are *Desh ke Fankaar*, *Samiksha Keshav*, *Fran Mena Gomez*, Many thanks *Gusto* for the oscilloscope at the right moment.

Time for another special person Mr. *Aafaque Karim*, your role as a friend is marvelous and cannot be left acknowledged. You are since my schooldays and your humorous nature, living in the moment, as well as sober and simplicity, are the special things that I want inside myself. Thank you very much, dear. Thanks, Mr. *Abhishek Chatterjee*, I learned many many things from you. You have kept yourself enriched with the knowledge, books and many more scientific and non-scientific things. I remember the day when we met in the RUF, what a wonderful time we spent in Porto doing lots of activities. You are truly my friend.

I want to show my deepest respect and thanks to Dr. *Chetak Kandaswamy* and Mr. *Bharat Chetry*, you both are a wonderful friend and a superb person. I like the way you are called as *Sirji* and your constant belief in me, projecting my strengths, minimizing my weaknesses and admiring me, many thanks, *Sirji*. Lots and lots of hearty gratitude to Bharat Bhai, you are a very nice person. You always helped me and kept me going, sending the positive energy and boosting my moral. Many thanks, *Ataollah Mokhberdoran*, the time we spent together as a friend is marvelous and surely I learned many things from you as well. Thanks for boosting my moral and helping me out whenever I reached out to you.

Thanks, *José António* for the help from the administrative side.

Prof. *Helder Leite*, thank you for giving me this opportunity to carry out this task of Ph.D. and believing in me until the last moment. I felt happy when you said *Now I can see the light at the other end of tunnel.* Many special thanks to Prof. *Adriano Carvalho*, I like the way you are, the way you tackle the problems, the way you approach the students, the way you respect others, just superb or I should say Ótimo! Thanks for helping me out during my difficult times. I can't forget two things from you 1. *KIS method* (Keep It Simple) and 2. *Go step-by-step*. Thanks, Dr. *Jun Liang* for the support.

The research leading to these results has received funding from the People Programme (Marie Curie Actions) of the European Union's Seventh Framework Programme FP7/2007-2013/ under REA grant agreement no. 317221, project title MEDOW.

CONTENTS

I INTRODUCTION & LITERATURE REVIEW 1

1 INTRODUCTION 3
- 1.1 General Background & Motivation . . . 3
- 1.2 Problem Definition . . . 3
- 1.3 Distance Protection & Challenges . . . 5
- 1.4 Objective & Research Questions . . . 5
- 1.5 Outline & Approach . . . 6

2 VSC-HVDC SYSTEM 9
- 2.1 HVDC Transmission System Background . . . 10
- 2.2 Classic HVDC System . . . 11
- 2.3 VSC-HVDC Transmission System . . . 14
- 2.4 HVDC Transmission System Configuration . . . 18
- 2.5 VSC-HVDC Control . . . 19
- 2.6 VSC-HVDC Transmission System Behavior . . . 20
  - 2.6.1 During Normal Condition . . . 20
  - 2.6.2 During Abnormal Condition . . . 21
- 2.7 Conclusions . . . 21

3 DISTANCE PROTECTION & ITS CHALLENGES 23
- 3.1 Grid Protection . . . 24
  - 3.1.1 General Background . . . 24
  - 3.1.2 Changing Grid Scenario: A Highlight . . . 24
  - 3.1.3 Protection Methodologies . . . 25
- 3.2 Challenges Faced by Distance Protection . . . 26
- 3.3 Why To Assess Distance Protection . . . 26
- 3.4 Effects of VSC Based Technologies on Distance Protection . . . 27
  - 3.4.1 Effects of FACTS devices . . . 27
  - 3.4.2 Effects of Distributed Generation . . . 29
  - 3.4.3 Effects of DFIG . . . 30
  - 3.4.4 Effects of VSC . . . 30
- 3.5 Numerous Solutions of Problem . . . 31
  - 3.5.1 Modified Pilot Distance Protection . . . 31
  - 3.5.2 Adaptive Distance Relay . . . 33
- 3.6 Conclusions . . . 33

II PROBLEM SHOWCASE, SIMULATION & EXPERIMENTAL SETUP 35

4 IMPACT OF VSC-HVDC ON DISTANCE PROTECTION 37
- 4.1 History of Distance Relays . . . 38
- 4.2 Distance Relays . . . 39
- 4.3 Mho Function . . . 41
- 4.4 Quadrilateral Function . . . 44
- 4.5 Apparent Impedance Analysis . . . 45

4.5.1 Single line to Ground Fault . . . 49
4.5.2 Phase-to-Phase Fault . . . 51
4.6 Modern Network Codes for HVDC connection . . . 51
4.7 Current Limitation Strategies . . . 54
4.8 Study System . . . 56
4.8.1 AC Source Model . . . 57
4.8.2 Converter Transformer Model . . . 57
4.8.3 Converter Reactor Model . . . 57
4.8.4 Transmission Line Model . . . 57
4.8.5 VSC Based HVDC . . . 58
4.9 Simulation Results and Discussion . . . 59
4.9.1 Single Line to Ground Fault (SLG) . . . 60
4.9.2 Phase-to-Phase Fault (LL) . . . 63
4.9.3 Three-Phase Fault . . . 65
4.9.4 Impact of Saturation Limits of Converter . . . 68
4.10 Conclusions . . . 69
5 LABORATORY SETUP & TESTING OF DISTANCE RELAY USING RTDS 71
5.1 Short Circuit Behaviour of VSC-HVDC . . . 72
5.2 RTDS/RSCAD Description . . . 72
5.2.1 Processor Description . . . 72
5.2.2 Channel Description . . . 73
5.2.3 Analog & Digital Signal . . . 73
5.2.4 RSCAD & RunTime Environment . . . 74
5.3 RTDS Based Modeling . . . 74
5.3.1 Power System Model in RTDS . . . 75
5.3.2 VSC-HVDC Model . . . 76
5.3.3 VSC-HVDC Control . . . 76
5.3.4 Outer Control Loop - Positive Sequence . . . 76
5.3.5 Outer Control Loop - Negative Sequence . . . 77
5.3.6 Inner Current Control Loop – Positive & Negative Sequence . . . 78
5.3.7 Fault Response of VSC Controller . . . 78
5.3.8 Transmission Line model . . . 78
5.4 Signal Amplifier & Distance Relay . . . 79
5.4.1 Voltage & Current Signal Amplifier . . . 79
5.4.2 Distance Relay . . . 79
5.5 Relay Performance During Faults with VSC-HVDC Using Closed-Loop Test in RTDS . . . 80
5.6 Results and Analysis . . . 81
5.6.1 Single Phase to Ground Fault . . . 82
5.6.2 Phase-to-Phase Fault . . . 88
5.6.3 Three-Phase Fault . . . 95
5.7 Conclusions . . . 100
III ADAPTIVE DISTANCE RELAYING, CONCLUSIONS & FUTURE RESEARCH WORK 103
6 ADAPTIVE DISTANCE RELAYING SCHEME 105
6.1 General Background . . . 106
6.2 Experimental test setup using RTDS . . . 106

6.3 Relay Performance with Fixed Setting Scheme . . . 107
6.3.1 Non-Pilot Distance Relaying Scheme . . . 107
6.4 Pilot Distance Relaying Scheme . . . 113
6.4.1 Permissive Underreach Transfer Trip (PUTT) . . . 113
6.4.2 POTT . . . 114
6.4.3 DCB . . . 114
6.5 Adaptive Distance Relaying Scheme . . . 118
6.5.1 Mathematical Evaluation . . . 118
6.5.2 Algorithm . . . 121
6.6 Relay Performance with Adaptive Scheme . . . 122
6.7 Flowchart . . . 125
6.8 Conclusions . . . 125
7 CONCLUSIONS 129
7.1 Final Conclusions . . . 130
7.2 Recommendations for Future Research . . . 131

IV APPENDIX, BIBLIOGRAPHY & DECLARATION 133
A STUDY SYSTEM PARAMETERS 135
B TRANSMISSION LINE IMPEDANCE CALCULATION 137

BIBLIOGRAPHY 141

LIST OF FIGURES

Figure 2.1 Thury's six-pole dynamo [1]. . . . 10
Figure 2.2 Thury System balancing voltage of supply with voltage of load [2]. . . . 10
Figure 2.3 Mercury arc valves of ASEA design with four anode columns in parallel located at HVDC Inter-Island link [3]. . . . 11
Figure 2.4 A map of transmission lines in New Zealand with the High Voltage Direct Current (HVDC) Inter-Island link shown as dashed line. . . . 11
Figure 2.5 Examples of classic HVDC links in India [4]. . . . 11
Figure 2.6 Thyristors of different sizes [5]. . . . 12
Figure 2.7 A 12-pulse HVDC converter using thyristor valves. . . . 12
Figure 2.8 The Xiangjiaba Shanghai ±500 kV 6400 MW HVDC link. . . . 12
Figure 2.9 The Talchar Kolar classic HVDC link in India [4]. . . . 13
Figure 2.10 Global HVDC link [6]. . . . 13
Figure 2.11 Global Voltage Source Converter (VSC)-HVDC link. . . . 14
Figure 2.12 Inelfe VSC-HVDC link between France and Spain. . . . 14
Figure 2.13 Converter station layout between France and Spain [7]. . . . 15
Figure 2.14 Murraylink VSC-HVDC link between Berri and Red Cliffs. . . . 15
Figure 2.15 Murraylink VSC-HVDC cables [8]. . . . 15
Figure 2.16 Single phase H-Bridge scheme (a) Single bridge. (b) Cascaded bridge. . . . 16
Figure 2.17 Three phase Neutral Point Clamped converter 17
Figure 2.18 Modular Multilevel converter and Half Bridge sub-module 17
Figure 2.19 Modular Multilevel converter and Full Bridge sub-module 18
Figure 2.20 Monopole HVDC configuration. . . . 18
Figure 2.21 Bipole HVDC configuration. . . . 18
Figure 2.22 Multi Terminal HVDC configuration. . . . 19
Figure 2.23 Back to Back HVDC configuration. . . . 19

Figure 3.1 Production of Electricity worldwide from different sources [9]. . . . 24
Figure 3.2 General layout of electricity networks [9]. . . . 24
Figure 3.3 Differential protection scheme. [10]. . . . 25
Figure 3.4 Overcurrent protection scheme. [10]. . . . 25
Figure 3.5 Mho distance scheme. . . . 26
Figure 3.6 USA eastern coast blackout in 2003. . . . 27
Figure 3.7 HVDC links in European mainland. . . . 27
Figure 3.8 STATCOM installed in Cerro Navia, Chile by ABB [8]. . . . 28
Figure 3.9 Static Var Compensator (SVC) PLUS VSC technology by Siemens [11]. . . . 28
Figure 3.10 Typical Unified Power Flow Controller (UPFC) layout. . . . 29
Figure 3.11 Wind farms [9]. . . . 30
Figure 3.12 Study system with VSC 31
Figure 3.13 Study system with Thyristor Controlled Series Capacitor (TCSC) 31
Figure 3.14 Blocking Trip Logic for (a) RD1, RC2, RA1, RB2 (b) RA2, RB1 32
Figure 3.15 Blocking Trip Logic for (a) RD1, RC2, RA1, RB2 (b) RA2, RB1 32

Figure 3.16 Unblocking Trip Logic 33

Figure 4.1 H. E. Tudor - founder of distance relay. 38
Figure 4.2 Schematic diagram of distance relay cz, Westinghouse, 1923 [12]. 38
Figure 4.3 RAZOG distance relay. (source: www.pacw.org) 39
Figure 4.4 Zones of distance protection. 40
Figure 4.5 Line distance protection relay SIPROTEC 7SA86 - a product of Siemens [11]. 40
Figure 4.6 (a) Impedance characteristic. (b) Mho characteristic. (c) Offset Mho characteristic. (d) Reactance characteristic. (e) Quadrilateral characteristic (f) Lenticular characteristic. 41
Figure 4.7 (a) Simple Mho function. (b) Variable Mho phase distance function. . . . 43
Figure 4.8 Effect of source-to-line ratio $\frac{Z_s}{Z_L}$ (a) $\frac{Z_s}{Z_L} = 20$ (b) $\frac{Z_s}{Z_L} = 0.1$. 44
Figure 4.9 Quadrilateral characteristics of distance protection. 45
Figure 4.10 A simple power system with a transmission line and two sources. 46
Figure 4.11 (a) Sequence network diagram of the power system with a single line to ground fault. (b) Sequence network diagram of the power system for a line-to-line fault. 46
Figure 4.12 A typical layout and devices in a substation. (source: www.primeraeng.com) 46
Figure 4.13 A typical layout of a converter station. [8] 47
Figure 4.14 (a) Simplified power system with VSC-connected line and a fault. 47
Figure 4.15 (a) Sequence network diagram of the system for a phase-to-phase-to-ground fault. (b) Sequence network diagram of the system for a three-phase fault. 48
Figure 4.16 A typical layout of a offshore converter station platform [8]. 52
Figure 4.17 (a) Reactive current slope for voltage support by the VSC-HVDC system. . 54
Figure 4.18 Equal current priority current limitation strategy. 55
Figure 4.19 Reactive current priority current limitation strategy. 55
Figure 4.20 (b) Active current blocked current limitation strategy. 56
Figure 4.21 Modified Prabha Kundur two-area system. 56
Figure 4.22 World's first 1100 kV converter Transformer[8] 57
Figure 4.23 HVDC projects all around the globe which can be seen in white dots.) . . 57
Figure 4.24 (a) Circuit diagram of Modular Multilevel Converter (MMC)-HVDC converter. (b) Simplified control scheme of MMC. (c) Circulating current suppressing control in MMC. (d) Inner current control of MMC with positive and negative sequence current control loops. 59
Figure 4.25 Phase A to ground fault on Line 1 at 60 km from R1 with $R_f = 0\Omega$ (a) Active power. (b) Reactive power. (c) RMS bus voltage. (Top: Converter side, Bottom: Grid side). 60
Figure 4.26 Phase A to ground fault on Line 1 at 60 km from R1 with $R_f = 0\Omega$ (a) Instantaneous bus voltage. (b) Instantaneous current contribution. (c) Bus voltage phase angle. (Top: Converter side, Bottom: Grid side). 61
Figure 4.27 Phase A to ground fault on Line 1 at 60 km from R1 with $R_f = 0\Omega$ (a) Sequence bus voltage. (b) Sequence current contribution. (c) DC link voltage and d and q-axis converter currents. (Top: Converter side, Bottom: Grid side). 62

Figure 4.28 Impedance trajectory of ground AG element with and without VSC for phase-A to ground fault on Line 1. (a) L = 60 km with Rf = 0, 10, 20 $R_f = 0\Omega$ (b) L = 50, 70, 90 km with $R_f = 10\Omega$. (Solid Red Line: with VSC; Dotted Orange Line: without VSC). 63
Figure 4.29 Phase-A to ground fault on Line 1 at 60 km from R1 with $R_f = 10\Omega$ (a) SLG Fault – magnitude of terms in the denominator. (b) SLG Fault – magnitude of terms in the expression (12). (c) SLG Fault – angle of terms in the expression (12). 63
Figure 4.30 Phase A to Phase B fault on Line 1 at 60 km from R1 with $R_f = 10\Omega$ (a) Instantaneous current contribution. (b) Sequence current contribution. (c) RMS bus voltage. (Top: Converter side, Bottom: Grid side). 64
Figure 4.31 Phase A to Phase B fault on Line 1 at 60 km from R1 with $R_f = 10\Omega$. (a) LL Fault – magnitude of terms in the expression (19). (b) LL Fault – angle of terms in the expression (19). 64
Figure 4.32 Impedance trajectory of phase AB element with and without VSC for phase-A to phase-B fault on Line 1. (a) L = 60 km with $R_f = 0, 10, 20\Omega$. (b) L = 50, 70, 90 km with $R_f = 10\Omega$. (Solid Red Line: with VSC; Dotted Orange Line: without VSC). 66
Figure 4.33 Three-phase fault on Line 1 at 60 km from R1 with $R_f = 10\Omega$ (a) Active power. (b) Reactive power. (c) RMS bus voltage. (Blue Solid Line: Converter side, Red Dotted Line: Grid side). 66
Figure 4.34 Three-phase fault on Line 1 at 60 km from R1 with $R_f = 10\Omega$ (a) DC link voltage. (b) I_d and I_q. (c) DC pole current. 67
Figure 4.35 Three-phase fault on Line 1 at 60 km from R1 with $R_f = 10\Omega$ (a) Instantaneous bus voltage. (b) Instantaneous current contribution. (c) Sequence component of current contribution. (Top: Converter side, Bottom: Grid side). 67
Figure 4.36 Impedance trajectory of phase AB element with and without VSC for a three-phase fault on Line 1. (a) L = 60 km with $R_f = 0, 10, 20\Omega$. (b) L = 50, 70, 90 km with $R_f = 10\ \Omega$. (Solid Red Line: with VSC; Dotted Orange Line: without VSC). 68
Figure 4.37 Impedance trajectory of distance elements with VSC for a fault on Line 1 at 60 km from R1 with $R_f = 10\Omega$. (a) Ground AG element. (b) Phase AB element. (c) Phase AB element. (Solid Red Line: 1.15 p.u.; Dotted Blue Line: 0.5 p.u.). 68

Figure 5.1 Real Time Digital Simulator (RTDS) cubicle with analog ports and front panel interface. 73
Figure 5.2 Oscilloscope output taken from the front panel analog interface of RTDS . 73
Figure 5.3 (a) 12 bit resolution analog front panel. (b) 16 bit resolution of analog ports. 74
Figure 5.4 (a) 16 bit resolution analog interface board. (b) Analog cable. 74
Figure 5.5 (a) Digital interface board. (b) Digital channel cable. 75
Figure 5.6 Sample power system with VSC-HVDC connection modelled in RTDS platform 75
Figure 5.7 VSC-HVDC system with control block modeled in RTDS platform. 77
Figure 5.8 Reactive current slope for voltage support by the VSC-HVDC system. . . . 78

Figure 5.9 Multimeter during closed-loop test. 79
Figure 5.10 F6350e signal amplifier. 79
Figure 5.11 EtherCAT ports on a signal amplifier. 79
Figure 5.12 (a) Low level signal cable. (b) Low level signal channel. 80
Figure 5.13 A commercial distance relay TPU L500. 80
Figure 5.14 Experimental closed-loop test setup using RTDS, F6350e amplifier, and TPU L500 relay. 81
Figure 5.15 A pictorial representation of a commercial distance relay in a closed-loop arrangement using RTDS. 81
Figure 5.16 Phase A to ground fault on Line 1 at 70 km from *R1* with $R_f = 10\Omega$ (a) PCC voltage (RMS). (b) VSC side active power. (c) VSC side reactive power. (d) Grid side voltage (RMS). (e) Grid side active power. (f) Grid side reactive power. 82
Figure 5.17 Phase A to ground fault on Line 1 at 85 km from *R1* with $R_f = 20\Omega$ (a) PCC voltage (RMS). (b) VSC side active power. (c) VSC side reactive power. (d) Grid side voltage (RMS). (e) Grid side active power. (f) Grid side reactive power. 84
Figure 5.18 Oscilloscope output for a phase A to ground fault on *Line 1* at 70 km from *R1* with $R_f = 10\Omega$ (a) VSC side voltage. (b) VSC side current. [Yellow (channel 1): Phase A, Green (channel 2): Phase B, Blue (channel 3): Phase C, Red (channel 4): RMS (a) current (b) voltage. 85
Figure 5.19 Impedance trajectory of ground AG element with and without VSC for phase-A to ground fault on Line 1. (a) L = 70 km with $R_f = 0, 10\Omega$ (b) L = 60, 80 km with $R_f = 10\Omega$ (Solid Red Line: with VSC; Dotted Orange Line: without VSC). 86
Figure 5.20 Impedance trajectory of ground AG element with and without VSC for phase-A to ground fault on Line 1. (a) L = 70 km with $R_f = 0, 10\Omega$ (b) L = 60, 80 km with $R_f = 10\Omega$ (Solid Red Line: with VSC; Dotted Orange Line: without VSC). 86
Figure 5.21 Disturbance report recorded by relay R1 for a Phase A to ground fault on Line 1 at 70 km from R1 with $R_f = 10\Omega$ and active current blocked current limitation strategy. 88
Figure 5.22 Disturbance report recorded by relay R1 for a Phase A to ground fault on Line 1 at 70 km from R1 with $R_f = 10\Omega$ and reactive current priority current limitation strategy. 89
Figure 5.23 Phase A to Phase B fault on Line 1 at 70 km from *R1* with $R_f = 10\Omega$ (a) Bus voltage (RMS). (b) Active power. (c) Reactive power. 90
Figure 5.24 Phase A to Phase B fault on Line 1 at 70 km from *R1* with $R_f = 10\Omega$ (a) VSC current contribution (RMS). (b) VSC side sequence current. (c) VSC side sequence voltage. (d) Grid current contribution (RMS). (e) Grid side sequence current. (f) Grid side sequence voltage. 91
Figure 5.25 Oscilloscope output for a phase A to phase B fault on *Line 1* at 70 km from *R1* with $R_f = 10\Omega$ (a) VSC side voltage. (b) VSC side current. [Yellow (channel 1): Phase A, Green (channel 2): Phase B, Blue (channel 3): Phase C, Red (channel 4): RMS (a) current (b) voltage. 91

Figure 5.26 Impedance trajectory of phase AB element with and without VSC for phase-A to phase-B fault on Line 1. (a) L = 70 km with $R_f = 0, 10\Omega$ (b) L = 60, 80 km with $R_f = 10\Omega$ (Solid Red Line: with VSC; Dotted Orange Line: without VSC). 92
Figure 5.27 Impedance trajectory of phase AB element with and without VSC for phase-A to phase-B fault on Line 1. (a) L = 70 km with $R_f = 0, 10\Omega$ (b) L = 60, 80 km with $R_f = 10\Omega$ (Solid Red Line: with VSC; Dotted Orange Line: without VSC). 92
Figure 5.28 Disturbance report recorded by relay R1 for a phase A to phase B fault on Line 1 at 70 km from *R1* with $R_f = 10\Omega$. 94
Figure 5.29 Three phase fault on Line 1 at 70 km from R1 with $R_f = 10\Omega$ and active current blocked current limitation strategy. (a) Bus voltage (RMS). (b) Active power. (c) Reactive power. (d) VSC current contribution. (e) VSC side sequence current. (f) VSC side sequence voltage. (g) Grid current contribution. (h) Grid side sequence current. (i) Grid side sequence voltage. 95
Figure 5.30 Three phase fault on Line 1 at 50 km from R1 with $R_f = 0\Omega$ and active current blocked current limitation strategy. (a) Bus voltage (RMS). (b) Active power. (c) Reactive power. (d) VSC current contribution. (e) VSC side sequence current. (f) VSC side sequence voltage. (g) Grid current contribution. (h) Grid side sequence current. (i) Grid side sequence voltage. 96
Figure 5.31 Oscilloscope output for a three phase fault on *Line 1* at 70 km from *R1* with $R_f = 10\Omega$ (a) VSC side voltage. (b) VSC side current. [Yellow (channel 1): Phase A, Green (channel 2): Phase B, Blue (channel 3): Phase C, Red (channel 4): RMS (a) current (b) voltage. 96
Figure 5.32 Impedance trajectory of phase AB element with and without VSC for phase-A to phase-B fault on Line 1. (a) L = 70 km with $R_f = 0, 10\Omega$ (b) L = 60, 80 km with $R_f = 10\Omega$ (Solid Red Line: with VSC; Dotted Orange Line: without VSC). 97
Figure 5.33 Impedance trajectory of phase AB element with and without VSC for phase-A to phase-B fault on Line 1. (a) L = 70 km with $R_f = 0, 10\Omega$ (b) L = 60, 80 km with $R_f = 10\Omega$ (Solid Red Line: with VSC; Dotted Orange Line: without VSC). 97
Figure 5.34 Disturbance report recorded by relay R1 for a three-phase fault on Line 1 at 50 km from R1 with $R_f = 10\Omega$ and active current blocked current limitation strategy. 99
Figure 5.35 Disturbance report recorded by relay R1 for a three-phase fault on Line 1 at 50 km from R1 with $R_f = 10\Omega$ and reactive current priority current limitation strategy. 100

Figure 6.1 RTDS based closed-loop test-bed with signal amplifier and Siemens distance relays 7SA86. 107
Figure 6.2 Apparent fault distance calculated by the distance relays R1 and R2 for a phase A-phase B fault with $P_{HVDC} = 0$p.u. 108
Figure 6.3 Duration of pickup by the distance relays R1 and R2 for a phase A-phase B fault with $P_{HVDC} = 0$p.u. 108
Figure 6.4 Time taken to trip by the distance relays R1 and R2 for a phase A-phase B fault with $P_{HVDC} = 0$p.u. 109

Figure 6.5 Apparent fault distance calculated by the distance relays R1 and R2 for a phase A-phase B fault with $P_{HVDC} = 0.5$p.u. 111
Figure 6.6 Duration of pickup by the distance relays R1 and R2 for a phase A-phase B fault with $P_{HVDC} = 0.5$p.u. 111
Figure 6.7 Time taken to trip by the distance relays R1 and R2 for a phase A-phase B fault with $P_{HVDC} = 0.5$p.u. 112
Figure 6.8 Apparent fault distance calculated by the distance relays R1 and R2 for a phase A-phase B fault with $P_{HVDC} = -0.5$p.u. 114
Figure 6.9 Time taken to trip by the distance relays R1 and R2 for a phase A-phase B fault with $P_{HVDC} = -0.5$p.u. 114
Figure 6.10 A simplified sketch of a Permissive Underreaching Transfer Trip (PUTT) communications assisted tripping scheme. 116
Figure 6.11 A simplified sketch of a Permissive Overreaching Transfer Trip (POTT) communications assisted tripping scheme. 116
Figure 6.12 A simplified sketch of a DCB communications assisted tripping scheme. 117
Figure 6.13 Apparent fault distance calculated by the distance relays R1 and R2 for a phase A-phase B fault with $P_{HVDC} = 0$p.u. 117
Figure 6.14 Time taken to trip by the PUTT element of distance relays R1 and R2 for a phase A-phase B fault with $P_{HVDC} = 0$p.u. 118
Figure 6.15 Time taken to trip by the POTT element of distance relays R1 and R2 for a phase A-phase B fault with $P_{HVDC} = 0$p.u. 118
Figure 6.16 Power system with VSC-HVDC connected to transmission line. 118
Figure 6.17 Apparent impedance calculated by the distance relays R1 and R2 for a phase A-phase B fault with $P_{HVDC} = 0$p.u. 123
Figure 6.18 Duration of pickup by the distance relays R1 and R2 for a phase A-phase B fault with $P_{HVDC} = 0$p.u. 123
Figure 6.19 Time taken to trip by the distance relays R1 and R2 for a phase A-phase B fault with $P_{HVDC} = 0$p.u. 124
Figure 6.20 Non-Pilot distance relay performance with and without adaptive Scheme. 125
Figure 6.21 Pilot distance relay performance with and without adaptive Scheme. . . 125
Figure 6.22 Flowchart for Adaptive Distance Relaying Scheme. 126

LIST OF TABLES

Table 4.1 Operating Times for Various Types of Distance Relays [13] 39

Table 5.1 Distance Relay performance for phase A to ground fault for different fault location. 87
Table 5.2 Distance Relay performance for phase A to ground fault for different fault resistance. 87
Table 5.3 Distance Relay performance for phase A to phase B fault for different load angle. 88
Table 5.4 Distance Relay performance for phase A to phase B fault for different fault location. 93
Table 5.5 Distance Relay performance for phase A to phase B fault for different fault resistance. 93
Table 5.6 Distance Relay performance for phase A to phase B fault for different load angle. 94
Table 5.7 Distance Relay performance for three-phase fault for different fault location. 98
Table 5.8 Distance Relay performance for three-phase fault for different fault resistance. 98
Table 5.9 Distance Relay performance for three-phase fault for different load angle. 99

Table 6.1 Distance relay performance for phase A-phase B fault for different fault locations at $P_{HVDC} = 0MW$, $R_f = 0.1\Omega$. 109
Table 6.2 Distance relay performance for phase A-phase B fault for different fault locations at $P_{HVDC} = 0MW$, $R_f = 10\Omega$. 110
Table 6.3 Distance relay performance for phase A-phase B fault for different fault locations at $P_{HVDC} = 0MW$, $R_f = 20\Omega$. 110
Table 6.4 Distance relay performance for phase A-phase B fault for different fault locations at $P_{HVDC} = 500MW$, $R_f = 0.1\Omega$. 112
Table 6.5 Distance Relay performance for phase A-phase B fault for different fault locations at $P_{HVDC} = 500MW$, $R_f = 10\Omega$. 113
Table 6.6 Distance Relay performance for phase A-to-phase B fault for different fault location at $P_{HVDC} = 500MW$, $R_f = 20\Omega$. 113
Table 6.7 Distance relay performance for a phase A-phase B fault for different fault locations at $P_{HVDC} = -500MW$, $R_f = 0.1\Omega$. 115
Table 6.8 Distance relay performance for phase A-phase B fault for different fault locations at $P_{HVDC} = -500MW$, $R_f = 10\Omega$. 115
Table 6.9 Pilot-distance relay performance for phase A-phase B fault for different fault locations at $P_{HVDC} = 0MW$ and $R_f = 0.1\Omega$. 119
Table 6.10 Pilot-distance relay performance for phase A-phase B fault for different fault location at $P_{HVDC} = 0MW$, $R_f = 10\Omega$. 119

Table 6.11 Pilot-distance relay performance for phase A-phase B fault for different fault location at $P_{HVDC} = 0MW$, $R_f = 20\Omega$ and active current blocked limitation strategy. 120
Table 6.12 Adaptive distance relay performance for phase A-phase B fault for different fault locations at $P_{HVDC} = 0MW$, $R_f = 10\Omega$. 124
Table 6.13 Adaptive Distance Relay performance for phase A-to-phase B fault at 75 km and $R_f = 10\Omega$. 124

Table A.1 Study System Parameters. 135

ACRONYMS

FFT	Fast Fourier Transform
VSC	Voltage Source Converter
LCC	Line Commutated Converter
HVDC	High Voltage Direct Current
LCP	Line Constant Program
PV	Photovoltaic
VRE	Variable Renewable Energy
SG	Synchronous Generator
TSO	Transmission System Operator
PES	Power Electronic Switch
PCC	Point of Common Coupling
NPC	Neutral Point Clamped
FC	Flying Capacitor
MMC	Modular Multilevel Converter
IGBT	Insulated Gate Bipolar Transistor
PWM	Pulse Width Modulation
CCSC	Circulating Current Suppression Control
SM	submodules
FP	Firing Pulses
NC	Network Code
PI	Proportional Integral
FRT	Fault Ride Through
UHV	Ultra High Voltage
EHV	Extra High Voltage
HV	High Voltage
CT	Current Transformer
PT	Potential Transformer

RTDS Real Time Digital Simulator

PLL Phase Locked Loop

SRF Synchronous Reference Frame

ARCI Additional Reactive Current Injection

CB Circuit Breaker

EMTP Electromagnetic Transient Program

GUI Graphical User Interface

GTWIF GT Workstation Interface

WIF Workstation Interface

LAN Local Area Network

GTAO Gigabit Transceiver Analogue Output

DAC Digital to Analog Converter

GTDI Gigabit Transceiver Digital Input

DAC Digital to Analog Converter

GTO Gate Turn-Off

DCB Directional Comparison Blocking

DCUB Directional Comparison Unblocking

DTT Direct Transfer Trip

PTT Permissive Transfer Trip

PUTT Permissive Underreaching Transfer Trip

POTT Permissive Overreaching Transfer Trip

PLC Power Line Carrier

OPGW Optical Phase ground Wire

SSR Sub-Synchronous Resonance

CBPWM Carrier Based PWM

SVPWM Space Vector PWM

PSB Power Swing Blocking

FACTS Flexible AC Transmission System

DFIG Doubly-Fed Induction Generator

SCIG Squirrel Cage Induction Generator

IIDG Inverter Interfaced Distributed Generation

DG Distributed Generation

WPP Wind Power Plant

SCR Short Circuit Ratio

ESCR Effective Short Circuit Ratio

SVC Static Var Compensator

STATCOM Static Synchronous Compensator

UPFC Unified Power Flow Controller

TCSC Thyristor Controlled Series Capacitor

SSSC Static Synchronous Series Capacitors

IPFC Interline Power Flow Controller

GIPFC Generalized Interline Power Flow Controller

GUPFC Generalized Unified Power Flow Controller

LVRT Low Voltage Ride Through

FSC Full-Scale Converter

Part I

INTRODUCTION & LITERATURE REVIEW

This part of the thesis describes the general introduction and problem statement of the research work, state-of-the-art on HVDC with VSC technology, and the power system protection philosophy. Part I of the thesis is divided into three chapters namely Chapter 1, which is an Introduction chapter presenting the rationale behind the research work conducted, the objective of the thesis, the problem in distance relay operation and the adaptive approach to target this problem.

Chapter 2 discusses the cutting edge status of HVDC system and VSC technology, their modeling methods, operation and control architectures. This chapter presents various HVDC system projects already in operation in different parts of the world. Moreover, it also highlights the operational behavior of VSC-HVDC during balanced and unbalanced system conditions.

Chapter 3 of part I reviews the power system protective relays, for instance, overcurrent relay, differential relay, and distance relay. Additionally, the operational challenges of distance relay with the VSC-HVDC system in the grid is expanding by the introduction of renewable energy based power sources is also explained in this chapter.

1 INTRODUCTION

Contents

1.1 General Background & Motivation 3
1.2 Problem Definition 3
1.3 Distance Protection & Challenges 5
1.4 Objective & Research Questions 5
1.5 Outline & Approach 6



Thales of Miletus (624-546 BC) was a pre-Socratic Greek/Phoenician philosopher, mathematician and astronomer from Miletus in Asia Minor (present-day Milet in Turkey). He was one of the Seven Sages of Greece. Many, most notably Aristotle, regard him as the first philosopher in the Greek tradition, and he is otherwise historically recognized as the first individual in Western civilization known to have entertained and engaged in scientific philosophy.

1.1 GENERAL BACKGROUND & MOTIVATION

Extra High Voltage (EHV) and High Voltage (HV) transmission lines are usually protected by the distance protection which is robust in nature, providing different zones of protection so as to identify and eliminate faults in necessary time. Distance protection based on communication serves as main/primary protection employed upon long lines and an aberration in its behavior is unacceptable. For the proper operation of power system without putting it in jeopardy, the main protection scheme must be all time reliable.

One of the main concern of power system protection engineers is the correct tripping of distance protection during the fault condition even if the power system network is ever expanding and growing in complexity.

In recent years, it has been found that major blackouts have been caused by the malfunctioning of protective devices due to the network effect. The blackout in USA 2003, European blackout in 2006, Indian power system blackout are some of the main examples. The malfunctioning of distance protection is one of the reasons for these power system blackouts.

Moreover, the installation of power electronic components in power system for power system reliability and efficiency enhancement have adverse effects on the distance protection, which has been presented later in the section of thesis research aim. The kind of hurdle and disturbance attributed by power electronic components on the distance relay is one of the main motivation for this research on analyzing the impact of VSC-HVDC on the distance protection.

1.2 PROBLEM DEFINITION

HVDC technology has become a mature technology in the field of power system to transfer bulk amount of energy with fewer losses and minimum expenditure. In future, Line Commutated Converter (LCC) and the forced commutated converter i.e. Voltage Source Converter will be utilized to transmit power over long distances due to their merits over AC lines as discussed in Chapter 2. The VSC based HVDC can be utilized to form a multi-terminal HVDC network, which will serve the foundation for DC grids. Much of the talk in the scientific community is based on establishing a multi-terminal DC grid and its integration to existing mainland AC grids.

The integration of VSC-HVDC network with mainland AC grid has several advantages:

1. Improve power system stability,
2. Reduce power system oscillations,

3. Eliminate Sub-Synchronous Resonance (SSR) phenomena,
4. Low power losses and more economical for the same length of AC transmission lines, and
5. Best suited for offshore wind system

In spite of these advantages there are issues related to VSC-HVDC system, which needs an urgent focus that can be illustrated as below:

1. Vulnerability towards DC short circuit current,
2. Vulnerability towards AC short circuit current,
3. Requirement of DC circuit breaker,
4. Reduction in Effective Short Circuit Ratio (ESCR) of AC grid, and
5. Impact upon AC protection system

The integration of VSC-HVDC to the existing mainland AC system is a difficult task posing a number of challenges as mentioned before. One of the main challenges for the grid protection engineers is to analyze the influence of voltage source converter on existing protection equipment's, for instance, distance protection.

The impact of power electronic components on the AC network and its associated control actions have not yet been analyzed. The behavior of converter and its controllers during any normal and abnormal condition is totally different from each other and from the synchronous generator. Moreover, the fast response time of VSC controllers leads to rapid changes in system parameters like Point of Common Coupling (PCC) voltage, and line currents.

During an event of a short circuit on a transmission line, the converter cannot supply more than its saturation limit. This saturation limits of VSC[1] depend upon the thermal limit of switches that are set to carry 15-20% more than the nominal current. Therefore, the VSC can only supply fault currents of 1.2 p.u. magnitude, thus restricting the fault level and affecting the conventional grid protection system that is based on the fault responses of conventional generators. Moreover, the converter responses to such faults on the grid side are entirely different from the Synchronous Generator (SG), which forms an integral part of the power system.

The distance protection, which is primarily an important protection scheme employed upon the AC transmission lines, is mostly affected by the VSC-HVDC. When the VSC-HVDC is connected to the transmission lines with the distance relay, a fault on the line cannot be seen by the distance relay at an appropriate location due to the fast changes caused by the converter controllers following the grid codes of reactive current injection, which ultimately leads to no operation or delayed operation of the distance relay. This delayed operation or no operation of the distance relay puts the entire power system in jeopardy.

Power system planners and protection engineers have been preparing the blueprints of protective relays and analyzing the power system based on the reality that synchronous generator forms an integral part of the system[2]. But, with the continuous push of renewable energy players and high power consumption towards super grid or DC grid based on VSC, the structure of power system is changing, which is bringing a negative impact on the distance protection such as under reach during the fault and loss of insensitivity due to the blocking of converter, with a critical question in mind, "will the distance protection of line connected to VSC-HVDC perform optimally?" unfortunately, which has been left without being discussed widely in the research community.

Furthermore, a firm solution for the problem faced by the distance protection in the presence of VSC-HVDC system following Network Code (NC) for HVDC connections during the fault has to be proposed so as to accommodate the future VSC-HVDC grids into the existing AC grid.

[1] VSC characteristics:
- Converter saturates to a maximum of 15-20% more than the nominal current during a short circuit,
- Converters can only supply fault currents of 1.2 p.u. magnitude,
- Restricted fault level,
- Different fault response of converters with respect to conventional synchronous generator,

[2] Changing power systems scenarios:
- Integration of renewable energy sources,
- Rapid increase in Energy usage,
- Acceptance of DC grids,
- Increase use of power electronics based load and components,

1.3 DISTANCE PROTECTION & CHALLENGES

Distance protection[3] is used for the protection of high voltage transmission lines. The protection is a non-unit scheme as signals are fetched from one end of the protected line. The protection is arranged in overlapping zones so that no part of the system is left unprotected. The relay measures the current and voltage at the point of relay location and calculates an apparent impedance based on this measured current and voltage.

The apparent impedance is an indication of the distance to a fault by which a distance element decides the zone of fault location. The operating time of step distance relay depends upon the zones of protection. In general, a step distance protection provides backup protection of the communication assisted distance protection.

The main features of the step distance protection scheme are different zones of protection. The different zones of protection are provided in order to prevent the relay from overreach and any possible mis-operation. The zones of protection are also overlapping with each other so that none of the transmission line sections are left unprotected. Each zone has an associated operating time as well. Nonetheless, the distance function comes with many drawbacks and should not be considered as the morning star.

The main problems of distance protection of transmission lines are as follows:

- Inaccurate estimation of the distance to fault with high arc resistance,
- Risk of mal-operation during fast power swing on the line,
- Mal-operation of zone 3 distance relay because of load encroachment to relay characteristics,
- Impact of power electronic converters on apparent impedance seen by the relay.

[3] Distance relay characteristics:

- Serves as a primary and backup protection,
- Non-unit scheme,
- Multiple overlapping zones,
- Estimates the fault distance and apparent impedance using the current and voltage,

1.4 OBJECTIVE & RESEARCH QUESTIONS

The main goal of this Ph.D. thesis[4] is to investigate the impacts of control actions of VSC-HVDC system on distance protection following the NC guidelines to support the network reactively during the fault. The effect of current saturation limits, fault resistance, Fault Ride Through (FRT) capability of HVDC, current limitation strategies, negative sequence current suppression, and different fault current behavior of the converter, which is responsible for malfunction of the distance relay, by analyzing its apparent impedance trajectory on RX plane is studied. The thesis aims to assess the distance relay during symmetrical and unsymmetrical faults in a line connected to VSC-HVDC using analytical, simulation and RTDS based closed loop test methods. Furthermore, a solution is proposed for the problem faced by the distance relays in the form of novel adaptive relaying scheme. The research carried out to analyze, assess and present the following:

1. Analytical explanation,
    - Analyze mathematically the relay behavior during single line to ground, double line, double line to ground and three-phase fault in zone 1 and zone 2.
2. PSCAD/EMTDC environment,
    - Assess the impact of VSC-HVDC system on the distance relay behavior with different types of the converter (2-level, 3-level, half bridge and full bridge MMC).
    - Investigate the impact of VSC-HVDC system on the distance protection of transmission line when supplying the reactive current into the grid as per the grid codes.

[4] Thesis main objectives:

- Impacts of VSC control on the distance relay,
- Effects of network connection guidelines to supply reactive current,
- Effects of saturation limits,
- Effects of fault resistances,
- Effects of negative sequence current suppression,

- Assessment of the distance relay behavior in the presence of VSC-HVDC system with the current limitation strategies and negative sequence current suppression.

3. RTDS/RSCAD environment,
   - Closed-loop test of a commercial distance relay using RTDS to validate its operation in a VSC-HVDC environment.
4. Novel Adaptive Relaying Scheme
   - An adaptive relaying logic as a solution to the problem for both the standalone and communication channel assisted distance function for the correct operation is proposed and discussed.
   - Validation of the proposed adaptive relaying logic using RTDS/RSCAD.

1.5 OUTLINE & APPROACH

In order to achieve the objectives of the research laid down in objective&research questions, a systematic approach to identify and investigate the behavior of distance protection in the presence of VSC-HVDC is adopted. Apart from the analytical study involving a mathematical explanation of the problem, simulation study and Hardware in Loop testing of the distance relay is done to evaluate the misoperation of distance relay.

Chapter 2

The research work starts with the state-of-the-art review of the HVDC technology. This chapter discusses the historical development of this technology from Thury system, mercury-arc valves, thyristor to the latest VSC technology. It also explains the advantages of VSC technology over the other HVDC technologies. Further, the fault behavior of VSC-HVDC during a fault is compared with the conventional power system.

Chapter 3

This chapter elaborates the grid protection system and then the impact of VSC based systems like Flexible AC Transmission System (FACTS) devices, Doubly-Fed Induction Generator (DFIG), Inverter Interfaced Distributed Generation (IIDG) on the distance relays installed in AC transmission lines. The reasons behind the mal-operation of the distance relay in the form of relay under-reach and overreach in presence of VSC are studied. The possible solution for the correction of distance relay behavior is also discussed.

Chapter 4

Continuing the work further, the behavior of distance relay is analyzed in a power system with a VSC-HVDC network, modeled in PSCAD/EMTDC simulation platform. The details of power system components such as voltage sources parameters, transmission line parameters, transformer rating and configuration parameters, length of the line, distance relay protection zone settings, and finally the type of distance relays characteristics are explained. The grid codes for the reactive current injection during the fault and the current limitation strategies are explained.

Based on the transmission line parameters, sequence impedance of the line is obtained from Line Constant Program (LCP) of PSCAD/EMTDC to design the reach setting of conventional distance protection. The distance relay installed on both the ends of the trans-

mission line is then tested for different fault conditions like fault types, fault locations, power flow direction, system loading and fault resistance. The apparent impedance seen by the distance relay is plotted on R-X diagram for all the scenarios and compared with the distance relay impedance trajectory without VSC-HVDC to mark the difference.

Chapter 5

To validate the simulation results obtained in PSCAD/EMTDC, a similar system is modeled in RTDS/RSCAD, which is a real-time simulation platform with the enhanced functionality of closed-loop testing of a physical device. A commercial numerical distance relay is then put into closed-loop test so as to receive signals from the RTDS and send trip signals back to RTDS to open the AC breakers. The distance relay in the closed loop test is analyzed for breaker signal, operating time, assertive zone of operation, relay reach, and apparent impedance trajectory and compared with the results obtained in PSCAD.

Chapter 6

After the real-time digital simulator closed-loop testing, an adaptive relaying logic is proposed and modeled in RTDS for the correct operation of the distance relay in case of asymmetrical faults fault while following grid code guidelines.

Chapter 7

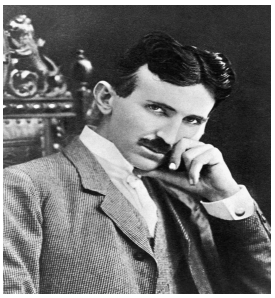
Finally, this chapter presents the final conclusions and final remarks for the future research.

2

VSC-HVDC SYSTEM

Contents

2.1 HVDC Transmission System Background 10
2.2 Classic HVDC System 11
2.3 VSC-HVDC Transmission System 14
2.4 HVDC Transmission System Configuration 18
2.5 VSC-HVDC Control 19
2.6 VSC-HVDC Transmission System Behavior 20
2.7 Conclusions 21



Nikola Tesla (1856-1943) was a Serbian-American inventor, electrical engineer, mechanical engineer, physicist, and futurist who is best known for his contributions to the design of the modern alternating current electricity supply system. Born and raised in the Austrian Empire, Tesla received an advanced education in engineering and physics in the 1870s and gained practical experience in the early 1880s working in telephony and at Continental Edison in the new electric power industry.

The introduction Chapter 1 presented a general background and rationale behind the investigation of distance protection operation in the presence of VSC-HVDC system. It has been discussed in brief that the grid code requirement for the operation of HVDC connection such as reactive current support during the event of a fault, FRT capability of HVDC system, control strategies and current limitation capability of VSC actually affects the performance of distance relaying scheme.

At the center of this discussion, regarding the performance evaluation of distance function, lies the HVDC system based on VSC with different control architecture, physical layout and behavior during normal and abnormal conditions. Therefore, the main aim of this chapter is to present the behavior of VSC-HVDC system during the normal and abnormal condition when integrated with the network. This Chapter 2 begins with the historical developments of HVDC system and its existing types in operation nowadays. Later on, the physical and control architecture is discussed, which progresses into its behavior during a normal and abnormal situation.

2.1 HVDC TRANSMISSION SYSTEM BACKGROUND

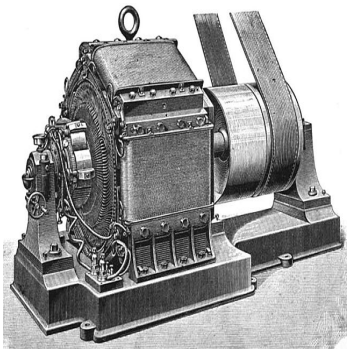


Figure 2.1: Thury's six-pole dynamo [1].

Since the beginning, there were huge discussions among the pioneers of electricity regarding the pros and cons of Alternating and Direct currents, which is historically termed as "War of Currents" [14]. This war was famously fought between Nikola Tesla who supported Alternating Current and Thomas Edison who was in favour of Direct Current. But, at that time the real advantages of DC system was not known.

The 100th anniversary of operation of the first truly commercial HVDC transmission cable, the Moutiers-Lyon line, was celebrated in 2007, which was the largest HVDC transmission line installed up to that time. It was laid between the power station at Moutiers and the city of Lyon to supply power to the railway terminal. It was also the time when mass-impregnated HVDC underground cable was used [15]. Nonetheless, the HVDC system is even older than 1906 and dated back to 1888. A system had been designed by the Swiss engineer René Thury and is still referred to as the 'Thury system'.

The Thury System

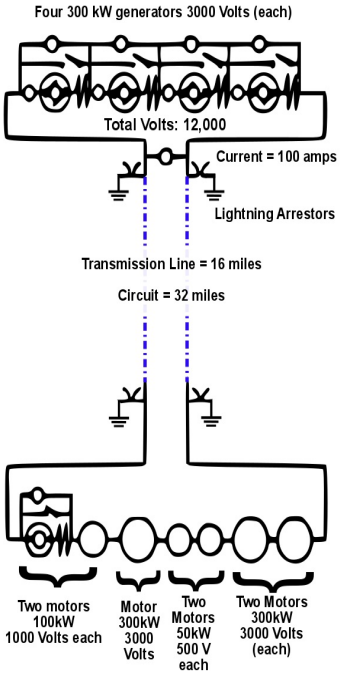


Figure 2.2: Thury System balancing voltage of supply with voltage of load [2].

René Thury was known as the "King of DC" for his work with High Voltage Direct Current electricity transmission. Thury continued the idea of Marcel Deprez to develop the first commercial system for high-voltage DC transmission, using generators in series to attain high transmission voltages [16]. In 1889, the system was first put into service in Italy by the Acquedotto de Ferrari-Galliera. Earlier the company had built a water supply for Genoa from the Gorzente River and were interested whether turbines for electrical generation might address their long-standing problem of reducing excess pressure. The first turbine of 140 hp (100 kW) was installed at Galvani station, which turned the two Thury 6-pole dynamos, as shown in Figure 2.1 that each produces 1000 to 1100 volts at 45 amperes. In order to keep the same current, their speed varies from 20 to 475 rpm, regulated by changing the flow through the water turbine. The circuit supplied 15 motors along the line stretching to Genoa, including a 60 hp (44 kW) motor at the railway station, and motor transformers at Central Electric Lighting Station in Genoa [15].

Thury system consisted of several DC generators connected in series to feed a high-voltage transmission line. The loads consisted of DC motors (also connected in series) which could drive machinery directly or drive other types of generators to supply whatever electric power was required, as shown in Figure 2.2. The series connection of generators and motors eliminated the need to design these machines to withstand the high transmission voltage. Between the years 1888 and 1912, Thury transmission systems were installed in Italy, Switzerland, Spain, Hungary, Russia and France [15], [17].

The Moutiers-Lyon HVDC Scheme

The Moutiers-Lyon system transmitted 20 megawatts of hydroelectric power a distance of 124 miles (200 km), including 6 miles (10 km) of underground cable. The system used eight series-connected generators with dual commutators for a total voltage of 150,000 volts between the poles, was steadily upgraded from 4.3 to 20 MW and ran from about 1906 until 1936 [17]. Most of the route was covered using overhead lines but in Lyon itself, a pair of mass-impregnated HVDC underground cables were laid over a 4 km route [15].

The Elbe-Berlin Project

The Elbe-Berlin transmission line would bring power from the power plant Vockerode on the river Elbe to Berlin. Due to the extreme scarcity of raw materials in those days of

World War II, the German government ordered the line to be built as a pair of underground cables. Despite the war, the Elbe-Berlin transmission line was completed in April 1945, but after the defeat of Germany, the cable system was uninstalled as part of war reparation payments [15].

The Moscow-Kashira Project

Commissioned in 1950, the Kashira–Moscow project was the first HVDC system in the world. It is a two-pole system that is comprised of a 120-km (75-mile) ±100 kV underground cable circuit, with a load-transfer capacity of 30 MW. The system was built using equipment designed and manufactured by German companies Siemens and AEG for the Elbe–Berlin project, which was never put into service by Germany. By 1953, the underground cable was replaced with cable manufactured at the Soviet plant Moscabel [18].

The Mercury-Arc Valve System

A mercury-arc valve is a type of electrical rectifier used for converting AC into DC. It is a type of cold cathode gas-filled tube made from a pool of liquid mercury and is therefore self-restoring. As a result, mercury-arc valves were much more rugged and long-lasting and could carry much higher currents than most other types of gas discharge tube [16].

The Swedish government decided in 1950 to connect the island of Gotland electrically to the Swedish mainland. The limited transmission power and moderate voltage made this project an ideal starting point. It was the first fully commercial static plant for high voltage direct current transmission in the world. Gotland 1 went into service in 1954. It could transfer 20 megawatts over a 98-kilometer-long submarine cable between Västervik on the mainland and Ygne on the island of Gotland, with a voltage of 100 kV. As a static inverter, Mercury arc valves were used. In 1970 the service was re-engineered to the transmission capacity of 30 megawatts at a voltage of 150 kV by using the first thyristor module for HVDC applications [16].

The HVDC Inter-Island link is a 610 km long, 1200 MW bipolar HVDC transmission system connecting the electricity networks of the North and South Islands of New Zealand together, as shown in Figure 2.4. It is commonly referred to as the Cook Strait cable because only a short section of the complete link is in cable, and there are actually three operational HVDC power cables across Cook Strait. The HVDC link was first commissioned in April 1965 to primarily transport electricity from the generation-rich South Island to the more populous North Island. The link originally was a bipolar 600 MW link with mercury arc valves (see Figure 2.3), until the original equipment was paralleled onto a single pole (Pole 1) in 1992, and a new thyristor-based pole (Pole 2) was commissioned alongside it, increasing the link capacity to 1040 MW.

2.2 CLASSIC HVDC SYSTEM

High Voltage DC technology is a power electronic devices based technology and has proven its mettle in transferring bulk amount of active power over a very long distance keeping the cost and losses below par than an Ultra High Voltage (UHV)/EHV/HV AC transmission lines. It has been observed that HVDC is cheaper in comparison to AC transmission when utilized for a distance more than 800km long [19].

Furthermore, it is more beneficial to transfer power through sub-marine cables using HVDC due to the absence of charging current in DC cables, reducing losses [20, 21]. It can interconnect unsynchronized grids (operating at 50Hz and 60Hz) to transfer power between them as well as power flowing through the DC link can be controlled indepen-



Figure 2.3: Mercury arc valves of ASEA design with four anode columns in parallel located at HVDC Inter-Island link [3].

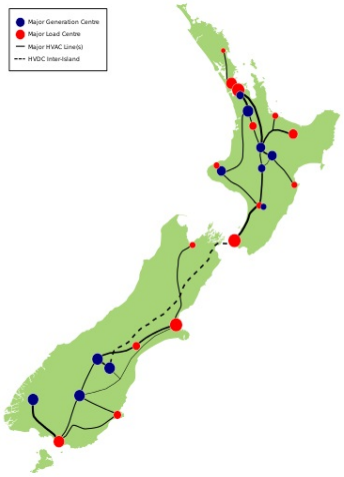


Figure 2.4: A map of transmission lines in New Zealand with the HVDC Inter-Island link shown as dashed line.

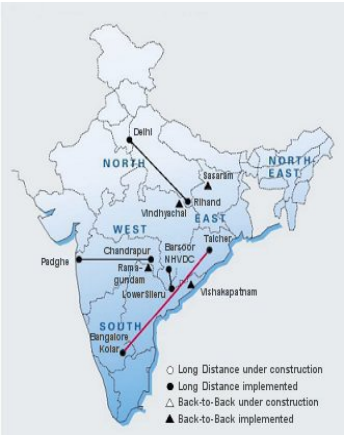


Figure 2.5: Examples of classic HVDC links in India [4].

dently by each of the source voltage and phase angles. It is also helpful in stabilizing the AC grids under the event of disturbance and faults. Numerous other good impacts of HVDC has aided it in capturing Power market and running parallel or even competing with AC power market [21].

Since 1977, HVDC systems are using Thyristor valves to transfer power which are also called by the name of LCC based HVDC, as an example Figure 2.7. The first project based on LCC-HVDC was established in Canada on the river Eel. But, line commutated converter has its own limitation, such as, power reversal can only be done by changing the polarity of DC link voltage which is itself a cumbersome task. It has no tendency to support black start capability, in case of grid re-synchronization after grid outages [22].



Figure 2.6: Thyristors of different sizes [5].

HVDC technology is now widely used around the world, for instance, Xiangjiaba-Shanghai, (China), Talchar-Kolar (India) (refer Figure 2.5), Rio Madeira (Brazil), Manitoba, Canada etc. For transferring power through under water cables/sub-marine cables, HVDC technology are more beneficial due to the absence of charging current from DC cables, therefore reduce losses [23]. Until recently, Thyristor based HVDC has been used for AC-DC-AC conversion which is also called as classic HVDC or traditional HVDC [21].

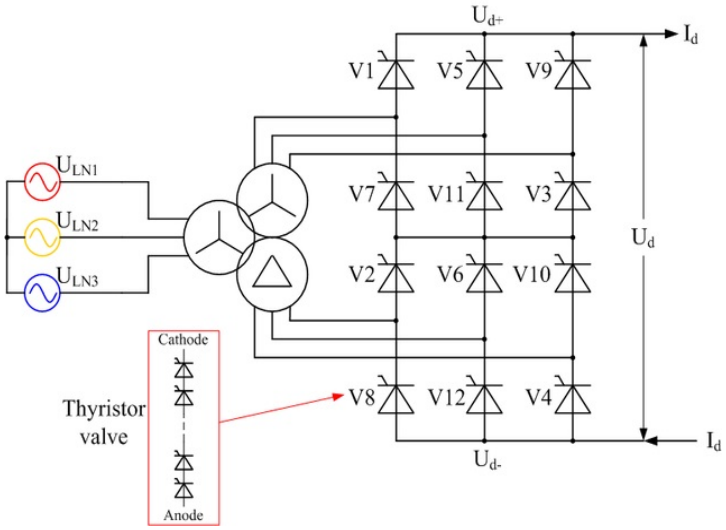


Figure 2.7: A 12-pulse HVDC converter using thyristor valves.

The thyristor valve was first used in HVDC systems in 1972 on the Eel River Converter Station in Canada [24]. The thyristor is a solid-state semiconductor device similar to the diode, but with an extra control terminal that is used to switch the device on at a defined instant, as shown in Figure 2.6. Because thyristors have breakdown voltages of only a few kilovolts each, HVDC thyristor valves are built using large numbers of thyristors connected in series. Additional passive components such as grading capacitors and resistors need to be connected in parallel with each thyristor in order to ensure that the voltage across the valve is shared uniformly between the thyristors. The thyristor plus its grading circuits and other auxiliary equipment are known as a thyristor level.



Figure 2.8: The Xiangjiaba Shanghai ±500 kV, 6400 MW HVDC link.

As of 2012, thyristor valves had been used on over 100 HVDC schemes, with many more still under construction or being planned. The highest power rating of any single HVDC converter (twelve-pulse bridge) in operation was 2000 MW in 2010, on the ±660 kV Ningdong–Shandong scheme in China. Two such converters are provided at each end of the scheme, which is of conventional bipolar construction [25]. Since 2007 the highest voltage rating of a single HVDC converter has been the ±450 kV NorNed scheme linking Norway to the Netherlands, which has only a single converter at each end in an arrangement that is unusual for a LCC-HVDC scheme.

Xiangjiaba–Shanghai HVDC system

In July 2010, the Xiangjiaba–Shanghai HVDC system, which is a ±800 kV, 6400 MW high-voltage direct current transmission system in China became the world's largest-capacity HVDC system, presented in Figure 2.8. The system was built to export hydro power from Xiangjiaba Dam in Sichuan province, to the major city of Shanghai. The design is a bipolar system with overhead lines for the high-voltage conductors and ground return for the neutral current. However, because of the very high operating voltage and power, each pole contains two twelve pulse bridges in series at each end.

Talcher–Kolar HVDC system

The Talcher–Kolar HVDC system, otherwise known as the East–South interconnection II (refer Figure 2.9) is a 1450 km HVDC transmission connection between the eastern and southern regions in India connecting four states namely Odisha, Andhra Pradesh, Tamil Nadu and Karnataka. The system has a transmission voltage of ±500 kV and was originally put into service in March 2003,[26] with a rated power of 2000 MW. In 2007 the scheme was upgraded to 2500 MW. The Talcher–Kolar HVDC system is owned by Power Grid Corporation of India and the converter stations were built by Siemens. The scheme is a conventional bipolar system with overhead lines for the high-voltage conductors and ground return for the neutral current.

The scheme includes two ground electrodes, of ring construction, located at Rohila, 28.5 km northeast of the Talcher converter station and at Chikkadasarahalli, 30 km northwest of the Kolar converter station.



Figure 2.9: The Talchar Kolar classic HVDC link in India [4].

Rio Madeira HVDC system

The Rio Madeira HVDC system is a high-voltage direct current transmission system in Brazil, built to export power from new hydro power plants on the Madeira River in the Amazon Basin to the major load centres of southeastern Brazil. The system consists of two converter stations at Porto Velho in the state of Rondonia and Araraquara in Sao Paulo state, interconnected by two bipolar ±600 kV DC transmission lines with a capacity of 3,150 megawatts each. In addition to the converters for the two bipoles, the Porto Velho converter station also includes two 400 MW back-to-back converters to supply power to the local 230 kV AC system. Hence the total export capacity of the Porto Velho station is 7100 MW: 6300 MW from the two bipoles and 800 MW from the two back-to-back converters. When Bipole 1 commenced commercial operation in 2014, Rio Madeira became the world's longest HVDC line, surpassing the Xiangjiaba–Shanghai system in China.

Some of the most famous classic HVDC projects implemented around the globe are as shown in Figure 2.10:

- Three Gorges-Changzhou
- Ningdong - Shandong
- Rihand-Delhi
- Chandrapur-Padghe
- HVDC Inter-Island 2
- Inga-Shaba
- Basslink

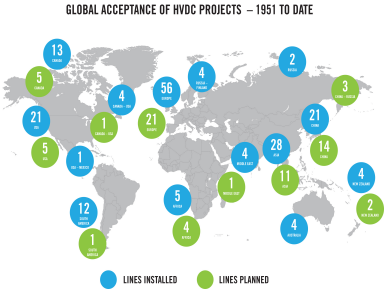


Figure 2.10: Global HVDC link [6].

2.3 VSC-HVDC TRANSMISSION SYSTEM

A new emerging technology based on more advanced semiconductor devices such as Insulated Gate Bipolar Transistor (IGBT) and Gate Turn-Off (GTO)s are being used in HVDC which are different from Thyristors and are called as Voltage Source Converter [20, 21, 27]. The VSCs operate at a high switching frequency of 1-2 kHz and utilize Pulse Width Modulation (PWM). Today a maximum rating of 1000 MW and ±320kV is commercially available. The positive aspect of VSC based HVDC are [28]:

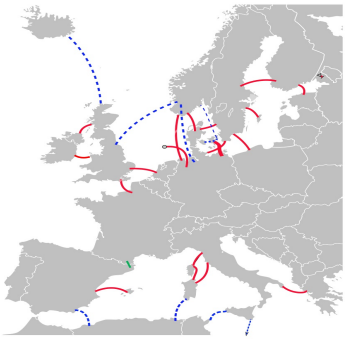


Figure 2.11: Global VSC-HVDC link.

1. No need of any external voltage source for commutation,
2. Active power and Reactive power can be controlled independently and rapidly,
3. Power reversal is easy without voltage polarity reversal,
4. Small filtering equipment,
5. Black start capability, and
6. Best suited for offshore wind farm and Multi-Terminal HVDC grids

These features enables VSC based HVDC system to connect weak AC system, islands, offshore wind system for example BorWin-1 (Germany) [29], BorWin-2 (Germany) [30], Inelfe (France and Spain) [31], East-West Inter-connector Project (EWIP)(Ireland and Wales) [22], as shown in Figure 2.11.

BorWin-1 Project

HVDC BorWin1 is the first HVDC facility in Germany to use VSC, and the first in the world to be built for importing power from an offshore wind park to shore. It is used for the power connection of the offshore wind park BARD Offshore 1 and other offshore wind farms in Germany near Borkum to the European power grid. The facility was built by ABB and can transfer a power of 400 MW at a bipolar voltage of ±150 kV. HVDC BorWin1, which leads from BorWin Alpha Offshore Platform to Diele substation, consists of a 75 km of underground and 125 km of submarine cable.

Unlike the later (and more powerful) HVDC connections that have been built for transmitting wind power to shore in Germany, Borwin 1 uses two-level converters in which several hundred IGBT are connected directly in series in each valve. PWM is used to improve the level of harmonics but filtering is still needed. One converter is provided at each end of the link, in the symmetrical monopole configuration. Borwin 1 is operated by the German Transmission System Operator TenneT and construction and commissioning was completed in 2009



Figure 2.12: Inelfe VSC-HVDC link between France and Spain.

Inelfe Project

The Inelfe project is a VSC-HVDC project inter-connector between France and Spain started in October 2015 between the Baixas-Santa Llogaia electricity interconnection to increase the interchange capacity between the Iberian Peninsula and the rest of Europe. It is developed under the flagship of Zaragoza Agreement, which was signed on 27 June 2008 between the governments of Spain and France to build this interconnection. The interconnection capacity between France and Spain will be doubled from 1,400 MW before its construction to 2,800 MW as it a bipolar connection, see Figure 2.12.

The connection established is a mix of underground cable and overhead lines. The power electronic devices used are IGBT. The stations use HVDC Plus technology from Siemens with a transmission voltage of ±320 kV direct current (DC) (see Figure 2.13). The distance

between the two power converter stations is around 65 km. Underground DC cables in an 8 km tunnel that leads into the Pyrenees Mountains will transmit the power in both directions.

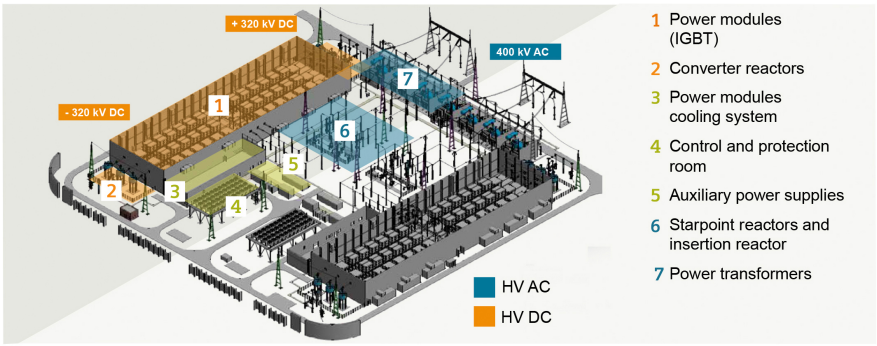


Figure 2.13: Converter station layout between France and Spain [7].

Murraylink

Murraylink is an Australian HVDC based electricity transmission link between Berri in South Australia and Red Cliffs in Victoria, connecting the two state electricity grids, as shown in Figure 2.14. It consists of two 180 km long bipolar HVDC cables, which for environmental protection reasons are underground, with an operating voltage of 150 kV and a transmission capacity of 220 MW. The link operates an "HVDC Light" VSC system, a product of ABB [8]. This link is considered to be the world's longest underground cable transmission system and is owned by Energy Infrastructure Investments consortium as depicted in Figure 2.15.

But, VSCs are also associated with major vulnerability for instance [21]

1. High power losses,
2. High converter cost, and
3. Highly vulnerable towards DC side faults

With the continuous progress in semiconductor technology, a parallel development in power electronics converter based on high power semiconductors was also taking place. Researchers and industries have already developed many converter models based on Voltage Source technology such as H-Bridge converter, Flying Capacitor (FC) converter, Neutral Point Clamped (NPC) and MMC [20].



Figure 2.14: Murraylink VSC-HVDC link between Berri and Red Cliffs.



Figure 2.15: Murraylink VSC-HVDC cables [8].

H-Bridge Converter

The name has been derived from the schematic arrangement of semiconductor devices which is shown as an English letter "H". The load is connected to the H-Bridge. For a single phase converter, the bridge requires at least four semiconductor devices which can be stacked together to produce multilevel H bridge converter. The number of voltage levels depends upon the number of H bridge cells stacked together.

Figure 2.16(a) presents a schematic diagram of single phase H-Bridge converter with four semiconductor devices while Figure 2.16(b) presents a single phase cascaded H-Bridge converter connected in series. Similarly, a number of H-Bridge cells can be cascaded to produce numerous levels of voltages. Many research has been done in the past

regarding topologies of the cascaded multi-level H-Bridge converter to minimize losses, semiconductor devices, minimize harmonics and improve power quality.

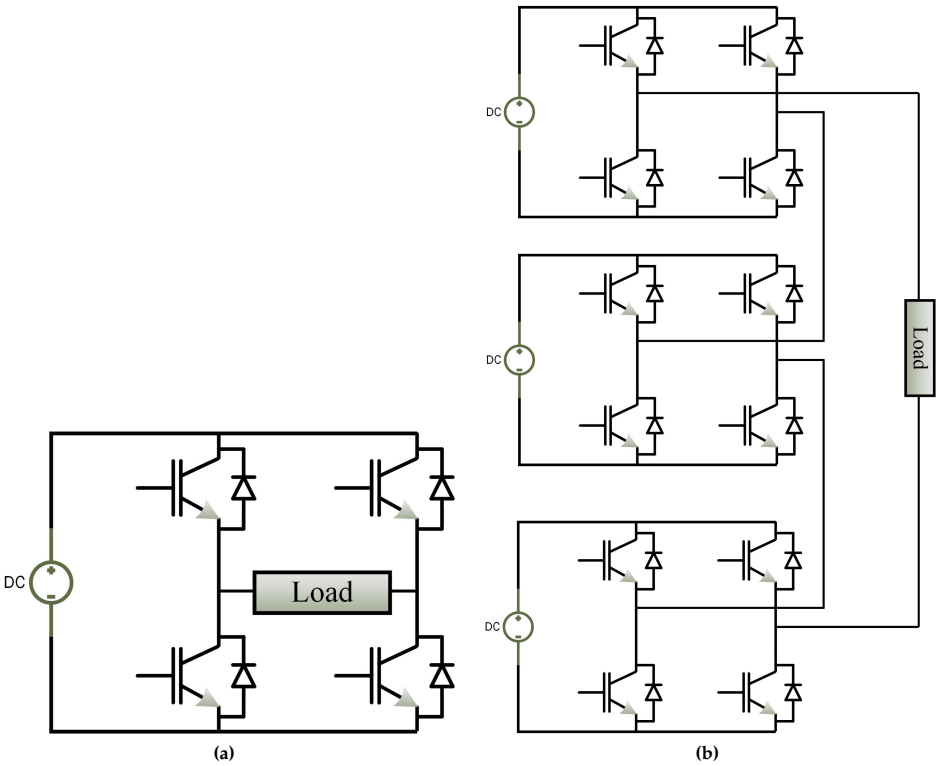


Figure 2.16: Single phase H-Bridge scheme (a) Single bridge. (b) Cascaded bridge.

Neutral Point Clamped Converter

As we already know that multilevel converter has attracted researchers and industries for various industrial application because of their advantages, Neutral Point Clamped scheme is one of the widely accepted among multilevel converter for high power drives and utility systems. A three phase, three level, NPC consist of four semi-conductors (IGBT) in each phase with a diode path connecting each leg and capacitor branch as shown in Figure 2.17 [32, 33]. When compared with other multilevel converter, the NPC converter uses fewer number of capacitors and switches per phase for a desired voltage output level, hence more economical and reliable [34]. One of the main tasks/challenges in NPC are:

1. Voltage balancing of DC link capacitors, and
2. Eliminate low-frequency oscillation from neutral point voltage which arises due to a certain condition

As the number of levels increases in a Neutral Point Clamped converter, the complexity to balance DC link capacitor voltage increases as well. A number of PWM techniques and control methods are presented in different literature's which correlate problem in NPC. As a matter of fact, PWM techniques utilized to fire semiconductor devices in NPC are generally categorized into [35]:

1. Carrier Based PWM (CBPWM) which is mostly based on Sinusoidal PWM technique where sine wave is used as modulating signal and a triangle wave is used a carrier signal, and
2. Space Vector PWM (SVPWM)

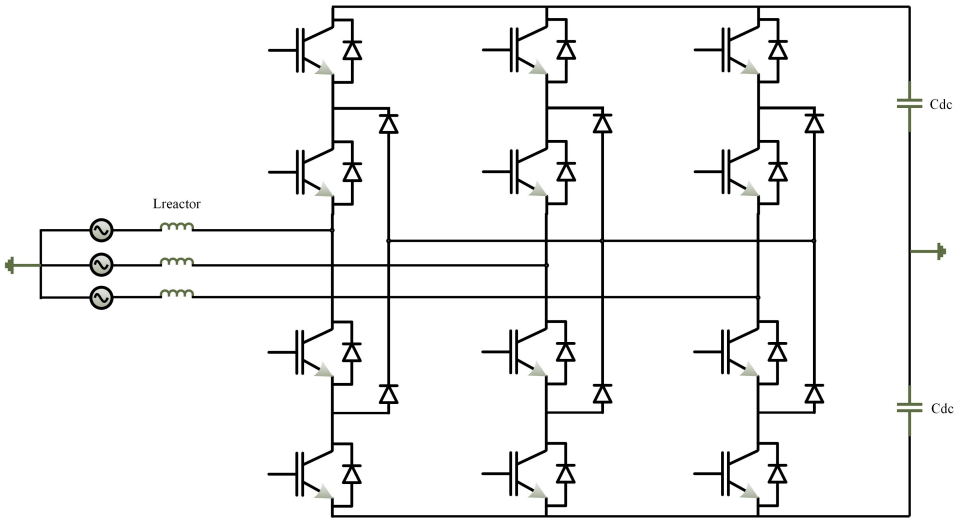


Figure 2.17: Three phase Neutral Point Clamped converter

Modular Multilevel Converter

The MMC is a series connection of identical elements called as MMC cells or sub-module. The sub-modules in MMC are the building block when connected in phase are termed as phase leg as shown in Figure 2.18 and Figure 2.19. The phase legs are divided into upper and lower arms connected at the common point of AC voltage terminal. Arm inductors are placed in series with the sub-modules to limit transient currents [36]. Each sub-modules has dc link capacitors which share dc link voltage hence no need arises to place a bulky dc link capacitors as used in H-bridge, NPC and FC [37, 38].

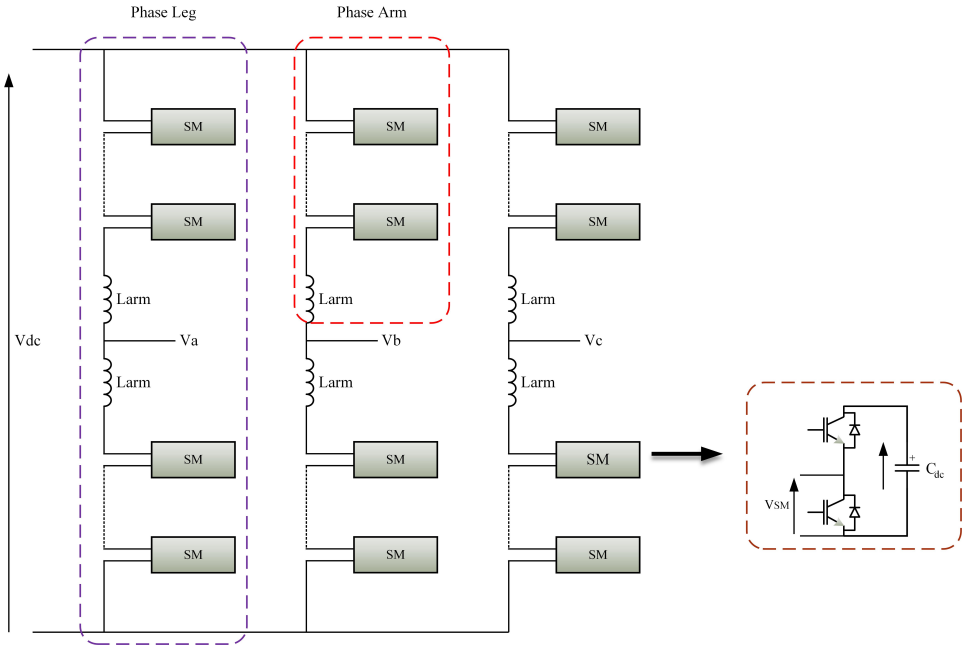


Figure 2.18: Modular Multilevel converter and Half Bridge sub-module

A different arrangement of sub-modules produces different configuration of MMC based on the purpose of implementation. The arrangements of cells produce different voltage levels at the sub-modules [39, 40]. But as the number of cells increases, capacitor voltage balancing become more complex and tough to maintain. It is found that half bridge sub-

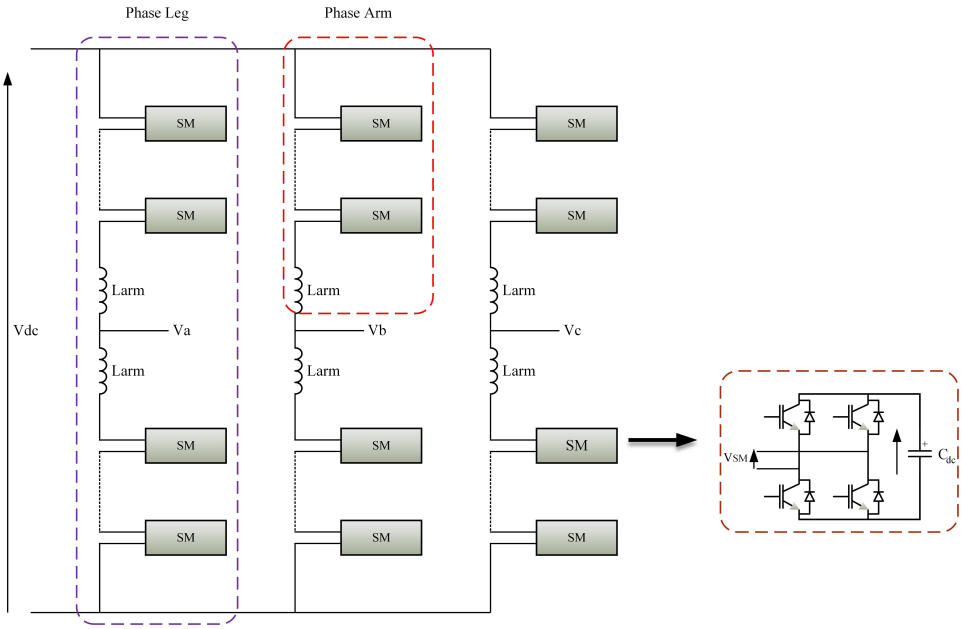


Figure 2.19: Modular Multilevel converter and Full Bridge sub-module

modules are more beneficial in terms of low power losses and capacitor balancing than a full bridge MMC when bidirectional power conversion required [41–44].

2.4 HVDC TRANSMISSION SYSTEM CONFIGURATION

Monopolar

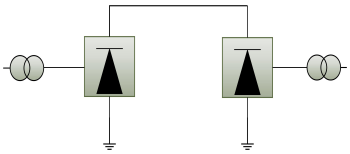


Figure 2.20: Monopole HVDC configuration.

In this configuration two converters are connected by single pole line either positive pole or negative pole as shown in Figure 2.20. There is only one conductor and ground or sea serves as a ground return path. A metallic return conductor can also be used as return path [45].

In the Monopolar link, two converters are placed at the end of each pole. Earthing of poles is done by earth electrodes placed about 15 to 55 km away from the respective terminal stations. But this link has several disadvantages because it uses earth as a return path. The monopolar link is not much in use nowadays.

Bipolar

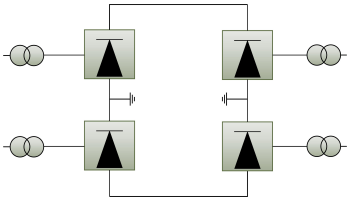


Figure 2.21: Bipole HVDC configuration.

This configuration is the most common HVDC configuration where the converters are connected by two conductors serving as positive and negative poles as shown in Figure 2.21. The bipolar configuration can be operated independently when both the neutrals are grounded. A bipolar HVDC has higher power transfer capability and carries positive and negative currents in both the poles under normal operating condition [45].

Since one conductor is at the positive polarity on earth and other is at negative polarity on earth. In bipolar link when one pole goes out of operation, the system may be changed to the monopolar mode with the ground return. Thus, the system continues to supply the half rated power.Bipolar links are most commonly used in all high power HVDC systems [46].

MultiTerminal

Three or more converter stations are connected together, present at different location either in series or parallel connection in multi-terminal HVDC system by the use of transmission lines or cables as shown in Figure 2.22. Multi-Terminal HVDC system are considered to be strong contender of future DC grids based on VSC [29, 47]. Future DC grids that are promoted mostly in Europe are based on clustering of renewable source of energy like offshore wind farms, solar plants backed by VSC based HVDC. This kind of multi-terminal DC grids is favourable in meeting future energy demands and harnessing the potentials of renewable sources available [48]. Although, many thyristor-based multi-terminal HVDC projects are already implemented and in use but have fewer benefits than VSC.

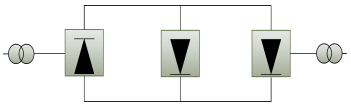


Figure 2.22: Multi Terminal HVDC configuration.

Back-to-Back

In a back to back HVDC, two system situated at the same point can be connected to each other without the need of cables or transmission lines with incompatible frequency, voltage level, short circuit power level as depicted in [45].



Figure 2.23: Back to Back HVDC configuration.

1. connect asynchronous high-voltage power systems with different frequencies,
2. stabilize weak AC links,
3. supply more active power where the AC system is at the limit of its short-circuit capability,
4. power-flow control within synchronous AC systems.

2.5 VSC-HVDC CONTROL

The conventional control system of VSC is a cascaded control of outer and inner control arranged sequentially in such a fashion that inner current controller runs faster than the outer controller. The outer controller can be chosen as either DC voltage control/Active Power control/Frequency control, where reference command/signal is fed into the outer controller depending upon the type of control implemented which generates d-axis reference current command for inner current control. While to generate the q-axis reference current, either reactive power control or AC voltage control can be chosen [49, 50].

Inner Current Control

The d-axis and q-axis reference current command generated from the outer control loop is fed into the inner controller. The inner controller consists of the actual measured value of d-axis and q-axis currents which are then compared with the references and passed through the Proportional Integral (PI) controller. Current decoupling and voltage feedforward control are also implemented to completely decouple the currents. The output is passed through the limiter and obtained as PWM firing pulses for semiconductor devices [51, 52].

Outer Current Control

The outer controller generates reference commands for d-axis and q-axis currents by passing the error signal through a PI controller and a limiter.

Negative Sequence Current Control

During voltage sag on the PCC side of VSC which leads to reduction of PCC voltage, conventional outer and inner control of VSC does not work at all. This is because of the fact that when an unbalanced voltage sag occurs like L-G fault on the PCC side then negative sequence components of current and voltage comes into existence which causes a ripple in power injected [53, 54]. This also leads to double line ripple in DC voltage. Therefore a negative sequence current controller is designed on grid side VSC.

The conventional vector current control is utilized in the form of inner current control that is based on the control of two independent current components, d-axis and q-axis in the dual Synchronous Reference Frame (SRF) to control simultaneously the positive and the negative sequence currents while the Phase Locked Loop (PLL) helps in the synchronization [51, 53].

Fault Ride through Control

Several controls have been proposed in literature for both AC side and DC side fault ride through capabilities associated with voltage source converter. In order to ride through DC side faults, one of the methods is to use DC circuit breaker with fast current interrupting capability while the other method is to use converter station with DC fault reverse blocking capability [49]. MMC with half bridge modules is one of the converter stations which have inherited quality of quenching DC side fault because of the absence of common capacitor. However, VSC should also be designed to withstand AC side faults by designing proper controls so that converters continue supplying power into the network maintaining DC voltage [55].

Zero Sequence Current Control

A line to ground fault on the DC side of converter puts the DC capacitor of the converter in an unbalanced condition which can only be balanced by discharging zero sequence component. On the other hand, a line to ground fault on the AC side leads to flow of zero sequence component of current between fault point and capacitor grounding. Therefore a DC link voltage balancing method is introduced based on zero sequence current controls [56, 57].

2.6 VSC-HVDC TRANSMISSION SYSTEM BEHAVIOR

The continuous increase in demand for electricity because of non-stop growth in population led to the expansion in mainland AC grid. Furthermore, a simple, radial AC grid structure has evolved into a highly complex and meshed grid with time. In addition to this, a push from the electricity market players in order to harness renewable energy technologies[5] and putting them into operation along with other conventional sources of energy has brought another dimension of complexity in the grid. The present-day AC grid now constitutes conventional power plants, for instance, coal, hydro, etc. as well as renewable power plants like wind, solar in transmission as well as sub transmission levels, AC transmission and distribution feeders, converters based HVDC and Distributed Generation resources.

[5] Effective utilization:

- Power supply to islands.
- Small isolated loads.
- Offshore generation and deep sea crossing.
- Connection to weak AC grids to provide stability.

2.6.1 *During Normal Condition*

One of the key feature of VSC-HVDC is independent control of active and reactive power injections at both converter terminals. This benefit of increased flexibility can be used by

the network operators to optimize power flows of the AC grid. In addition to this, fast dynamic properties of VSC-HVDC control actions can actually support the network during critical conditions, for instance, line outages or inter-area oscillations [58].

The synchronization of VSC-HVDC link to a grid is a very important phenomenon in order to transfer active and reactive power into and out of the grid [59]. The control action designed to operate VSC plays an important role in grid synchronization of VSC-HVDC links. Several control methods have been proposed in many literature's out of which power angle control, vector-current control and power synchronization control are widely discussed. Power angle control although simple suffers from the demerits of the absence of current limiting capability. On the contrary, vector-current control possesses the current limiting capability by virtue of its fast inner current loop. PLL is utilized to synchronize the converter with the grid. Unfortunately, this control suffers when the network is very weak. Therefore, to counter this problem, a power synchronization control is discussed in literature where it does not require any PLL to synchronize with the grid and effective to connect weak ac grid and islands.

2.6.2 *During Abnormal Condition*

Nevertheless, integration of VSC-HVDC with the ac grid requires a lot more attention and even more, when offshore wind farms are connected through VSC-HVDC due to their feature to be uncertain and random. In general, the electrical collection system for offshore wind parks is divided into the offshore and onshore collection system. Since the collection system and the main grid are not synchronously coupled, the VSC do not contribute significantly to short-circuit currents in the main grid. Besides this, economic and environmental feasibility studies have revealed that VSC-HVDC is 20% costlier than its AC counterpart for a distance less than 90 km between onshore converter station and offshore wind turbines. Nonetheless, future investments in offshore wind VSC-HVDC system altogether with existing 25 GW wind parks is going to create transmission congestion in mainland Europe [19, 46].

The most frequent grid disturbances are voltage sags, which are either balanced or unbalanced voltage sags. When the reduction in voltage magnitude is equal for all the three phases then a balanced voltage sag takes place and vice-versa for an unbalanced voltage sag. During a balanced voltage sag in the AC grid, the voltage at the PCC reduces due to which VSC reaches its maximum allowed current, which in turn causes the voltage of the dc bus to rise due to excess power input to the bus[6] [55].

On the other hand, unbalanced voltage sag due to asymmetrical faults in the ac grid causes a ripple in the power injected into the ac grid due to the presence of negative sequence components in the voltage. This causes a second harmonic ripple in the power flow as well as a ripple in dc voltage [53, 54]. Besides this, VSC's have an inherent property of fault current limitation beyond which they will saturate. This saturation limits of VSC depend upon the thermal limit of switches that are set to carry 20% more than the nominal current. During a short circuit in the AC grid, the VSC can only supply 1.2 p.u. of fault current, thus restricting the fault level and affecting the grid protection system. Moreover, the converter responses to such faults on the grid side are entirely different from the synchronous generators which form an integral part of the power system.

[6] Characteristics:

- Low Short Circuit Ratio.
- High Impedance.
- Low Inertia problems.
- Nominal short-circuit currents.
- Absence of sub-transient and transient duration.
- Fault currents depend upon the control system.

2.7 CONCLUSIONS

This chapter concludes that the HVDC technology has proven its mettle/worth in today's fast-changing power transfer scenario. It has broken the barrier of long distance transmission of power more economically than its AC counterpart. The advent of thyristor technology removed the earlier version of mercury-arc valve based HVDC system. At present,

the VSC technology is mostly adopted converter technology for high voltage transmission. Many projects have already been implemented in the past, present and in the coming future on VSC technology, out of which, MMC based technology is given more priority due to numerous advantages over other two-level, neutral-point clamped etc. converters. It causes fewer harmonics, less number of filters, fewer losses and high efficiency that is why it is utilized in offshore and onshore grid integration.

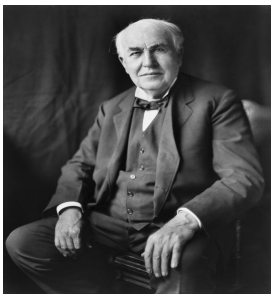
Based on the discussion in this chapter regarding the behavior of VSC-HVDC during the fault, its impact has been studied on the distance protection of transmission line in Chapter 4 when the VSC is supplying power into the ac grid. The grid codes are also considered during the event of a fault, which has been discussed later on in Chapter 4. The protection of networks is discussed in the next Chapter 3. Furthermore, an experimental setup has been established using RTDS to analyze the effect of VSC.

3

DISTANCE PROTECTION & ITS CHALLENGES

Contents

3.1	Grid Protection	24
3.2	Challenges Faced by Distance Protection	26
3.3	Why To Assess Distance Protection	26
3.4	Effects of VSC Based Technologies on Distance Protection	27
3.5	Numerous Solutions of Problem	31
3.6	Conclusions	33



Thomas Alva Edison (1847-1931) was an American inventor and businessman, who has been described as America's greatest inventor. He developed many devices that greatly influenced life around the world, including the phonograph, the motion picture camera, and the long-lasting, practical electric light bulb. Dubbed "The Wizard of Menlo Park", he was one of the first inventors to apply the principles of mass production and large-scale teamwork to the process of invention, and because of that, he is often credited with the creation of the first industrial research laboratory.

Chapter 3 presented the state-of-the-art about the HVDC technology and its growth from the past 125 years. The technology has seen tremendous growth and potential over the years re-surging from the ashes of war of electricity. Nowadays, renewable sources of energy are being implemented in mass scale at a distant location away from the load centers to reduce the carbon emission. This done by using long distance favourable HVDC technology especially in case of offshore wind platforms.

However, an important point has been discussed in the Chapter 3 regarding the fault behavior of VSC that is entirely different from the SG. This difference in the fault characteristics is also caused by the grid codes of HVDC operation, which affects the protective relaying performance. Therefore, this chapter presents a state-of-the-art on the subject of protective relaying and their responses to faults. Moreover, a comparison is presented between the early and modern grid scenarios in continuation of distance protection and its impacts due to the VSC-HVDC.

This chapter is based on the following publication:

M. M. Alam, H. Leite, and A. S. Carvalho, "Investigating Distance Relay Behaviour on an EHV AC Lines Connected with Voltage Source Converter Based HVDC," in Proc. CIGRE Symp., Across Borders-HVDC Systems And Market Integration, Lund, Sweden, 2015.

3.1 GRID PROTECTION

3.1.1 *General Background*

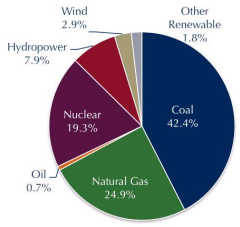


Figure 3.1: Production of Electricity worldwide from different sources [9].

Electric energy is needed by the human being in order to perform a number of day to day tasks. The power stations are the hub where a bulk amount of electric energy is produced by a number of sources, for instance, Thermal, Hydro, Nuclear and more recently Photo-voltaic, Wind, shown in Figure 3.1. The electrical energy produced in powerhouses are transported to consumers like industries, factories, households through the use of networks and network components. The overall structure which includes electrical power stations, generators, transmission and distribution lines, transformers, circuit breakers, loads is termed as "Power System" [60].

Power System quite often is exposed to short circuits, major as well as minor disturbances. The large magnitude of fault current associated with short circuits can even damage equipment's like generators, transformers, loads unless they are protected by relays and circuit breakers to isolate such short circuit faults from the power system. When a fault occurs in an element of a power system, protective devices must operate as quickly as possible, within 2 or 3 cycles to isolate the fault and maintain the overall healthiness of system. If a fault is not cleared within the required time, this can lead to heavy damage to the system and its components. Therefore, a need for power system protective devices arises [61].

One of the main objectives of Transmission System Operator is to maintain continuity of Electricity supply which can be achieved by the installation of protective relaying devices and circuit breakers. The protective relaying devices are responsible for the correct identification of fault types, accurate estimation of fault location and selective operation of circuit breakers in order to eliminate the faulty elements from the power system and minimize the adverse impact of fault [62].

3.1.2 *Changing Grid Scenario: A Highlight*

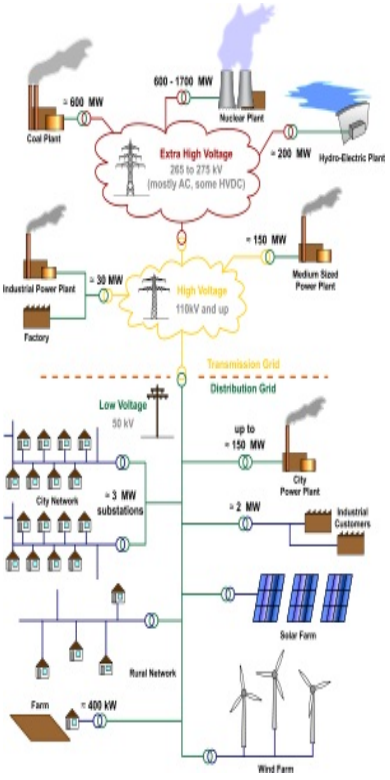


Figure 3.2: General layout of electricity networks [9].

The continuous increase in demand for electricity because of non-stop growth in population led to an expansion in mainland AC grid. Furthermore, a simple, radial AC grid structure has evolved into a highly complex and meshed grid with time. In addition to this, a push from the electricity market players in order to harness renewable energy technologies and putting them into operation along with other conventional sources of energy has brought another dimension of complexity in the grid. The present-day AC grid now constitutes conventional power plants, for instance, coal, hydro, etc. as well as renewable power plants like wind, solar in transmission as well as sub transmission levels, AC transmission and distribution feeders, converters based HVDC and Distributed Generation (DG) resources, as shown in Figure 3.2.

Nowadays AC grid, which constitutes thousands of kilometers of transmission lines (UHV/EHV/HV) also accommodates High Voltage DC technology so as to transfer bulk amount of electrical power over a very long distances offering many other benefits including interconnecting major electrical grids serving as tie-lines and supplying offshore wind energy to onshore AC grid.

Transmission lines are often exposed to major as well as minor disturbances. The fault current associated with major disturbances can jeopardize the power system unless protected by the relays and circuit breakers [61]. These protective relays are responsible for the correct detection and isolation of faults to minimize the damage [62]. Therefore, transmission lines are always protected by the relays, for instance, line differential protection, directional overcurrent protection, directional earth fault and distance protection (pilot and non- pilot), which are selective, robust and sensitive in nature [63].

3.1.3 *Protection Methodologies*

Differential Protection

Differential protection is also known as Merz-Price scheme. This kind of protection scheme is utilized to protect unit feeder, generators, transformers or any apparatus. The protection is provided by the efficient use of pilot communication channels to exchange local information and status of both the ends of protected region [63] (see Figure 3.3). Differential protection separates an internal fault from an external fault. It is categorized into two kinds:

- Current balance method
- Voltage opposed method

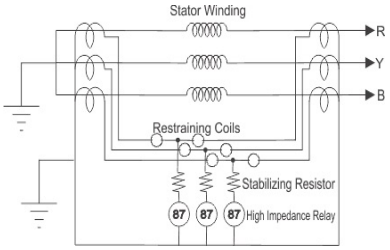


Figure 3.3: Differential protection scheme. [10].

Overcurrent Protection

When a short circuit takes place which results in a large magnitude of short circuit current, for instance, short circuit near the terminals of generator and/or transformer, the fault current can be utilized as basis for selectivity for a current magnitude device, such as fuse or an instantaneous relay or trip device to isolate such faults. This kind of protective devices is called as over-current protection. Different time-current grading schemes are used as over-current protection, for instance [63] (see Figure 3.4)

- Definite Time-Current Relays,
- Inverse Time-Current Relays, and
- Inverse Definite Time-Current Relays

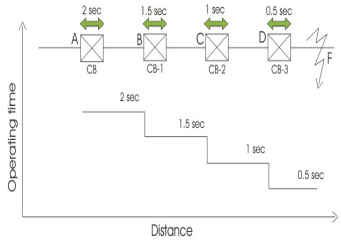


Figure 3.4: Overcurrent protection scheme. [10].

Tele-Protection

A tele protection scheme or communication assisted protection helps duplicate protection, for instance, distance, directional overcurrent, current differential and directional earth fault to provide 100 percent transmission line coverage. There are three kinds of communication assisted tripping schemes [13]:

- Direct Transfer Trip (DTT) - In this scheme, the remote relay trips instantaneously upon receipt of a signal from the local relay without verification. This happens during remote breaker failure, blind spot tripping, transformer ended feeder and when a weak source is connected at one end of a line, the remote relay may not see a fault due to high infeed from a strong source.
- Permissive Transfer Trip (PTT) - This scheme differs from acDTT that local relay sends a permissive signal when it detects a fault in its forward reach, the remote relay, upon receipt of signal verifies whether the fault lies in its zone 2. When correct verification, the remote relay zone 2 timer must be bypassed to trip to internal fault otherwise zone 2 timer will be initiated for an external fault. and
- Directional Comparison Blocking (DCB) - The local relay will send two blocking signal through redundant paths, one serving as a duplicate path, to block remote relay from tripping for any external fault which remote relay tripping element can detect.

Distance Protection

Protective relays especially the distance protection form the backbone of the transmission line protection due to its simple operating principle. It provides high speed instantaneous primary protection (tele protection scheme with 100 percent feeder coverage and total fault clearance time of less than 6 cycles) and slow speed backup protection (pilot as well as non-pilot scheme) [13, 63]. A distance protection utilizes measured local voltage and current at the relay location in order to compute the apparent impedance to a fault [64].

In doing so, a distance relay fulfills its objective to decide whether a fault is internal or external to the protected feeder zones based on its reach setting. That is why; a distance relay is associated with the different zones of protection, which essentially demarcate the speed of operation of fault isolation. With an instantaneous zone 1 protection that covers 80 to 90 percent of the transmission line and subsequent time delayed, and coordinated zone 2 and zone 3 protection (refer Figure 3.5), a distance relay has been able to win the hearts of protection engineers over the years.

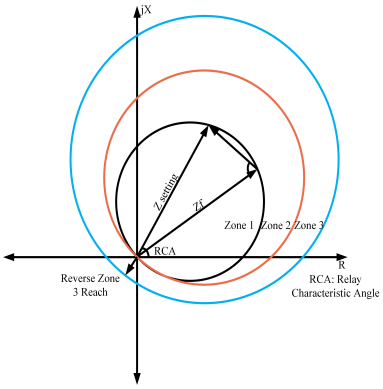


Figure 3.5: Mho distance scheme.

3.2 CHALLENGES FACED BY DISTANCE PROTECTION

Although the distance protection is widely chosen to protect transmission lines because of their simple operating principle, they too are associated with many challenges. The main problems of distance protection employed upon UHV/EHV/HV transmission lines are [65]:

1. Faults with high arc resistance lead to inaccurate computation of fault distance between the relay point and resistive fault that will cause incorrect tripping of relay if the relay characteristics are not designed properly to cover such arc resistances [66–68].

2. A sudden load/generation imbalance may edge to power swing phenomena ultimately pushing load impedance to pass through the characteristics and activating relay trip. Therefore, to avoid such problems Power Swing Blocking (PSB) schemes are implemented [69, 70].

3. Transmission lines carrying power close to or more than their limit causes load encroachment, which the relay observes as load impedance approaching zone 3 or zone 2 region.

   Many incorrect tripping and blackout in the past took place because of load encroachment and it has been proposed to utilities to verify the presence of overreaching zone 3 element [61, 71].

4. Presence of power electronic converters in transmission levels in the form of FACTS to regulate power flow and voltage of line are affecting the performance of distance relays by changing line impedance and load currents [72].

5. Power electronic converters directly interfaced to transmission lines, which serve as an intermediary between the source and the load, such as in DFIG, VSC-HVDC, IIDG, decouples the generation from the load, reduces inertia and decreases the fault level and short circuit capacity, finally affects the relay performance.

3.3 WHY TO ASSESS DISTANCE PROTECTION

Transmission lines are usually protected by distance protection which is robust in nature, providing different zones of protection so as to identify and eliminate faults in necessary time. Distance protection based on communication serve as primary protection and any aberration in its behavior is unacceptable. For proper operation of power system without

putting it in jeopardy, the primary protection scheme must be all time reliable. However, one of the main concern of power system protection engineer is correct tripping of the distance protection during the fault even if the network is expanding into complexity.

However, the distance protection comes with major drawbacks of overreach and tripping during overload and power swing, which consequently led to major blackouts, such as USA 2003 (see Figure 3.6) and Europe 2006 [73]. Furthermore, the present day power system is evolving from what it was a decade ago by the replacement of conventional SG with the renewable energy sources and VSC based HVDC connection.



Figure 3.6: USA eastern coast blackout in 2003.

This change in the power system is leading to a low or very low Short Circuit Ratio (SCR) because of increase in the network impedance as the point of connection between the ac system and VSC is remotely located [51]. In addition to this, the system inertia is also reducing when a considerable amount of power is supplied by the VSC station [43, 74, 75], and any load-generation imbalance causes frequency excursion and line overloading leading to the malfunction of the distance relay.

Nowadays, VSC-HVDC is utilized for the grid integration of far offshore Wind Power Plant (WPP) and interconnection of WPPs to each other or to multiple infeed points leading to Multi-Terminal HVDC (MTDC) by the efficient use of multilevel converter technologies [45, 76], as shown in Figure 3.7.

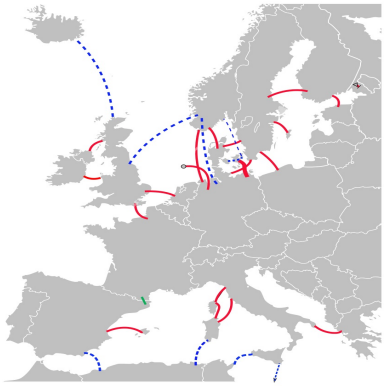


Figure 3.7: HVDC links in European mainland.

Furthermore, one of the important benefits of VSC based HVDC or MTDC is that the onshore VSC's can provide limited reactive current during faults as per the NC decided by the Transmission System Operator (TSO) to support the network voltage [77–79]. Since this reactive current injection is the positive sequence current and the presence of negative sequence current in addition to the positive sequence current limits the amount of available positive sequence reactive current during an unbalanced fault [80, 81].

Moreover, the negative sequence current causes an extra stress on the Power Electronic Switch (PES) due to large unbalanced ac fault currents [82]. Consequently, the negative sequence current can be suppressed to zero to give room to the positive sequence reactive current support from the VSC and to de-stress the PES by keeping the ac currents balanced under unbalanced grid conditions. Additionally, the grid code does not stipulate any specific requirement regarding the negative sequence current supplied by the VSC during the fault [80, 83].

This eventually modifies the overall fault behaviour of VSC's compared to SG in terms of both magnitude and waveform [84]. Therefore, the network operator is facing challenges in handling the grid protection systems due to these exclusive behaviours of VSC, which affect the current and voltage measured by the protective relays during the fault leading to an inaccurate computation of the apparent impedance and malfunction of the distance relay [84–86]. Hence, it is highly relevant to look into the performance of the distance relays in the presence of VSC-HVDC system.

3.4 EFFECTS OF VSC BASED TECHNOLOGIES ON DISTANCE PROTECTION

3.4.1 *Effects of FACTS devices*

One of the important power electronic component widely utilized in power system is FACTS devices. FACTS devices either series or shunt or combination of both are effectively implemented to achieve system controllability and improve system performance. There are different kinds of FACTS devices presently installed in power system depending upon the objective of installation, for instance, SVC, Static Synchronous Compensator (STATCOM), UPFC, TCSC, Static Synchronous Series Capacitors (SSSC), Interline Power Flow Controller (IPFC) etc. All of these FACTS devices are Series compensators and/or shunt compensators. The location of their installation depends upon the purpose, for instance, to obtain voltage



Figure 3.8: STATCOM installed in Cerro Navia, Chile by ABB [8].

control and power flow control, shunt compensators are utilized (look Figure 3.8) [35, 87, 88].

FACTS devices are currently employed for various application [89]:

1. Improve power transfer capability of a transmission line,
2. Improve transient state stability as well as steady-state stability limits,
3. Damp power system oscillation,
4. Improve voltage stability,
5. Reduce sub-synchronous resonance, and
6. Improve HVDC links

However, the introduction of FACTS devices produces some other undesirable effects upon the protection coordination of distance relays. The FACTS devices which consist of fully controlled power electronic switches, for instance, Gate Turn-off Thyristors, Insulated Gate Bipolar Transistors etc. and its associated fast control actions cause rapid changes in primary system parameters e.g. line impedance, line voltage, load currents during normal conditions as well as fault situation.

Effects of SVC & STATCOM

Nevertheless, the impact of shunt-FACTS devices (refer Figure 3.9) leads to an error in apparent impedance seen by the distance relay (under reaching/overreaching), transient impact leads to a delayed operation, wrong phase selection by the commercial relay. The distance relay with communication perform better than stand-alone relay but it fails to provide correct operation for all types of faults [90–92].



Figure 3.9: SVC PLUS VSC technology by Siemens [11].

The work in [93] specifies that distance protection in presence of STATCOM connected at the midpoint of transmission lines is not the best protection scheme. Even communication aided scheme is unable to provide effective protection to lines compensated by midpoint FACTS devices. The adverse effects are in terms of apparent impedance seen, phase selection and operating times. Moreover, when single-pole tripping is required, distance protection either stand-alone or communication aided will not perform correctly. The operation of STATCOM during fault condition where voltage dips to a low value and STATCOM tries to maintain the voltage of midpoint transmission line by boosting reactive power into the network causes an error in apparent impedance seen by the relay [94].

Effects of UPFC & IPFC

The study in [95] presents analytically, the apparent impedance seen by the distance relay in presence of Unified Power Flow Controller, as shown in Figure 3.10, first and then illustrate its adverse effects. Later on, simulations results in MATLAB show the impact of UPFC when it is operated as STATCOM and UPFC. The adverse impact is due to the injection/absorption of reactive power by STATCOM which results in under reaching/overreaching of distance relays [31]. The impact of UPFC is more pronounced for UPFC than operated as STATCOM due to the fact that former operates as both SSSC and STATCOM [96].

The multiline FACTS devices such as IPFC, Generalized Interline Power Flow Controller (GIPFC), Generalized Unified Power Flow Controller (GUPFC) which are used to control power flows of multi-lines simultaneously have a remarkable impact on the operation of distance relays which is shown in [97, 98]. The work concludes that GUPFC, when installed in the middle of the line, causes the trip characteristics to split into two parts and it also causes the relay to underreach. However, the impact of IPFC is less pronounced than GUPFC

due to the absence of shunt controller in IPFC [92, 99]. The work in [100] also highlights that detailed modeling of devices produces more realistic results. provide correct operation for all types of faults [90–92].

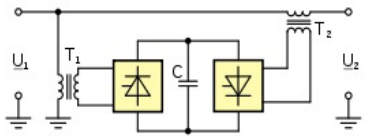


Figure 3.10: Typical UPFC layout.

Effects of TCSC

A complete analysis of impact of TCSC upon distance protection by modeling transient behavior of TCSC during disturbance in PSCAD/EMTDC and validating the results by performing a closed loop test with a commercial relay is done in [101, 102]. The paper modeled different modes of operation of TCSC in normal and disturbance situation to visualize the impact of transit of TCSC upon the relay. The shift in modes of operation of TCSC is considerably in the range of operating time of distance relay. TCSC dynamics have a serious impact not only on the compensated lines but also on the adjacent lines protection scheme [103, 104].

Similar studies regarding the impact of TCSC dynamics on communication aided distance protection, for instance, Directional Comparison Blocking (DCB), Permissive Overreaching Transfer Trip (POTT) and Directional Comparison Unblocking (DCUB) is presented in [105, 106]. The work comprehensively analyzed comparison distance scheme for TCSC and presented solutions for maloperation as well. The problems associated with TCSC are forward and reverse overreach, directional integrity issues and pilot distance malfunctions. A modified pilot communication scheme with a new protection logic to improve the directional integrity and eliminate under reach/overreach is also presented [107].

Another analysis in [107] highlights the issue of directional relaying in the presence of TCSC. The capacitive mode of operation of TCSC causes problems in current and voltage inversion which ultimately leads to directional complications in relaying. A single classifier based on the phase angle of sequence components is inadequate to provide direction of fault for faults in TCSC compensated lines. A novel three positive sequence voltage based classifier is combined with the voting method to obtain the direction of fault. The method is tested is for voltage and current inversion.

The work in [102] analyzes equivalent dynamic power frequency impedance of TCSC and its integrated impedance, which is the ratio of sum of the voltage phasors across the two ends of transmission lines and the sum of current phasors at one end of the same line. This integrated impedance is utilized to decide whether there is a fault inside or outside of protected line section or not. The scheme is tested on 750 kV China Northwest Grid. The integrated impedance is a capacitive value of line impedance with real and imaginary parts.

3.4.2 *Effects of Distributed Generation*

Besides all of the above, the renewable energy power plants at the distribution level, more appropriately, inverter interfaced distributed generation, is deemed to be leaving a negative footprint on distribution level protection as well. It has been discussed in [108]-[109] that fault current contribution from IIDG is highly dependent on their control systems, that may lead to fast or slow fault transients, eventually jeopardizing the protective schemes. Furthermore, the emphasis has been given on the fault current limitation, which can go a maximum up to 2 p.u., responsible for protection insensitivity. However, the affected protection schemes are overcurrent protection rather than distance protection in distribution level. But, it perspicuously forms the opinion that controllers for power electronics based converters actually intervenes the functioning of protective devices.

[110] discussed that addition of DG at distribution level along with inverter actually results in loss of protection sensitivity, loss of protection coordination and out of zone tripping, ultimately leading to incorrect operation of the relay. Similarly, [111] presents that

as a power electronic based converter, the fault behavior of an IIDG is largely determined by its control system. The fault current characteristics observed has no sub-transient and transient period rather it settles to steady state instantly giving a different fault behavior altogether.

3.4.3 *Effects of DFIG*

Studies have also been performed on the impact of Low Voltage Ride Through (LVRT) capability of wind generators as a new grid code, in order to maintain wind farm connection during voltage dips, on distance protection [112]. It is reported that the crowbar circuit activation during any short circuit fault in a DFIG, transforms it into a Squirrel Cage Induction Generator (SCIG), which, in turn, demands reactive power from the grid, aggravating voltage dip and resulting in protection mis-coordination of the distance relays [112]. Furthermore, the conventional reach setting of distance relays for bus differential protection does not hold sufficient to protect the grid, equipped with DFIG, because of LVRT control [113]. A distance relaying problem in a Belgian grid topology is studied, which concludes that the distance relay is not performing correctly in case of three phase faults due to small currents resulting from the loss of excitation. Moreover, varying parameters such as the crowbar resistance and the wind turbine loading have a significant impact on the relay performances as well. Nonetheless, control is lost during a grid fault very close to the generator and the fault current is determined by the machine characteristics. A lower crowbar resistance causes an unpredictable detection behavior resulting in a backward detection and an early, incorrect fault removal [113].



Figure 3.11: Wind farms [9].

Technical rule for connecting wind farm into power grid suggests that the capacity of wind farm should be smaller than the 15% of the short circuit capacity of the connecting point. Comparing with the power system, the capacity of a wind farm is much small. Because the wiring type of the main transformer is Ynd, the three-phase current detected by the distance relay is almost the same in phase and amplitude when a ground fault occurs. The protection relays detect the weak power source characteristic of the wind farm and block the distance protection functions [114]-[115].

Moreover, wind farm conditions, such as varying wind farm loading level, voltage level and source impedance also affect the trip boundaries of distance relay significantly. A fixed reach setting of distance protection is not suitable for lines connecting DFIG based wind farm [116].

3.4.4 *Effects of VSC*

when a three-phase short circuit on a transmission line, as shown in Figure 3.12, near to a PCC, is scrutinized closely and thoroughly in a grid-connected offshore wind HVDC system, the backup distance protection fails to operate because of interference of reactive power control strategy of the converter station [85]-[86]. Moreover, a reach setting calculation method based on bus impedance matrix has been proposed to accurately determine apparent impedance seen by the distance relay in presence of offshore wind VSC-HVDC system.

In addition to this, FRT schemes proposed in grid codes for wind generators based on Full-Scale Converter (FSC), to maintain the security of supply to network during faults, in fact, impede with the distance protection [86]. It has been revealed in [86]-[117] that the converter control strategy not only affects the zone 1 fault detection, it also influences detection of faults lying in zone 2 with in-between infeed. The relay under reaches as well as overreaches for the different fault situation.

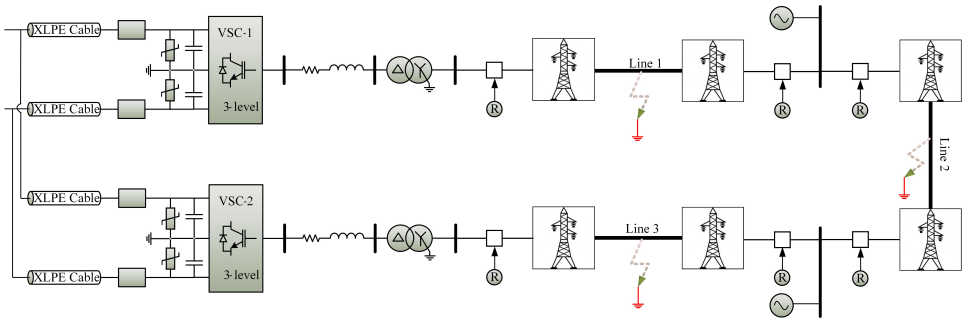


Figure 3.12: Study system with VSC

3.5 NUMEROUS SOLUTIONS OF PROBLEM

As seen above, the distance protection (both pilot and non-pilot) are experiencing problems, in terms of overreaching, under reaching, directional integrity, trip boundaries modification, fault classification, reduced fault levels, when operated to protect lines at transmission and sub-transmission levels in presence of Induction wind generators, FACTS devices, Inverter Interfaced Distributed Generation, and VSC's. The problems are grave and critical in nature, which if not countered, is going to pose serious challenges to the security of the entire network. Fortunately, studies have been done to address these challenges faced by the distance protection and solutions have been floated in many pieces of literature.

3.5.1 *Modified Pilot Distance Protection*

Series compensation of transmission lines produces aberration in the operation of distance protection (refer Figure 3.13), but several solutions have also been presented such as in [89, 105] where communication aided distance protection scheme utilizing comparison principle are modified to perform well in the vent of faults. Directional comparison systems can be classified as:

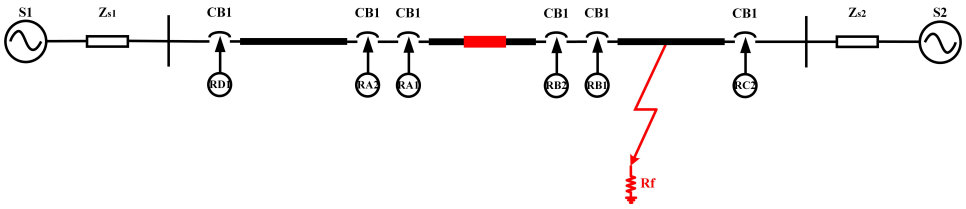


Figure 3.13: Study system with TCSC

- Based on DCB: This method requires two distance zones: a fast starter zone which sends blocking signal to remote end when the fault is in reverse direction and a directional overreaching zone in the forward direction, which inhibits the blocking signal during faults in the forward direction, and initiates tripping if no blocking signal from the remote end is present.

  For faults on the main line involving series compensation, the blocking signal will not be sent by both RA1 and RB2, hence tripping command is issued after the tripping delay time. When the fault is on the line Line3, RA1 overreaches but does not trip due to receiving the blocking signal from RB2. The same situation applies for the faults in line Line1. The adjacent lines cannot be protected by this method, since for some cases when the fault is on the main line, the directional integrity concerns by RA2 causes the fault to be seen in Zone 1 by this relay so blocking signal will not be sent to the remote relay RD1, which has already seen the fault in Zone 1 due

to its overreaching effect. Nonoperating of RA1 in Zone I is a pre-requisite for the operation of RA2 in the forward reach, and also its operation triggers sending the blocking signal to RD1, as does the operation of RA2 in Zone 3 [105], as shown in Figure 3.14.

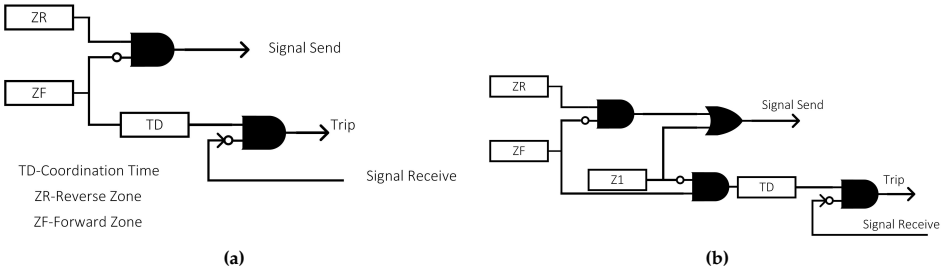


Figure 3.14: Blocking Trip Logic for (a) RD1, RC2, RA1, RB2 (b) RA2, RB1

- Based on POTT: When the relays at both ends of the line detect a fault in the overreaching zone and send each other a release signal. Usually zone1 with 80% to 90% coverage of the line trips unconditionally, while zone 2, which extends beyond the remote end trips instantaneously upon receipt of permissive trip signal. POTT with unconditional zone 1 trip cannot be used here, so the only possibility is releasing an overreaching distance zone by the received signal. In this method, sending the signal is triggered by the forward overreaching zone.

  For the main line, POTT can be used successfully. For the faults on the main line, both end line relays see the fault in their overreaching zone and send transfer trip signal to each other, so the only delay is channel time. For faults on the adjacent line, the overreaching of RA1 or RB2 can be compensated by the refraining of the remote relay to send the trip signal. The permissive trip signal transfer is dependent on the nonoperation of the main line relays RA1 and RB2, so when the RA2 or RB1 relays incorrectly see the fault in the forward direction, false tripping is avoided. The proposed scheme can be used for both main line and the adjacent lines [89, 105], as presented in Figure 3.15.

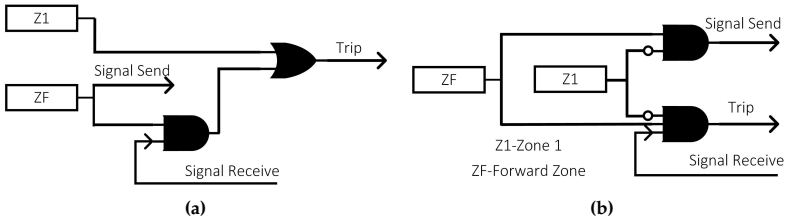


Figure 3.15: Blocking Trip Logic for (a) RD1, RC2, RA1, RB2 (b) RA2, RB1

  In the case of lines connecting to wind farms, a modified POTT scheme is proposed with a minimal bandwidth requirement of communication channel [118] because of incorrect measurement of impedance. The relay detects the fault not based on the impedance but based on the current wave shape.

- Based on Directional Comparison Unblocking (DCUB): The blocking procedure has the disadvantage that during un-faulted system operation no signal is transmitted. The communication channel is therefore not monitored. The unblocking technique does not have this disadvantage; moreover, this technique is also somewhat faster. During internal faults, the signal is changed to a permissive signal similar to the POTT method. This implies that no trip delay is required to wait for an eventual

block signal. This procedure offers a good compromise of both high dependability (channel not required to trip) and high security (blocking is continuous), as shown in Figure 3.16.

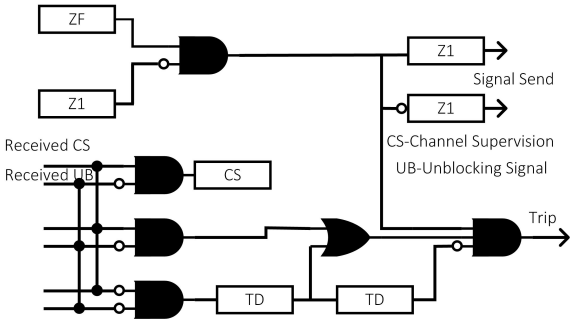


Figure 3.16: Unblocking Trip Logic

3.5.2 *Adaptive Distance Relay*

A trip boundary modification based adaptive reach setting is discussed in [98] for FACTS compensated transmission lines. In [119] power output and voltage fluctuation of wind farm affects trip boundary of distance relay dominantly. To mitigate this effect, adaptive setting method is discussed for distance relay. For this, the relay requires bus voltage, current and number of generating unit's information at an instant. Reference [120] also presents a new method to calculate zone 2 distance relay setting so as to provide better line coverage through adaptive relay reach.

3.6 CONCLUSIONS

This chapter discussed the changes taking place in the modern day electrical grid scenario from fossil fuel dependent electrical sources to renewable energy dependent sources. This changes in the grid along with the addition of distributed resources is taking place not only at the transmission level but also at the distribution level, which is affecting the conventional behavior of the grid during disturbances. Furthermore, power electronics based converters utilized to improve transmission capacity is known to be interacting with the grid protection systems like FACTS, IIDG etc.

The chapter presented a glimpse of the state-of-the-art about the challenges faced by the distance protection due to changing grid scenario and raised a critical question about its performance. Moreover, Chapter 3 formed the basis for the investigation of distance protection of lines connected to VSC-HVDC in Chapter 4. The proven and accepted the impact of DFIG, DG, FACTS devices on the distance relaying scheme formed the basis of investigation with the hypotheses that VSC-HVDC can also influence distance relays.

Part II

PROBLEM SHOWCASE, SIMULATION & EXPERIMENTAL SETUP

Part II of the thesis consists of Chapter 4 and Chapter 5, which elaborates a distance relay, its working principle, investigation of the problem in the operation of distance relay, mathematical formulation of the apparent impedance, Electromagnetic Transient Program based simulation and real-time simulation using RTDS of the study system.

Chapter 4 mainly covers the distance relay, its history of development, its working principle, types of operational characteristics, the grid code for HVDC connections, more specifically about the reactive current injection during the fault depending on the slope of current vs voltage curve, the negative sequence current suppression strategy, the VSC current limitation scheme and the apparent impedance seen by the distance relay. Firstly, an analytical approach is adopted to derive the apparent impedance during a single line to ground fault and a line-line fault assuming a VSC-HVDC system is connected to one end of a transmission line. The study system is then modeled and simulated on PSCAD, an Electromagnetic Transient Program (EMTP) based simulation package. Later on, the mathematical expression of apparent impedance is compared with the results obtained from the simulation.

Chapter 5 presents a real-time closed-loop simulation of a commercial distance relay using the RTDS and signal amplifier. Firstly, the rationale behind a real-time closed-loop simulation is explained and later on the modeling approach of study system with VSC-HVDC is discussed in detail. The chapter then examines the relay behavior in a closed-loop setup for different fault conditions and further compares it with the simulation results.

4

IMPACT OF VSC-HVDC ON DISTANCE PROTECTION

Contents

4.1 History of Distance Relays 38
4.2 Distance Relays 39
4.3 Mho Function 41
4.4 Quadrilateral Function 44
4.5 Apparent Impedance Analysis 45
4.6 Modern Network Codes for HVDC connection 51
4.7 Current Limitation Strategies 54
4.8 Study System 56
4.9 Simulation Results and Discussion 59
4.10 Conclusions 69



Michael Faraday (1791-1867) was an English scientist who contributed to the study of electromagnetism and electrochemistry. His main discoveries include the principles underlying electromagnetic induction, diamagnetism and electrolysis. It was by his research on the magnetic field around a conductor carrying a direct current that Faraday established the basis for the concept of the electromagnetic field in physics.

The previous Chapter 2 discusses about the HVDC technology, recent developments, configuration and its behavior during normal as well as abnormal condition. Moreover, Chapter 3 focuses on the comparison between the characteristics of the early grid without the renewable and the modern grid with the renewable source of energy. It addresses an important question about the performance of grid protection system in the modern grid scenario. This chapter is an extension of previous Chapter 3 with the main focus on the distance protection.

This chapter discusses about the impact of VSC-HVDC system on the operation of distance protection of transmission lines. Firstly, the modeling of Mho and quadrilateral characteristics based distance relays are presented. Later on, the apparent impedance seen by the distance protection is evaluated analytically for symmetrical and asymmetrical faults. Furthermore, the chapter presents the performance of distance relay during faults VSC-HVDC system embedded into the network using PSCAD/EMTDC simulation platform.

This chapter is based on the following publication:

M. M. Alam, H. Leite, J. Liang, and A. da Silva Carvalho, "Effects of VSC based HVDC system on distance protection of transmission lines," International Journal of Electrical Power & Energy Systems, vol. 92, pp. 245-260, 11// 2017.

4.1 HISTORY OF DISTANCE RELAYS

Initial Days of Distance Relays



Figure 4.1: H. E. Tudor - founder of distance relay.

At the beginning of 20th century, Distance relays were introduced for the first time in order to overcome the problems of high clearing times and operation with radial lines and ring circuits associated with over-current or directional over-current relays [12]. In 1904, Krämer, chr., F&G proposed a protection device with the basic structure of distance relay. Later on, distance relay based on balanced beam mechanism was developed, which led to the birth of impedance circle, typical for electromechanical relays. At that time, the relays were used to protect the radial lines with single infeed. Therefore, Wecken, W. proposed to use ring operation and voltage drop relays to protect the ring in 1912. However, a directional element wasn't used to determine the direction of the relay. One year later, Meyer, G.J. developed current and voltage dependent relay for ring operation. The directionality was not taken into consideration for ring or parallel line operation because only one circuit breaker was used in the substations at that time [12].

Industrial Installation of Early Distance Relays

After 4 years, Westinghouse El. & Mfg. Co. developed a relay whose operating time was dependent on the ratio $R/X = Z$ (refer Figure 4.2). This device was equipped with a directional element. In addition to this, Meyer, G.J. proposed another relay called N-relay (Netzschutz for protection system in German) in 1918[7]. Later on, a combined voltage and current relay using the resistance principle was proposed in 1920 by Ackerman, P. and implemented in 1921 by Cansfield Electrical Works, Toronto. This was the first time that a step distance characteristic was used. The same technique was then used by Siemens, Westinghouse Co., and General Electric Co. The Westinghouse Co. launched their distance relays in 1923 while BBC and Siemens & Halske produced it in 1928 [12].

[7]Prior to this, the distance relay was installed on 4 kV network of Karlsruhe (Germany) in 1913.

The utilities "Thueringenwerk" and "Kraftwerk Thueringen AG" decided to use Siemens and Westinghouse Relays for their 50 kV network in 1927[8]. The name impedance protection was proposed because the operating time was dependent upon the voltage and current ratio. However, Biermans proposed the name "distance protection" as the operating time was dependent upon the length of the line. In those days, three relays were used per feeder as they were single pole devices and the operating times of those relays were also very high. The operating times were in a range of 0.5 to 1s due to the limitations of the breakers (short circuit currents were not that high in those days).

[8]The first substation in Europe that used Westinghouse relays was the double-circuit line from power station "Hedwigschacht" (Seestadl) to Prague in 1925.

Arc Resistance Coverage in Early Design

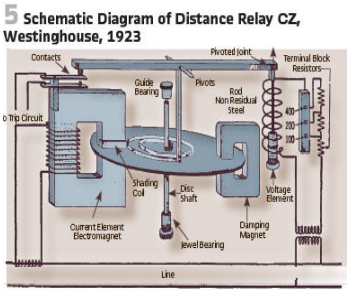


Figure 4.2: Schematic diagram of distance relay cz, Westinghouse, 1923 [12].

In 1915, a method to switch the voltage from phase-phase to phase-ground was developed that helped in detecting double line to ground fault. Distance relays provided by BBC and impedance relays of Siemens in 1928 had similar designs. The first distance relays that used the reactance principle were developed by BBC and S&H in 1928. Unlike impedance relays, they were used for super-grid applications due to the possibility of high arc resistances in such applications. Reactance relays were the preferred choice for the high voltage lines in order to eliminate the impacts of arc resistance [12].

Wide Acceptance and Rapid Development

Many patents were granted between 1908 to 1920 to inventors like Kuhlmann, K.; Wecken, W.; Chrichton, L.N.; Meyer, G.J., Ackermann, P. and Biermanns, J. Kesselring, Fr. Unlike

these developments, distance protection met with criticism in magazines and at conferences at that time. The idea was new for utilities although the distrust and skepticism decreased with increasing numbers of successful short-circuit and double earth-fault operational trials[9]. Unfortunately, the impact of the arc resistance was not considered at that time, which was later investigated by German utility "Bayernwerke" in 1926/27. After a series of successful tests with 30 relays, a Norwegian interconnection Samkjöringen decided to use distance relays to protect their networks in 1936.

[9]For instance, Ackermann, P. performed short circuit tests on Shawinig Water and Power Co.'s 50 kV transmission network in 1920 and found that the overcurrent failed to trip due to low short circuit currents.

Electromechanical and Solid State Distance Relays

Line distance relays were introduced in 1940's which represented the state-of-the-art in electromechanical relays. In 1950, distance relays type RYZKC was introduced and was last manufactured in 1985. Later on, in 1970, RAZOG was introduced which was world's first line distance relay with quadrilateral characteristics (see Figure 4.3). This was a switched scheme static relay suitable for protecting overhead lines and cables with an operating time of 21 ms, as given in Table 4.1. A switched scheme relay type RAZOA was implemented in 1976, which was a successful line distance relay for sub-transmission level.

Relay Type	Speed (0-60% reach)	Speed (60-100% reach)	Directional Sensitivity	Close-in Fault selection
Analog Relay-Full scheme	25-35 ms	$\leqslant$ 45 ms	Acceptable	Acceptable
Analog Relay-Switched scheme	30-50 ms	$\leqslant$ 65 ms	Acceptable	Special measure applied
Solid State Relay	25-35 ms	$\leqslant$ 45 ms	Better	Good
Numerical Relay (conventional)	20-30 ms	$\leqslant$ 35 ms	Best	Good
Numerical Relay (high speed)	15-30 ms	$\leqslant$ 35 ms	Best	Good

Table 4.1: Operating Times for Various Types of Distance Relays [13]

4.2 DISTANCE RELAYS

Since the beginning of 20th century, the design, efficiency, and performance of distance relays have continuously improved. It has progressed from the electro-mechanical type through analog type up to digital type [121]. The distance protection is a non-unit scheme as signals are fetched from one end of the protected line. The protection is arranged in overlapping zones so that no part of the system is left unprotected. The relay measures current and voltage at the point of relay location and calculates apparent impedance based on this measured current and voltage. The relay operates if the calculated apparent impedance falls inside the relay's zones of protection settings. This can be utilized to protect both phase and ground faults by the use of relay characteristics on R-X plane [63].



Figure 4.3: RAZOG distance relay. (source: www.pacw.org)

Zones of Step Distance Protection

The apparent impedance is an indication of distance to a fault by which a distance element locate the zone of fault. The operating time of step distance relay depends upon the zones of protection. In general, a step distance protection provides back up protection to communication assisted distance protection. The main feature of step distance protection scheme is different zones of protection, as shown in Figure 4.4. The different zones of protection are provided in order to prevent the relay from over reach and any possible mal operation. The zones of protection are also overlapping with each other so that none of the transmission line section is left unprotected [73][10].

[10]http://www.pes-psrc.org/Reports

1. Zone 1 covers 80-90% length of transmission line and relay operates instantaneously,

[11] Zone 2, is set to protect the remainder of the line plus an adequate margin. Zone 2 relays need to be time delayed to coordinate with relays at the remote bus. Typical time delays are in the order of 15–30 cycles although, depending on the application, they may be set faster or slower. The minimum setting for the Zone 2 that ensures full coverage of the line, with safety margin, is usually 120% of the line impedance [122].

2. Zone 2[11] covers 100% length of transmission line plus minimum 20% of shortest line connected to remote terminal and relay operates after a time delay of 15-30 cycles,
3. Zone 3 protects 200% of line length and relay operates after a time delay of 50 cycles,
4. Reverse Zone 3 provides backup to the lines behind a relay by reversing zone 3 coverage upto 50%.

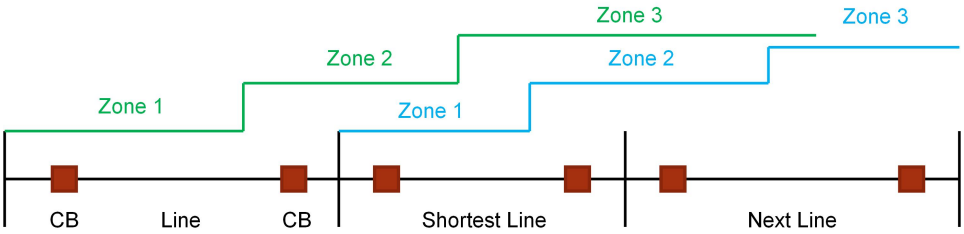


Figure 4.4: Zones of distance protection.

Distance Protection Types and Characteristics

The distance relay characteristics are defined based on their settings decided by the positive and zero sequence impedance of the transmission line. In general, a "distance relay" is sometimes called by the name of "impedance relay" although it is one of the type of distance relay. The basic distance relay characteristics are as follows:



Figure 4.5: Line distance protection relay SIPROTEC 7SA86 - a product of Siemens [11].

1. *Impedance*: The impedance characteristic on R-X plane is a circle with its center at the origin, as depicted in Figure 4.6(a). The relay operates when the measured impedance falls within the circle. It is independent of the phase angle between the voltage and current supplied to it, which leads to operation in all the four quadrants. Therefore, in order to utilize this relay, a separate directional sensing element is necessary [123].
2. *Mho*: The characteristic of this type of relay is also a circle passing through the origin. The relay operates when the apparent impedance falls within the Mho circle by determining the angle between the operating quantity $(IZ - V)$ and the polarizing quantity (IZ_f), as shown in Figure 4.6(b) [121].
3. *Offset Mho*: Figure 4.6(c) shows the characteristic of an offset Mho relay, which is a circle similar to Mho characteristic but shifted including the origin. An offset Mho relay provides a better coverage for close-in faults in the forward and reverse directions. It can be utilized along with a directional element for tripping or time delayed if not intended to operate during the fault [121].
4. *Reactance*: The reactance relay characteristic is a straight line parallel to X-axis (Resistance axis) (refer Figure 4.6(d)) and measures only the reactive component of the apparent impedance. This element should be supervised by another function to ensure directionality and prevent wrong tripping due to load encroachment [24].
5. *Quadrilateral*: The quadrilateral characteristic is obtained by combining the reactance and directional element together along with two resistive blinders, as unveiled in Figure 4.6(e) [122].
6. *Lenticular*: This distance relay characteristic is important to prevent tripping during load encroachment by reducing the area of Mho characteristic in the form of lens as can be seen in Figure 4.6(f) [24].

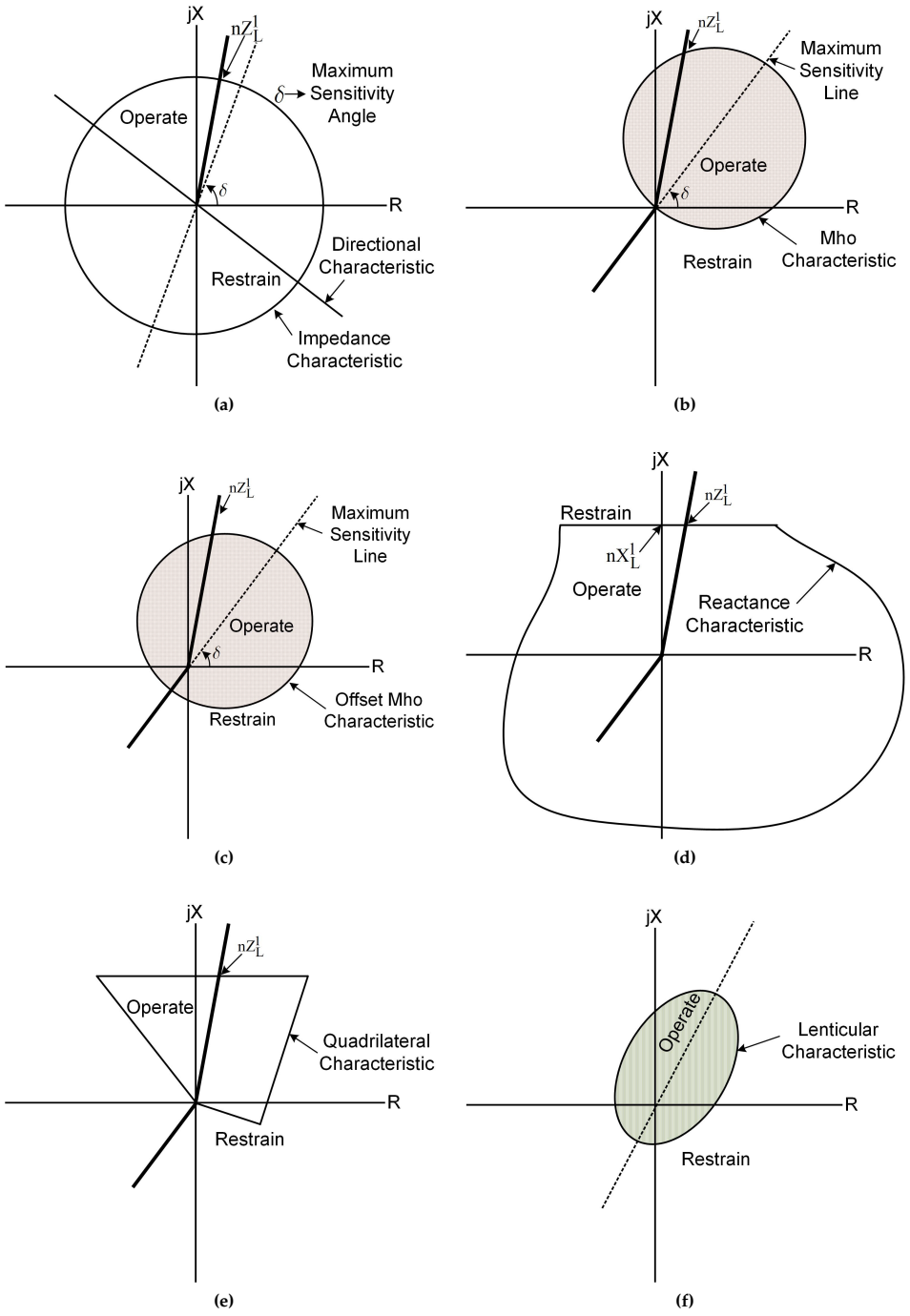


Figure 4.6: (a) Impedance characteristic. (b) Mho characteristic. (c) Offset Mho characteristic. (d) Reactance characteristic. (e) Quadrilateral characteristic (f) Lenticular characteristic.

4.3 MHO FUNCTION

Mho Function Operation Principle

A simple Mho function measures the current and the voltage at the relay location and compares the angle between the operating quantity and the polarizing quantity to determine the apparent impedance falls within the Mho characteristic. Equation (4.1), (4.2), and (4.3) present that the Mho function will operate if the angle is less than or equal to 90^0 that

means the apparent impedance falls within the characteristic otherwise the function will not operate if the angle is greater than 90^0 [124]. Inside Mho circle (Operate):

$$-90^0 < arg(\frac{dZ}{Z}) < 90^0 \tag{4.1}$$

On the Mho circle (At reach point):

$$arg(\frac{dZ}{Z}) = \pm 90^0 \tag{4.2}$$

Outside Mho circle (Restrain):

$$90^0 < arg(\frac{dZ}{Z}) < -90^0 \tag{4.3}$$

The polarizing quantity for a simple Mho function[12] is equal to the fault voltage ($V = I * Z_f$), therefore the function is said to be self-polarized and has the simple characteristic shown in Figure 4.7(a). However, when a Mho function is polarized by a voltage different than the fault voltage then the function is called as cross-polarized.

[12]For the balance point fault, $IZ - V$ is zero, therefore no operation occurs, which is expected. For an internal fault, $IZ - V$ and V are in phase, therefore the function operates as expected. For the external fault, operation does not occur because $IZ - V$ and V are 180^0 out of phase.

Mho Function Polarization Technique

A Mho relay can be polarized using quantities other than the fault voltage ($V = I * Z_f$) for phase and ground functions out of which some of them are mentioned here [121]:

1. *Self Polarized:* When phase-A voltage (V_a) for phase-A function and phase-A to phase-B voltage (V_{ab}) for the phase AB function is utilized as polarizing quantity.
2. *Positive Sequence Voltage Polarized:* When (V_a^1) for phase-A function and (V_{ab}^1) for the phase AB function is utilized as polarizing quantity.
3. *Quadrature Voltage Polarized:* When (V_{bc}) shifted and leading 90^0 for phase-A function is utilized as polarizing quantity.
4. *Median Voltage Polarized:* When Midpoint of (V_{bc}) to (V_a) for phase-A function is utilized as polarizing quantity.
5. *Leading Phase Polarized:* When (V_c) shifted and leading 240^0 for phase-A function is utilized as polarizing quantity.

Nonetheless, the cross-polarization still leads to circular characteristics but causes swivel based on system conditions shown in Figure 4.7(b). The reasons of swivel for the cross-polarized Mho function depends upon the source impedance directly behind the function, the amount and the direction of load-flow [125]. This is to accommodate more arc resistance in comparison to a self-polarized function[13].

[13]For a fault right at the relay location, the voltage will be very small (approaching zero for a bolted fault), and a self-polarized Mho function may not operate for such a fault, whereas a cross-polarized function will, except for a three-phase fault. For a three-phase close-in fault, all three voltages will be very small, therefore operation of any of the cross-polarized functions will be jeopardized because there will be very little, or no voltage available to develop the polarizing quantity. To overcome this deficiency, memory is added to the polarizing circuits.

Mho Function Design Methodology

For a generic phase angle comparator ground distance element the operating quantity is given by (4.4) as [68]:

$$I * Z - V = (I^a + K * I^0) * Z^G - V^a \tag{4.4}$$

I^a Phase-A current [A]

V^a Phase-A voltage [V]

Z^G Mho relay reach setting [Ω]

I^o Zero sequence current [A]

K Zero sequence compensation factor

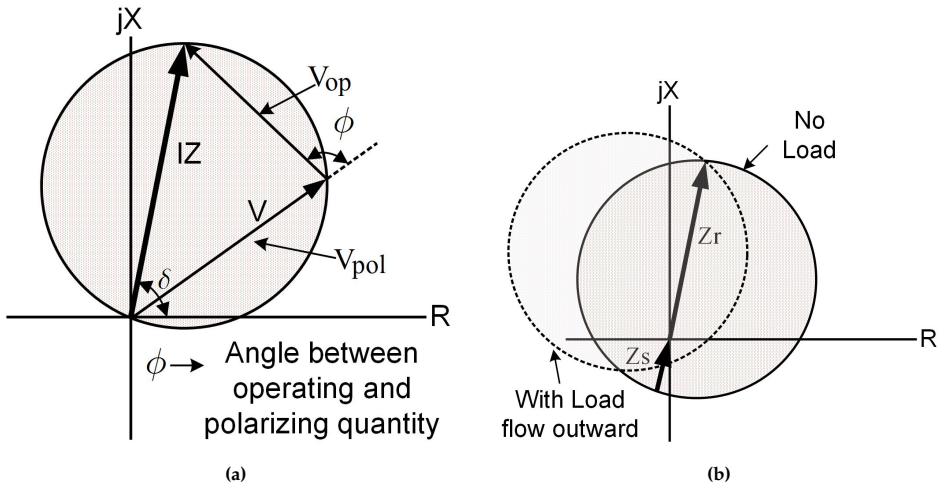


Figure 4.7: (a) Simple Mho function. (b) Variable Mho phase distance function.

Distance protection system is used in medium and long lines with different zones of protection acting as a primary as well as backup protection [63]. The three zones of protection[14] are as follows:

[14] Protective zones:

- Zone 1: 80-85% of line length in order to avoid over-reach tripping effect.
- Zone 2: 100% of protected line and 20-50% of the next shortest line.
- Zone 3: 100% of protected line and 120% of the next line.
- Length of line = 100 km
- Positive sequence impedance of the line = $0.009 + j0.2643\ \Omega/km$

Zone 1 Reach

Zone 1 reach setting = $80 * (0.009 + j0.2643)\ \Omega$
Zone 1 reach setting = $21.16\angle 88.05\ \Omega$

Zone 2 Reach

Zone 2 reach setting = 100% of transmission line length + 20% of adjacent line
Zone 2 reach setting = $100 * (0.009 + j0.2643) + 20 * (0.009 + j0.2643)\ \Omega$
Zone 2 reach setting = $31.74\angle 88.05\ \Omega$

Zone 3 Reach

Zone 3 reach setting = 100% of transmission line + 120% of adjacent line
Zone 3 reach setting = $100 * (0.009 + j0.2643) + 120 * (0.009 + j0.2643)\ \Omega$
Zone 3 reach setting = $58.19\angle 88.05\ \Omega$

Arc Resistance Coverage

Generally, single line to ground faults (AG, BG, and CG) are associated with high fault resistances (R_{arc}). On the other hand, phase-to-phase faults are less susceptible to high fault resistance values (R_{arc}) [126]. Furthermore, short lines are much more affected by higher fault resistances that means the protective relaying with the maximum fault detecting capabilities should be used to detect these kind of faults shown in Figure 4.8(a) and (b)[15].

Out of many components that contribute to fault resistance, the tower footing resistance is a critical parameter. The practical values of footing resistance range from 5 to 20 Ω and in rocky surface the resistance can go up to 100 Ω [67]. Ideally, the smaller is the footing resistance, the better will be the ground fault detection performance. For the majority of transmission line protection, Mho function performed unarguably well. Nonetheless, the

[15] Short circuits on a transmission line are associated with additional impedance or more specifically resistance either in the form of arc or foreign object. If this resistance is negligible then the angle of apparent impedance is equal to line angle otherwise there exits a difference between them.

challenge is to protect short lines as they have low impedance values, which lies far away from the expected maximum load.

The problem arises when the tower footing resistance is close to the line impedance, the Mho element will face difficulty in detecting ground fault even without the presence of arc resistance [67]. Quadrilateral ground distance element can provide a larger margin to

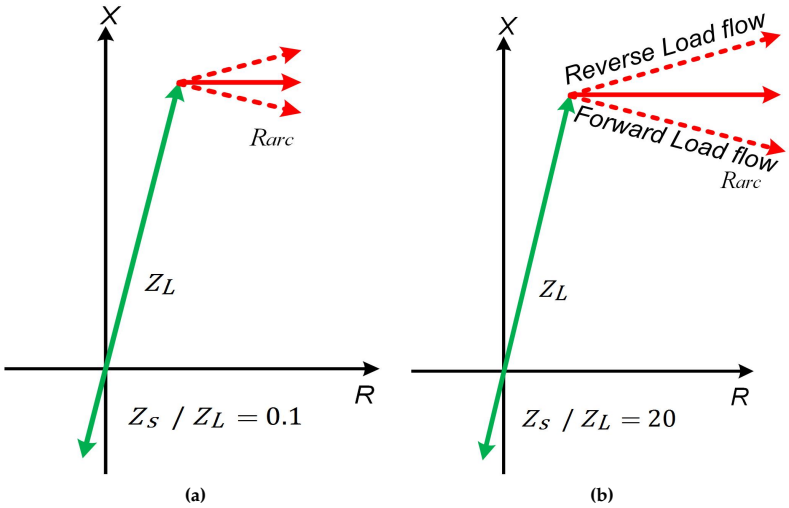


Figure 4.8: Effect of source-to-line ratio $\frac{Z_s}{Z_L}$ (a) $\frac{Z_s}{Z_L} = 20$ (b) $\frac{Z_s}{Z_L} = 0.1$.

accommodate R_{arc}. They are better suited to protect short lines however, with some limitations in the amount of R_{arc} that they can accommodate. Nevertheless, their performance is better than the Mho function [67].

4.4 QUADRILATERAL FUNCTION

Operation Principle

A quadrilateral function is a form of reactance function with a directional supervision as it is inherently non-directional in nature. The reason for the use or selection of a quadrilateral or a reactance function is to enhance the apparent resistive reach in comparison to the conventional self-polarized Mho function [96]. On the other hand, a quadrilateral function also suffers from the problem of overreach for faults with arc resistance if not designed properly. Moreover, some quadrilateral function may not work properly for faults at the relay location[16].

[16]For a fault right at the relay location, the voltage will be very small (approaching zero for a bolted fault), and a quadrilateral function may not operate for such a fault.

Quadrilateral Function Modeling Technique

The measured voltage and current are digitized by using sampling rate of 96 kHz, and they are digitally filtered by using a second-order Butterworth low-pass filter at a cutoff frequency of 200 Hz, and using an anti-aliasing filter [72]. Later on, the resultant is down-sampled to 16 samples per cycle of base frequency before decomposing into fundamental phasor quantities by using online Fast Fourier Transform (FFT). Furthermore, the fundamental components of current and voltage are decomposed into sequence components, after which they are passed through a distance protection block to calculate the apparent impedance.

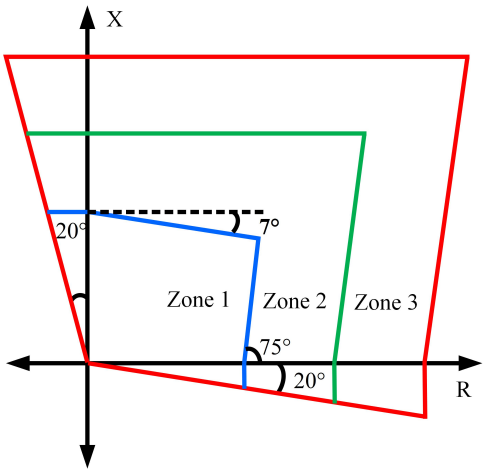


Figure 4.9: Quadrilateral characteristics of distance protection.

Quadrilateral Relay Design

To visualize the problems pragmatically, a commercially available numerical distance relay with quadrilateral characteristics [127], where the resistance and reactance elements of the quadrilateral are adjusted accordingly for a 400 kV EHV transmission line [128] is modeled. The settings of the relay are outlined in the Appendix A. The instantaneous zone 1 of the relay is designed to reach 80%[17] of the line with no operating time delay, zone 2 can reach 120% of the line with an operating time of 250 ms, and zone 3 can reach 200% of the line with an operating time of 1000 ms.

As can be seen from Figure 4.9, zone 1 of the reactance element is given a tilt of 7^0 in order to surpass the steady state overreach problem because of resistive faults. Furthermore, the characteristic possess elements extending into the 3rd and 4th quadrant of R-X plane with an equal slope of 20^0 to bestow directionality and correct operation during close-in high resistance faults. Besides this, a resistance element with a slope of 75^0 is added to the distance relay protecting from incorrect tripping due to load encroachment [64].

[17]The distance relay is never designed to give complete coverage to the line due to over-reaching issue that may jeopardize the protection.

4.5 APPARENT IMPEDANCE ANALYSIS

Apparent Impedance During Normal & Abnormal Condition

As explained in Section 4.2, the distance elements have to be configured and selected in such a way that they will provide sufficient resistive reach and correct fault detection for all the faults lying inside a dedicated zone of protection and no operation for any kind of external faults [129]. This correct fault detection and sufficient impedance coverage completely rely on the transmission line positive Z_L^1 and zero sequence impedance Z_L^0 calculated either by using LCP[18] or fetched from the line commissioning records [130]. The line impedance parameters are utilized in setting the distance relays properly. Incorrect transmission line impedance parameters can lead to wrong relay reach settings, which can lead to distance relay misoperations forcing the power system into risk [131]. The positive sequence impedance of the line Z_L^1 is used directly for relay settings and zero sequence impedance of the line Z_L^0 is utilized to obtain zero-sequence compensation factor k for faults involving the ground as (4.5):

$$k = \frac{Z_L^0 - Z_L^1}{3 * Z_L^1} \tag{4.5}$$

[18]The program calculates the electrical parameters of overhead lines using Carson's formula for single pole lines. It calculates the impedance parameters for most conductors and designed to give engineers a straightforward way to check parameters for existing lines.

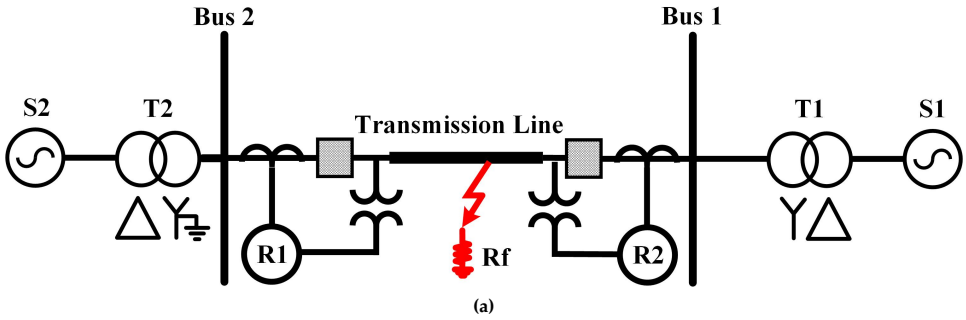


Figure 4.10: A simple power system with a transmission line and two sources.

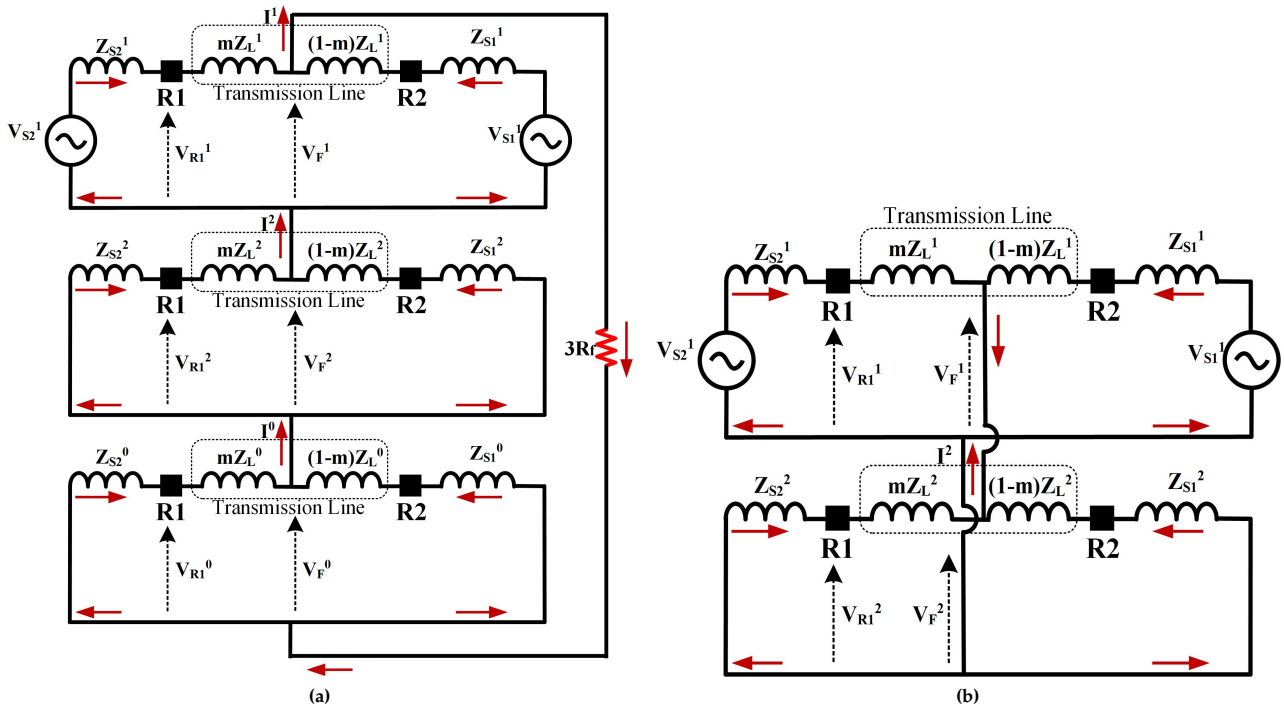


Figure 4.11: (a) Sequence network diagram of the power system with a single line to ground fault. (b) Sequence network diagram of the power system for a line-to-line fault.



Figure 4.12: A typical layout and devices in a substation. (source: www.primeraeng.com)

The distance relay operates by measuring the positive sequence apparent impedance, which is a time varying quantity depending upon the state of power system such as line loading, fault, power swing etc [131]. During a normal operation, the apparent impedance seen by the distance function lies far away from its designed reach [132]. On the other hand, the apparent impedance measured by the relay during a fault, line overloading or power swing comes very close to the relay reach or enters into the operating characteristics sending a trip or pickup signal.

Apparent Impedance

For a phase-to-ground fault on a transmission line shown in Figure 4.10, distance elements operate when the apparent impedance ($Z_{app}^{\phi G}$) becomes less than the zone reach setting. The sequence network diagram for the fault is highlighted in Figure 4.11. The apparent impedance is given by (4.6):

$$Z_{app}^{\phi G} = \frac{V_\phi}{I_\phi + k * (3 * I_0)} \tag{4.6}$$

where is k is the zero sequence compensation factor as explained before, I_0 is the zero sequence current, V_ϕ and I_ϕ are the measured voltage and current of the faulted phase, respectively. On the other hand, the apparent impedance ($Z_{app}^{\phi\phi}$) for a phase-to-phase fault is given by:

$$Z_{app}^{\phi\phi} = \frac{V_{\phi 1} - V_{\phi 2}}{I_{\phi 1} - I_{\phi 2}} \tag{4.7}$$

Apparent Impedance with Embedded VSC-HVDC

Figure 4.14(a) presents a simplified arrangement of a power system consisting of a VSC like Figure 4.13 connected to the grid through a delta-star winding transformer and a transmission line. The distance relay R1 and R2 located at both the ends of the transmission line protects the line. Figure 4.15(a) and (b) illustrate the sequence networks of the power system arrangement for a single line to ground and phase-to-phase faults. Figure 4.15(c) and (d) also present the sequence network of the power system during phase-to-phase-to-ground and three phase faults. The VSC is represented as a controlled current source both in the positive and negative sequence networks because the inner current control is the main control that tracks the current references coming from the outer control [133]. From the sequence networks, the sequence component of the voltage, V_{R1}^x at the relay location *R1* can be derived for the different fault types. Henceforth, (4.8) gives the positive sequence component of the voltage at the fault location, V_F^1, from the relay R1 as follows.

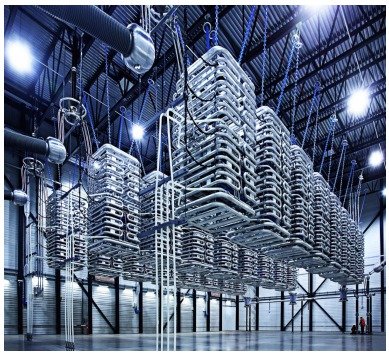
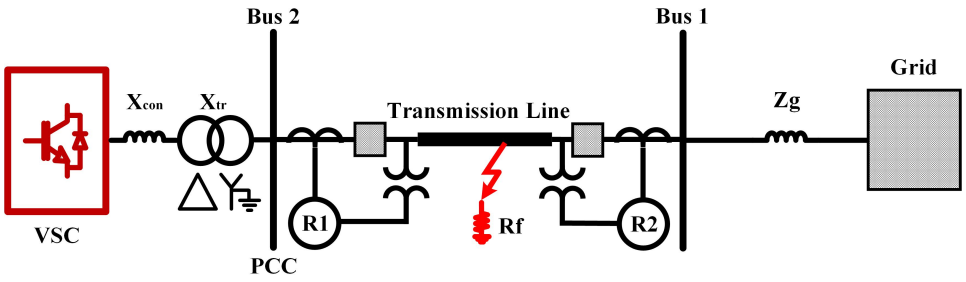


Figure 4.13: A typical layout of a converter station. [8]



(a)

Figure 4.14: (a) Simplified power system with VSC-connected line and a fault.

Where

Z_L^x	Seq. impedance of the line	Z_g^x	Seq. Thev. grid impedance
X_{tr}^x	Seq. reactance of transformer	X_{con}^x	Seq. reactance of converter reactor
I_{con}^x	Converter seq. fault current	I^x	Seq. fault current
I_g^x	Grid seq. fault current	I_{tr}^0	Transformer zero seq. current
V_g^1	Pos. seq. Thev. grid voltage	V_F^x	Fault point voltage on the line
V_{R1}^x	Seq. voltage at *R1*	m	Length of the transmission line
R_f	Fault resistance	x	0, 1, 2
I_{R1}^{abc}	Phase currents through *R1*	V_{R1}^{abc}	Phase voltages at *R1*
I_{R1}^x	Seq. currents through *R1*	I_g^{abc}	Phase currents through *R2*

$$V_F^1 = V_{R1}^1 - I_{con}^1(mZ_L^1) \tag{4.8}$$

With reference to the negative sequence network[19] of the simplified power system for any unbalanced faults, as depicted in Figure 4.15(a), (b), and (c), the negative sequence voltage V_F^2 at the fault location is given by (4.9), which is similar to (4.8) except the superscript. Therefore,

$$V_F^2 = V_{R1}^2 - I_{con}^2(mZ_L^2) \tag{4.9}$$

[19]Fortescue theorem states that an unbalanced three phase system can be decomposed into symmetrical components of positive, negative and zero sequence components.

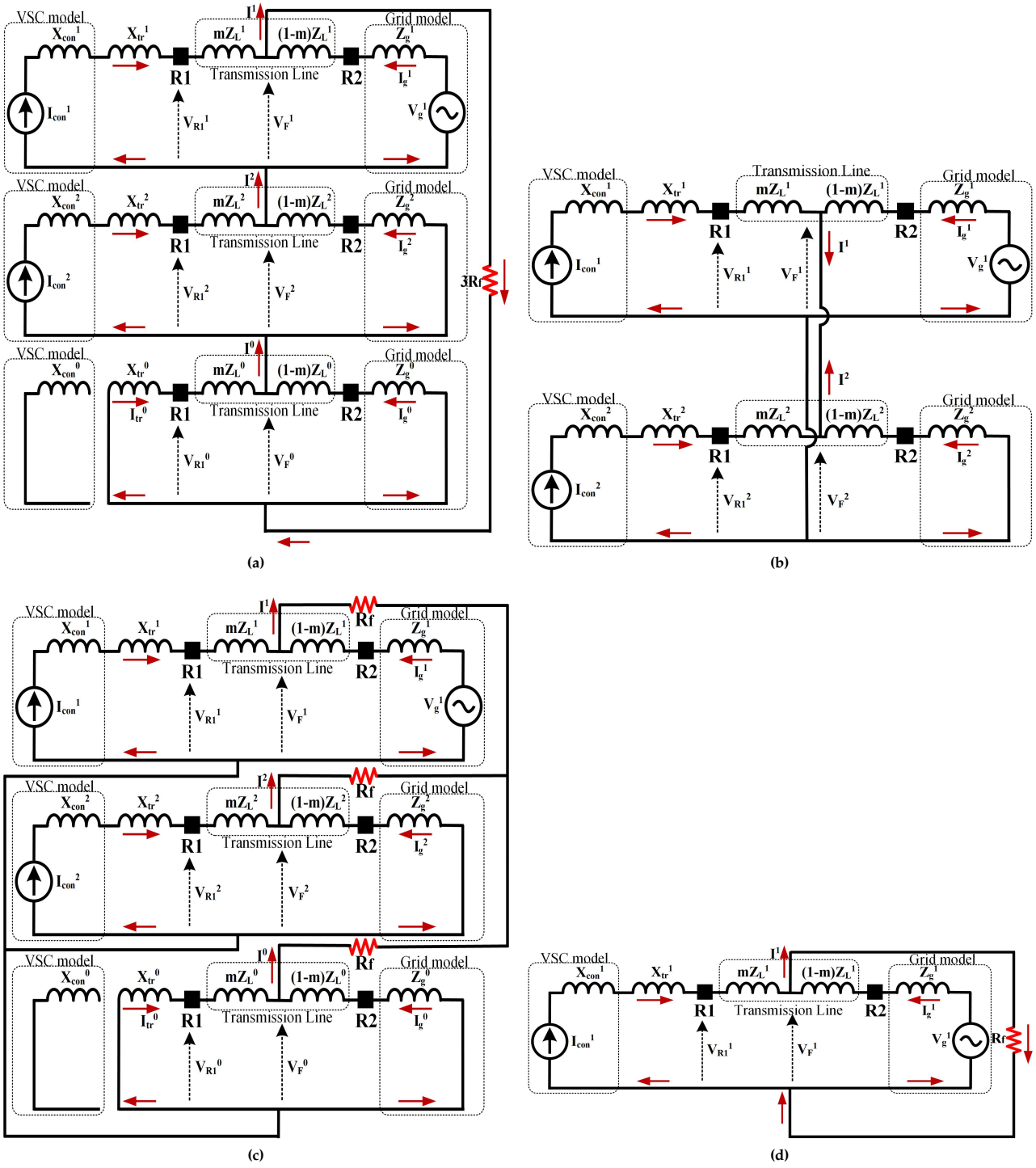


Figure 4.15: (a) Sequence network diagram of the system for a single line to ground fault. (b) Sequence network diagram of the system for a phase-to-phase fault.(c) Sequence network diagram of the system for a phase-to-phase-to-ground fault. (d) Sequence network diagram of the system for a three-phase fault.

Apart from this, the ground faults such as the single line to ground and phase-to-phase-to-ground faults involve the zero sequence component of the fault current and zero sequence network of the system as unveiled in Figure 4.15(a) and Figure 4.15(c). It is evident from the figures that the converter does not supply the zero sequence component of the fault current due to the delta-star winding of the transformer. Thus, the converter controller is independent from the zero sequence current regulation and the grounded neutral of the

transformer[20] is the only path for its flow through the line (I^0_{tr}). The zero sequence voltage at the fault V^0_F is given by (4.10):

$$V^0_F = V^0_{R1} - I^0_{tr}(mZ^0_L) \tag{4.10}$$

According to the Fortescue's methodology, a three phase unbalanced system can be decomposed into three independent and symmetrical sequence components which can be converted into phase currents and voltages using matrix vector A [81]. This results in the following equations:

$$V^{abc} = AV^{012} \tag{4.11}$$

$$I^{abc} = AI^{012} \tag{4.12}$$

where,

$$A = \begin{bmatrix} 1 & 1 & 1 \\ 1 & \alpha^2 & \alpha \\ 1 & \alpha & \alpha^2 \end{bmatrix} \tag{4.13}$$

$$\alpha = -0.5 + 0.866i \tag{4.14}$$

Thus,

$$\begin{bmatrix} V^a_{R1} \\ V^b_{R1} \\ V^c_{R1} \end{bmatrix} = \begin{bmatrix} 1 & 1 & 1 \\ 1 & \alpha^2 & \alpha \\ 1 & \alpha & \alpha^2 \end{bmatrix} \begin{bmatrix} V^0_{R1} \\ V^1_{R1} \\ V^2_{R1} \end{bmatrix} \tag{4.15}$$

$$\begin{bmatrix} I^a_{R1} \\ I^b_{R1} \\ I^c_{R1} \end{bmatrix} = \begin{bmatrix} 1 & 1 & 1 \\ 1 & \alpha^2 & \alpha \\ 1 & \alpha & \alpha^2 \end{bmatrix} \begin{bmatrix} I^0_{R1} \\ I^1_{R1} \\ I^2_{R1} \end{bmatrix} \tag{4.16}$$

$$\begin{aligned} V^a_{R1} &= V^0_{R1} + V^1_{R1} + V^2_{R1} \\ V^b_{R1} &= V^0_{R1} + \alpha^2 V^1_{R1} + \alpha V^2_{R1} \\ V^c_{R1} &= V^0_{R1} + \alpha V^1_{R1} + \alpha^2 V^2_{R1} \end{aligned} \tag{4.17}$$

$$\begin{aligned} I^a_{R1} &= I^0_{R1} + I^1_{R1} + I^2_{R1} \\ I^b_{R1} &= I^0_{R1} + \alpha^2 I^1_{R1} + \alpha I^2_{R1} \\ I^c_{R1} &= I^0_{R1} + \alpha I^1_{R1} + \alpha^2 I^2_{R1} \end{aligned} \tag{4.18}$$

4.5.1 *Single line to Ground Fault*

The sequence components of voltage and current as well as the sequence network depends upon the type of fault that can be seen from Figure 4.15. The voltage phasors measured by the distance relay *R1* can be written using (4.8), (4.9), and (4.10) in (4.19) for a phase A to ground fault[21] as:

$$V^a_{R1} = V^0_F + I^0_{tr}(mZ^0_L) + V^1_F + I^1_{con}(mZ^1_L) + V^2_F + I^2_{con}(mZ^2_L) \tag{4.19}$$

Equation (4.19) is rearranged in (4.20) as:

$$V^a_{R1} = (V^0_F + V^1_F + V^2_F) + m(I^0_{tr}Z^0_L + I^1_{con}Z^1_L + I^2_{con}Z^2_L) \tag{4.20}$$

From the Fortescue methodology:

$$V^a_F = (V^0_F + V^1_F + V^2_F) = R_f(I^a_{R1} + I^a_g) \tag{4.21}$$

[20] In general, the transformer utilized in a VSC-HVDC scheme is a delta-star grounded winding type transformer with the delta winding on the VSC side. This is because the delta winding restricts the 3rd harmonic and disturbance produced by the VSC to enter into the grid

[21] A single line to ground fault is the most common type of fault that occurs in a power system. It has been estimated that nearly 85% of faults taking place in a power system is single line to ground fault with fault resistance.

Hence, (4.22) gives the voltage seen by the relay *R1* as:

$$V^a_{R1} = R_f(I^a_{R1} + I^a_g) + mZ^1_L(4I^0_{tr} + I^1_{con} + I^2_{con}) \tag{4.22}$$

where, $Z^1_L = Z^2_L$ and $Z^0_L = 4Z^1_L$ from Table in the Appendix A. Moreover, expression (4.22) can be arranged using (4.18) as:

$$V^a_{R1} = (R_f + mZ^1_L)I^a_{R1} + R_f I^a_g + 3mZ^1_L I^0_{tr} \tag{4.23}$$

The apparent impedance seen by the relay R1 for a phase A to ground fault (Z^{AG}_{app}) is given by (4.24) [63]:

$$Z^{AG}_{app} = \frac{V^a_{R1}}{I^a_{R1} + 3KI^0_{tr}} \tag{4.24}$$

Using $Z^1_L = 0.2645\angle 88.05^o\,\Omega/km$ and $Z^0_L = 1.0588\angle 77.83^o\,\Omega/km$ (refer Table in the Appendix A), we get $K = \frac{Z^0_L - Z^1_L}{3Z^1_L} = 1.01\angle -14^o$ as the zero sequence compensation factor. Substituting (4.23) in (4.24) gives (4.25):

$$Z^{AG}_{app} = \frac{(R_f + mZ^1_L)I^a_{R1} + R_f I^a_g) + 3mZ^1_L I^0_{tr}}{I^a_{R1} + 3KI^0_{tr}} \tag{4.25}$$

Expression (4.25) constitutes three terms:

1. $(R_f + mZ^1_L)I^a_{R1}/(I^a_{R1} + 3KI^0_{tr})$: The numerator of the first component highlights the dependence of the apparent impedance on the current contribution from the converter side that cannot deliver the fault current more than its saturation limit (i.e. 1.15 p.u.)[22]. The denominator $I^a_{R1} + 3KI^0_{tr} = I^1_{con} + I^2_{con} + (3K+1)I^0_{tr}$ is dominated by the zero sequence current (approx. four times I^0_{tr} that flows through the neutral of the transformer because $|K| \cong 1$ (see Appendix A), $I^1_{con} \leqslant 1.15$p.u. and I^2_{con} is suppressed to zero to de-stress the PES of VSC as the negative sequence current leads to an additional stress on the PES and oscillating power component [81]. Furthermore, the reactive current injection is the positive sequence current and the presence of negative sequence current[23] in addition to the positive sequence current limits the amount of available positive sequence reactive current support from the VSC during the fault.

2. $R_f I^a_g/(I^a_{R1} + 3KI^0_{tr})$: This part reflects the effect of R_f in conjunction with the fault current contribution from the grid I^a_g. If $R_f = 0$, this term eventually reduces to zero. Since, the grid consists of conventional generator[24]; the fault current has sub transient, transient, and steady state characteristics affecting the overall trajectory of the positive sequence impedance of the line.

3. $3mZ^1_L I^0_{tr}/(I^a_{R1} + 3KI^0_{tr})$: This expression presents the impact of the zero sequence current upon the measured impedance. The zero sequence current flows through the grounded neutral of the transformer for faults involving the earth and remains independent of the VSC controller due to the delta winding of the transformer on the converter side. Since, the zero sequence current (I^0_{tr}) dominates the denominator $\cong 4 * I^0_{tr}$ as explained before, the third term is approximately $(3/4)mZ^1_L$, seen by the relay in case of a single line to ground fault.

Consequently, it is evident from (4.25) that the restricted I^1_{con} from VSC I^0_{tr} contribution through the transformer, I^a_g and R_f directly decide the performance of the relay *R1*.

[22] Any unbalanced condition resulting from any unbalanced fault leads to a large unbalanced fault currents that might lead to over current situation and damage the PES.

[23] The present grid code does not stipulate any requirement for the flow of negative sequence current during an unbalanced fault.

[24] The fault characteristics of synchronous generators based power system is different that depends upon the physics of generator and transmission lines.

4.5.2 *Phase-to-Phase Fault*

For a phase A-to-phase B fault, the apparent impedance seen by the relay *R1* (Z_{app}^{AB}) is:

$$Z_{app}^{AB} = \frac{V_{R1}^{a} - V_{R1}^{b}}{I_{R1}^{a} - I_{R1}^{b}} \tag{4.26}$$

where, V_{R1}^{a}, V_{R1}^{b}, I_{R1}^{a} and I_{R1}^{b}, are the voltages and currents of phase A and B, respectively, at the relay point *R1*. Using (4.17) to express V_{R1}^{b}, we have:

$$V_{R1}^{b} = (V_F^0 + \alpha^2 V_F^1 + \alpha V_F^2) + m(I_{tr}^0 Z_L^0 + \alpha^2 I_{con}^1 Z_L^1 + \alpha I_{con}^2 Z_L^2) \tag{4.27}$$

$$V_{R1}^{b} = V_F^b + mZ_L^1(4I_{tr}^0 + \alpha^2 I_{con}^1 + \alpha I_{con}^2) \tag{4.28}$$

Therefore, keeping (4.22) and (4.28) in (19) gives:

$$Z_{app}^{AB} = \frac{(V_F^a - V_F^b) + mZ_L^1((4I_{tr}^0 + I_{con}^1 + I_{con}^2) - (4I_{tr}^0 + \alpha^2 I_{con}^1 + \alpha I_{con}^2))}{(I_{R1}^0 + I_{R1}^1 + I_{R1}^2) - (I_{R1}^0 + \alpha^2 I_{R1}^1 + \alpha I_{R1}^2)} \tag{4.29}$$

$$Z_{app}^{AB} = \frac{(V_F^a - V_F^b) + mZ_L^1(I_{con}^1(1-\alpha^2) + I_{con}^2(1-\alpha))}{(I_{con}^1(1-\alpha^2) + I_{con}^2(1-\alpha))} \tag{4.30}$$

$$Z_{app}^{AB} = mZ_L^1 + \frac{R_f((I_{R1}^a - I_{R1}^b) + (I_g^a - I_g^b))}{(I_{con}^1(1-\alpha^2) + I_{con}^2(1-\alpha))} \tag{4.31}$$

$$Z_{app}^{AB} = mZ_L^1 + R_f\left(1 + \frac{(I_g^a - I_g^b)}{(I_{con}^1(1-\alpha^2) + I_{con}^2(1-\alpha))}\right) \tag{4.32}$$

Expression (4.32) presents an apparent impedance observed by the relay *R1* for a phase A-to-phase B fault constituting two terms:

1. mZ_L^1: The first term highlights the correct value of the impedance, which should be seen by the relay *R1*.
2. $R_f\left(1 + /(I_g^a - I_g^b)(I_{con}^1(1-\alpha^2) + I_{con}^2(1-\alpha))\right)$: The effect of this component is on the resistive part of Z_{app}^{AB}. Since, the current supplied through the relay *R1* mainly consists of the positive sequence current from the converter[25], which is even limited in magnitude ($I_{con}^1 \leqslant 1.15$p.u.) in order to protect the converter from overcurrent, therefore, this term is dominated by the grid current contribution in conjunction with the fault resistance that decides the apparent impedance of the relay *R1*. The denominator reduces to a smaller value eventually magnifying the overall value of the second term.

[25] The absence of zero sequence current during the fault involving ground is due to the delta winding transformer configuration.

4.6 MODERN NETWORK CODES FOR HVDC CONNECTION

General Description

A mammoth change is taking place in the present day power system with the continuous addition of sustainable energy regime that led to overall capacity additions of more than 100 GW in the form of renewable since 2011. The share of renewables in total electricity production have exceeded 22% in 2014 out of which hydro power accounted for 16.4% and renewable like wind and Photovoltaic (PV) for 3.6%. The renewable source of energy like wind and PV are also termed as Variable Renewable Energy (VRE). Few European countries like Denmark, Germany, Spain, and Ireland have their individual share of VRE more than 15%, which is higher than the global share. Moreover, the global share of VRE is expected to rise by 20% by the end of 2030 [134].

The rapid development in the renewable energy technologies is leading to their rapid installation and implementation ultimately replacing their conventional counterpart like SG based thermal and nuclear power plants. This development represents a challenge for the network operators. These must ensure the security of the networks – in tandem with significantly rising shares of VRE based electricity. System services therefore have to be increasingly provided by VRE plants, which have so far only been required from conventional power stations [83].



Figure 4.16: A typical layout of a offshore converter station platform [8].

Grid codes are essential for the successful integration of VRE. For the operation of power systems, VRE generators pose challenges that contrast with conventional generation. In response to these challenges, VRE generation technology is rapidly developing, accompanied by enabling technologies like storage and control systems, and facilitating new operational practices for power systems. These technological and operational developments create greater flexibility for operating electricity networks and enable a higher share of VRE. Grid codes need to be established to ensure that electricity service for consumers is secure while deploying new technologies and adopting new operational practices. If VRE is to be successfully integrated into electricity networks, then all the three components need to be considered: technology, operation and regulation [135].

Grid codes provide the rules for the power system and energy market operation, ensuring operational stability, security of supply and well-functioning wholesale markets. A set of grid codes can include, for instance, connection codes, operating codes, planning codes, market codes [79].

Grid codes are set of rules for power system and energy market operation. It enables the network operators, generators, suppliers and consumers to function more effectively across the market. This ensures operational stability and security of supply, and contributes to well-functioning wholesale markets. Connection codes, operating codes, planning codes and market codes are a few examples of grid codes.

Fault Ride Through

The code provides exact description of conditions when VRE generators like offshore wind power parks shown in Figure 4.16 must remain connected to the grid after the initial voltage dip due to short circuit. The desired feature to inject reactive current for fault detection is also demanded of VRE generation above a minimum voltage level [134]. Conventional generators are inherently capable of providing high short circuit currents. However, the provision of these higher than nominal currents from VRE generators must be considered in the generator design.

The grid code clearly specifies a voltage against time profile for any power park modules that shall be applied at the grid connection point for any fault conditions [55], [27]. The code suggests the following [78, 83]:

1. The HVDC Converter Station shall be capable of staying connected to the Network and continue stable operation after the power system has recovered following fault clearance unless the protection scheme for internal faults requires the disconnection of the HVDC Converter Station from the Network.

2. The Voltage-against-Time-profile shall be expressed by a lower limit of the phase-to-phase Voltages on the Network Voltage level at the Connection Point(s) during a symmetrical fault, as a function of time before, during and after the fault.

3. The ride through period shall be defined by the relevant TSO.

4. Relevant TSO shall have the right to specify Voltages (U_{block}) at the Connection Point(s) under specific network conditions whereby the HVDC system is allowed to block.

Active Power Output

Every generating plant must be capable of operating at a reduced power output and to allow constant power control of 1% of the rated power per minute across the entire range between minimum and continuous power. However, following actions are to be implemented during fault conditions [79]:

1. Disconnection from the grid upon reaching a frequency at the grid connection point of less than 46.5 Hz or greater than 53.5 Hz and after a time delay of 300 ms.
2. Disconnection from the grid upon reaching a frequency at the grid connection point of less than 47.5 Hz or greater than 51.5 Hz and after a time delay of 10 s.

After a disturbance with zero residual voltage at the grid connection point a restart of the generation plant with maximum 10% per minute of the maximum installed active power is allowed.

Reactive Power Exchange & Voltage Stability

With the active power output, every generating plant must fulfill at the grid connection point, the range of reactive power provision. In the case of online specification of set point value, the respective new specifications for the operating point of the reactive power exchange must be realized at the grid connection point after no more than one minute. Changes in the reactive power corresponding to a reactive power of more than 5% of the grid connection capacity in the extra high voltage grid are not permissible, if the gradient is more than 1% per second.

The generating plant is expected to set any operating point within 30 s. The reactive power supply in a frequency range of 47.5-51.5 Hz must be possible.

Active Power Reduction during over frequency

In a frequency range of 47.5 – 50.2 Hz, the generating units must be able to unrestrictedly feed active power into the grid. Below a frequency of 47.5 Hz, the active power supply may be shortened due to justified technical restrictions.

Above a frequency of 50.2 Hz, as defined in NAR[26]., a frequency dependent active power reduction is required. The technical solution implemented for this purpose must achieve a maximal power variation gradient of 25% of the currently available active power of the generation unit per second.

[26] Netzanschlussregeln Höchstspannung

Frequency Support

All generating plants meeting the necessary technical and operational requirements can be used for the provision of primary control power, secondary control power and minute reserve[27].

Following are the requirements:

1. Primary control band must be at least $\pm 2\%$ of the rated power.
2. Frequency power droop characteristic must be adjustable.
3. Insensitivity range must be less than ± 10 mHz.
4. Activation of the total primary control power range required by the generating plant must be in 30s and for at least 15 min.

[27] Every generating plant with a rated capacity of $\geqslant$ 100 MW must be capable of supplying primary control power. Furthermore, every generating plant with a rated capacity of less than $\leqslant$ 100 MW are also used to secure primary control

Reactive Current Support During Faults

Modern grid codes authorize the system operators to support the grid during faults by meeting the reactive short circuit current injection from the HVDC converter station to support the network voltage [77, 79]. The network code specify the priority of additional reactive current contribution in the event of a significant voltage deviation during a fault and staying connected to the network with regard to the FRT capability of the HVDC system [78, 80]. This additional reactive current (ΔI_q) support by the converter must be proportional to the voltage drop (ΔU) at the PCC such that $\Delta I_q / I_N = k * \Delta U / U_N$ [83].

The reactive current droop (k) is adjustable between 2 p.u. to 10 p.u. In order to achieve this, the voltage control is activated within 20 ms after fault detection if the network voltage deviates more than 10% of the rms value i.e. a dead band ($\pm$0.1p.u.) as per Figure 4.17 [78],[83]. Additionally, this voltage support is maintained for the fault duration after the voltage returns to the dead band. The ac voltage control of the VSC-HVDC, which outputs the reactive current reference component for the inner current control and determines the additional reactive current, utilizes PI control. The proportional gain of this ac voltage control is set to the reactive current droop ($2 < k < 10$) and the integrator is continuously operating during the fault.

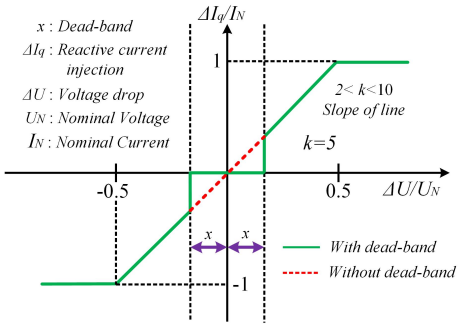


Figure 4.17: Reactive current slope for voltage support by the VSC-HVDC system.

4.7 CURRENT LIMITATION STRATEGIES

Equal Current Priority Limitation Strategy

As it is widely known that the current contribution from the VSC should not exceed its maximum current rating, which is usually assigned between 1.15-1.2 times the nominal current of the converter during either normal or fault condition. The current limitation strategies are adopted for VSC during any fault condition to keep the active as well as reactive current component within the range of maximum current rating of the converter.

This equal current priority limitation strategies during the fault prevents the converter from overloading while maintaining the priority of both the active and reactive power supply. In this strategy as in Figure 4.18, the q-axis and d-axis current limit are assigned as given in (4.33) and (4.34) by defining the angle between the d-axis current and the fault current phasor i.e. β. The magnitude of the total fault current is kept within the maximum current of the VSC i.e. 1.15 p.u.

$$\beta = \arctan \frac{i_{q+}^{ref}}{i_{d+}^{ref}} \tag{4.33}$$

$$i_{q+}^{lim} = I_{max} * \sin \beta \tag{4.34}$$

$$i_{d+}^{lim} = I_{max} * \cos\beta \tag{4.35}$$

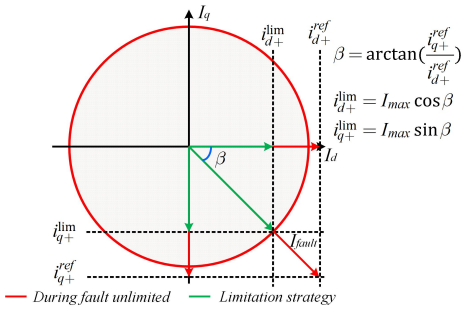


Figure 4.18: Equal current priority current limitation strategy.

Reactive Current Priority Limitation Strategy

Another VSC-HVDC current limitation strategy i.e. reactive current priority limitation strategy during the fault to restrain the VSC from overloading by giving priority to the reactive current and examining its impact on the performance and operation of the distance relay. In this strategy, q-axis current limit (i_{q+}^{lim}) is assigned equal to the reactive current reference command (i_{vq+}^{ref}) coming out of the outer ac voltage controller such that the reactive current limit should be less or equal to 1 ($i_{q+}^{lim} \leqslant 1$), as showcased in Figure 4.19. On the other hand, the active current limit (i_{d+}^{lim}) is dynamic in nature and uses the q-axis current limit (i_{q+}^{lim}) as an input signal. The strategy then computes the available over current capability left for the d-axis current limit (i_{d+}^{lim}) as given in (4.36) and (4.37).

$$i_{d+}^{lim} = \sqrt{(I_{max})^2 - (i_{q+}^{lim})^2)} \tag{4.36}$$

$$i_{q+}^{lim} = i_{vq+}^{ref} \leqslant 1 \tag{4.37}$$

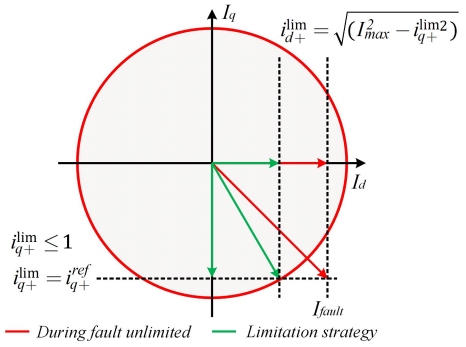


Figure 4.19: Reactive current priority current limitation strategy.

Active Current Blocked Limitation Strategy

The current contribution of a VSC should not exceed its rating (1.15 p.u.) during the fault to avoid damage to the PES. Thus, supplying the active current along with the reactive current

during the fault limits the amount of reactive current injection (red arrow in Figure 4.20). Hence, the active current can be reduced by the TSO to ensure system stability and benefit reactive current injection by providing it with a sufficient room during significant voltage deviation. The grid side VSC outer control adopts the active current blocked limitation strategy by setting the active current limit ($i_{dlim} = 0$p.u.) and assigning the reactive current limit equal to the converter maximum current ($i_{qlim} = I_{max} = 1.15$p.u.) during the fault as in [136], elaborated in Figure 4.20. This is done in order to dedicate the full capacity of the converter to the reactive current support (green arrow in Figure 4.20). On the other hand, the active current reference is quickly forced to drop to zero with the help of active current limiter at the output of d-axis outer control given by (4.38) and (4.39).

$$i_{d+}^{lim} = 0 \tag{4.38}$$

$$i_{q+}^{lim} = I_{max} = 1.15\text{p.u.} \tag{4.39}$$

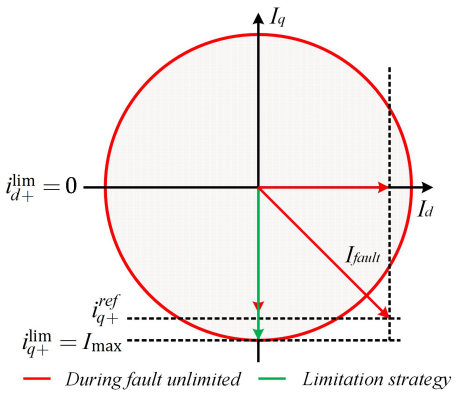


Figure 4.20: Active current blocked current limitation strategy.

4.8 STUDY SYSTEM

A 400 kV, 50 Hz, modified Kundur two-area, four-machine system [137] is modelled and simulated in PSCAD/EMTDC platform to study the distance protection of the line connected to the VSC-HVDC as shown in Figure 4.21. The analyzed distance relay is R1 situated on Line 1 between Bus 5 and Bus 6. The PCC is Bus 5 in the power system. The system constitutes voltage sources behind Thevenin Equivalent impedances, sufficient for fault studies. The parameters of the study system are given in the Appendix A in Table.

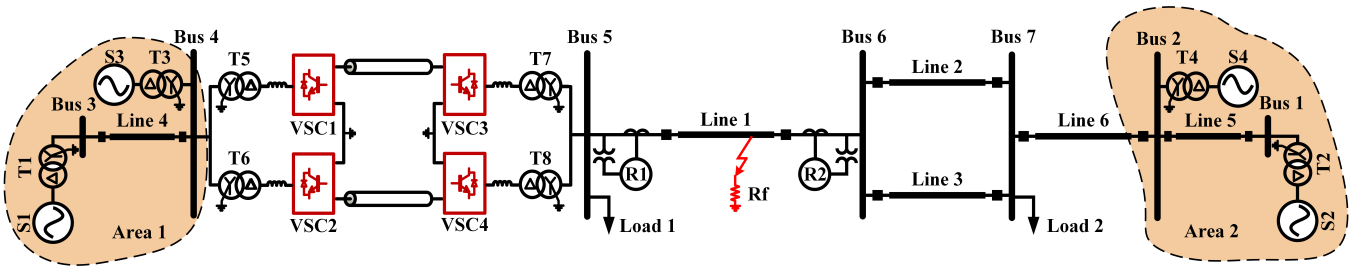


Figure 4.21: Modified Prabha Kundur two-area system.

4.8.1 *AC Source Model*

The AC sources presented in the study system are constant voltage source models behind Thevenin equivalent grid impedance S1, S2, S3, and S4 as shown in Figure 4.21. The Thevenin equivalent grid impedance model is adopted in terms of the positive and zero sequence impedance and represented as (R–RL) with a constant voltage source. The model of voltage source along with positive and zero sequence circuit is chosen in PSCAD/EMTDC at a voltage level of 400kV (Line-to-Line rms) and steady state frequency of 50 Hz.

4.8.2 *Converter Transformer Model*

The transformer (refer Figure 4.22) models T5 to T8 utilized to step-up the voltage level in PSCAD are star-delta transformers with the star side grounded, which serve as the primary winding as depicted in Figure 4.21. The grounding of star side serves as a source for zero sequence currents and helps in detecting the earth faults. The voltage ratio of star-delta transformer is 400/175 kV. The star-delta transformer model in PSCAD is a detail model with a tap changing options and transformer saturation making transformer non-ideal. However, the transformer is considered ideal with no winding saturation and no copper and iron losses.



Figure 4.22: World's first 1100 kV converter Transformer[8]

4.8.3 *Converter Reactor Model*

The point to point VSC-HVDC system is interfaced with the AC grid at the PCC by the use of converter reactor which helps in active and reactive power regulation between the converter and the PCC. The converter reactor value can be chosen from 0.05 p.u. to 0.25 p.u. depending upon the system rating. In this study system, the converter reactor is chosen as 0.10 p.u.



Figure 4.23: HVDC projects all around the globe which can be seen in white dots.)

4.8.4 *Transmission Line Model*

A frequency dependent phase model of the transmission lines, Line 1 and Line 2, at a voltage level of 400kV is utilized in PSCAD/EMTDC platform. The chosen conductors belong to "chukar" class and are bundled (4 conductors per bundle). The ground wire conductor is a stainless steel conductor at a height of 40m from the ground. The conductors are placed in a triangular form with the ground wires exactly above the middle conductor.

The phase impedance matrix of transmission line can be calculated manually or using LCP. The phase impedance matrix in the form of self (diagonal elements) and mutual impedance (off-diagonal elements) of the transmission line can be processed to obtain a sequence impedance matrix of the transmission line using (4.40) and (4.41). The sequence impedance matrix of the transmission line has zero off-diagonal elements when the transmission lines are completely transposed.

$$Z_{abc} = \begin{bmatrix} 0.1381 + 0.5077i & 0.0697 + 0.2481i & 0.0697 + 0.2481i \\ 0.0697 + 0.2481i & 0.1381 + 0.5077i & 0.0697 + 0.2481i \\ 0.0697 + 0.2481i & 0.0697 + 0.2481i & 0.1381 + 0.5077i \end{bmatrix} \tag{4.40}$$

$$Z_{012} = A^{-1} * Z_{abc} * A \tag{4.41}$$

$$Z_{012} = \begin{bmatrix} 0.2775 + 1.0039i & 0 & 0 \\ 0 & 0.0684 + 0.2596i & 0 \\ 0 & 0 & 0.0684 + 0.2596i \end{bmatrix} \tag{4.42}$$

The zero sequence impedance can be given from the above matrix using (4.42) as the first diagonal element of the matrix. The positive sequence impedance is the second diagonal element while the third diagonal element is the negative sequence impedance of the line. If the sequence impedance matrix has non-zero off-diagonal elements, then the sequence impedance are closely coupled and can cause under-reach and over-reach of the relay if not compensated properly.

4.8.5 *VSC Based HVDC*

Physical Model

The work adopts the detailed model of a half bridge MMC as the converter in a VSC-HVDC scheme. Figure 4.24(a) presents a three-phase MMC circuit diagram that consists of six arms with N submodules (SM)s and an arm inductance (L_{arm}) in each of the arms. Each SM of the MMC consists of a half bridge cell that includes two IGBT and a parallel capacitor (see Figure 4.24(a)). The ac terminal of the MMC is connected to the PCC through a reactor and a delta-star grounded transformer, as depicted in Figure 4.21. The MMC are in bipolar arrangement with the dc side pole-to-ground voltage of 320 kV. Physical parameters of the MMC are presented in the Appendix A in Table.

Control Model

Figure 4.24(b) portrays a simplified control scheme employed for the MMC topology that consists of an outer control, an inner current control, a Circulating Current Suppression Control (CCSC), a voltage balancing control and a PWM control in *dq* synchronous rotating frame of reference with *d*-axis aligned with phase-A voltage (u_a). The outer control includes the active power control and ac voltage control, which generates i_{d+}^{ref} and i_{q+}^{ref} reference currents for the inner current control, respectively. Since, an unbalanced voltage condition in the grid leads to the appearance of the negative sequence current in the line, which limits the reactive current injection and causes an additional stress on the PES of the VSC. Therefore, to give space to the positive sequence reactive current injection and to de-stress the PES during an unbalanced grid condition, the negative sequence current is suppressed to zero. This is done by implementing a fast decoupled, dual inner current control in the form of positive and negative sequence current control, which regulates i_{dq+} and i_{dq-} with respect to i_{dq+}^{ref} coming from the outer control and $i_{dq-}^{ref} = 0$, respectively, as unveiled in Figure 4.24(b) and (d) [82].

Furthermore, the summation of the upper and lower arm voltages may not be equal to V_{dc} due to the variation of SM capacitor voltages. This unbalance in the arm-phases of the MMC result in circulating currents i_{abc}^{diff} which is a negative sequence current at double the fundamental frequency, as shown in Figure 4.24(a). The circulating currents distort and increase the rms value of the arm currents that leads to increased converter losses. Additionally, this also induce ripples in the SM voltages. The CCSC implements a *dq* decoupled control with the reference $i_{dqcirc}^{ref} = 0$ to suppress the second harmonic circulating currents (refer Figure 4.24(c)) [44]. The MMC control also requires a capacitor voltage balancing control to balance the capacitor voltage of all SMs and PWM control to generate Firing Pulses (FP). In addition to the normal operation of the aforementioned MMC controller, where power requirements are fulfilled by tracking preset active/reactive power values, the control system administers the fault current behaviour as well by dictating the

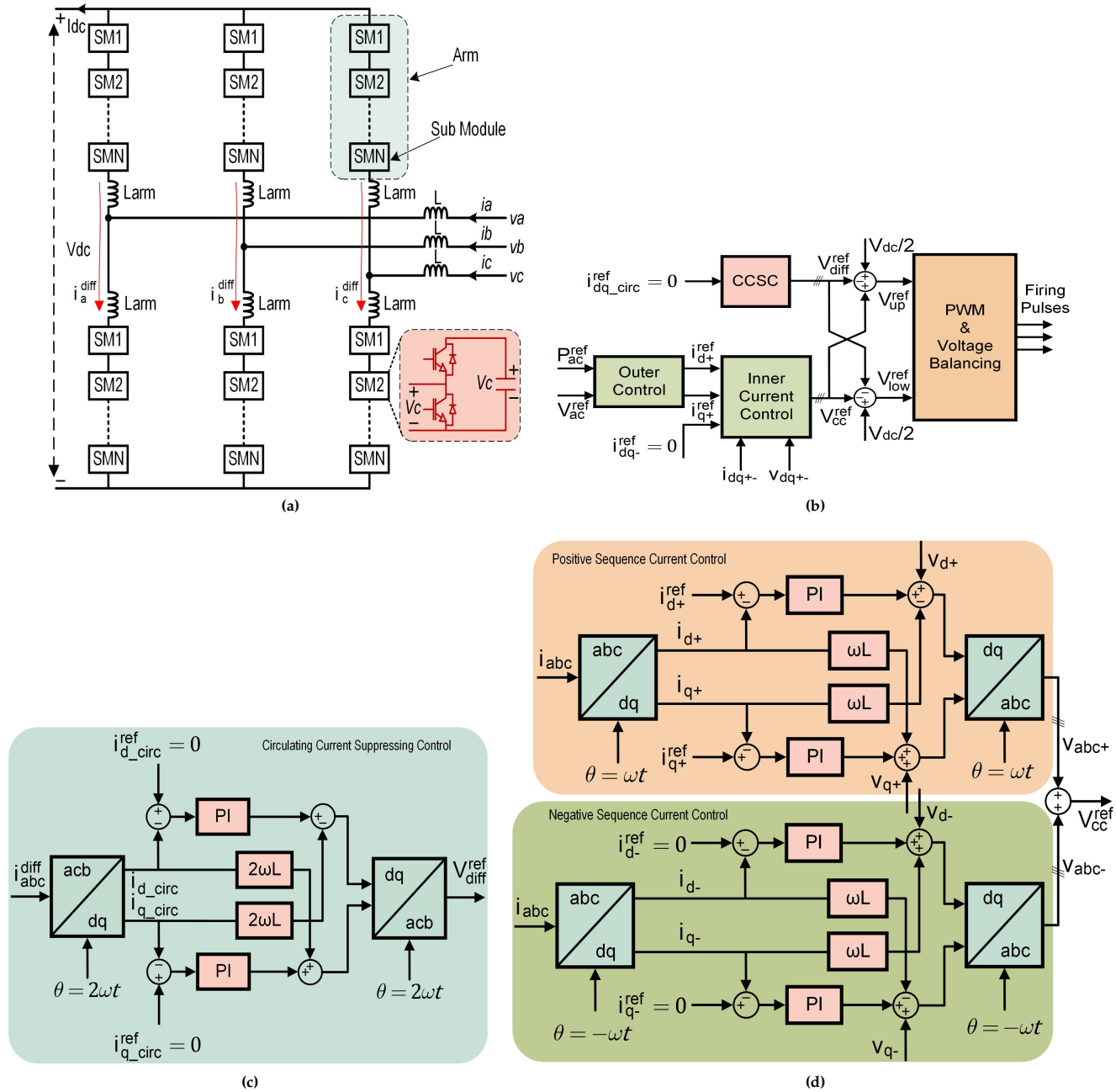


Figure 4.24: (a) Circuit diagram of MMC-HVDC converter. (b) Simplified control scheme of MMC. (c) Circulating current suppressing control in MMC. (d) Inner current control of MMC with positive and negative sequence current control loops.

firing pulses for the converter [108]. The set points for the controller are governed by the grid codes decided by the network operators and regulatory authorities to attain a specific regulation in the active/reactive power and/or grid voltage during any faulty scenario [79]. The study performed upon the impact of the distance protection is irrespective of the type of the converter, for instance, 2-level, 3-level, MMC etc. commonly implemented in VSC-HVDC scheme.

4.9 SIMULATION RESULTS AND DISCUSSION

Simulations have been conducted by following the NC for HVDC connection, which state the priority of reactive current support and current limitation strategies during the fault condition, to analyze its impact on the distance relay. The faults are studied on Line 1, as

shown in Figure 4.21, for a duration of 200 ms (i.e. 10 cycles), to provide sufficient time for the impedance locus to reach a steady state, and for the distance relay to detect faults. Several study scenarios have been examined, which are stated as follows:

4.9.1 *Single Line to Ground Fault (SLG)*

At t = 1 s, phase-A to ground fault is simulated on Line 1 at a distance of 60 km from R1. The fault resistance, R_f is kept equal to zero, initially. Taking into account the network code for HVDC connections, the controller shifts the priority from active power control to reactive power support during the fault, as explained above. Furthermore, the amount of reactive current support depends upon the drop in the PCC voltage as governed by the slope of the line (k), presented in Figure 4.17. Figure 4.25 unveils the pre-fault, during the fault, and post-fault active power, reactive power, and the bus voltage for the converter (Bus 5) and the grid side (Bus 6). Figure 4.25(a) presents that the active power flow from the VSC-HVDC drops to 0.0 MW from 400 MW after the phase-A to ground fault due to the current limitation strategy of $i_{dref} = i_{dlim} = 0$p.u. and starts re-injecting 400 MW (reference power) into the network, once the fault is removed from Line 1. This is evident that the limitation strategies and control priorities of VSC stations are functioning properly. On the other hand, the active power contribution from the grid side reverses from -400 MW to +500 MW (peak) for 200 ms in order to feed the fault, as depicted in Figure 4.25(a).

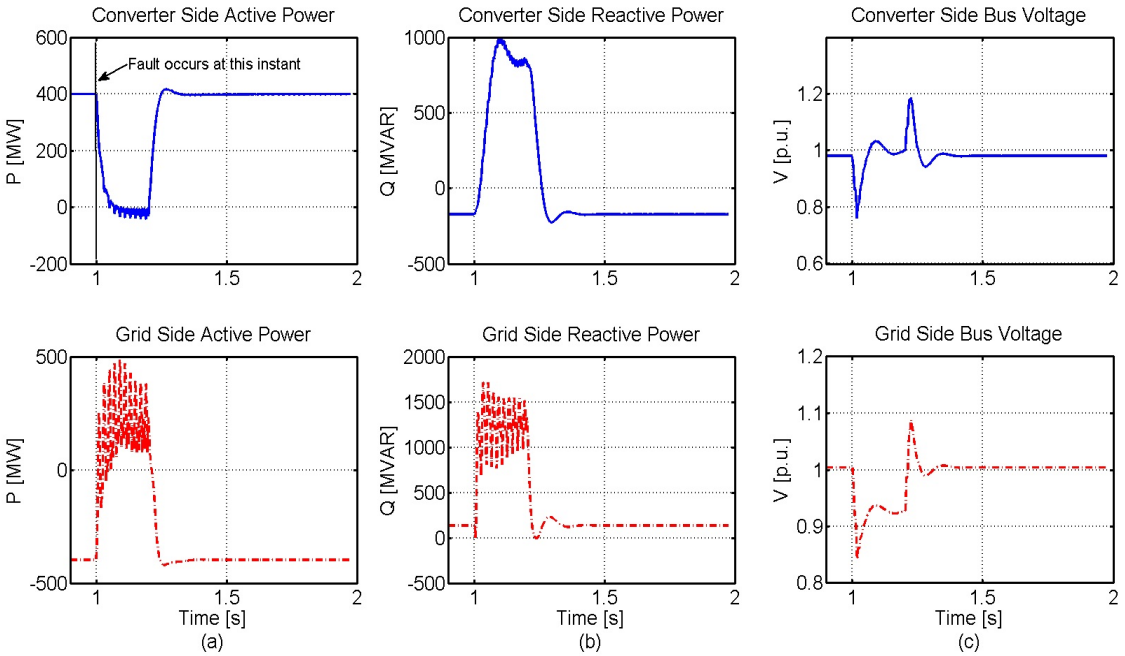


Figure 4.25: Phase A to ground fault on Line 1 at 60 km from R1 with $R_f = 0\Omega$ (a) Active power. (b) Reactive power. (c) rms bus voltage. (Top: Converter side, Bottom: Grid side).

The PCC rms voltage i.e. the converter side bus voltage (Bus 5), after the phase-A to ground fault drops to 0.76 p.u. in comparison to the grid side bus voltage (Bus 6) of 0.84 p.u., as shown in Figure 4.25(c). Since, the PCC voltage drop is more than the dead band limit of ±0.1 p.u., the controllers of the VSC-HVDC station (VSC 3 and VSC 4) inject the reactive current proportional to the voltage drop at PCC determined by the slope of the line (k) (see Figure 4.17). Figure 4.25(b) also highlights the reactive power change from 172 MVAR (drawn) to 850 MVAR (injection) by the VSC during the fault in comparison to the grid side reactive power contribution. The presence of negative sequence component of voltage

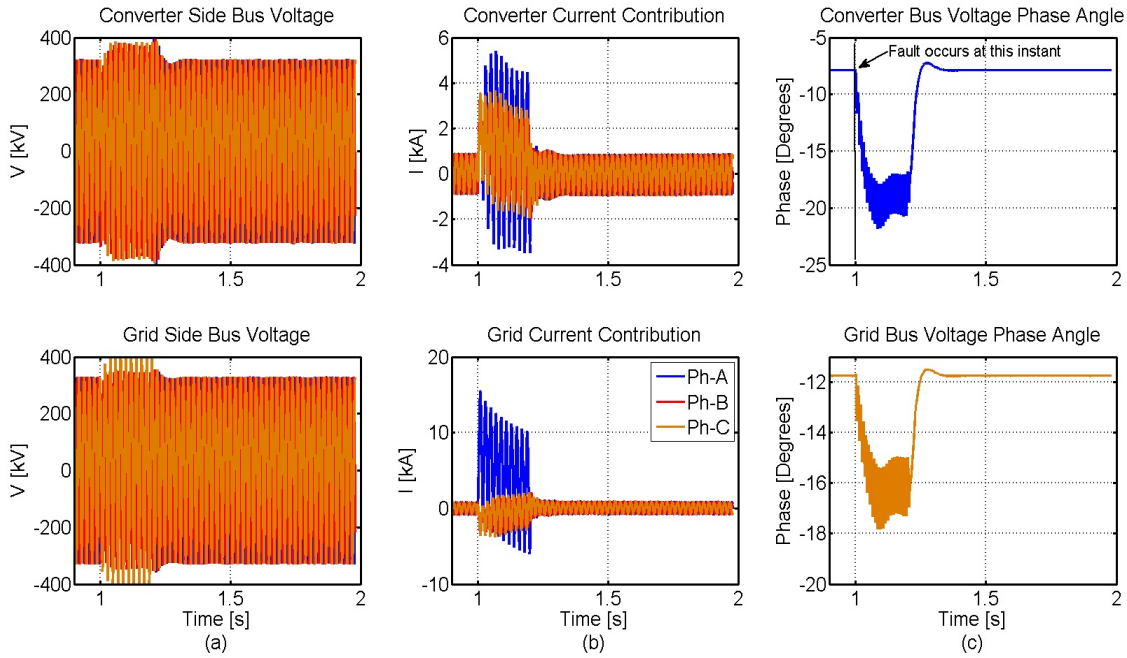


Figure 4.26: Phase A to ground fault on Line 1 at 60 km from R1 with $R_f = 0\Omega$ (a) Instantaneous bus voltage. (b) Instantaneous current contribution. (c) Bus voltage phase angle. (Top: Converter side, Bottom: Grid side).

and current due to an unbalance in the three-phase system causes the instantaneous active and reactive power flowing through the network to consist of sinusoidal double-line frequency component leading to a second harmonic oscillating nature of instantaneous power contribution during the fault (see Figure 4.25(a) and (b)). The instantaneous power ripple disappears as soon as the voltage and current become balanced after the clearance of fault.

Apart from the reactive compensation of unhealthy phases, the reactive current support from the VSC is also found to pose the risk of temporary over voltages in healthy phases during unbalanced faults. This is because the reactive current injection are not phase-selective in nature and an equal amount of reactive current is supplied through all the three phases during the fault [86]. Thus, proper care has been taken in reactive current support so that all the phase voltages are maintained within acceptable limits during any unbalanced condition. Likewise, Figure 4.26(a) demonstrates the instantaneous voltages of the VSC side bus, where the phase voltage including the healthy phases (phase-B and phase-C) are boosted due to equal reactive support. Furthermore, the negative sequence voltage increases during the fault because of the negative sequence current suppression, which eventually leads to more voltage asymmetry. The behaviour of the instantaneous fault current supplied by the converter (5.4 kA peak) is modest and limited in nature than the grid side fault current contribution (15.5 kA peak) due to the converter maximum current limitation strategy and the gain of ac voltage controller, as depicted in Figure 4.26(b). The VSC side bus voltage is approximately in the same phase with small phase difference as compared to the grid side voltage, shown in Figure 4.26(c).

Since, the gain of the ac voltage controller (k) decides the reactive current support from the converter; the ac voltage control is continuously operating during the fault while the PI control of the active power controller is made to freeze. That is why; the dc link voltage rises to 340 kV from 320 kV due to continuous active power injection from the rectifier end of the VSC-HVDC (see Top: Figure 4.27(c)). Bottom curve of Figure 4.27(c) also expose that $i_{dref} = i_{dlim} = 0$p.u. is assigned as the output of outer control soon after the fault because of the active current blocked current limitation strategy. This $i_{dref} = 0$p.u. is given to the d-axis inner current control that reduces i_d to zero. Furthermore, $i_{qlim} = I_{max} = 1.15$p.u. is

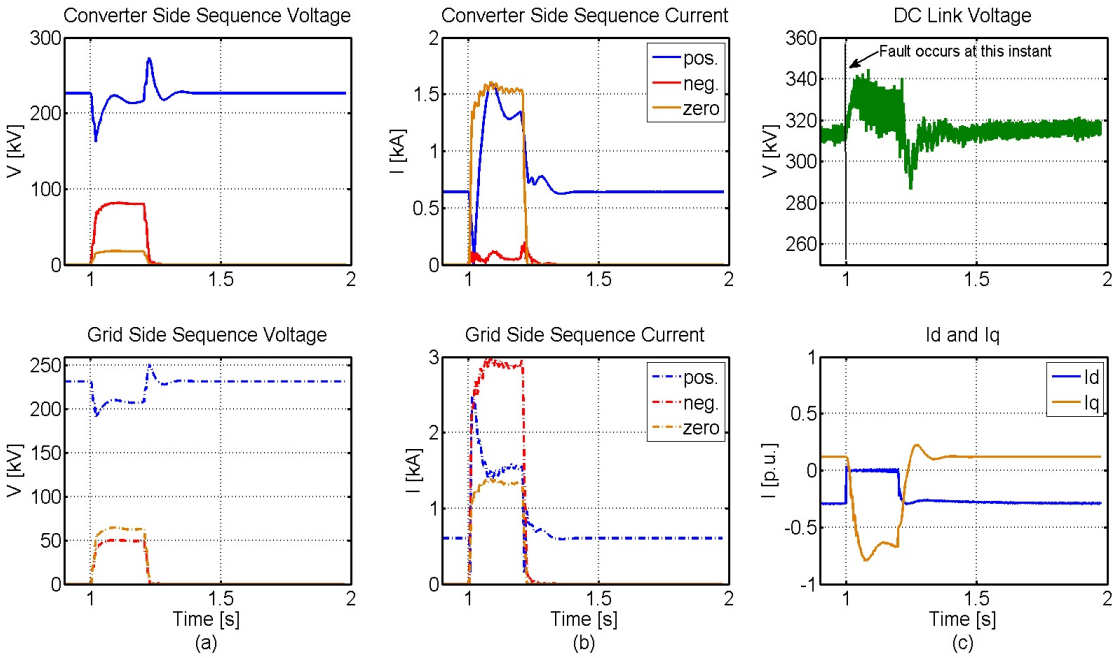


Figure 4.27: Phase A to ground fault on Line 1 at 60 km from R1 with $R_f = 0\Omega$ (a) Sequence bus voltage. (b) Sequence current contribution. (c) DC link voltage and d and q-axis converter currents. (Top: Converter side, Bottom: Grid side).

assigned to the output of fast ac voltage control, which essentially boosts i_q by providing $i_{qref} = 0.65$p.u. to the *q*-axis inner current control of the VSC-HVDC depending upon the PCC voltage drop, as presented in Figure 4.27(c). The fast ac voltage control is a PI control with the rise time ($< 20ms$) and proportional gain (k) [83]. Figure 4.27(a) and (b) illustrate the sequence components of voltages and currents during the fault, pre and post fault. Remarkably, the difference between the negative and zero sequence voltages during the fault is larger for the VSC than the grid side voltage. Similarly, the negative sequence component of fault current from the converter is suppressed to zero to give space to the positive sequence reactive current injection and to de-stress the PES while the zero sequence component of fault current from the *R1* side is uncontrolled by the converter due to the delta winding of the transformer, as reflected in Figure 4.27(b). The zero sequence current supplied through the transformer is 1.52 kA whereas the positive sequence current drops to zero initially due to blocking of the active current then increases to 1.52 kA and then settles to 1.32 kA, which is entirely different from the grid side fault current sequence components illustrated in Figure 4.27(b). The impedance locus for the phase-A to ground fault are portrayed in Figure 4.28. Figure 4.28(a) sketches the positive sequence apparent impedance for a fault at 60 km from R1 with different fault resistances of 0, 10, and 20 Ω with and without VSC-HVDC. It is clear from the Figure 4.28(a) that the increase in the fault resistance causes a large deviation in the impedance seen by the distance relay *R1*. This is because of increase in the magnitudes of 1st and 2nd components of (4.25). The distance relay under reaches because of VSC control strategy. Similarly, the apparent impedance trajectory for the different fault location of 50, 70, 90 km with VSC is different from without VSC, as shown in Figure 4.28(b). In the case of fault at 70 km with 10 Ω, the locus enters into zone 1 but leaves it achieving a steady state in zone 2, which is an under reach.

For a phase-A to ground fault on *Line 1* with a fault resistance of $R_f = 10\Omega$ at a distance of 60 km from R1, the positive sequence component of converter fault current decreases to zero kA initially, before rising to $1.32\angle 153.07^0$ kA. On the other hand, the zero sequence component increases to a value of $I^0_{con} = 1.37\angle -176.3^0$ kA supplied through the grounded neutral of the star winding of the transformer. Analyzing (4.25) and calculating

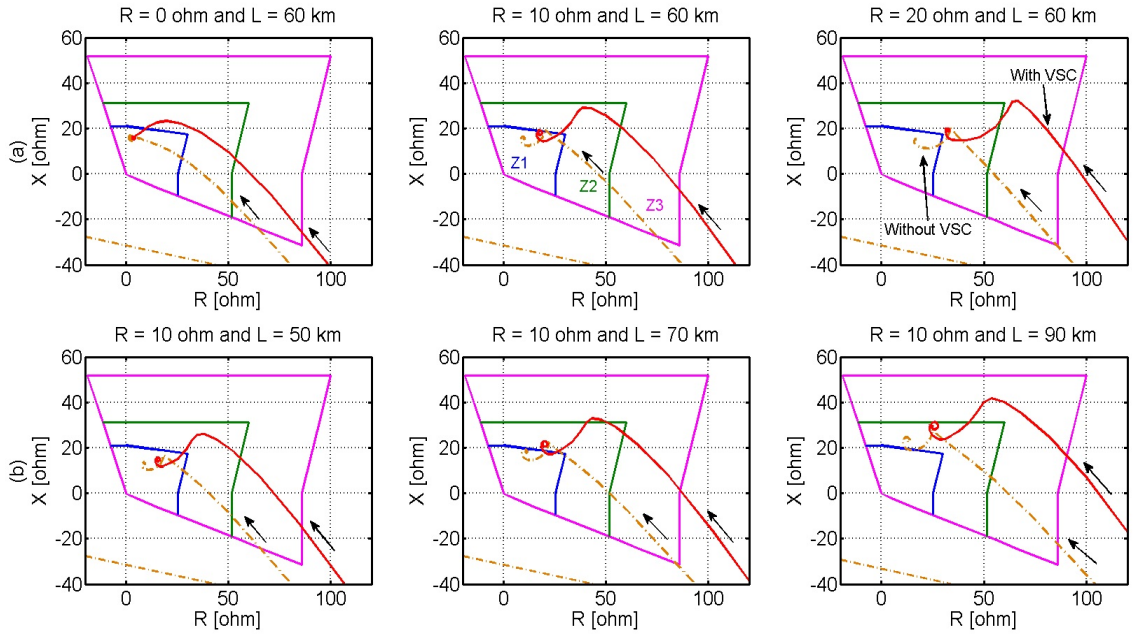


Figure 4.28: Impedance trajectory of ground AG element with and without VSC for phase-A to ground fault on Line 1. (a) L = 60 km with Rf = 0, 10, 20 $R_f = 0\Omega$ (b) L = 50, 70, 90 km with $R_f = 10\Omega$. (Solid Red Line: with VSC; Dotted Orange Line: without VSC).

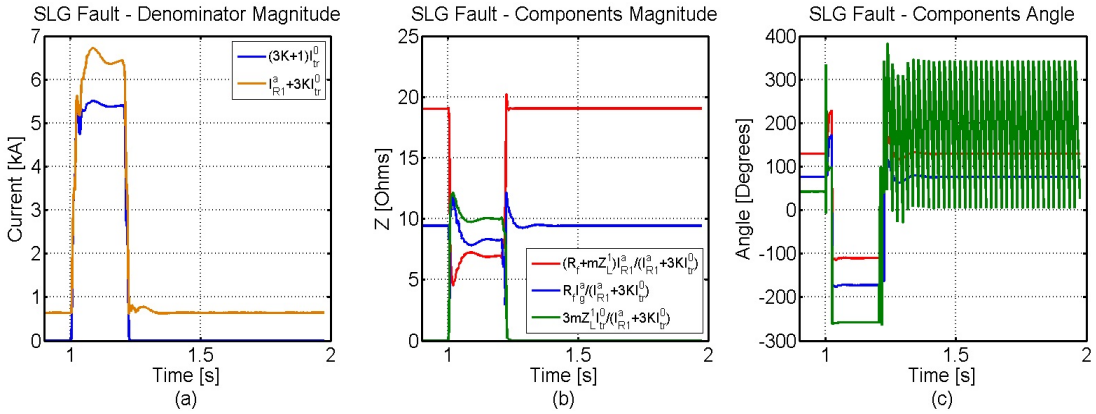


Figure 4.29: Phase-A to ground fault on Line 1 at 60 km from R1 with $R_f = 10\Omega$ (a) SLG Fault – magnitude of terms in the denominator. (b) SLG Fault – magnitude of terms in the expression (12). (c) SLG Fault – angle of terms in the expression (12).

the individual terms of the expression gives a clear idea about the apparent impedance seen by the distance relay during a SLG fault. At t = 1.1 s, the magnitude of the denominator of (4.25) is $|(I^a_{R1} + 3KI^0_{tr})| = 6.675$ kA, where the magnitude of $|(3K + 1)I^0_{tr})| = 5.49$ kA (see Figure 4.29(a)), which gives the first component $(R_f + mZ^1_L)I^a_{R1}/(I^a_{R1} + 3KI^0_{tr}) = 7.2\angle -110^0\Omega$, as shown in Figure 4.29(b) and (c). Furthermore, the second and the third component of (4.25) are $R_f I^a_g/(I^a_{R1} + 3KI^0_{tr}) = 7.86\angle -172.76^0\Omega$ and $3mZ^1_L I^0_{tr}/(I^a_{R1} + 3KI^0_{tr}) = 9.77\angle -258^0\Omega$, which gives the apparent impedance $Z^{AG}_{app} = 20.42\Omega$, as shown in Figure 4.28(a) for 60 km fault location and $R_f = 10\Omega$, highlighting the relay under reach when compared without VSC-HVDC.

4.9.2 *Phase-to-Phase Fault (LL)*

In another instance, a phase A to phase B fault is simulated on Line 1 at a distance of 60 km from R1 with $R_f = 10\Omega$ at t = 1 s. The PCC (Bus 5) voltage after the inception of phase A-phase B fault drops to 0.73 p.u. in comparison to the grid side voltage of 0.77 p.u., as

depicted in Figure 4.30(c). Since, the drop in the voltage is outside of the dead-band range (±0.1 p.u.); the VSC controller activates the active and reactive current limitation strategy by completely blocking i_d and setting i_q limit equal to I_{max}. The ac voltage controller starts injecting reactive current proportional to the PCC voltage drop multiplied by the gain of the controller (k) to support the network. Fault currents flowing through the local relay (*R1*) and the remote relay (*R2*) are presented in Figure 4.30(a) and (b), which indicates that the instantaneous fault current from the VSC is limited and modest in magnitude with a maximum peak of 3.85 kA in comparison to the remote relay *R2* current of 15 kA peak. Figure 4.30(a) also presents the difference in the fault current wave shape with the sub-transient, transient and steady state nature of current from the grid side.

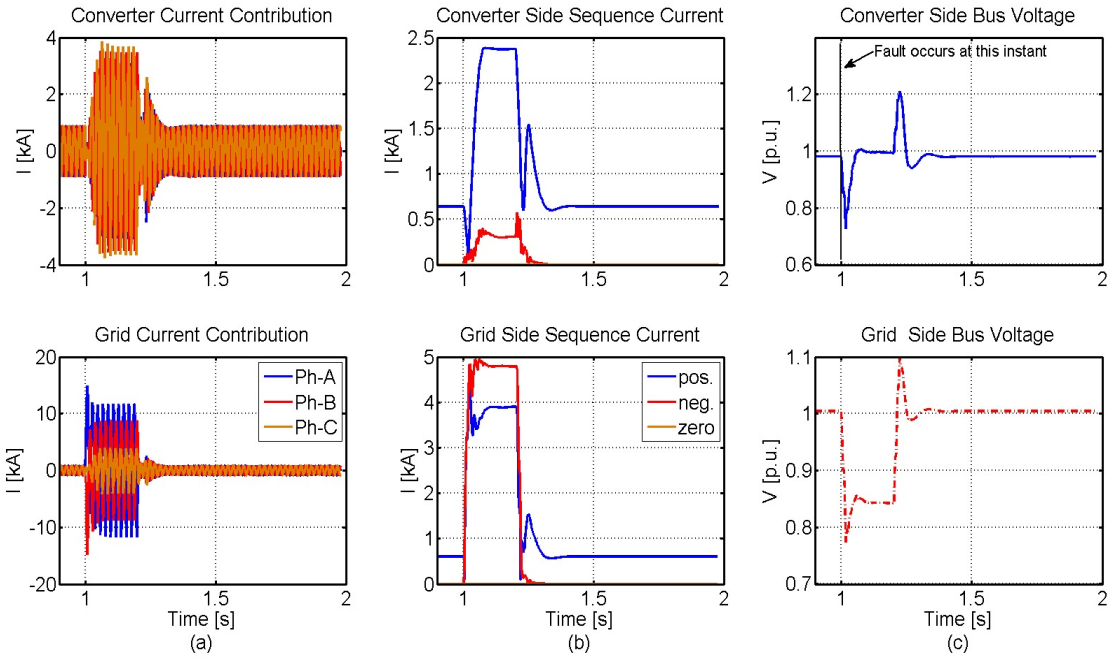


Figure 4.30: Phase A to Phase B fault on Line 1 at 60 km from R1 with $R_f = 10\Omega$ (a) Instantaneous current contribution. (b) Sequence current contribution. (c) RMS bus voltage. (Top: Converter side, Bottom: Grid side).

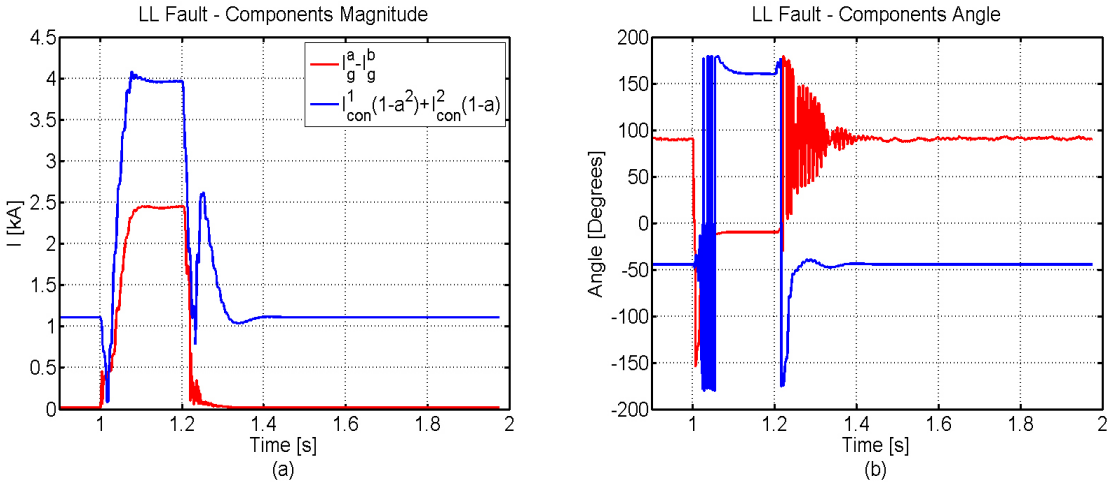


Figure 4.31: Phase A to Phase B fault on Line 1 at 60 km from R1 with $R_f = 10\Omega$. (a) LL Fault – magnitude of terms in the expression (19). (b) LL Fault – angle of terms in the expression (19).

It is important to assess the individual components of (4.32) to calculate the apparent impedance for a phase-phase fault. Figure 4.30(b) presents the sequence components of

currents supplied through the local (*R1*) and remote relay (*R2*) to feed the phase-phase fault. The positive sequence component of the fault current from the VSC drops to 0.02 kA in the 1st cycle after the fault, before rising to a value of 2.4 kA. The converter side negative sequence current (0.3 kA) is marginal with respect to the grid side negative sequence current (4.8 kA) due to the negative sequence current suppression, as shown in Figure 4.30(b). The first part of (4.32) corresponds to the positive sequence impedance of the line up to the fault point, which should be the actual impedance. The numerator of the second term consists of $(I_g^a - I_g^b)$ which is the difference between the faulted phase currents coming from the grid side with its magnitude and phase angle depicted in Figure 4.31(a) and (b), respectively. Similarly, the variation in the magnitude and phase angle of the denominator of the second term of the expression (4.32) are also elaborated in Figure 4.31. From the Figure 4.31, it can be noticed that $(I_g^a - I_g^b) = 2.45\angle -9.9^0$ kA and $(I_{con}^1(1-\alpha^2) + I_{con}^2(1-\alpha)) = 3.99\angle 160^0$ kA at t = 1.1 s. Consequently, the apparent impedance seen by the phase AB element of the distance relay R1 for the resistive fault at 60 km under reaches severely, as shown in Figure 4.32(a).

Moreover, Figure 4.32(a) presents the apparent impedance seen by the phase AB element of the distance relay *R1* with VSC for $R_f = 0\ \Omega$ and fault location of 60 km, where the locus enters into zone 1 with a different trajectory and reaches a steady state value similar to the case without VSC. On the other side, the locus fails to enter into zone 1 with fault resistances of 10 Ω and 20 Ω, although, the fault takes place in zone 1 reach of the relay i.e. 60 km. The relay under-reaches during a phase-phase fault with $R_f = 10\ \Omega$ and 20 Ω along with the reactive current injection from the VSC station as shown in Figure 4.32(a). For the $R_f = 10\ \Omega$ and fault location 60 km, the trajectory reaches a steady state value of R = 39 Ω, and X = 40 Ω, far from the actual fault impedance estimated in the absence of VSC-HVDC.

Furthermore, Figure 4.32(b) presents the case for the different fault locations of 50, 70 and 90 km with $R_f = 10\ \Omega$. It can be seen from Figure 4.32(b) that the locus of the apparent impedance for a zone 1 fault at 70 km without VSC-HVDC enters into zone 1 correctly and reaches a steady state before sending a correct trip signal to the breaker. Nonetheless, for the case of $R_f = 10\ \Omega$ and 70 km with VSC-HVDC connected to Line 1, the impedance locus of the AB element enters into zone 3 region, as appended in Figure 4.32(b), at 55 ms after the fault, finally reaching a steady state value of R = 41.7 Ω and X = 44 Ω, which is larger than expected. This is due to the reactive current injection and suppressed negative sequence current effect of VSC-HVDC on the distance relay operation. The relay under reaches heavily and is unable to operate successfully, jeopardizing the reliability of the protection scheme. The difference in trajectories of the fault impedance, in both the cases, highlights the impact of VSC-HVDC on the distance relay, which is evident from Figure 4.32.

4.9.3 *Three-Phase Fault*

Similar to the previous cases, this section discusses three-phase faults simulated on Line 1 with and without VSC-HVDC connection in the study system whose sequence network diagram is depicted in Figure 4.15(d). Figure 4.33(a) and (b) present the active and reactive power responses of the VSC side and the grid side for a three phase fault at 60 km and $R_f = 10\ \Omega$. It is clear that the VSC controller quickly adopts the limitation strategy by reducing the converter side active power to 0.0 MW from 400 MW (injection) and increasing the reactive power injection to +440 MVAR. The PCC voltage measured by *R1* drops to 0.25 p.u. (see Figure 4.33(c)) for a three-phase fault on Line 1 due to which the VSC controller injects reactive current into the network. Figure 4.34(b) is a clear representation of active and reactive current control, where active current i_d is limited to 0.0 p.u. and i_q boosts to achieve the maximum current $(I_{max} = 1.15\text{p.u.})$ allowed for the converter. Moreover,

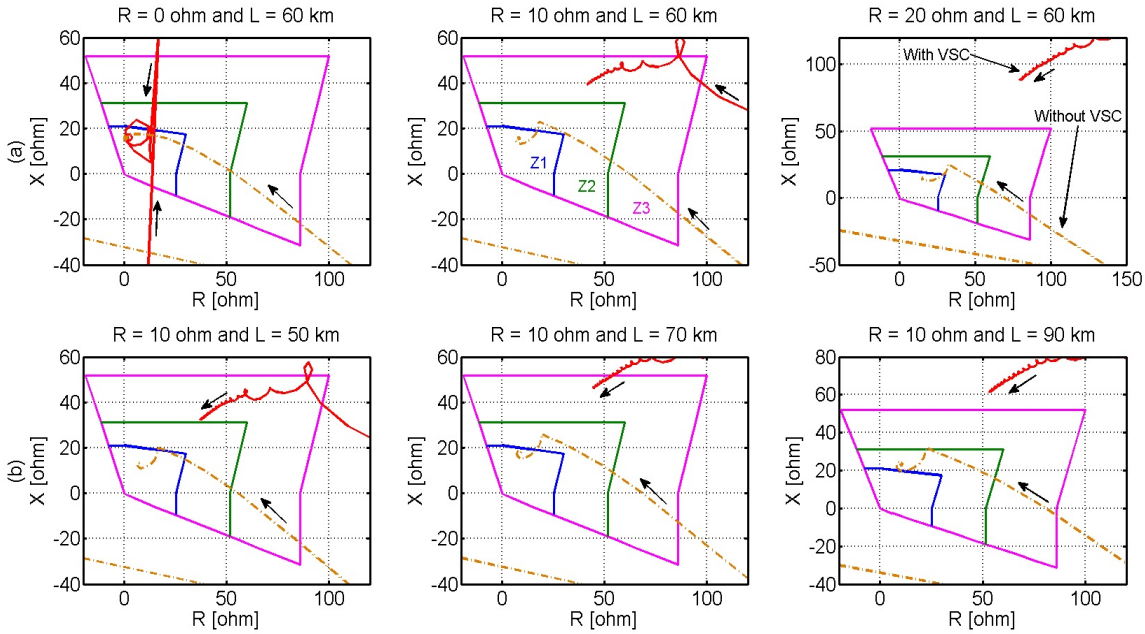


Figure 4.32: Impedance trajectory of phase AB element with and without VSC for phase-A to phase-B fault on Line 1. (a) L = 60 km with $R_f = 0, 10, 20\Omega$. (b) L = 50, 70, 90 km with $R_f = 10\Omega$. (Solid Red Line: with VSC; Dotted Orange Line: without VSC).

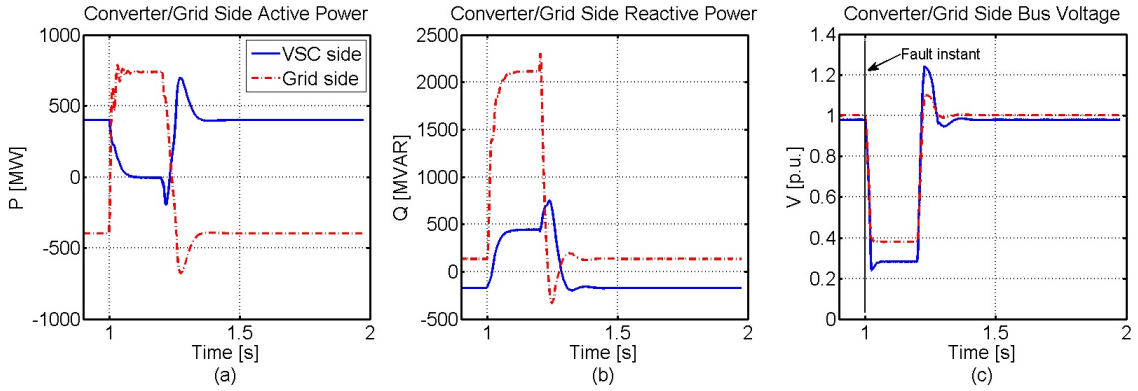


Figure 4.33: Three-phase fault on Line 1 at 60 km from R1 with $R_f = 10\Omega$ (a) Active power. (b) Reactive power. (c) RMS bus voltage. (Blue Solid Line: Converter side, Red Dotted Line: Grid side).

Figure 4.34(a) and (c) present the magnitude of dc link voltage and dc current in the both the positive and negative poles. The dc link voltage during the three-phase fault rises to 335 kV while the positive and negative pole currents drop to 0.0 kA. The rise in the dc link voltage is due to the sudden decrease in the dc pole current.

Figure 4.35(a) unveils the comparison between the instantaneous voltage of the VSC and grid side bus for a fault at 60 km and $R_f = 10\ \Omega$. The voltage is non-zero due to fault resistance and reactive support from the converter. However, the fault current from the VSC is completely reactive in nature, which can also be verified from Figure 4.34(b). The instantaneous fault current contribution from the converter is limited to 1.15 p.u. from each converter. Since, the arrangement is a bi-pole, thus the peak current reaches to 2.3 p.u., as depicted in Figure 4.35(b). Additionally, the sequence currents only consist of positive sequence current from both the VSC and the grid in Figure 4.35(c) because of balanced fault without involving the ground that is why neither negative nor zero sequence network is shown in Figure 4.15(d).

Figure 4.36 unfolds the transient trajectory of the impedance calculated by the phase distance element AB of the distance relay R1 for various fault resistances and fault locations.

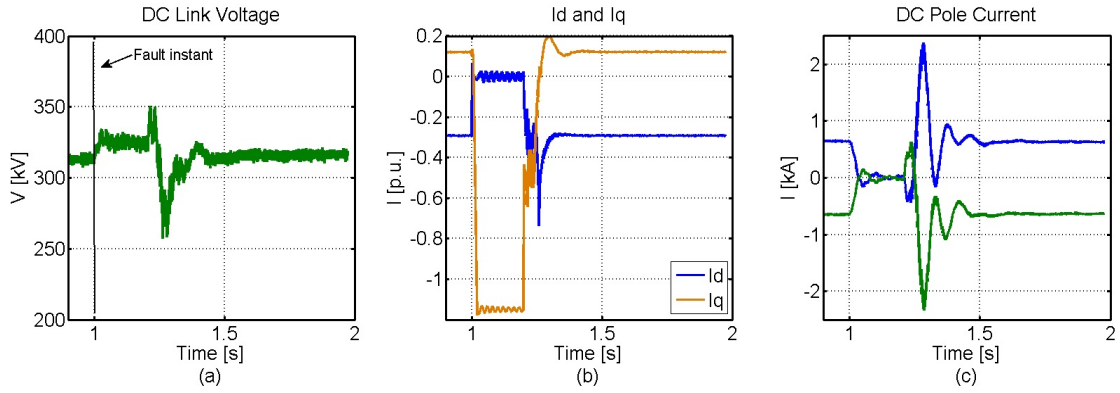


Figure 4.34: Three-phase fault on Line 1 at 60 km from R1 with $R_f = 10\Omega$ (a) DC link voltage. (b) I_d and I_q. (c) DC pole current.

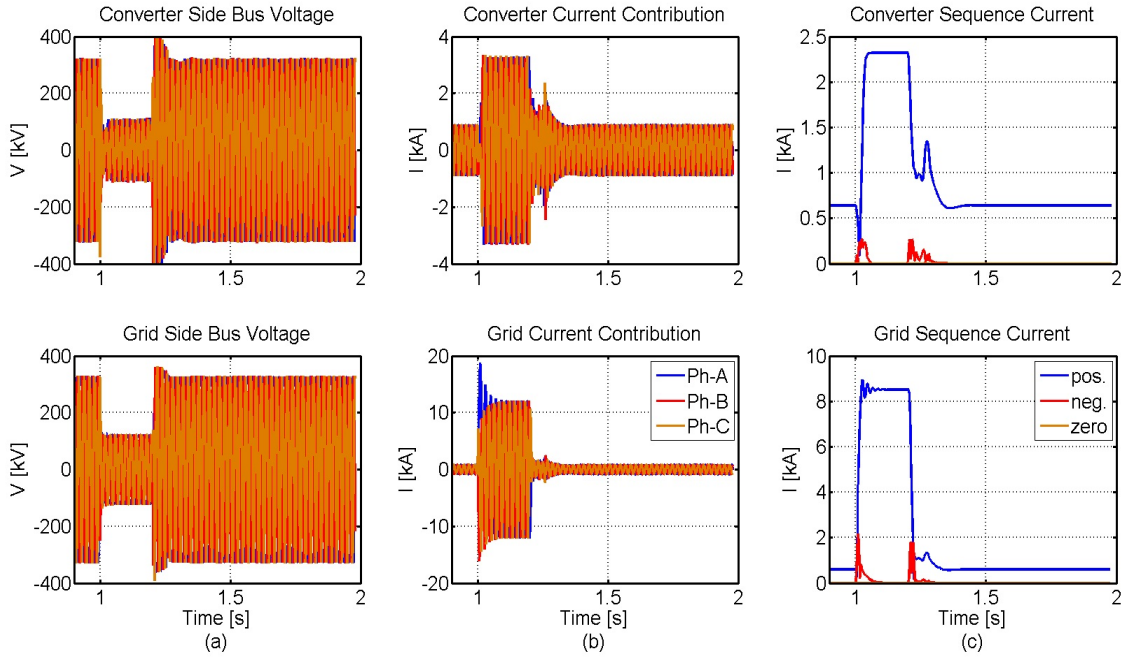


Figure 4.35: Three-phase fault on Line 1 at 60 km from R1 with $R_f = 10\Omega$ (a) Instantaneous bus voltage. (b) Instantaneous current contribution. (c) Sequence component of current contribution. (Top: Converter side, Bottom: Grid side).

The phase AB element enters into zone 1 for fault location at 60 km and $R_f = 0\Omega$ correctly similar to the condition without VSC. However, it under reaches heavily as R_f increases, as presented in Figure 4.36(a). The impedance seen by the phase distance element AB is far from the actual impedance due to the dominance of the grid positive sequence current and limited magnitude of converter positive sequence currents, as can be seen in Figure 4.35(c). Moreover, during a three-phase fault on Line 1 at a distance of 50, 70, and 90 km from *R1* with $R_f = 10\ \Omega$, the converter affects the distance relay R1 performance causing an under reach. The trajectory for 50 km fault is unable to enter into zone 1, as shown in Figure 4.36(b) and subsequently, the trajectory moves far away from the scenario without VSC-HVDC as the distance to the fault increases. The locus enters into zone 2 at 30 ms after the fault for 70 km. However, it does not settle in zone 2 and enters into zone 3 at 63 ms, as illustrated in Figure 4.36(b). The distance relay is unable to pick up for zone 1 because a steady state impedance has not been achieved.

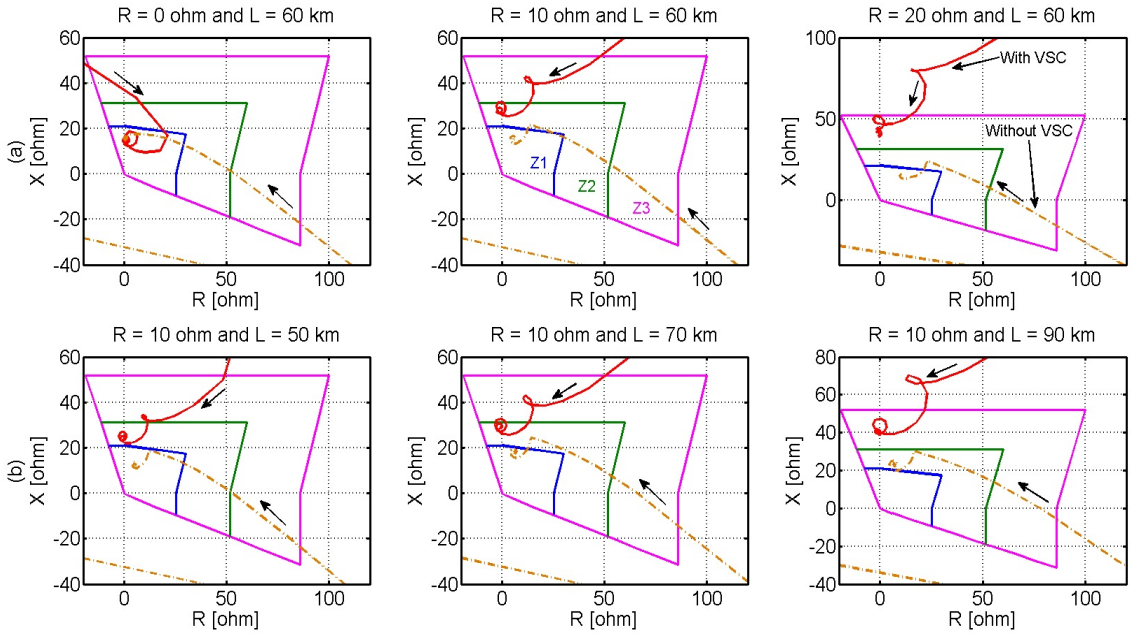


Figure 4.36: Impedance trajectory of phase AB element with and without VSC for a three-phase fault on Line 1. (a) L = 60 km with $R_f = 0, 10, 20\Omega$. (b) L = 50, 70, 90 km with $R_f = 10\Omega$. (Solid Red Line: with VSC; Dotted Orange Line: without VSC).

4.9.4 *Impact of Saturation Limits of Converter*

The impact of saturation limit of the converter is studied during phase-A to ground, phase-A to phase-B and three phase faults at 60 km from R1 with $R_f = 10\ \Omega$. The locus of the distance elements are plotted in Figure 4.37 for different saturation limits of the converter. Figure 4.37(c) narrates that the impedance seen by the distance element is R=-0.75 Ω, X=28.9 Ω for the saturation limit of 1.15 p.u. and R=-0.7 Ω, X=44 Ω for 0.50 p.u. during a three-phase fault. The impedance seen by the relay for different saturation limit of the converter has no effect during the phase to ground fault from Figure 4.37(a). However, Figure 4.37(b) presents the impact during phase-to-phase fault. Figure 4.37 concludes that the saturation limit of the converter affects the performance of the distance relay as under reach is higher for lower value of saturation.

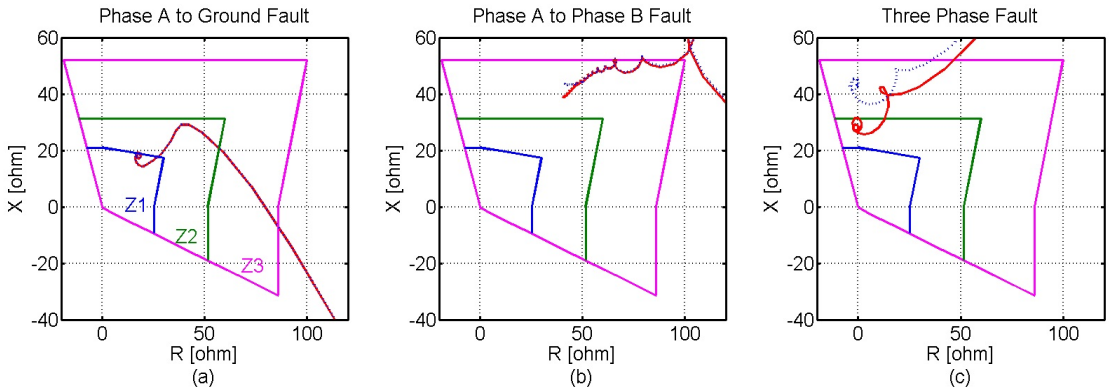


Figure 4.37: Impedance trajectory of distance elements with VSC for a fault on Line 1 at 60 km from R1 with $R_f = 10\Omega$. (a) Ground AG element. (b) Phase AB element. (c) Phase AB element. (Solid Red Line: with VSC; Dotted Orange Line: without VSC).

4.10 CONCLUSIONS

This chapter unveils that the distance protection of transmission lines connected to VSC-HVDC fails to operate during symmetrical and asymmetrical faults, when the converter provides reactive current support to the network along with the limitation strategy as suggested by the network guidelines for HVDC connections. The main conclusions of this chapter are extracted as follows.

1. Firstly, an analytical investigation is presented for the apparent impedance seen by the distance relay during asymmetrical faults for a VSC-HVDC connected transmission line. The mathematical analysis presented that the limited reactive positive sequence and suppressed negative sequence fault current from the converter, zero sequence from the transformer, grid current and fault resistance impacts the distance relay heavily.

2. The simulations presented that the impact of the reactive current injection to support the network voltage along with the active current blocking limitation strategy on the distance relay results in relay underreach of symmetrical and asymmetrical fault scenarios, which lead to wrong trip, eventually threatening the power system. The distance relay is also affected by the saturation limits of the converter in a way that the smaller is the saturation limit, the higher is the under reach.

3. Future power system will consist of more VSC based HVDC connected energy sources that poses a challenge to the operation of protection system due to the limited fault current, suppressed negative sequence current and reactive current support. Therefore, in order to accommodate VSC based HVDC connection into the network, an effective solution to update the protection system is the need of the hour that could either be an artificial intelligence based adaptive protection or wide area protection system based on synchrophasors. It is equally important to revise the grid codes for HVDC connections in order to include the VSC based new energy source technologies without influencing the protective devices.

5

LABORATORY SETUP & TESTING OF DISTANCE RELAY USING RTDS

Contents

5.1 Short Circuit Behaviour of VSC-HVDC 72
5.2 RTDS/RSCAD Description 72
5.3 RTDS Based Modeling 74
5.4 Signal Amplifier & Distance Relay 79
5.5 Relay Performance During Faults with VSC-HVDC Using Closed-Loop Test in RTDS 80
5.6 Results and Analysis 81
5.7 Conclusions 100



Georg Simon Ohm (1789-1854) was a German physicist and mathematician. As a school teacher, Ohm began his research with the new electrochemical cell, invented by Italian scientist Alessandro Volta. Using equipment of his own creation, Ohm found that there is a direct proportionality between the potential difference (voltage) applied across a conductor and the resultant electric current. This relationship is known as Ohm's law.

Chapter 4 presents the issues encountered by the distance protection of transmission line connected to Voltage Source Converter based High Voltage DC system when operated in conjunction with the modern network codes for HVDC connection. Modern NC codes supervise the TSO's to support the network voltage during any balanced or unbalanced voltage sag condition like faults by supplying the reactive current from the VSC-HVDC station into the network. The amount of reactive current injection by the VSC station depends upon the voltage drop of the PCC, which is governed by the slope of the line presented in Chapter 4. Furthermore, the grid codes do not stipulate any requirement of negative sequence current during any unbalanced fault condition. Thus, the impact of negative sequence current suppression on the performance of the relay is also studied. Firstly, the problem has been presented analytically and then an Electromagnetic transient based simulation on PSCAD/EMTDC is performed in the previous Chapter 4 .

Chapter 5 presents the experimental validation of hypotheses discussed in Chapter 4 to evaluate the performance of the distance relay by establishing a test setup utilizing RTDS, signal amplifier (F6350e) and a commercial distance relay (TPU L500), which validates the analytical & simulation study performed in the previous chapter. The experimental setup established is termed as a closed-loop test, which is an industrial practice to test any device before any field implementation.

This chapter is based on the following publication:

M. M. Alam, H. Leite, N. Silva, and A. S. Carvalho, "Performance Evaluation of Distance Protection of Transmission Lines Connected with VSC-HVDC System Using Closed-Loop Test in RTDS," Electric Power Systems Research, vol. 152, pp. 168-183, 11// 2017.

5.1 SHORT CIRCUIT BEHAVIOUR OF VSC-HVDC

The fault current characteristics of a conventional synchronous generator depends upon the transient and sub-transient reactance i.e. generator construction and represented by an equivalent voltage source behind the reactance[28] [133]. Contrary to this, the short circuit current from the VSC based HVDC is governed by its control systems (recommended by the grid code) and independent from the physics of transmission lines [138]. Moreover, the fault current contribution from the VSC is limited to a maximum of 1.15 times the rated nominal current in order to protect the power electronic devices from being damaged due to over current [139]. Hence, there is no significantly large difference between the nominal and the short circuit currents in both amplitude and wave shape during the fault in a VSC [139], [140].

This uncommon feature of a VSC based HVDC system during the fault or transient makes it hard to investigate for short circuits using any conventional short circuit analysis tools because an accurate transient model depicting its dynamic behaviour cannot be modelled [133], [141]. This unusual dynamic behaviour poses a challenge to the protection engineers regarding the reach setting calculation of the distance relay in the presence of VSC based HVDC system[29]. Nonetheless, the impacts of VSC-HVDC on the distance protection by studying its electromagnetic dynamic characteristics can be realized under small time scale in RTDS. This dynamic analysis of VSC's impact on the distance protection in RTDS has many advantages over the traditional methods. The traditional dynamic stability methods of relay testing are not helpful because they skip transient computation and possess limited ability to predict the relay behaviour. On the other hand, RTDS can model power system components in detail and considers the effect of transient phenomena, thereby testing the protective devices under realistic condition [142].

[28] The conventional voltage behind reactance equivalent circuit of synchronous machines is a physics-based equivalent circuit, in which the fault current is determined by the initial flux in the machine and time constants of decay.

[29] Fault analysis and setting of the protective relays throughout the grids have been historically founded upon the fact that SGs energize power systems that have high short circuit MVA level.

5.2 RTDS/RSCAD DESCRIPTION

RTDS performs fully digital electromagnetic transient power system simulation in real time; it utilizes, the Dommel Algorithm [143] similar to non-real time EMTP-type programs. Unlike analog simulators, which output continuous signals, digital simulators compute the power system at discrete instants of time. The time between the discrete instants is referred to as the time step. Typical time steps are in the order of 50–80 μsec [144].

The simulator with parallel processing architecture is specifically designed for power system simulations, which ensures continuous real-time operation. This type of simulator is an ideal tool[30] for designing, studying, and testing protection schemes. With features like closed-loop testing and batch processing, the simulator provides more flexibility for applications like single-pole tripping and reclosing, out-of-step conditions, remedial action schemes, etc. Using a real time digital simulator, the protective systems are continuously fed with the voltage and current signals resembling a realistic environment. Feedback signals, such as breaker status and relay trip and close, are interfaced between the software model and the protection system through a digital interface, as shown in Figure 5.1.

[30] RTDS is also very useful in modeling IGBT based converters very accurately as it consists of specific small time step library components, which helps in accurate computation.

5.2.1 *Processor Description*

Each RTDS rack includes either a GT Workstation Interface (GTWIF) card or a Workstation Interface (WIF) card to communicate between the RTDS rack and the computer workstation running the RTDS software. The communication is over an Ethernet based Local Area Network (LAN). The RSCAD/RunTime software of RTDS communicates with the GTWIF card's real-time operating system to send and receive messages associated with plot updates and user initiated events[31].

[31] e.g. change of a set-point via a Slider, Switch, push button, dial or other such RunTime component.

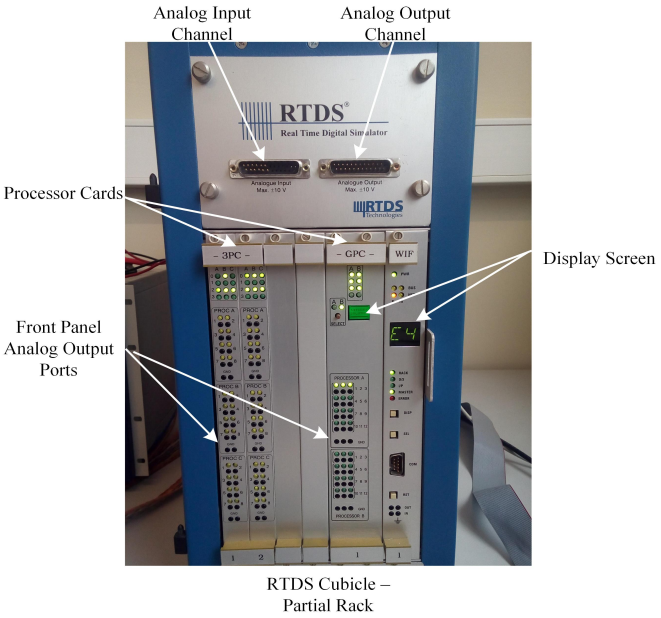


Figure 5.1: RTDS cubicle with analog ports and front panel interface.

The RTDS consists of GPC/PB5 processor cards used to solve the equations representing the power system and control system components modelled within the RTDS. An RTDS rack typically contains between 2 to 6 GPC/PB5 cards. Each GPC card includes two IBM Power PC 750GX processors running at 1 GHz and each PB5 card includes two Free scale PowerPC MPC7448 processors running at 1.7 GHz [144].

5.2.2 *Channel Description*

Each GPC card[32] includes two sets of twelve analogue output channels. The first set of twelve channels is accessible by the GPC's 'A' processor and the second set by the 'B' processor, as shown in Figure 5.3(a). The front panel analogue outputs from the GPC cards are provided for monitoring of selected signals on oscilloscope, as depicted in Figure 5.2. The analogue outputs are not optically isolated and do not include over-sampling. The front panel interface has a resolution of 12 bits and a voltage output of ±10 Volts, which is advised not to be used to test an external device [144].

[32]The earlier version of RTDS also consists of another processor called 3PC that has now become obsolete and has been replaced by PB5.

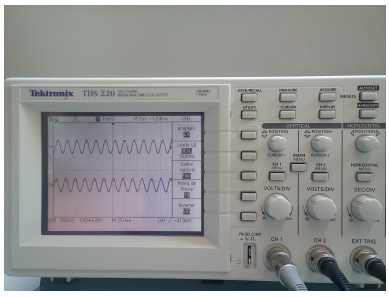


Figure 5.2: Oscilloscope output taken from the front panel analog interface of RTDS

5.2.3 *Analog & Digital Signal*

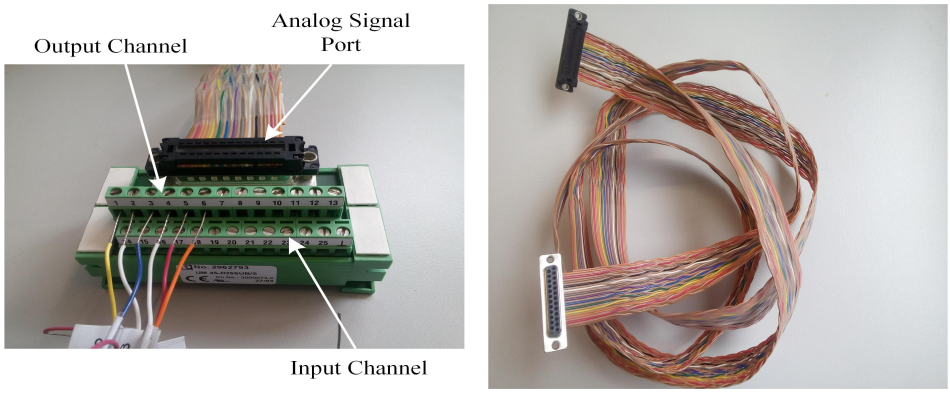
The Gigabit Transceiver Analogue Output (GTAO) Card is used to interface analogue signals from the RTDS to external devices. The GTAO card includes twelve, 16 bit analogue output channels with an output range of ±10 volts, as shown in Figure 5.3(b). The 16 bit Digital to Analog Converter (DAC)s provide a wide dynamic range. Such a wide dynamic range may be required when using the GTAO to send measured current signals to an external protection device [144]. The output's are over sampled at a rate of 1 µs and the card's output channels are updated synchronously. Figure 5.4(a) and (b) depicts the analog board and cable to fetch signals from the RTDS.

The Gigabit Transceiver Digital Input (GTDI) Card is used to interface digital signals from an external device to the RTDS. The GTDI card includes 64 optically isolated digital input channels. A digital board and a special cable is utilized to transfer externally generated digital signals back into the RTDS, as shown in Figure 5.5(a) and (b).



(a) (b)

Figure 5.3: (a) 12 bit resolution analog front panel. (b) 16 bit resolution of analog ports.



(a) (b)

Figure 5.4: (a) 16 bit resolution analog interface board. (b) Analog cable.

5.2.4 *RSCAD & RunTime Environment*

RSCAD is the Graphical User Interface (GUI) based software module of the RTDS to design and model the power system and study the behavior through real-time simulation. RSCAD software platform helps the RTDS to generate the signals required for closed-loop testing and batch processing. It has its own rich library of components that helps the user to build the study system and analyze it in RunTime environment[33].

[33] RunTime environment is a real-time simulation environment in RSCAD during which the study system is solved in RTDS using Dommel algorithm.

5.3 RTDS BASED MODELING

The RTDS solves the power system model in discrete and fixed time step of 50-80 µs, which actually depends upon the network size and the available RTDS processors [13]. Furthermore, it also provides small time step computational feature in order to solve the VSC model in 1.4 to 2.5 µs. Nowadays, the relay manufacturers and utilities are completely relying on the RTDS to perform extensive transient fault studies to verify the performance

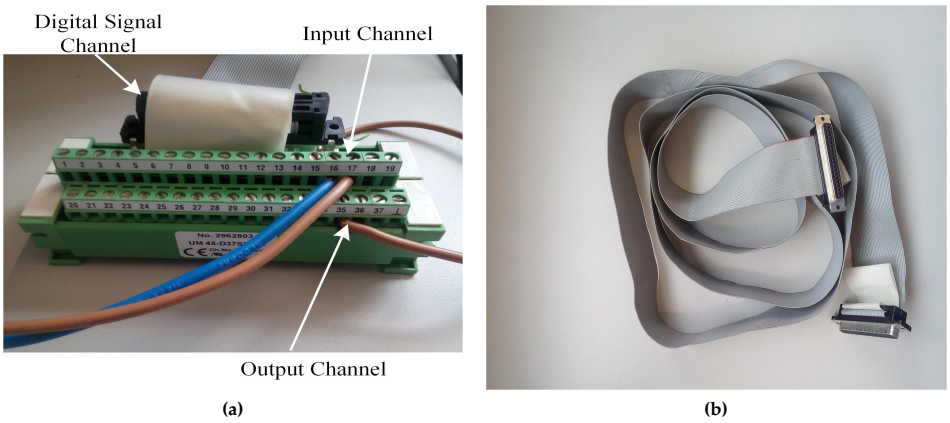


Figure 5.5: (a) Digital interface board. (b) Digital channel cable.

of the protection system and the applied settings before commissioning them into service [145].

5.3.1 *Power System Model in RTDS*

An important requirement of the electromagnetic transient based study is an accurate representation of the electrical and electromechanical properties of the power system components [142]. Nonetheless, the detail model[34] of power system components occupies a large chunk of space and drastically reduces the processing speed. Thus, it is a common practice to reduce the remaining power system into its equivalent and represent the small portion of the system under study in detail, ultimately saving the computer resources.

[34]Each of the component in RTDS occupies space in its processor cards like power system and control system components occupies space in PB5 cards while VSC small time-step components occupy space in GPC cards.

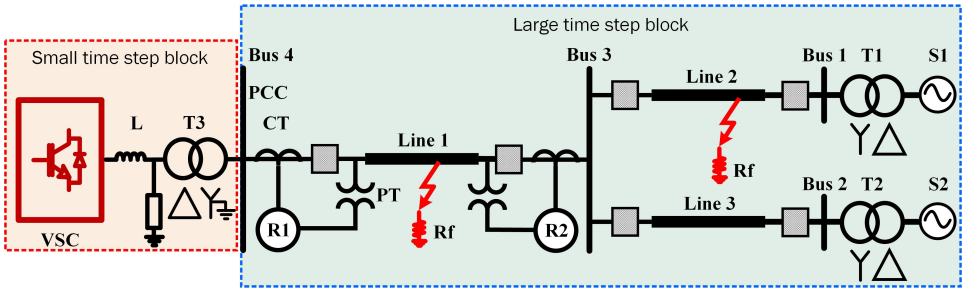


Figure 5.6: Sample power system with VSC-HVDC connection modeled in RTDS platform

Figure 5.6 presents a 400 kV, 50 Hz, sample power system that includes transmission lines, generators, transformers, circuit breakers, Current Transformer (CT) (3000 A/1 A), Potential Transformer (PT) (400 kV/110 V), VSC station, and distance relays. The transmission lines between Bus 1, Bus 2, Bus 3, and Bus 4 are each of 100 km long and modeled with distributed parameters. The CT and PT are modeled to supply the current and voltage to the distance relay under test. The MVA rating of the VSC transformer[35] is 1000 MVA and in delta/star grounded configuration with delta winding on the VSC side. The power system components are modeled in detail and solved with a large time step of 80 µs. On the other hand, the entire VSC station along with the converter reactor (L), and interface transformer (T3) is modeled and solved with a small time step of 1.4 µs. This is because a small time step of 1.4 µs assists in processing the high frequency (1.5 to 2 kHz) PWM signals and firing the switches more precisely [146]. The small time step VSC block is interfaced with the large time step ac system through the interface transformer, as shown in Figure 5.6.

[35]The three-phase transformer studied in RTDS has been modeled in detail and serve as an interface between the VSC and large time step power system..

5.3.2 *VSC-HVDC Model*

[36]The RTDS is capable of simulating IGBT and GTO devices modeled as ideal switches. Furthermore, each RTDS GPC processor card can simulate 18 single phase switches

The VSC is a two-level converter[36] based on IGBT and anti-parallel diode modeled in detail inside small time step VSC subnetwork of RTDS. The dc side of VSC has a voltage level of $\pm$320 kV. The ac side of VSC-HVDC is connected to the 400 kV ac network through a reactor of inductance (0.1 p.u.) and a converter transformer (0.1 p.u. leakage reactance) of voltage ratio 320/400 kV in delta/star grounded configuration. The converter transformer in the RTDS model serves as an interface between the small time and large time step blocks, as unveiled in Figure 5.7. The VSC subnetwork also consists of a high-pass filter to provide a low impedance path to ground for the high-frequency harmonic currents. The VSC-HVDC specifications are listed in the Appendix A.

5.3.3 *VSC-HVDC Control*

The control block diagram of the VSC-HVDC system, as presented in Figure 5.7, is modeled in large time step block, which includes a PLL, a positive and a negative sequence inner current (i_{vdq+}, i_{vdq-}) control loops, the outer active power (P_{ac}), and the ac voltage (U_{PCC}) control loops. The conventional vector current control is utilized in the form of inner current control that is based on the control of two independent current components, *d*-axis and *q*-axis in the dual SRF to control simultaneously the positive and the negative sequence currents while the PLL helps in the synchronization [51].

5.3.4 *Outer Control Loop - Positive Sequence*

The outer positive sequence control consists of an active power (P_{ac}) control and the PCC voltage control (U_{PCC}), which generates positive sequence *d*-axis and *q*-axis current references for the fast inner current control, respectively. The mathematical representation for the active power control can be given by (5.1) as:

$$i_{vd+}^{ref} = (k_p^{P_{ac}} + \frac{k_i^{P_{ac}}}{s})(P_{ac}^{ref} - P_{ac}) \tag{5.1}$$

where $k_p^{P_{ac}}$ is the proportional gain, $k_i^{P_{ac}}$ is the integral gain of the PI controller and P_{ac} is the measured active power flow from the VSC-HVDC station into the grid. The PCC voltage control consists of a slow reactive current control loop operating during the normal condition and a fast reactive current injection scheme activated during ac network disturbance/fault, as per grid code guidelines for HVDC connections [78]. Equation (5.2) presents the ac voltage control as:

$$i_{vq+}^{ref} = (k_p^{U_{PCC}} + \frac{k_i^{U_{PCC}}}{s})(U_{PCC}^{ref} - U_{PCC}) + i_{vq+}^{ARCI} \tag{5.2}$$

where $k_p^{U_{PCC}}$ is the proportional gain, $k_i^{U_{PCC}}$ is the integral gain of the PI controller, U_{PCC} is the rms value of measured PCC voltage and i_{vq+}^{ARCI} is the positive sequence Additional Reactive Current Injection (ARCI) from the VSC station during any ac faults. Figure 5.7 also highlights the positive sequence outer control loops where the fast reactive current injection i_{vq+}^{ARCI} implemented as a proportional control with gain (k) operates in parallel to the slow PI-based PCC voltage control. The additional reactive current injection scheme is activated only when the PCC voltage (U_{PCC}) drops or rises by 0.1 p.u. (i.e. dead-band).

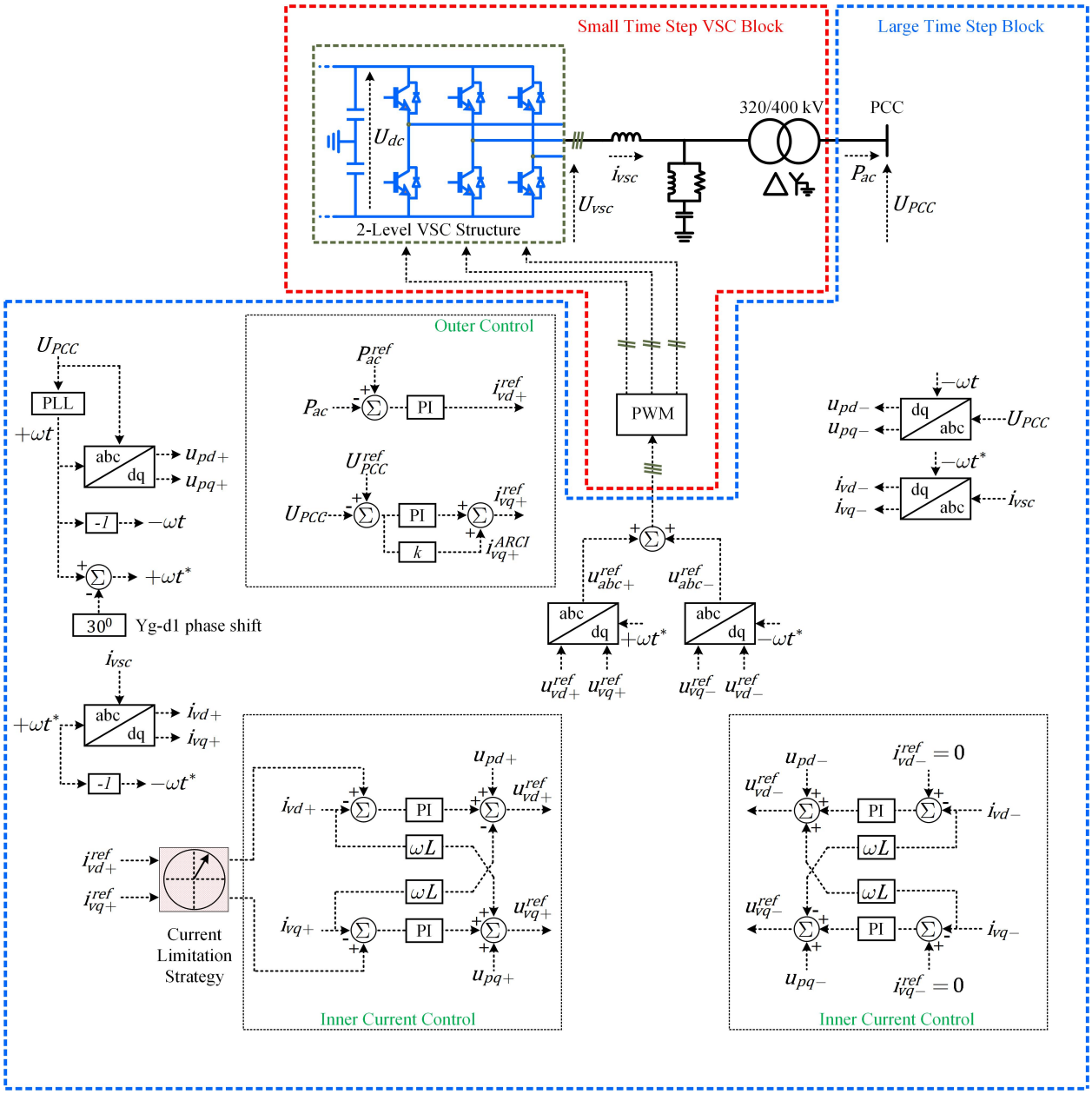


Figure 5.7: VSC-HVDC system with control block modeled in RTDS platform.

5.3.5 *Outer Control Loop - Negative Sequence*

It is well known that any unbalanced ac network condition like asymmetrical fault gives birth to the negative sequence current in the system, ultimately leading to the flow of large unbalanced fault currents. These large unbalanced fault currents might damage the converter switches if not controlled properly. Furthermore, the combined flow of positive and negative sequence current during the fault limits the amount of positive sequence reactive current injection (i_{vq+}^{ARCI}) needed to support the ac network voltage or might violates the overcurrent capacity of the converter. Consequently, a negative sequence current suppression strategy is implemented as the negative sequence outer control loop to balance the ac fault currents and provide room for the positive sequence reactive current injection. The negative sequence current can be suppressed to zero by supplying d-axis and q-axis negative sequence reference currents ($i_{vd-}^{ref} = 0$) and ($i_{vq-}^{ref} = 0$) to inner current control, as shown in Figure 5.7.

5.3.6 *Inner Current Control Loop – Positive & Negative Sequence*

Consequently, the generated *d*-axis and *q*-axis positive (i^{ref}_{vdq+}) and negative (i^{ref}_{vdq-}) sequence reference currents are passed to the inner current control loops from where *d*-axis and *q*-axis positive (u^{ref}_{vdq+}) and negative (u^{ref}_{vdq-}) sequence reference voltages are generated after the decoupling of active and reactive currents by the addition of feed-forward compensation terms to the outputs of the *d*-axis and *q*-axis inner current controllers. Furthermore, the *d*-axis and *q*-axis reference voltages (u^{ref}_{vdq+}) and (u^{ref}_{vdq-}) are passed through the *dq-abc* block to generate the positive sequence and the negative sequence three-phase modulation signals, as depicted in Figure 5.7. The three-phase modulation signals are further exported into the VSC small time step subnetwork block to generate high precision firing pulses to fire the IGBTs.

5.3.7 *Fault Response of VSC Controller*

In addition to the normal behavior of the VSC-HVDC station when the PCC voltage (U_{PCC}) is in the range of 0.9 to 1.1 p.u, the behavior of VSC-HVDC is also governed by the control system during any abnormal grid condition. Once the PCC voltage drops below 0.9 p.u., the grid code for HVDC connections suggest the TSO to support the ac network voltage by injecting an additional reactive current from the VSC-HVDC station during any faults explained in Chapter 4.

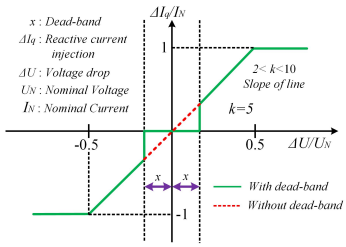


Figure 5.8: Reactive current slope for voltage support by the VSC-HVDC system.

During the fault condition, the fast positive sequence reactive current injection (i^{ARCI}_{vq+}) is activated with the proportional gain of the controller (k) set in the range between 2 p.u. to 10 p.u., as shown in Figure 5.8. In addition to this, the outer active power PI controller and the slow PCC voltage PI controller are freezed throughout the fault duration. Furthermore, the active current blocked or reactive current priority limitation strategy is activated as soon as the voltage drops below the dead-band. If the active current blocked current limitation strategy is selected then the positive sequence active current (i_{vd+}) is reduced to zero whereas the fault current contribution from the VSC comprises of only the positive sequence reactive current injection. On the other hand, if the reactive current priority strategy is selected then the short circuit current from the VSC-HVDC station comprises of both the positive sequence active and reactive current.

Apart from the VSC control block, the model also includes fault control block, circuit breaker control block, and input/output control block. The fault control block is used to control fault duration, fault location, fault resistance and fault inception time. The circuit breaker control block allows the breaker to be controlled by the digital signals from the distance relay. Moreover, the input/output block sends the analog and digital signals in and out of the RTDS.

5.3.8 *Transmission Line model*

Travelling wave transmission line models and PI section models are both available to represent transmission lines on the RTDS. However, travelling wave models are generally preferred unless the line in question is very short, in which case a PI section model must be used. Travelling wave models are distributed parameter representations of transmission lines and are much more accurate for modelling long lines than the lumped parameter representation inherent in PI section models. It provide a means for separating the power system into mathematically isolated sub-systems which can be run on separate RTDS Racks, if required.

5.4 SIGNAL AMPLIFIER & DISTANCE RELAY

5.4.1 *Voltage & Current Signal Amplifier*

Signal Amplifier

The analog channel of the RTDS can only give an output signal between ±10 V (peak), which is insufficient to operate the distance relay. Hence, a signal amplifier is needed to enhance the voltage and current signals to the relay operating magnitude, as depicted in Figure 5.10. A special low-level signal cable is used for this purpose in order to transmit the signals from the RTDS to the signal amplifier. The secondary current and the secondary voltage of the CT and PT from the RTDS, respectively, are passed through the signal amplifier to obtain 110 V phase-to-phase (rms) (see Figure 5.9) and 1 A under normal operating condition. The signal amplifier can only accept a maximum of 6.78 V (rms) as a low level input signal for voltage amplification and a maximum of 3.4 V (rms) for current amplification from the RTDS, as presented in Figure 5.15.

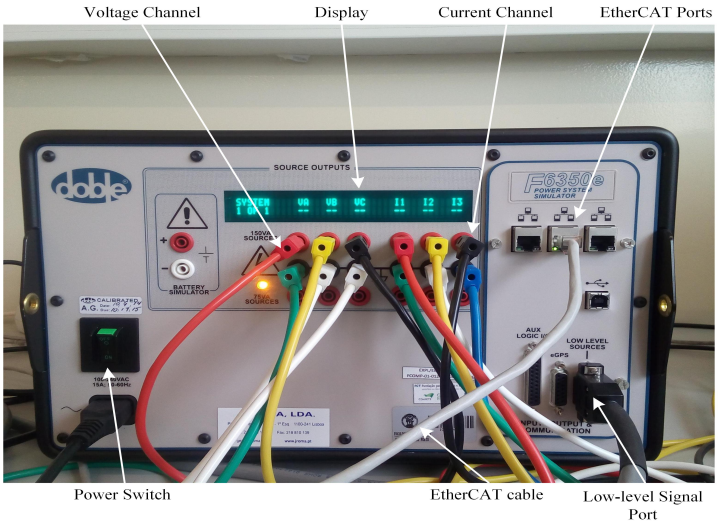


Figure 5.10: F6350e signal amplifier.



Figure 5.9: Multimeter during closed-loop test.

Low Level Signal Channel & EtherCAT Communication

Once an instrument is configured to perform as an amplifier, you must inject the proper voltage signals from a simulator, such as the RTDS system, to produce the desired outputs. This is done by using the Universal Low-Level Sources cable for each F6350e, as shown in Figure 5.12(a). This cable contains 12 twisted-pair leads that connect to the pins of the Low Level Sources connector. Each of these pins controls the output from one of the upper or lower channels of the amplifier, as shown in the Figure 5.12(b). The amplifier is being controlled through EtherCAT communication, as shown in Figure 5.11.



Figure 5.11: EtherCAT ports on a signal amplifier.

5.4.2 *Distance Relay*

A commercial distance relay TPU L500 with quadrilateral characteristics based reach settings (given in Appendix A) to protect Line 1 (see Figure 5.6) is utilized. The distance relay is classified into three zones of protection where Zone 1 covers 80% of Line 1 i.e. 80 km from R1 with an instantaneous operating time. Zone 2 covers unto 120 km from relay R1



(a) (b)

Figure 5.12: (a) Low level signal cable. (b) Low level signal channel.

with an operating time of 250 ms and Zone 3 up to 200 km and an operating time 1000 ms.

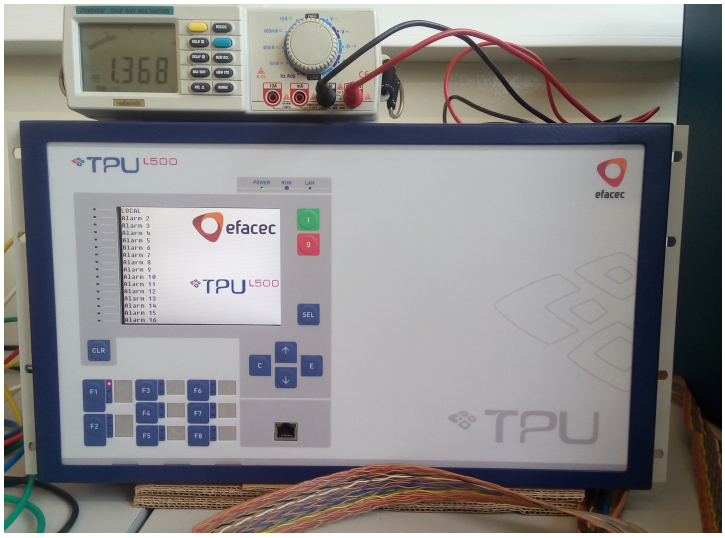


Figure 5.13: A commercial distance relay TPU L500.

5.5 RELAY PERFORMANCE DURING FAULTS WITH VSC-HVDC USING CLOSED-LOOP TEST IN RTDS

A closed-loop experimental setup has been established using RTDS, voltage and current signal amplifier (F6350e), and commercial distance relay (TPU L500), as presented in Figure 5.14.

Experimental Closed-Loop Test Setup

The setup of the closed-loop test in RTDS involves following steps:-

- Model the power system in RSCAD software module of RTDS.
- Model the CT & PT and send the secondary current and voltage out of RTDS through the analog output channel, as shown in Figure 5.15 and Figure 5.14.
- Amplify the current and voltage signals using F6350e signal amplifier in the range of 1 A and 110 V (phase-phase rms), as presented in Figure 5.15.

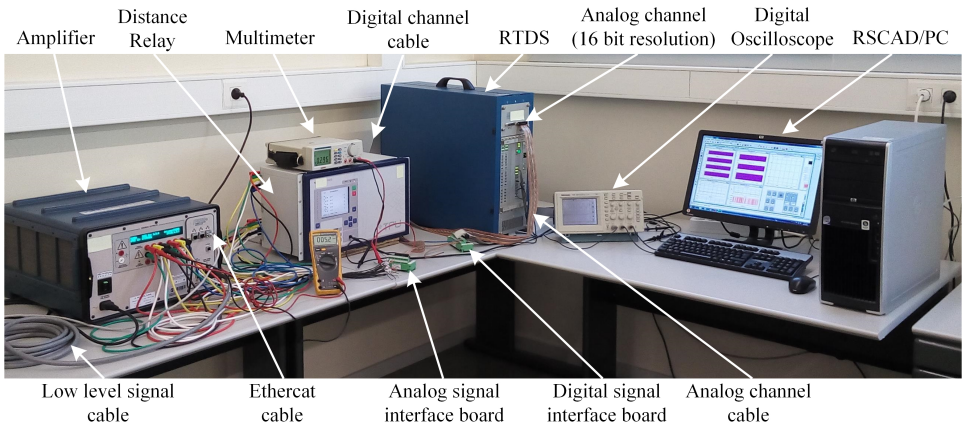


Figure 5.14: Experimental closed-loop test setup using RTDS, F6350e amplifier, and TPU L500 distance relay.

- Pass the amplified current and voltage signal from the amplifier to the TPU L500 commercial distance relay.
- The logical outputs from the relay as digital signals in terms of Circuit Breaker (CB) trip are supplied back into the RTDS forming a closed loop.

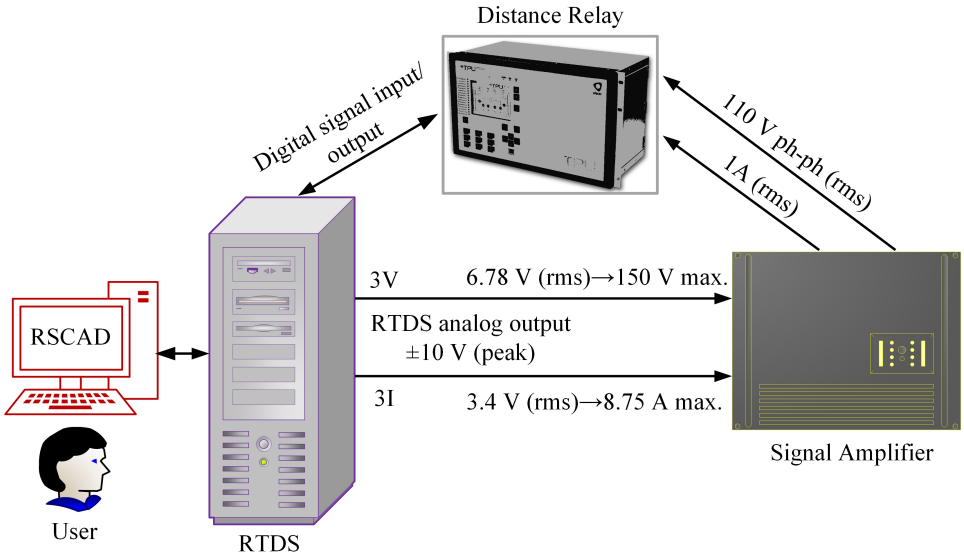


Figure 5.15: A pictorial representation of a commercial distance relay in a closed-loop arrangement using RTDS.

5.6 RESULTS AND ANALYSIS

The impact of the VSC-HVDC connection on the performance of the distance relay is evaluated using the closed-loop test in RTDS for different fault scenarios by following the grid code of reactive current support and current limitation strategy. Different faults are studied on *Line 1* for a duration of 200 ms (10 cycles). The oscillograph responses of the distance relay are recorded for these fault scenarios in terms of digital pickup and trip signals. The voltage and current signals coming out from the analog output channel of the RTDS are also recorded using an oscilloscope and compared with the simulation results.

5.6.1 *Single Phase to Ground Fault*

Case 1: Fault Location = 70 km, $R_f = 10\Omega$ with Active Current Blocked Limitation Strategy

At t = 1 s, a Phase A to ground fault is created on *Line 1* at a distance of 70 km from Bus 4 (PCC) for a duration of 200 ms with $R_f = 10\Omega$ and the active current blocked limitation strategy. Figure 5.16 presents the bus voltage, active power, reactive power, current contribution, sequence currents and sequence voltages on the VSC side (Bus 4) and on the grid side (Bus 3) during the fault as well as pre and post-fault duration. The PCC voltage drops to 0.80 p.u. soon after the inception of phase-A to ground fault in comparison to the grid side rms voltage of 0.87 p.u. (see Figure 5.16(a)). Since, the drop in the PCC side voltage is more than the dead band (0.1 p.u.), the VSC controller activates the additional positive sequence reactive current injection control within 20 ms after the fault detection. The VSC also adopts the current limitation strategy by completely blocking the positive sequence active current ($i_{d+}^{lim} = 0.0$p.u.) and fixing the reactive current limit (i_{q+}^{lim}) equal to 1.15 p.u.).

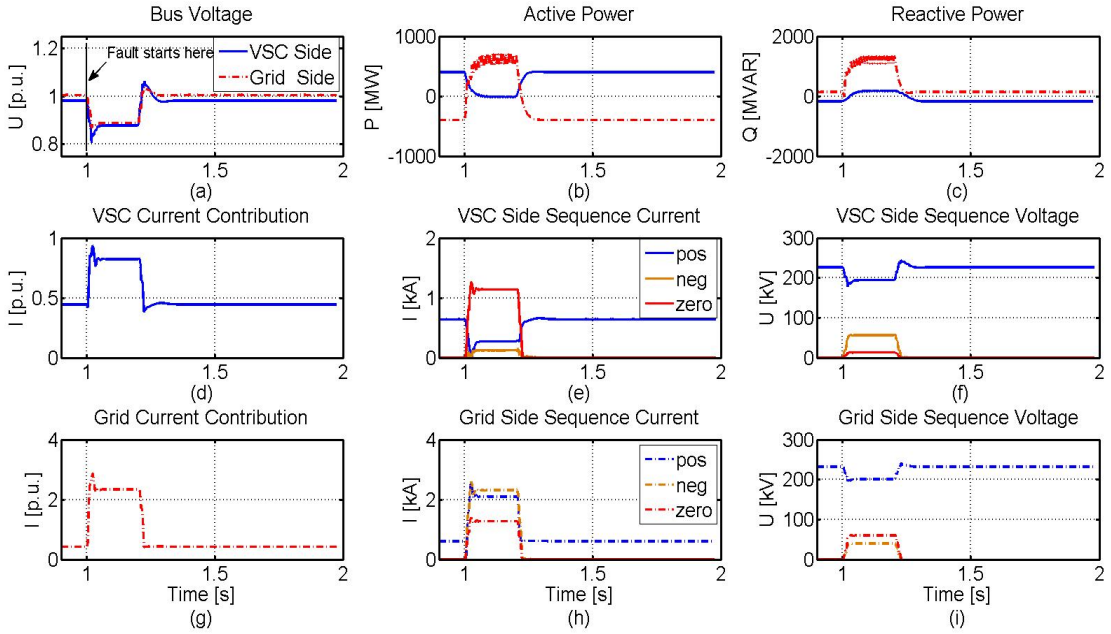


Figure 5.16: Phase A to ground fault on Line 1 at 70 km from *R1* with $R_f = 10\Omega$ and active current blocked current limitation strategy. (a) Bus voltage (RMS). (b) Active power. (c) Reactive power. (d) VSC current contribution. (e) VSC side sequence current. (f) VSC side sequence voltage. (g) Grid current contribution. (h) Grid side sequence current. (i) Grid side sequence voltage.

Due to the activation of this limitation strategy, the active power contribution from the VSC drops from 400 MW to 0.0 MW during the fault, as can be seen in Figure 5.16(b). The VSC recovers the active power contribution from 0.0 MW to 400 MW after the limitation strategy is removed due to the disappearance of fault from *Line 1* at t = 1.2 s. Similarly, the reactive power jumps from -172 MVAR (drawn from the network) to 200 MVAR (injected into the network by the VSC) (refer Fig. Figure 5.16(c)), which is evident that the reactive current injection controller and limitation strategy are performing correctly during the fault.

On the other hand, the active and reactive power flow from the grid side reverses from -400 MW to 698 MW (maximum peak) and 134 MVAR to 1332 MVAR (maximum peak) for the period of fault, as depicted in Figure 5.16(b) and Figure 5.16(c). The instantaneous active and the reactive power flowing through the network consist of second harmonic oscillating component due to the unbalance in the voltage and current during the asymmet-

rical fault that disappear as soon as the fault is cleared from the Line 1 (refer Figure 5.16(b) and Figure 5.16(c)). Furthermore, it is evident from the Figure 5.16(a) that not only the PCC voltage improved from 0.80 p.u. to 0.88 p.u., the grid side voltage also improved from 0.87 p.u. to 0. 89 p.u. due to the reactive current support by the VSC.

Figure 5.16(d) and Figure 5.16(g) unveils the rms fault current contribution from the VSC and the grid during the phase A to ground fault. The VSC starts injecting 0.82 p.u. of reactive fault current, as the active current is limited to zero value in comparison to the grid side contribution of 2.33 p.u., which indicates the modest fault behaviour of VSC. Furthermore, the investigation into the sequence currents contribution highlight the suppression of the negative sequence current supplied from the VSC due to the negative sequence inner current controller to provide complete room to the positive sequence reactive current support, as shown in Figure 5.16(e). The zero sequence current during the ground fault is supplied through the star grounded winding of the VSC side transformer and independent from the VSC due to the delta winding. On the other hand, Figure 5.16(h) depicts the grid side positive, negative and zero sequence components of fault currents. The zero and the negative sequence voltage during the phase A to ground fault of the PCC bus rises to 13 kV and 56 kV in comparison to the grid side zero and negative sequence voltage of 60 kV and 39 kV, as presented in Figure 5.16(f) and Figure 5.16(i).

Case 2: Fault Location = 85 km, $R_f = 20\Omega$ with Reactive Current Priority Limitation Strategy

Similar to the previous case 1, another Phase A to ground fault is analyzed on Line 1 at a distance of 85 km from Bus 4 (PCC) for a duration of 200 ms with $R_f = 20\Omega$ and this time with the reactive current priority limitation scheme. The PCC and the grid side rms voltage drops to 0.93 p.u. soon after the inception of phase-A to ground fault, as seen in Figure 5.17(a). Since, the drop in the PCC side voltage (0.07 p.u.) is not more than the dead band (0.1 p.u.), the VSC controller does not activate the additional positive sequence reactive current injection after the fault detection. The VSC in this case adopts the reactive current priority current limitation strategy where the positive sequence reactive current limit is set equal to the positive sequence reactive current reference ($i_{q+}^{lim} = i_{vq+}^{ref} \leqslant 1$) and the remaining space is allocated to the positive sequence active current.

The active power contribution from the VSC side drops slightly from 400 MW to 375 MW during the phase A to ground fault with the reactive current priority current limitation scheme, as presented in Figure 5.17(b), which is entirely different from the previous case. Similarly, Figure 5.17(c) presents that the reactive power flow from the VSC reverses from -172 MVAR to near to zero, which validates that no reactive current support should be supplied from the VSC in case the PCC bus voltage does not breach the dead band. The active power and the reactive power acquire the pre-fault power level as soon as the fault disappears from the Line 1 (refer Figure 5.17(b) and Figure 5.17(c)). Figure 5.17(d) and Figure 5.17(g) present the rms fault current contribution from the VSC and the grid side, which is 0.7 p.u. and 2.0 p.u., respectively. The fault current contribution from the VSC consists of both the positive sequence active and the reactive current due to the reactive current priority limitation scheme.

Moreover, Figure 5.17(e) and Figure 5.17(h) show the sequence components of fault currents from the VSC side and the grid side, respectively. The zero sequence component of fault current from the VSC transformer rises to 0.8 kA while the negative sequence component of fault current from the VSC drops to 0.0 kA due to the negative sequence current suppression control. Contrary to this, the grid side zero and negative sequence current rises to 1.32 kA and 2.11 kA from zero during the phase A to ground fault. Analysing the sequence voltages of the PCC bus and the grid side bus in Figure 5.17(f) and Figure 5.17(i) highlight that the zero sequence voltage of the PCC bus is lowest i.e. 9 kV as the fault current through the PCC bus has the highest percentage of the zero sequence current. The

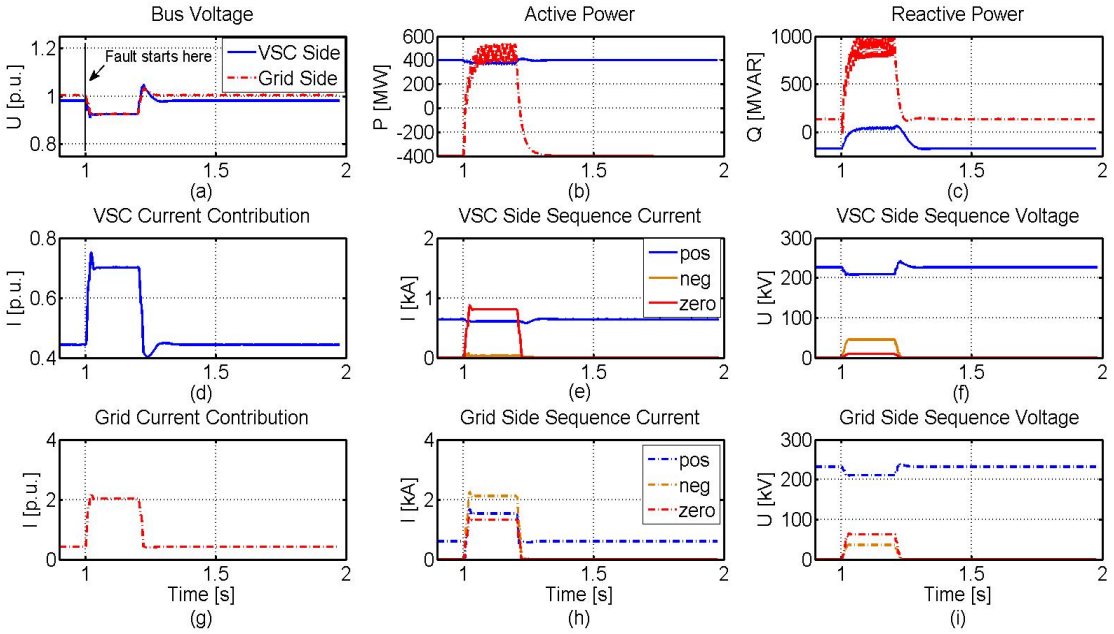


Figure 5.17: Phase A to ground fault on Line 1 at 70 km from *R1* with $R_f = 10\Omega$ and active current blocked current limitation strategy. (a) Bus voltage (RMS). (b) Active power. (c) Reactive power. (d) VSC current contribution. (e) VSC side sequence current. (f) VSC side sequence voltage. (g) Grid current contribution. (h) Grid side sequence current. (i) Grid side sequence voltage.

PCC bus negative sequence voltage rises to 45 kV in comparison to the grid side negative sequence voltage of 36 kV.

Analog Output: Fault Location = 70 km, $R_f = 10\Omega$

Figure 5.18(a) and Figure 5.18(b) unveil the oscilloscope output of instantaneous phase currents and rms voltage at the VSC side bus captured at the analog port of RTDS for a phase A to ground fault at 70 km and Rf = 10 Ω. The system is studied for both the active current blocked and the reactive current priority limitation strategy, which gives a clear picture about the limited fault currents behavior from the converter side in magnitude as well as in wave shape. For the active current blocked scheme during a phase-A to ground fault, the phase-A current increases but is limited to a peak-peak value of 16.1 A (5 A/div. and 1 div. = 1.022 kA) i.e. 3 kA (peak-peak), as depicted in Figure 5.18(a).

The fault currents do not exceed to a high value due to the maximum current limitation of the converter i.e. 1.15 p.u. The other healthy phase currents also increase instantaneously due to the reactive current supplied in all the three phases from the VSC. The rms voltage obtained in channel 4 (Red: 1st from the top) of Figure 5.18(a) is also in accordance with Figure 5.16(a) obtained from the simulation. Moreover, Figure 5.18(b) also unveil the instantaneous phase currents and rms voltage at the PCC side bus when the limitation strategy is reactive current priority. The instantaneous phase-A current rises to 18.1 A peak-peak value while on the other hand the healthy phase-C is not much affected since there is no additional reactive current supply from the VSC to the unhealthy and healthy phases. The rms voltage obtained in channel 4 (Red: 1st from the top) of Figure 5.18(b) is in accordance with Figure 5.17(a) for the reactive current priority strategy.

Apparent Impedance Trajectory – Phase-A to Ground Fault

The apparent impedance seen by the commercial relay R1 for a phase A to ground fault is showcased in Figure 5.19 and Figure 5.20 for different fault locations, fault resistances,

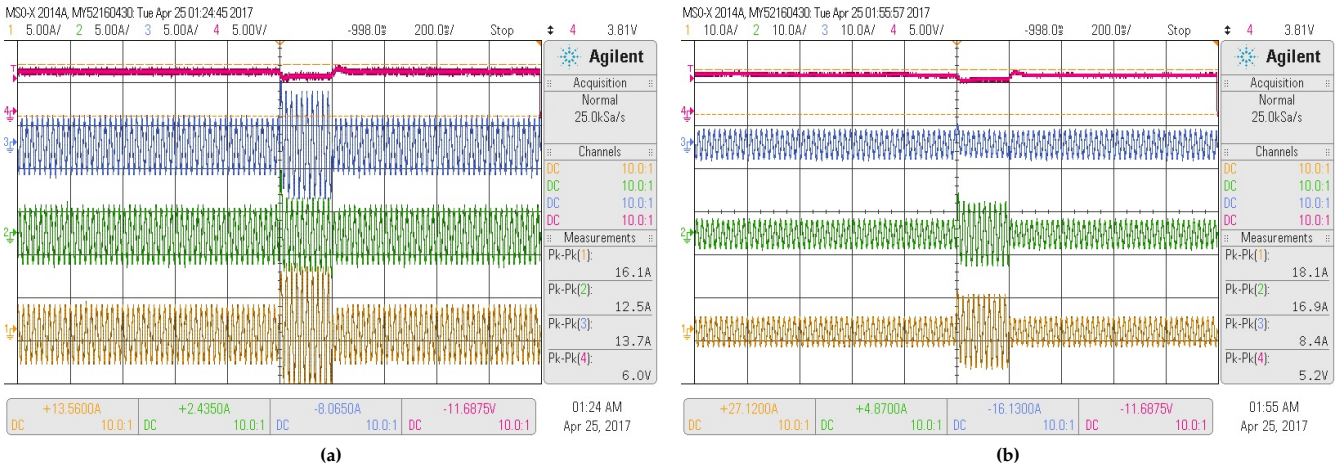


Figure 5.18: VSC side oscilloscope output for a phase A to ground fault on Line 1 at 70 km from R1 with $R_f = 10\Omega$ and (a) Active current blocked current limitation strategy. (b) Reactive current priority current limitation strategy. [Yellow (channel 1): Phase A current, Green (channel 2): Phase B current, Blue (channel 3): Phase C current, Red (channel 4): rms voltage].

loading angle and current limitation strategies. Figure 5.19(a) and Figure 5.19(b) clearly highlight that the distance relay under reach increases as the fault location and the fault resistance increases in the presence of VSC-HVDC control strategy. The locus of the positive sequence apparent impedance enters into zone 1 region but leaves quickly and settles into zone 2 region for a fault at 70 km with $R_f = 10\Omega$ and both the VSC current limitation strategies as compared to the same fault without VSC, as shown in Figure 5.19(a) and Table 1, which is an under reach. Similarly, in another case where $R_f = 10\Omega$ is kept constant and fault location is changed to 100 km (zone 2 fault), the relay under reaches heavily by reaching a steady state in zone 3 and deviates from the apparent impedance seen by the relay without VSC, (refer Figure 5.19(a)).

Moreover, the performance of the relay is also affected by the fault resistance. Figure 5.19(b) depicts the impedance locus for 0Ω, 20Ω, and 100Ω of fault resistance for a phase A to ground fault at 85 km (zone 2 fault). The relay detects the fault correctly for 0Ω and 20Ω of fault resistances and settles in zone 2 with the VSC reactive current priority strategy (see Figure 5.19(b)) but with the VSC active current blocked strategy the relay under reaches. The under reach is more pronounced as the resistance increases to a high value that is also evident from the Table 1 and Figure 5.19(b).

Similarly, the dynamic trajectory is also studied in Figure 5.20 for different loading angle of 0^0, 25^0 and 50^0 for faults at 50 km and $R_f = 20\Omega$. Although the dynamic impedance trajectory enters into zone 1 with both the VSC strategies for 0^0 and 25^0 loading angle, they slightly under reach in comparison to without the VSC condition, as shown in Figure 5.20(a) and Figure 5.20(b). Nonetheless, as the loading angle increases to a high value there are high possibilities of under reach for the active current blocked strategy (see Fig. Figure 5.20(c)).

Table 5.1, Table 5.2 and Table 5.3 also unveil the relay performance where '-' means no trip signal from the relay and 'x' means relay tripped/pickup. The distance relay operates for zone 2 and zone 3 region for faults greater than 70 km from R1 for both the limitation strategies that is a wrong operation of the relay. Similarly, the relay operates for zone 3 for $R_f = 20\Omega$ and 50 Ω for active current blocked strategy and $R_f = 50\Omega$ and 75 Ω for reactive current priority strategy at 85 km although the fault takes place inside zone 2. For resistance greater than 75 Ω and 100 Ω, the relay does not even pickup for active current blocked and reactive current priority strategies, respectively. The high loading angle creates problem when the active current blocked strategy is chosen (refer Table 5.3).

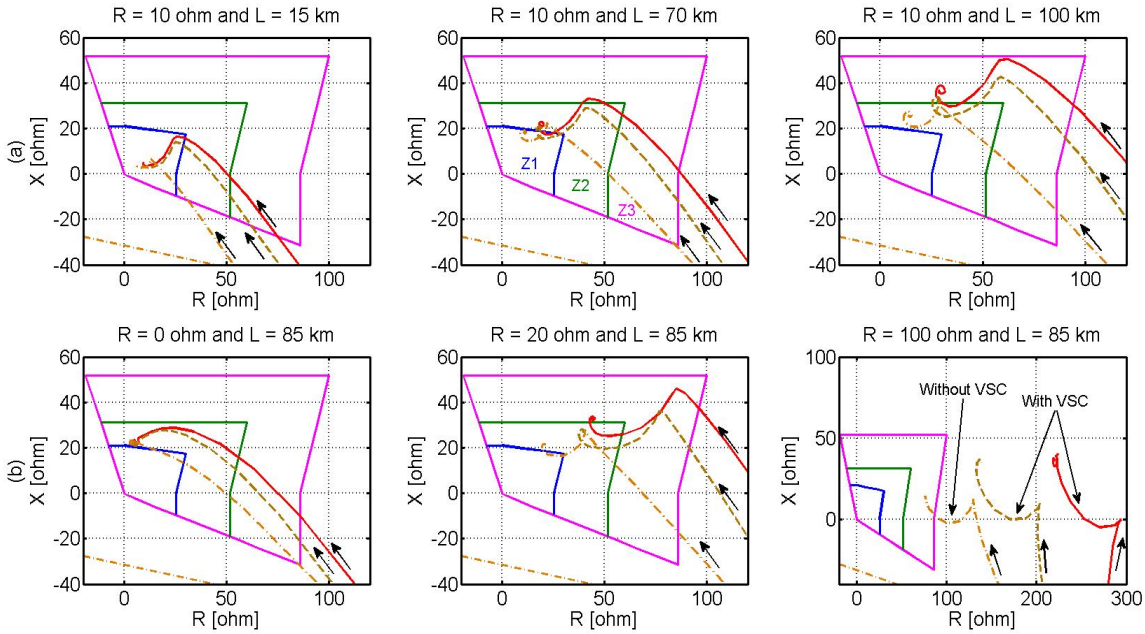


Figure 5.19: Impedance trajectories of ground AG element with and without VSC for phase-A to ground faults on Line 1. (a) L = 15, 70 and 100 km with $R_f = 10\Omega$. (b) L = 85 km with $R_f = 0, 20 and 100\Omega$. (Solid Red Line: with VSC and active current blocked current limitation strategy; Dotted Brown Line: with VSC and reactive current priority current limitation strategy; Dotted Orange Line: without VSC).

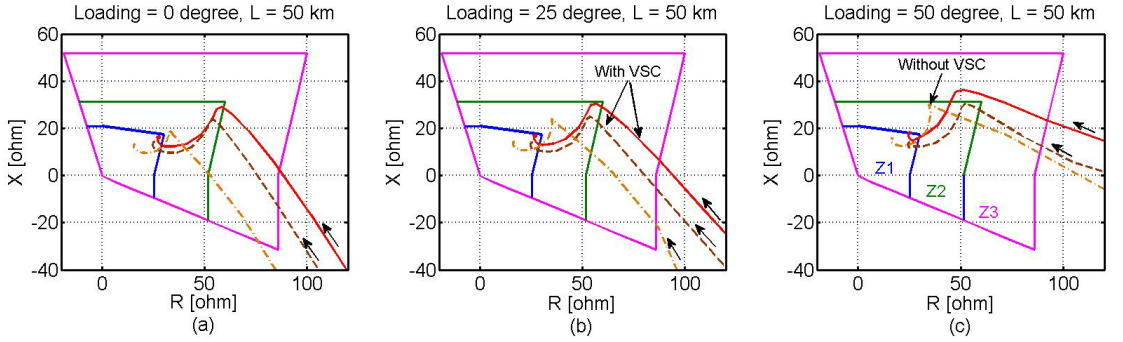


Figure 5.20: Impedance trajectories of ground AG element with and without VSC for phase-A to ground faults on Line 1 at 50 km from R1 with $R_f = 20\Omega$. (a) Loading = 0^0. (b) Loading = 25^0. (c) Loading = 50^0. (Solid Red Line: with VSC and active current blocked current limitation strategy; Dotted Brown Line: with VSC and reactive current priority current limitation strategy; Dotted Orange Line: without VSC).

Disturbance Records - Phase-A to Ground Fault

The impact of VSC-HVDC reactive current support and current limitation strategies on the performance of the commercial distance relay R1 located at the PCC is analyzed under the closed-loop test. The digital bits of pickup and trip signals are recorded using the disturbance recorder function of the relay. For a phase-A to ground fault at 70 km from R1 with $R_f = 10\Omega$ and active current blocked strategy, the relay picks up and sends a trip signal to the breaker for zone 1, as shown in Figure 5.21. Nevertheless, the fault report generated by the relay highlights that the relay wrongly detects a phase-A to ground fault as a phase-B to phase-C fault located at 7.28 km from R1 and issues a 3-pole trip signal. The fault impedance calculated by the relay is $Z^{AG}_{app} = 4.22\angle 152.84^0\Omega$ leading to wrong phase assertion.

On the other hand, for the same fault condition with the reactive current priority strategy, the relay neither issues any trip nor any pickup signal for the stage 1 or zone 1 function of the distance relay, although, the fault lies inside zone 1 region as per the standard settings (see Appendix A), as illustrated in Figure 5.22. The relay calculates the impedance to the

For different fault location from R1 with $R_f = 10\Omega$ and load angle -2.5^0				
Limitation Strategy	Location (in km)	Zone 1	Zone 2	Zone 3
Active Current Blocked	0	**X**	-	-
	15	**X**	-	-
	50	**X**	-	-
	70	-	**X**	-
	100	-	-	**X**
	120	-	-	**X**
Reactive Current Priority	0	**X**	-	-
	15	**X**	-	-
	50	**X**	-	-
	70	-	**X**	-
	100	-	**X**	-
	120	-	-	**X**

Table 5.1: Distance Relay performance for phase A to ground fault for different fault location.

For different fault resistance at fault location = 85 km from R1 and load angle -2.5^0				
Limitation Strategy	Resistance (in Ω)	Zone 1	Zone 2	Zone 3
Active Current Blocked	0	-	**X**	-
	10	-	**X**	-
	20	-	-	**X**
	50	-	-	**X**
	75	-	-	-
	100	-	-	-
Reactive Current Priority	0	-	**X**	-
	10	-	**X**	-
	20	-	**X**	-
	50	-	-	**X**
	75	-	-	**X**
	100	-	-	-

Table 5.2: Distance Relay performance for phase A to ground fault for different fault resistance.

phase A to ground fault more than its zone 1 reactive reach setting of 21.16Ω and under reaches in the presence of VSC-HVDC, which is also evident from the apparent impedance trajectory observed by the relay in Figure 5.19(a). The relay issues a zone 2 and zone 3 pickup signal as a backup if the primary zone 1 does not operate and if the fault duration is more than the threshold.

On the contrary, the stage 2 or zone 2 and stage 3 or zone 3 functions of the distance relay have picked up for 15 ms as soon as soon as the fault occurred but soon dropped off. The stage 2 and 3 functions of the relay again picks up after an interval of 20 ms for the duration of 180 ms, as depicted in Figure 5.21. This pick up highlights that the positive sequence apparent impedance measured by the distance relay falls inside the zone 2 tripping characteristics even though the fault lies in zone 1. The trip signals by the stage 2 and stage 3 function of the distance relay have not been issued because the fault duration is 200 ms (10 cycles) less than the operation delay of 250 ms for zone 2 and 1000 ms for zone 3 operation (see Figure 5.21 and Figure 5.22).

For different load angle at fault location = 50 km from R1 and $R_f = 20\Omega$.				
Limitation Strategy	Load angle (degree)	Zone 1	Zone 2	Zone 3
Active Current Blocked	0	-	-	-
	15	-	-	X
	25	-	-	X
	50	-	-	X
	75	-	X	-
	-	-	-	-
Reactive Current Priority	0	-	-	X
	10	-	-	X
	20	-	-	X
	50	-	-	X
	75	-	X	-
	-	-	-	-

Table 5.3: Distance Relay performance for phase A to phase B fault for different load angle.

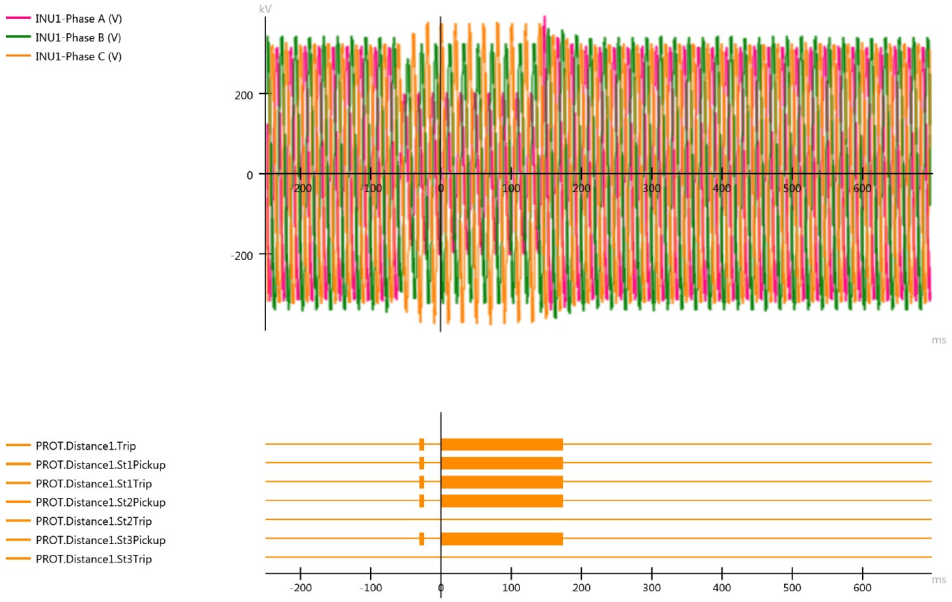


Figure 5.21: Disturbance report recorded by relay R1 for a Phase A to ground fault on Line 1 at 70 km from R1 with $R_f = 10\Omega$ and active current blocked current limitation strategy.

5.6.2 *Phase-to-Phase Fault*

Case 3: Fault Location = 70 km, $R_f = 10\Omega$ with Active Current Blocked Limitation Strategy

In another case, a phase-A to phase-B fault is created on Line 1 at a distance of 70 km from R1 with $R_f = 10\Omega$ at t = 1 s. Figure 5.23(a) highlights that the PCC voltage (Bus 4) drops to 0.74 p.u. in comparison to the grid side voltage (Bus 3) of 0.77 p.u. The converter control measures this drop in the PCC voltage and shifts the priority to the reactive current support. The PCC voltage improves from 0.74 p.u. to 0.88 p.u. due to the reactive power support of 600 MVAR during the fault from the VSC, as shown in Figure 5.23(c). The grid side rms voltage also improves to 0.81 p.u. due to this reactive support, as illustrated in Figure 5.23(a).

Since, the VSC controller implements the positive sequence active current blocked current limitation scheme such that $i_{(}d+)^{lim} = 0$ p.u., the active power flow from the VSC drops from 400 MW. On the other hand, the active power supply from the grid rises to a peak value of 1050 MW from -400 MW feeding the phase-A to phase-B fault (refer Fig-

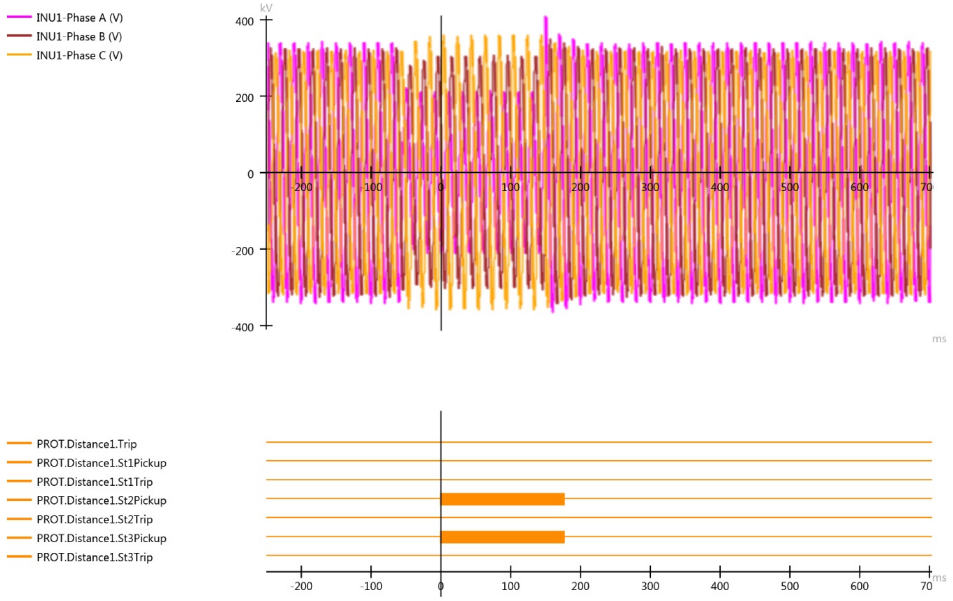


Figure 5.22: Disturbance report recorded by relay R1 for a Phase A to ground fault on Line 1 at 70 km from R1 with $R_f = 10\Omega$ and reactive current priority current limitation strategy.

ure 5.23(b)). The active and reactive power flow resumes the pre-fault values as soon as the fault disappears from Line 1 giving back the normal control strategy to the VSC station (see Figure 5.23(b) and Figure 5.23(c)). The active and reactive power due to the unbalanced voltage and current conditions contain the double line frequency component that leads to an oscillating power.

Similarly, Figure 5.23(d) and Figure 5.23(g) highlights the rms magnitude of fault current contribution from the VSC and the grid that rises to 0.86 p.u and 4.4 p.u, respectively. The fault current from the converter drops initially because of a sudden drop in the active power due to the active current blocking. Nonetheless, the fault current is completely reactive in nature due to the reactive current injection. In comparison to the fault current from the grid in Figure 5.23(g), the VSC fault current contribution is minimal and limited. If we examine the sequence components of the fault current from the VSC and the grid in Figure 5.23(e) and Figure 5.23(h) then it can be noticed that the negative sequence component of the fault current from the VSC is substantially smaller than the positive-sequence component of the current from the VSC. The small value of the negative sequence component of fault current from the VSC is due to the negative sequence current suppression control to balance the current.

The zero sequence component of the fault current is absent from both the grid side and the PCC side current contribution, as presented in Figure 5.23(e) and Figure 5.23(h). Moreover, there arises a difference between the negative sequence and positive sequence voltages at both the ends of Line 1, as shown in Figure 5.23(f) and Figure 5.23(i). The negative sequence component of PCC voltage rises to 120 kV as compared to the grid side negative sequence voltage of 83 kV due to the negative sequence current suppression.

Case 4: Fault Location $= 15$ *km,* $R_f = 100\Omega$ *with Reactive Current Priority Limitation Strategy*

In another case, a high resistance close-in phase-A to phase-B fault is studied at 15 km with $R_f = 100\Omega$ and Reactive Current Priority Limitation Strategy. Similar to the previous case 3, the PCC bus voltage drops to 0.9 p.u. during the fault in comparison to the grid side bus voltage of 0.95 p.u. illustrated in Figure 5.24(a). The PCC bus voltage drop does not pass the dead band test for the additional reactive current support from the VSC to improve the network voltage. To support the network with the reactive current, the PCC bus voltage

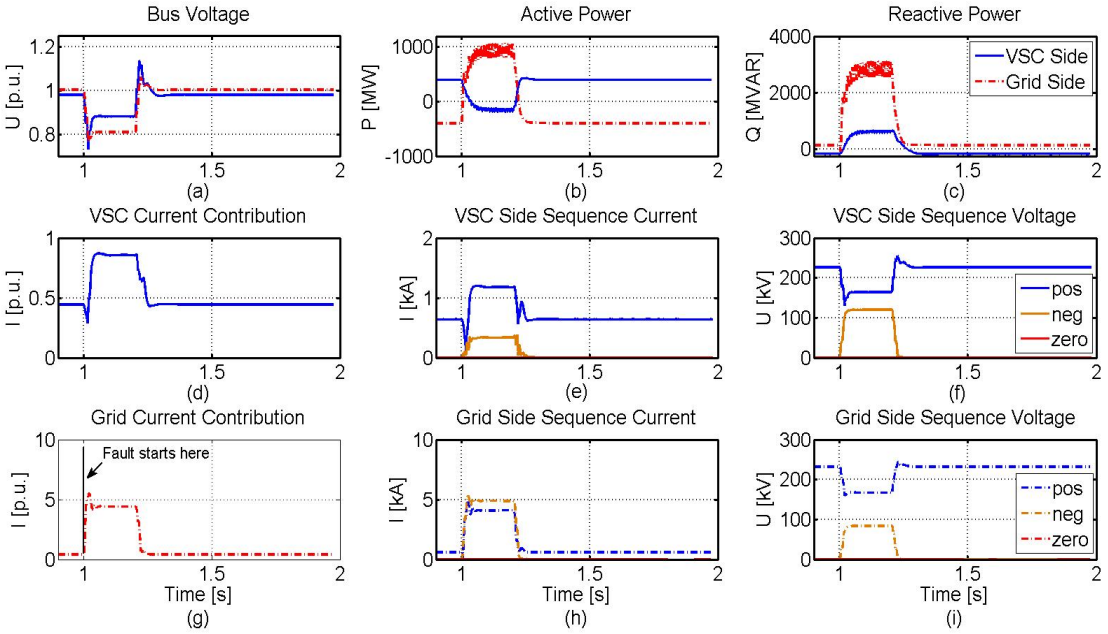


Figure 5.23: Phase A to phase B fault on Line 1 at 70 km from R1 with $R_f = 10\Omega$ and active current blocked current limitation strategy. (a) Bus voltage (RMS). (b) Active power. (c) Reactive power. (d) VSC current contribution. (e) VSC side sequence current. (f) VSC side sequence voltage. (g) Grid current contribution. (h) Grid side sequence current. (i) Grid side sequence voltage.

should be below 0.9 p.u. Moreover, Figure 5.24(b) presents that the change in the active power flowing from the VSC due to the phase-to-phase fault is 40 MW that is not significant. This is because of the reactive current limitation strategies where the current capacity is shared between both the positive sequence active and reactive currents. Similarly, the reactive power contribution from the VSC during the fault is reduced to approximately 0.0 MVAR because the controller does not activate the additional proportional reactive current controller, as depicted in Figure 5.24(c). However, the grid side active and reactive power jumps from -400 MW to 680 MW and 134 MVAR to 600 MVAR along with the second harmonic component.

Figure 5.24(d) and Figure 5.24(g) present the rms magnitude of the fault current contribution from the VSC and the grid, which are nominal values. The VSC side fault current drops to 0.43 p.u. due to the presence of high fault resistance while the grid side rms current contribution increases to 1.5 p.u., (see Figure 5.24(d) and Figure 5.24(g)). Due to the negative sequence current suppression control, the negative sequence component of the fault current from the VSC is 0.06 kA as compared to the grid side negative sequence current of 1.84 kA. The positive sequence fault current contribution consists of both the positive sequence active and reactive currents, as highlighted in Figure 5.24(e) and Figure 5.24(h). Figure 5.24(f) and Figure 5.24(i) unveil the sequence component of the PCC and the grid side voltage, which contain any 73 kV and 31 kV of negative sequence voltage, respectively.

Analog Output: Fault Location = 15 *km*, $R_f = 100\Omega$

Similarly, the oscilloscope output of instantaneous phase currents and rms voltage taken at the VSC end is presented in Figure 5.25 for two different current limitation strategies for a phase-A to phase-B fault at 15 km and Rf=100 Ω. The Phase-A, B and C instantaneous currents drop at t = 1 s during the close in high resistance fault due to the active current blocking where the fault current contribution from the VSC is marginal, as illustrated in Figure 5.25(a).

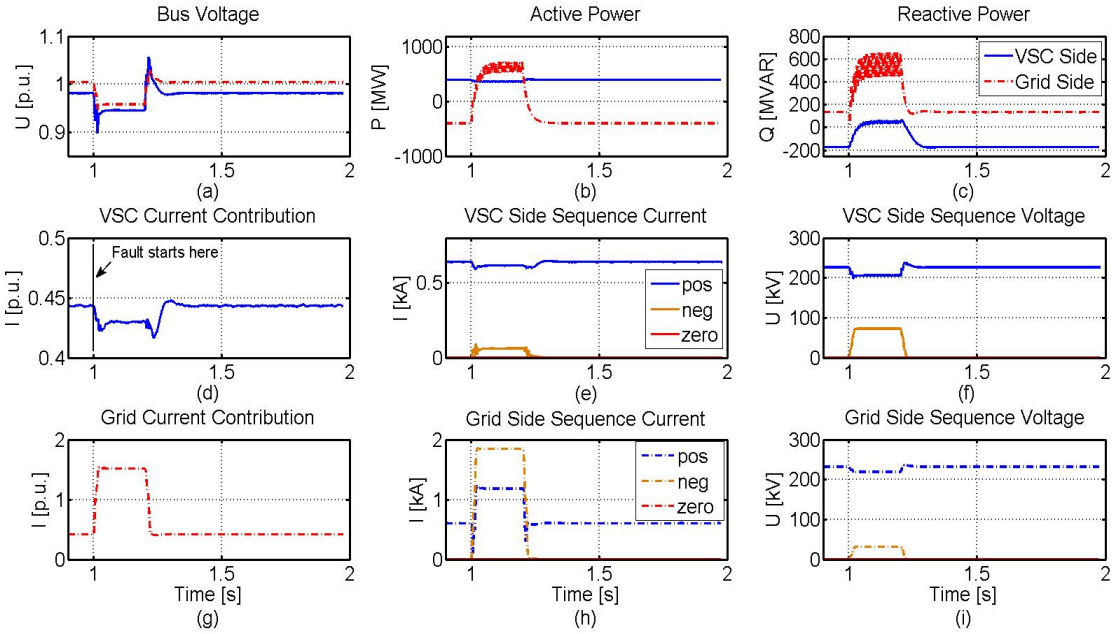


Figure 5.24: Phase A to phase B fault on Line 1 at 15 km from R1 with $R_f = 100\Omega$ and reactive current priority current limitation strategy. (a) Bus voltage (RMS). (b) Active power. (c) Reactive power. (d) VSC current contribution. (e) VSC side sequence current. (f) VSC side sequence voltage. (g) Grid current contribution. (h) Grid side sequence current. (i) Grid side sequence voltage.

On the other hand, for the same fault scenario with the reactive current priority limitation strategy the phase A, B and C instantaneous currents remain unchanged during the high resistance fault, as shown in Figure 5.25(b), which highlights insignificant amount of fault current supplied from the VSC in accordance with Figure 5.24(d). Figure 5.25(b) also present the rms magnitude of bus voltages on the VSC and the grid side, which is similar to the Figure 5.24(a) highlighting the coherency between the simulation and the experimental results.

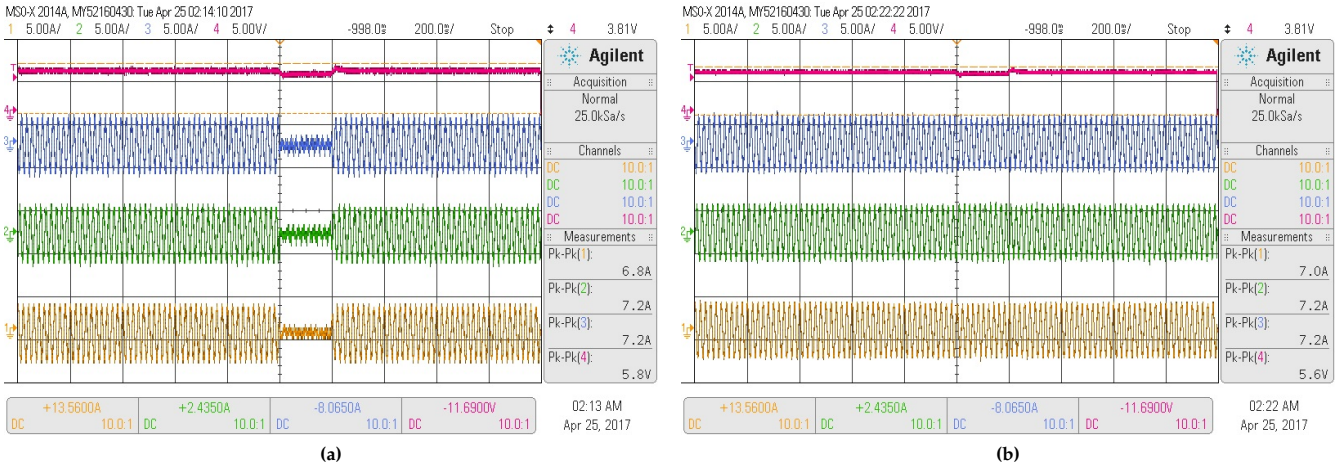


Figure 5.25: VSC side oscilloscope output for a phase-A to phase-B fault on Line 1 at 15 km from R1 with $R_f = 100\Omega$ and (a) Active current blocked current limitation strategy. (b) Reactive current priority current limitation strategy. [Yellow (channel 1): Phase A current, Green (channel 2): Phase B current, Blue (channel 3): Phase C current, Red (channel 4): rms voltage].

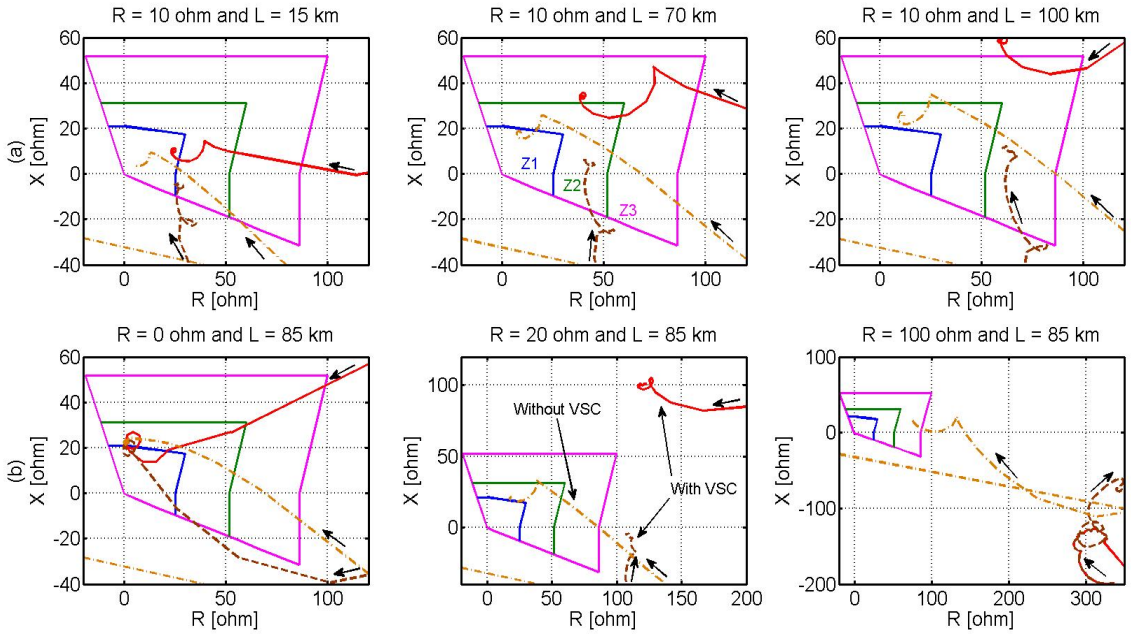


Figure 5.26: Impedance trajectories of phase AB element with and without VSC for phase-A to phase-B faults on Line 1. (a) L = 15, 70 and 100 km with $R_f = 10\Omega$. (b) L = 85 km with $R_f = 0, 20, 100\Omega$. (Solid Red Line: with VSC and active current blocked current limitation strategy; Dotted Brown Line: with VSC and reactive current priority current limitation strategy; Dotted Orange Line: without VSC).

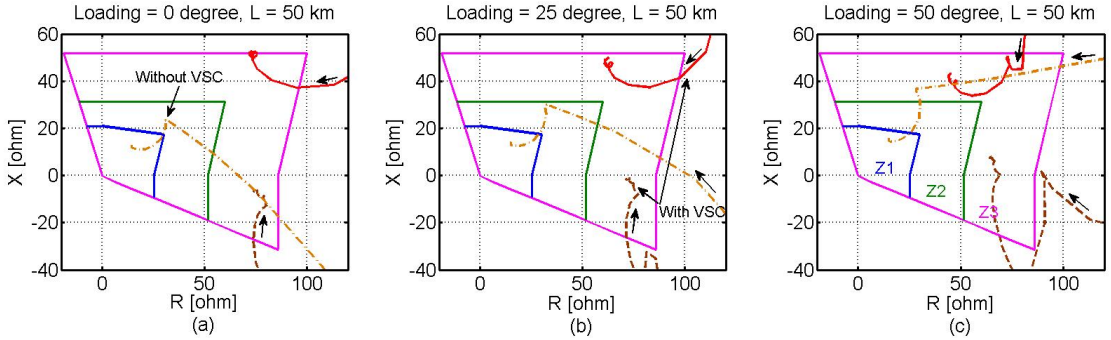


Figure 5.27: Impedance trajectories of phase AB element with and without VSC for phase-A to ground faults on Line 1 at 50 km from R1 with $R_f = 20\Omega$. (a) Loading = 0^0. (b) Loading = 25^0. (c) Loading = 50^0. (Solid Red Line: with VSC and active current blocked current limitation strategy; Dotted Brown Line: with VSC and reactive current priority current limitation strategy; Dotted Orange Line: without VSC).

Apparent Impedance Trajectory – Phase-A to Phase-B fault

Figure 5.26 and Figure 5.27 explain about the apparent impedance trajectory for a phase-A to phase-B fault at a distance of 15, 50, 70, 85 and 100 km with $R_f = 0, 10, 20, 100\ \Omega$ and loading angle of 0^0, 25^0 and 50^0. The locus enters into zone 1 and achieves steady state for a fault at 15 km with fault resistance 10 Ω for both the active current blocked and the reactive current priority (see Figure 5.26(a)). Nonetheless, the trajectory under reaches in comparison to the absence of VSC. Similar observation can be noticed from Figure 5.26(a) where $R_f = 10\Omega$ is kept constant and the distance to the fault location is varied for 15 km to 100 km. The locus under reaches severely as the fault distance increases from R1 for both the current limitation strategies.

For a fault at 85 km and $R_f = 0\Omega$, the locus enters into zone 2 correctly and settles at a steady state value similar to without VSC scenario. On the other hand, the locus enters into neither zone 1 nor zone 2 when the fault resistance is increased to 20 Ω concluding the malfunctioning of the relay and severe under reach (refer Figure 5.26(b)). Moreover, Figure 5.27(a), (b), (c) illustrate the impact of loading angle on the operation of the distance

relay during the phase A to phase B fault with the active current blocked and reactive current priority limitation strategies. With the loading angle 0^0 and the fault location of 50 km with $R_f = 20\Omega$, the relay under reaches severely while the under reach effect decreases as the loading is increased to 50^0.

Table 5.4, Table 5.5 and Table 5.6 also illustrate the commercial distance relay operation with the VSC-HVDC reactive current injection and the current limitation strategies. The relay does not issue any trip for resistances greater than 10Ω even though the fault takes place in zone 2 (i.e. 85 km) for both the limitation strategies, which is an indication of severe under reach evident from Figure 5.26 and Table 5.4 and Table 5.5 as well. In another cases with different loading angles, the relay does not perform correctly (see Table 5.6).

For different fault location from R1 with $R_f = 10\Omega$ and load angle -2.5^0				
Limitation Strategy	Location (in km)	Zone 1	Zone 2	Zone 3
Active Current Blocked	0	X	-	-
	15	X	-	-
	50	-	X	-
	70	-	-	X
	100	-	-	-
	120	-	-	-
Reactive Current Priority	0	X	-	-
	15	-	X	-
	50	-	X	-
	70	-	X	-
	100	-	-	X
	120	-	-	X

Table 5.4: Distance Relay performance for phase A to phase B fault for different fault location.

For different fault resistance at fault location = 85 km from R1 and load angle -2.5^0				
Limitation Strategy	Resistance (in Ω)	Zone 1	Zone 2	Zone 3
Active Current Blocked	0	-	X	-
	10	-	-	-
	20	-	-	-
	50	-	-	-
	75	-	-	-
	100	-	-	-
Reactive Current Priority	0	-	X	-
	10	-	-	X
	20	-	-	-
	50	-	-	-
	75	-	-	-
	100	-	-	-

Table 5.5: Distance Relay performance for phase A to phase B fault for different fault resistance.

Disturbance Records – Phase-A to Phase-B Fault

For a phase-A to phase-B fault, the effect of the VSC-HVDC reactive current injection on the performance of the distance relay R1 is recorded by plotting the digital output signals from the relay. Figure 5.28 presents the instantaneous phase voltages and the protection bits from the relay due to the fault. It can be seen from the Figure 5.28 that the commercial distance relay under test issues neither the pickup nor the trip signal from the stage 1 or zone 1 function for a fault at 15 km with $R_f = 100\Omega$. The distance relay R1 has calculated

For different load angle at fault location = 50 km from R1 and $R_f = 20\Omega$.				
Limitation Strategy	Load angle (degree)	Zone 1	Zone 2	Zone 3
Active Current Blocked	0	-	-	-
	15	-	-	**X**
	25	-	-	**X**
	50	-	-	**X**
	75	-	**X**	-
	-	-	-	-
Reactive Current Priority	0	-	-	**X**
	10	-	-	**X**
	20	-	-	**X**
	50	-	-	**X**
	75	-	**X**	-
	-	-	-	-

Table 5.6: Distance Relay performance for phase A to phase B fault for different load angle.

greater phase-A to phase-B fault impedance as compared to zone 1 reactive reach setting of 21.16Ω. That is why; the relay does not even picked up for the stage 1 function.

The stage 2 or zone 2 and stage 3 or zone 3 function of the distance relay picks up for the duration of 200 ms because the relay calculates the apparent impedance to be less than zone 2 and zone 3 reactive reach setting. This clearly highlights that the relay miscalculates the location of the fault and over reaches for a high resistive fault. Therefore, the presence of VSC-HVDC and its reactive control strategy leads to heavy under reach of the distance relay in case of phase-to-phase fault and put the entire power system at the risk of blackout.

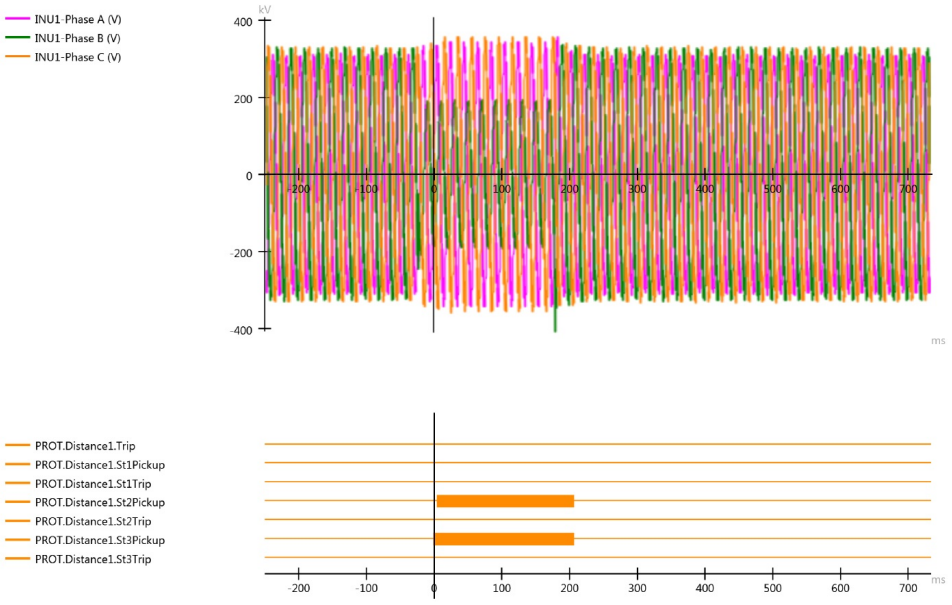


Figure 5.28: Disturbance report recorded by relay R1 for a phase A to phase B fault on Line 1 at 70 km from *R1* with $R_f = 100\Omega$ and active current blocked current limitation strategy.

5.6.3 *Three-Phase Fault*

Case 5: Fault Location = 70 km, $R_f = 10\Omega$ with Active Current Blocked Limitation Strategy

In another scenario, a three-phase fault is analyzed on Line 1 at 70 km from R1 with $R_f = 10\Omega$ at t = 1 s. The bus voltage, current contribution, active and reactive power are depicted in Figure 5.29 for the VSC side and the grid side. The limitation strategy adopted initially is the active current blocked when the PCC voltage drops due to the fault. As seen in Figure 5.29(a), the PCC voltage and the grid side bus voltage drops to 0.35 p.u. beyond the dead band that leads to the activation of additional reactive current injection from the VSC and simultaneously activating active current blocking strategy. Due to which the active power contribution from the VSC side drops to 0.0 MW and the reactive power rises to 505 MVAR, as shown in Figure 5.29(b) and Figure 5.29(c) for the duration of fault.

The grid side active and reactive power is free from second harmonic component due to the balanced nature of currents and voltages, which are evident from Figure 5.29(e), (f), (h) and (i) where there is no negative and zero sequence components of currents and voltages. The fault current from the VSC rises to 1.6 p.u. as the converter are arranged in bipolar configuration i.e. 0.8 p.u. per converter while the grid side current rises to a high value of 6.5 p.u., presented in Figure 5.29(d) and Figure 5.29(g).

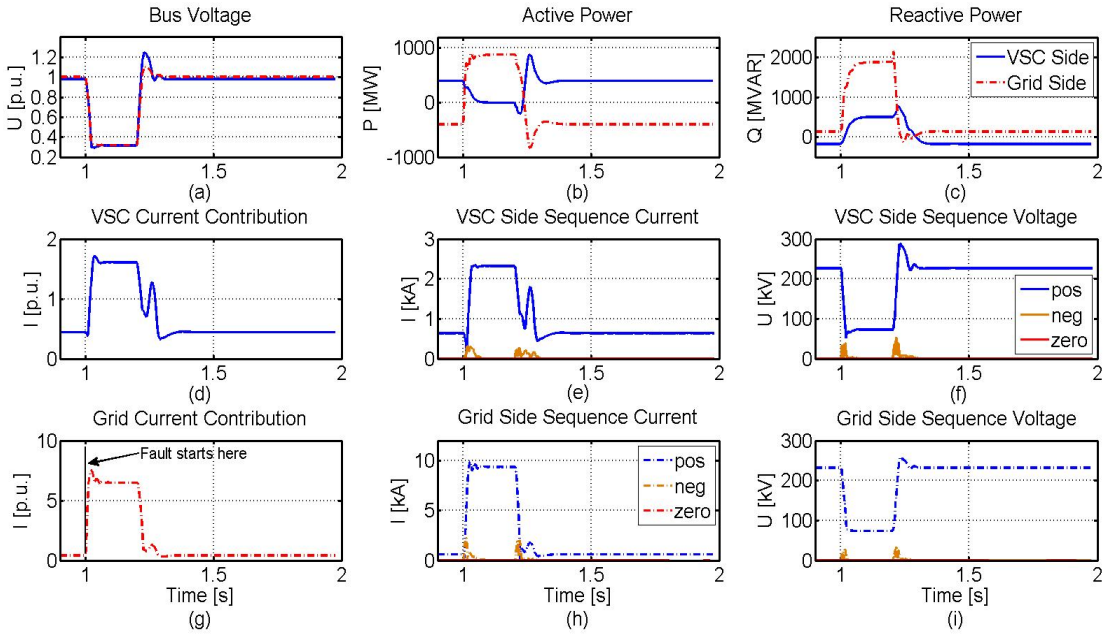


Figure 5.29: Three phase fault on Line 1 at 70 km from R1 with $R_f = 10\Omega$ and active current blocked current limitation strategy. (a) Bus voltage (RMS). (b) Active power. (c) Reactive power. (d) VSC current contribution. (e) VSC side sequence current. (f) VSC side sequence voltage. (g) Grid current contribution. (h) Grid side sequence current. (i) Grid side sequence voltage.

Case 6: Fault Location = 50 km, $R_f = 0\Omega$ with Reactive Current Priority Limitation Strategy

Another three-phase fault is studied on Line 1 at 50 km with $R_f = 0\Omega$ and reactive current priority. The VSC controller starts injecting reactive current into the network as soon as the PCC voltage drops below 0.9 p.u. (see Figure 5.30(a)). The fault current contribution from the VSC consists of the active current and the reactive current since the active current limit is dynamic in nature and depends upon the reactive current reference. The PCC voltage drops to 0.16 p.u. soon after the fault that leads the positive sequence reactive current to hit the maximum limit VSC overcurrent capability. Thus, the available active current space

reduces to zero that causes the active current limit to be set equal to zero. Due to this, the active power contribution from the VSC reduces to zero, as shown in Figure 5.30(b). Figure 5.30(c) presents the reactive current contribution from the VSC and the grid.

The VSC current contribution is 1.6 p.u. that mainly consists of the positive sequence reactive current injection while the grid current rises to 6.9 p.u. initially, as illustrated in Figure 5.30(d) and Figure 5.30(g). The sequence current contribution from the converter and the grid and the sequence bus voltages of PCC and the grid side bus have positive sequence components only, as presented in Figure 5.30(e), (f), (h) and (i).

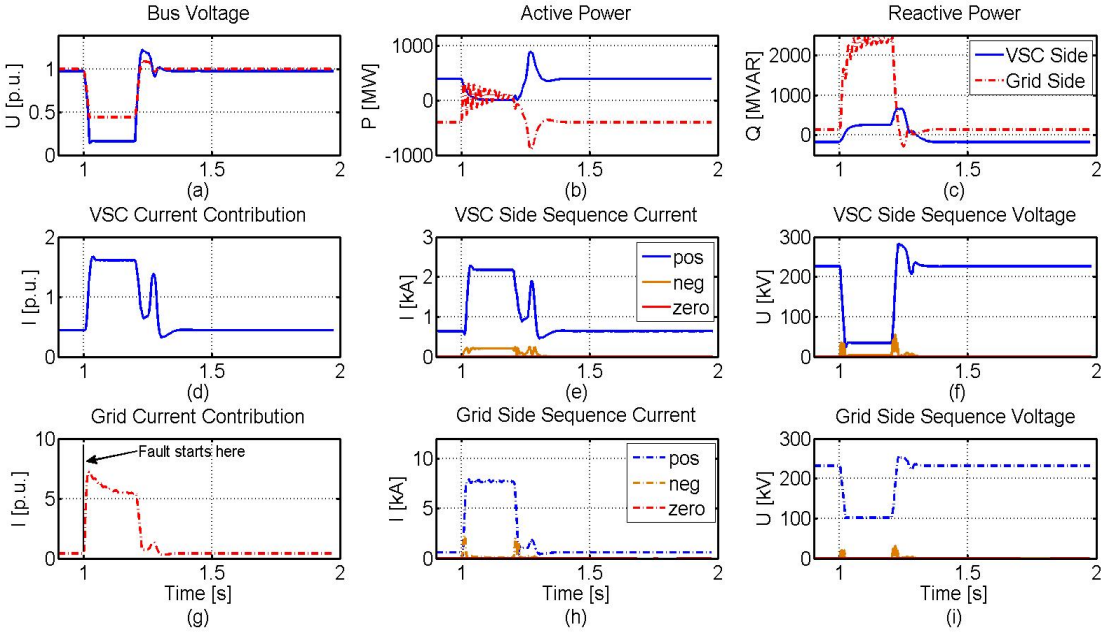


Figure 5.30: Three phase fault on Line 1 at 50 km from R1 with $R_f = 0\Omega$ and active current blocked current limitation strategy. (a) Bus voltage (RMS). (b) Active power. (c) Reactive power. (d) VSC current contribution. (e) VSC side sequence current. (f) VSC side sequence voltage. (g) Grid current contribution. (h) Grid side sequence current. (i) Grid side sequence voltage.

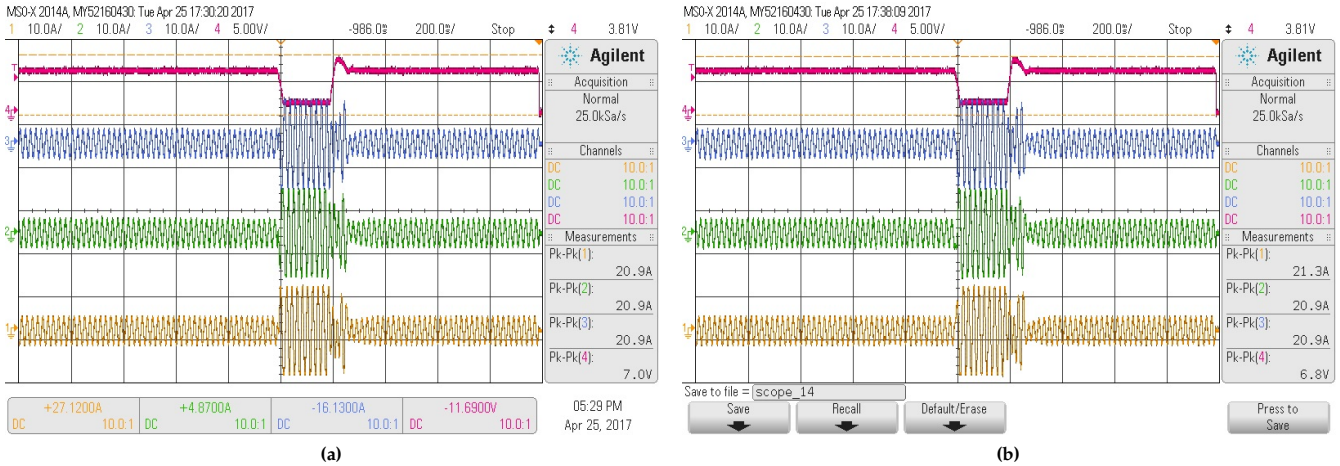


Figure 5.31: VSC side oscilloscope output for a three-phase fault on Line 1 at 50 km from R1 with ,$R_f = 10\Omega$ and (a) Active current blocked current limitation strategy. (b) Reactive current priority current limitation strategy. [Yellow (channel 1): Phase A current, Green (channel 2): Phase B current, Blue (channel 3): Phase C current, Red (channel 4): rms voltage].

Analog Output: Fault Location $= 50$ *km*, $R_f = 10\Omega$

In another case of a three-phase fault on Line 1 at the same distance of 50 km from R1 at t = 1 s, instantaneous phase currents and rms voltages are presented in Figure 5.31. It is shown in Figure 5.31(a) and Figure 5.31(b) that the instantaneous magnitude of fault currents from the converter increases sharply due to the three-phase fault on the line but is limited to the converter maximum current due to the activation of the active current blocked limitation strategy (channel 1, 2, and 3). The instantaneous phase currents shown in Figure 5.31 for the converter side are in accordance with the nature of the fault i.e. all the phase currents are increased in equal proportion, rises to 3.3 kA, and cannot exceed more than the maximum rating of the converter. Moreover, the VSC starts supporting the network voltage by initiating its reactive current compensation strategy. The instantaneous phase currents in each phase are almost the same because the VSC injects equal and symmetrical reactive current into each phase of the network, as shown in Figure 5.31.

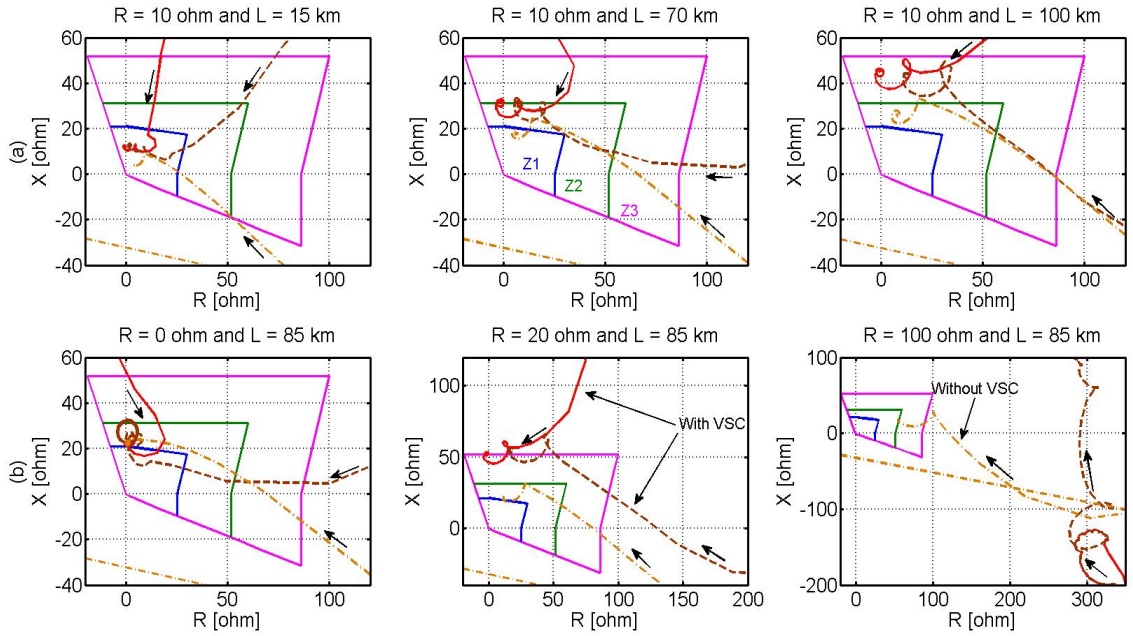


Figure 5.32: Impedance trajectories of phase AB element with and without VSC for three-phase faults on Line 1. (a) L = 15, 70 and 100 km with $R_f = 10\Omega$. (b) L = 85 km with $R_f = 0, 20, 100\Omega$. (Solid Red Line: with VSC and active current blocked current limitation strategy; Dotted Brown Line: with VSC and reactive current priority current limitation strategy; Dotted Orange Line: without VSC).

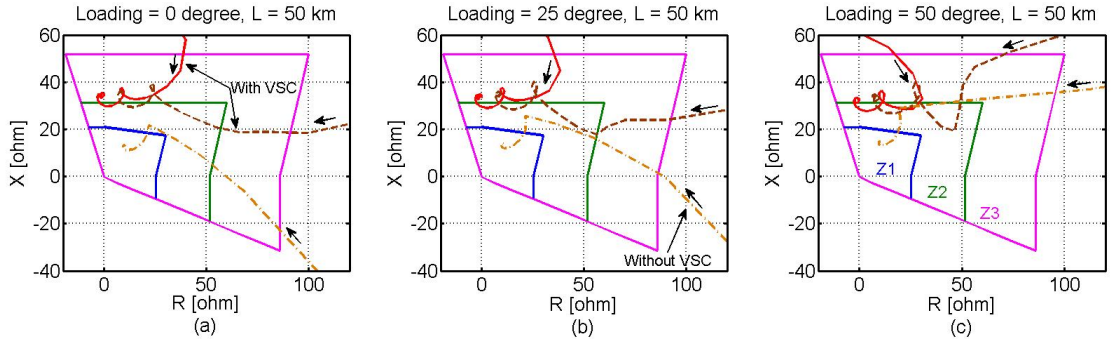


Figure 5.33: Impedance trajectories of ground AB element with and without VSC for three-phase faults on Line 1 at 50 km from R1 with $R_f = 20\Omega$. (a) Loading = 0^0. (b) Loading = 25^0. (c) Loading = 50^0. (Solid Red Line: with VSC and active current blocked current limitation strategy; Dotted Brown Line: with VSC and reactive current priority current limitation strategy; Dotted Orange Line: without VSC).

Apparent Impedance Trajectory – Three-Phase Fault

Figure 5.32 and Figure 5.33 unfold the time varying locus of the positive sequence impedance observed by the phase distance element AB of the distance relay R1 for different fault locations, fault resistances and loading angles. The impedance trajectories are plotted for the condition when the converter is injecting reactive current into the network and either of the two current limitation strategies are activated during the fault. The AB element enters into zone 1 for a fault at 15 km and $R_f = 10\Omega$ similar to the scenario without VSC-HVDC. However, the relay starts under reaching as the distance to the fault location increases, as highlighted in Figure 5.32(a). The relay settles in zone 2 for a fault at 70 km and in zone 3 for another fault at 100 km for both the active current blocked and the reactive current priority limitation strategies.

For different fault location from R1 with $R_f = 10\Omega$ and load angle -2.5^0				
Limitation Strategy	Location (in km)	Zone 1	Zone 2	Zone 3
Active Current Blocked	0	**X**	-	-
	15	**X**	-	-
	50	-	**X**	-
	70	-	**X**	-
	100	-	-	**X**
	120	-	-	**X**
Reactive Current Priority	0	**X**	-	-
	15	**X**	-	-
	50	-	**X**	-
	70	-	**X**	-
	100	-	-	**X**
	120	-	-	**X**

Table 5.7: Distance Relay performance for three-phase fault for different fault location.

For different fault resistance at fault location = 85 km from R1 and load angle -2.5^0				
Limitation Strategy	Resistance (in Ω)	Zone 1	Zone 2	Zone 3
Active Current Blocked	0	-	**X**	-
	10	-	-	**X**
	20	-	-	**X**
	50	-	-	-
	75	-	-	-
	100	-	-	-
Reactive Current Priority	0	-	**X**	-
	10	-	-	**X**
	20	-	-	**X**
	50	-	-	-
	75	-	-	-
	100	-	-	-

Table 5.8: Distance Relay performance for three-phase fault for different fault resistance.

On the other hand, the impact of increasing fault resistance is also portrayed in Figure 5.32(b), which concludes that the relay performs well when the fault resistance is zero i.e. bolted fault but creates problem and ultimately leads to wrong tripping when the resistance increases. For a zone 2 fault at 85 km, the relay lands in zone 2 correctly and generates a trip signal but it fails to operate as soon as the resistance increases to larger values (see Figure 5.32(b)). For another case with the increased loading conditions of 0^0, 25^0 and 50^0 for a three-phase fault at 50 km and $R_f = 20\Omega$ fault resistance, the apparent impedance affects the transient trajectories, as shown in Figure 5.33(a), (b) and (c). The

apparent impedance seen by the relay is far away from the impedance seen by the same relay without VSC-HVDC due to the limited fault current contribution from the converter.

Additionally, the tabular results of the performance of commercial relay is also illustrated in Table 5.7, Table 5.8 and Table 5.9 for three-phase faults for different fault conditions and limitation strategies. The relay under reaches for the faults greater than 50 km in both the current limitation strategies. Similarly, the effect of increasing resistances are pronounced when greater than 10 Ω, which leads to wrong trip or no trip.

For different load angle at fault location = 50 km from R1 and $R_f = 20\Omega$.				
Limitation Strategy	Load angle (degree)	Zone 1	Zone 2	Zone 3
Active Current Blocked	0	-	-	-
	15	-	-	**X**
	25	-	-	**X**
	50	-	-	**X**
	75	-	**X**	-
	-	-	-	-
Reactive Current Priority	0	-	-	**X**
	10	-	-	**X**
	20	-	-	**X**
	50	-	-	**X**
	75	-	**X**	-
	-	-	-	-

Table 5.9: Distance Relay performance for three-phase fault for different load angle.

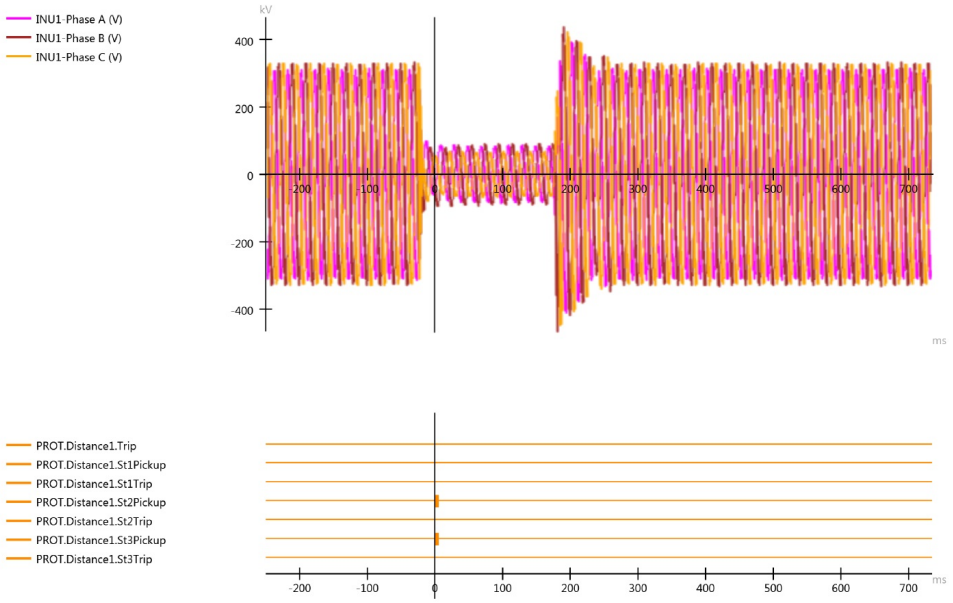


Figure 5.34: Disturbance report recorded by relay R1 for a three-phase fault on Line 1 at 50 km from R1 with $R_f = 10\Omega$ and active current blocked current limitation strategy.

Disturbance Records: Three-Phase Fault

Figure 5.34 and Figure 5.35 illustrate the instantaneous primary phase voltages of PT and the digital pick up and trip signals generated and recorded by the relay during a three-phase fault at 50 km and $R_f = 10\Omega$ for active current blocked and reactive current priority strategy, respectively. The disturbance report highlights that the distance relay has neither picked up nor issued any stage 1 trip signal. Since the fault lasts for 200 ms, the relay

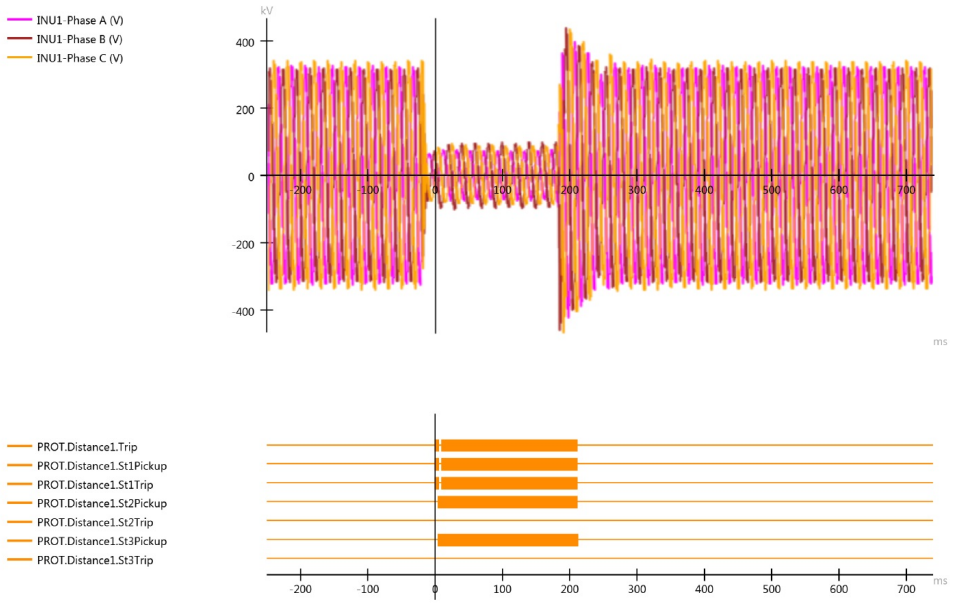


Figure 5.35: Disturbance report recorded by relay R1 for a three-phase fault on Line 1 at 50 km from R1 with $R_f = 10\Omega$ and reactive current priority current limitation strategy.

should have issued a stage 1 pickup and trip signals. The stage 2 and stage 3 picks up for 5 ms but soon drop off, as shown in Figure 5.34. On the contrary, the relay should have picked up for stage 2 and stage 3 for the entire duration of 200 ms. Although the fault report from the relay suggest that the relay correctly recognizes a three-phase fault but miscalculates the distance to the fault location as 134.07 km and the fault impedance as $Z_{app}^{BC} = 37.47\angle 71.09^0\Omega$.

Figure 5.35 also presents the disturbance record for a three-phase with reactive current priority scheme. The relay issues a stage 1 trip signal for 5 ms but drop off and after an interval of 5 ms the relay picks up again and trip, as presented in Figure 5.35. The distance relay is unable to achieve a steady state value of fault location and fault impedance that is why it shows a continuous pickup and drop off. On the other hand, the impedance locus for the three-phase fault in Table 3 suggests that it has entered into zone 2, which is not coherent with the trip signals obtained from the commercial relay.

5.7 CONCLUSIONS

The work presented in this chapter is the impact of the VSC-HVDC system on the operation of distance relay when the VSC provides reactive current support to the network along with the current limitation strategies by performing a closed loop test in RTDS under the more realistic scenario. Following are the main conclusions:

1. The results presented a serious concern regarding the distance relay performance with VSC-HVDC. The relay not only shown an under reach but also unstable or oscillating trip signals behavior.

2. For a successful opening of a circuit breaker, the relay should be able to detect the correct fault loop and assert for correct zones. On the other hand, the simulation and experiment presented that the distance relay wrongly measures the distance to fault and apparent impedance that leads to the wrong zones of assertion.

3. For the case of single phase to ground in zone 1, the relay measured the fault as a phase-phase fault in zone 1 and issued a zone 2 and zone 3 pickup signal.

4. Similarly, the relay issued a zone 2 and zone 3 pickup signal when the fault has high resistance during a zone 1 phase-to-phase fault leading to an over reach. Moreover, the relay picked up for zone 1 and dropped off soon for a zone 1 fault leading to an unstable behavior.

5. The relay also under reached due to the CT and PT error.

6. This concludes that the relay misoperated with VSC-HVDC reactive current limitation strategy.

Part III

ADAPTIVE DISTANCE RELAYING, CONCLUSIONS & FUTURE RESEARCH WORK

Part III of the thesis contains Chapter 6 and Chapter 7. Chapter 6 presents an adaptive distance relaying algorithm taking into account the power system condition, local bus measurements, sequence currents, VSC current limitation strategies and an optimal relay reach setting using RTDS. The chapter, firstly, presents the behavior of distance relay with the fixed reach setting, mathematical formulation of the adaptive algorithm and later on, it discusses the flowchart of an algorithm. Many power system fault conditions as test cases (with and without tele-protection scheme) are tested in a closed-loop to verify the correctness of the relaying algorithm.

Chapter 7 is the main conclusion chapter of this thesis where a chapter wise conclusions have been outlined in order to give a clear idea of the overall contribution of the thesis. Moreover, a bullet-list as a future research work per chapter is also highlighted in this part of the thesis.

6

ADAPTIVE DISTANCE RELAYING SCHEME

Contents

6.1 General Background 106
6.2 Experimental test setup using RTDS 106
6.3 Relay Performance with Fixed Setting Scheme 107
6.4 Pilot Distance Relaying Scheme 113
6.5 Adaptive Distance Relaying Scheme 118
6.6 Relay Performance with Adaptive Scheme 122
6.7 Flowchart 125
6.8 Conclusions 125



Benjamin Franklin (1706-1790) was one of the Founding Fathers of the United States. Franklin was a renowned polymath and a leading author, printer, political theorist, politician, freemason, postmaster, scientist, inventor, civic activist, statesman, and diplomat. As a scientist, he was a major figure in the American Enlightenment and the history of physics for his discoveries and theories regarding electricity. As an inventor, he is known for the lightning rod, bifocals, and the Franklin stove, among other inventions.

Chapter 4 and Chapter 5 presents the performance evaluation of a commercial distance relay applied to protect the transmission lines connected to VSC-HVDC system using an offline as well as a real-time simulation platform. It has been observed that the distance relays are not operating correctly for the different fault scenarios when operated with the grid codes of reactive current injection with the negative sequence current suppression and VSC current limitation strategy for HVDC connections. The relay wrongly calculates the fault distance, fault location, fault loop and fault phases. The modern grid codes for HVDC connections affect the operation of distance relays that has been verified by performing the closed-loop test in RTDS platform.

Chapter 6 presents a simple adaptive relaying scheme for the distance protection of transmission lines connected to VSC-HVDC system by computing a new set of relay reach settings during the fault using Z_{BUS} method and taking into account the VSC current limitation strategy and power system condition.

This chapter is based on the following publication:

M. M. Alam, H. Leite, D. V. Hertem, and A. S. Carvalho, "Adaptive Distance Relay Algorithm for Transmission Lines Connected to VSC Based HVDC System," IEEE Transactions on Power Delivery (To be submitted), 2018.

6.1 GENERAL BACKGROUND

Rapid changes are taking place in the modern day electrical network from fossil fuel dependent electrical sources to renewable energy dependent sources [147]. These changes in the grid are taking place not only at the transmission level but also at the distribution level, which is affecting the conventional behavior of grid during the network disturbances [148]. In addition to this, the behavior of renewable energy sources based on converters during any abnormal condition is totally different from the synchronous generator both in terms of fault current magnitude and wave-shape [112, 118, 149] that affects the performance of protection relays.

The VSC can only supply fault currents of magnitude 1.2 p.u., thus restricting the fault level and affecting the conventional grid protection system that is based on the fault responses of conventional synchronous generators [149]. Furthermore, the fast response of VSC controllers leads to rapid changes in the system parameters like PCC voltage and line currents, which affect the distance protection.

The authors in [113, 150] present the effect of type 3 and type 4 wind turbine on the distance protection of transmission line by simulating the turbine and converter. Moreover, the reference [117] elaborates the impact of full-scale converter based wind turbine on the distance relay of lines connecting the turbine. It has been discussed that the characteristics of fault current in a converter interfaced renewable energy source is different from the synchronous generator based system. Ref. [85] investigated the performance of a distance relay in a VSC connected transmission network during a three-phase fault without taking into consideration the grid codes for HVDC connections. Therefore, the authors in [149] have studied the impact of VSC-HVDC on the distance relays by considering the network code of reactive current injection from the VSC and the negative sequence current suppression strategy on PSCAD platform. Since very few research work have been performed on the performance of distance relay of transmission line connected to VSC-HVDC in a real-time platform, the previous work [151] is based on the performance evaluation of distance protection in RTDS.

Many works have been proposed based on the impact mitigation of converters on the distance relay in a transmission network. Ref. [152] discusses the integration of adaptive protection with optimal relay setting determination into a single scheme using closed-loop test. In another research, reference [153–155] presents an adaptive protection scheme for the converter interfaced wind turbine in a software simulation platform, where the accuracy and correctness of the model is a point of discussion. The contribution of this Chapter 6 is manifold. Firstly, the performance of a pilot and non-pilot distance protection is presented in a closed-loop test setup and then an adaptive protection scheme is implemented. The relay shows correct behavior in every disturbance scenarios.

6.2 EXPERIMENTAL TEST SETUP USING RTDS

A closed-loop test is established using an RTDS[37] to test a commercially available distance relay like the one from Siemens (7SA86), as shown in Figure 6.1. The RTDS depicted in Figure 6.1 has four racks with four PB5 processor cards in each rack. There is a front-panel interface with low-voltage level digital output channel of output ($\pm 10V$) and high-voltage level digital input channel of input unto ($\pm 200Vdc$), as unveiled in Figure 6.1. The analog output from the RTDS is fed into the distance relay under test via a signal amplifier. The distance relays are configured for standard relay reach settings.

[37] RTDS hardware features:

- 4 PB5 processor cards in each of 4 racks.
- GTAO's and GTAI's.
- GTFPI (Front Panel Interface).
- Low voltage level digital output channel ($\pm 10V$)
- High voltage level digital input channel ($\pm 200Vdc$)

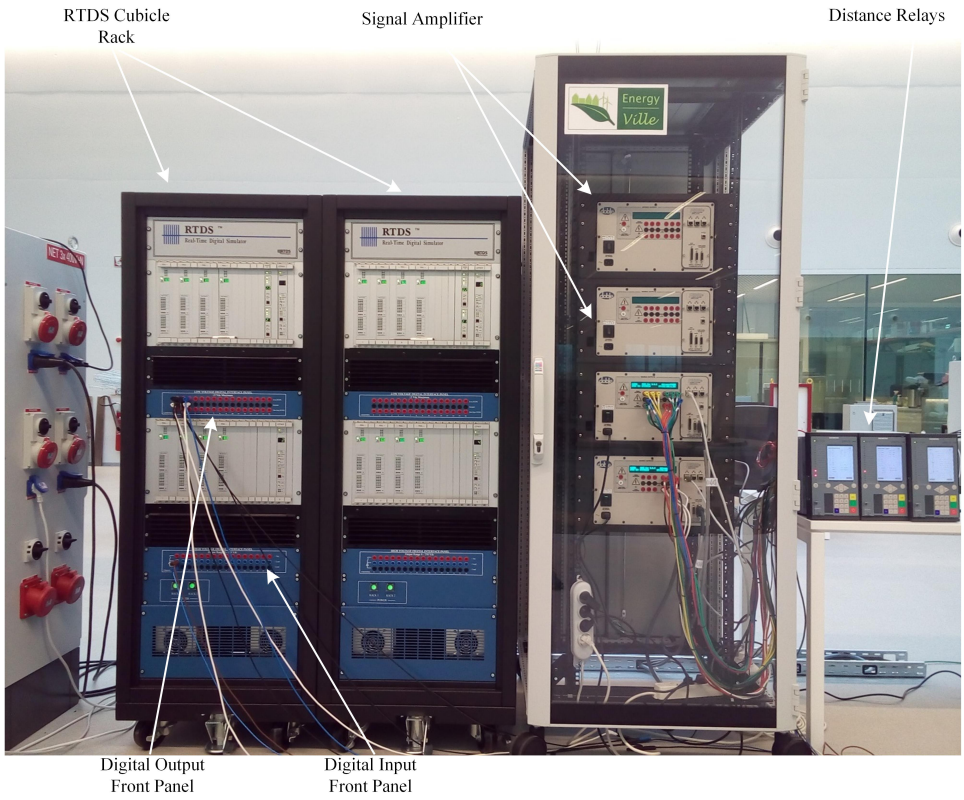


Figure 6.1: RTDS based closed-loop test-bed with signal amplifier and Siemens distance relays 7SA86.

6.3 RELAY PERFORMANCE WITH FIXED SETTING SCHEME

6.3.1 *Non-Pilot Distance Relaying Scheme*

Chapter 4 has already explained the working principle of a non-pilot distance protection scheme, which is often called as a step-distance relay with an inherent time delay. A fixed-setting based distance relay is conventional and commonly employed at the transmission level protection. However, when a power system accommodates VSC-HVDC connection, it has been found that the fixed-setting distance relaying scheme does not perform correctly.

This chapter[38] presents multiple operational scenarios of a distance relay during an unsymmetrical fault with different fault resistances, the direction of power flow, fault locations and VSC current limitation strategy. Later on, the chapter presents mathematical analysis to calculate an apparent impedance by computing the PCC voltage, reactive current injection from the VSC-HVDC system and current limitation strategies as an adaptive protection strategy. Consequently, the distance relay is loaded with the new reach settings in real-time to accommodate the VSC-HVDC connection. The performance of adaptive protection strategy is evaluated and results are presented in the latter part of this chapter in addition to a flowchart of the algorithm.

[38] Chapter 6 presents the performance of distance relays during unsymmetrical faults with:

- fault resistances,
- direction of power flows,
- fault locations,
- VSC current limitation strategy,

Effect of fault resistance

Figure 6.2 presents the performance of a non-pilot distance function for a phase A-phase B fault at different fault locations of 25, 50, 75, 85, and 115 km at $P_{HVDC} = 0MW$, $R_f = 0.1, 10, 20\ \Omega$ and active current blocked limitation strategy of VSC. It can be seen from the Figure 6.2 that the distance relay R1 has operated correctly for a low resistance phase-phase fault. The distance relay R1 has picked up for zone 1 for the duration of 214 ms during a phase A-phase B fault at 25 km from R1, as seen from Figure 6.3 and Table 6.1. The relay R1 identified the fault in zone 1 and operated in 1 ms by sending a three-pole

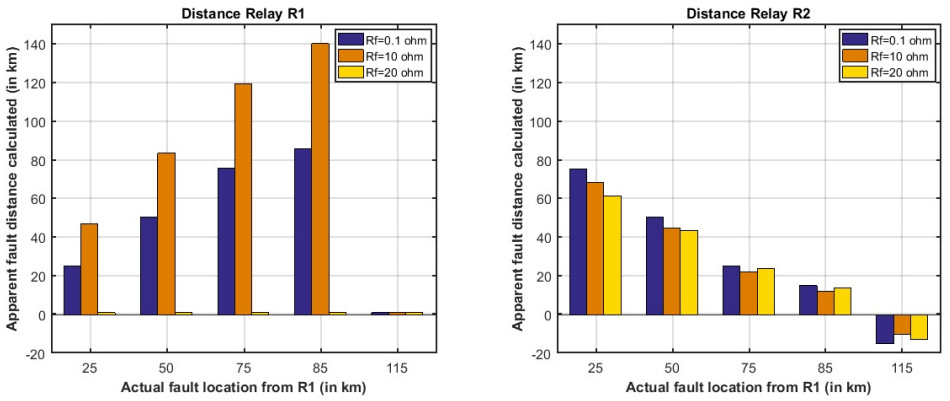


Figure 6.2: Apparent fault distance calculated by the distance relays R1 and R2 for a phase A-phase B fault with $P_{HVDC} = 0 p.u.$

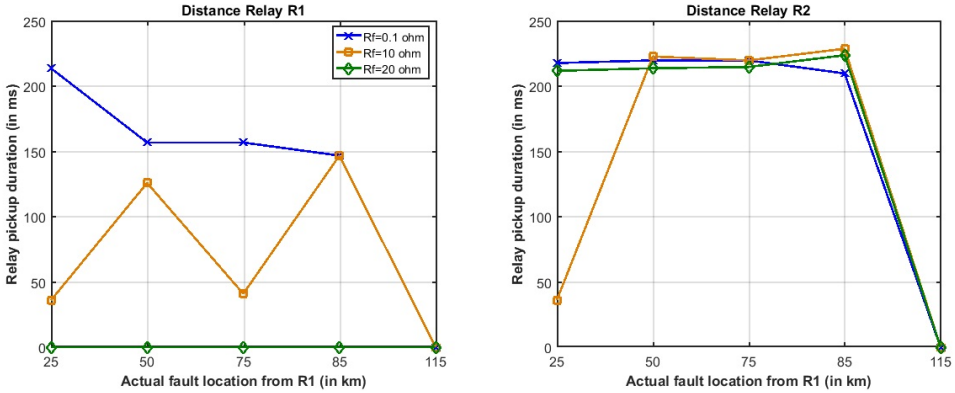


Figure 6.3: Duration of pickup by the distance relays R1 and R2 for a phase A-phase B fault with $P_{HVDC} = 0 p.u.$

trip signal (refer Table 6.1 and Figure 6.4). The apparent fault distance seen by the relay R1 is 25.2 km, which is close to the actual fault location.

Similarly, for a phase A-phase B fault[39] at 85 km from R1, the relay has picked up for a duration of 147 ms in zone 2, identifying correctly the fault loop as a phase A-phase B fault, as presented in Figure 6.3 and Table 6.1. The relay does not send the trip command as the duration of the fault is only 200 ms, which is lesser than the operating delay for a zone 2 fault. The relay R1 identifies the apparent fault location as 85.9 km, as depicted in Figure 6.2.

On the other hand, the distance relay R2 has operated for a phase A-phase B fault at 25 km from the relay R1, as shown in Table 6.1. The relay R2 picks up in zone 1 for a duration of 218 ms and issues a trip signal to the breaker estimating the apparent distance to the fault as 75.4 km, which lies in zone 1 of the relay R2 (see Figure 6.2 and Figure 6.3). In another instance, the relay R2 issues a three-pole trip signal in 2 ms for a fault at 85 km from relay R1.

In another situation as presented in Table 6.2, a phase A-phase B fault is studied at different fault locations with $P_{HVDC} = 0MW$, $R_f = 10\Omega$. It is observed from Figure 6.2 and Figure 6.3 that the relay R1:[40] calculates the apparent fault location at 47.1 km for a 25 km fault from R1. The distance relay R1 picks up for zone 1 for the duration of 36 ms and issues a trip signal in 4 ms. Similarly, for another phase A-phase B fault located at 50 km and 75 km from R1, the relay R1 estimates the distance to the fault at 83.5 km and 119.3 km, respectively without issuing any trip (refer Figure 6.2 and Figure 6.4). Moreover, the relay R1 picks up for zone 2 for both the above scenarios. Consequently, this corresponds that the distance relay performance degrades with the increase in the fault resistance.

[39] Operation of distance relay R1:
- Pickup zone: Zone 2,
- Pickup duration: 147 ms,
- Trip zone: none,
- Trip duration: none,
- Apparent fault location: 85.9 km,

[40] Operation of distance relay R1
- Pickup zone: Zone 1,
- Pickup duration: 36 ms,
- Trip zone: Zone 1,
- Trip duration: 4 ms,
- Apparent fault location: 47.1 km,

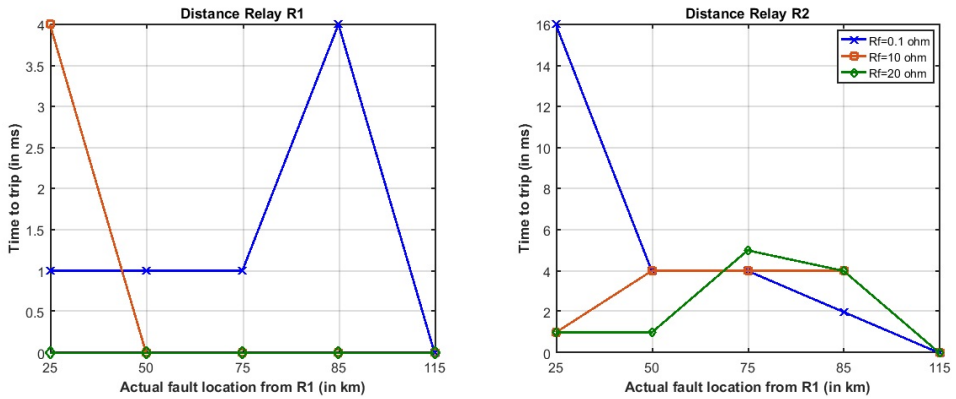


Figure 6.4: Time taken to trip by the distance relays R1 and R2 for a phase A-phase B fault with $P_{HVDC} = 0 p.u.$

For different fault locations from R1 with $P_{HVDC} = 0MW$, $R_f = 0.1\Omega$								
Relay	Location (in km)	Pickup Zone			Trip Zone			Phase loop
		Zone1	Zone2	Zone3	Zone1	Zone2	Zone3	
R1	25	X	-	-	X	-	-	ABC
	50	X	-	-	X	-	-	ABC
	75	X	-	-	X	-	-	ABC
	85	-	X	-	-	-	-	-
	115	-	-	-	-	-	-	-
R2	25	X	-	-	X	-	-	ABC
	50	X	-	-	X	-	-	ABC
	75	X	-	-	X	-	-	ABC
	85	X	-	-	X	-	-	ABC
	115	-	-	-	-	-	-	-

Table 6.1: Distance relay performance for phase A-phase B fault for different fault locations at $P_{HVDC} = 0MW$, $R_f = 0.1\Omega$.

On the other hand, the relay R2 operates precisely for a phase A-phase B faults at locations 25, 50, 75, 85, and 115 km. Comparing the operation of R1 and R2, it has been observed that the relay R2 pickup for a duration of 36 ms for zone 1 and issues a trip command for a fault at 25 km from R1. With respect to this, the relay R2[41] pickup during a phase A-phase B at 50 km for the duration of 223 ms (see Figure 6.3 and Table 6.2). The relay R2 estimates the fault location at 44.9 km and issues a trip signal in 4 ms. Similar is the case for other fault location, (see Table 6.2).

In another situation, the relay R1 does not operate during the unsymmetrical phase A-phase B fault at locations 25, 50, 75, 85, and 115 km with $P_{HVDC} = 0MW$ and $R_f = 20\Omega$ (see Figure 6.2, Figure 6.3 and Figure 6.4). The relay neither picks up nor issues any trip command to open the breaker. Consequently, the relay fails to estimate the fault location on the transmission line, as presented in Table 6.3. Table 6.3 elaborates that the phase A-phase B fault at 50 km from R1 has been picked up by the relay R2[42] as a fault in zone 1 for the duration of 214 ms. Finally, the relay R2 issues a three-pole trip in 1 ms estimating the fault to be located at 43.4 km from R2. Additionally, the relay R2 identifies the unbalanced fault on the line located at 75 and 85 km with $R_f = 20\Omega$ at 23.9 km and 13.6 km, respectively, as shown in Table 6.3. The relay picks up for the duration of 215 and 224 ms, respectively.

[41] Operation of distance relay R2:
- Pickup zone: Zone 1,
- Pickup duration: 223 ms,
- Trip zone: Zone 1,
- Trip duration: 4 ms,
- Apparent fault location: 44.9 km,

[42] Operation of distance relay R2:
- Pickup zone: Zone 1,
- Pickup duration: 214 ms,
- Trip zone: Zone 1,
- Trip duration: 1 ms,
- Apparent fault location: 43.4 km,

Effect of VSC-HVDC operating as an inverter

In another situation, when VSC-HVDC system is injecting 500 MW (0.5 p.u.) of active power into the network, the responses of distance relay have been recorded for phase A-phase B

For different fault locations from R1 with $P_{HVDC} = 0MW$, $R_f = 10\Omega$								
Relay	Location (in km)	Pickup Zone			Trip Zone			Phase loop
		Zone1	Zone2	Zone3	Zone1	Zone2	Zone3	
R1	25	X	-	-	X	-	-	ABC
	50	-	X	-	-	-	-	-
	75	-	X	-	-	-	-	-
	85	-	-	X	-	-	-	-
	115	-	-	-	-	-	-	-
R2	25	X	-	-	X	-	-	ABC
	50	X	-	-	X	-	-	ABC
	75	X	-	-	X	-	-	ABC
	85	X	-	-	X	-	-	ABC
	115	-	-	-	-	-	-	-

Table 6.2: Distance relay performance for phase A-phase B fault for different fault locations at $P_{HVDC} = 0MW$, $R_f = 10\Omega$.

For different fault locations from R1 with $P_{HVDC} = 0MW$, $R_f = 20\Omega$								
Relay	Location (in km)	Pickup Zone			Trip Zone			Phase loop
		Zone1	Zone2	Zone3	Zone1	Zone2	Zone3	
R1	25	-	-	-	-	-	-	-
	50	-	-	-	-	-	-	-
	75	-	-	-	-	-	-	-
	85	-	-	-	-	-	-	-
	115	-	-	-	-	-	-	-
R2	25	X	-	-	X	-	-	ABC
	50	X	-	-	X	-	-	ABC
	75	X	-	-	X	-	-	ABC
	85	X	-	-	X	-	-	ABC
	115	-	-	-	-	-	-	-

Table 6.3: Distance relay performance for phase A-phase B fault for different fault locations at $P_{HVDC} = 0MW$, $R_f = 20\Omega$.

fault with $R_f = 0.1\Omega$. It is described from Table 6.4 that the distance relay R1 acts perfectly at $P_{HVDC} = 500MW$, $R_f = 0.1\Omega$. The relay R1[43] issues a three-pole trip command in 1 ms by estimating the distance to a fault at 25.3 km for a phase A-phase B fault on the transmission line (refer Figure 6.5 and Figure 6.6). The relay R1 picks up for a duration of 146 ms for zone 1 (see Table 6.4). It is to be noticed that the relay R1 does not issue any trip command to the breaker for the fault beyond 85 km, however, the relay R1 picks up for zone 2 for the fault at 85 km for a duration of 167 ms, as shown in Figure 6.5, Figure 6.6 and Figure 6.7.

[43] Operation of distance relay R1:
- Pickup zone: Zone 1,
- Pickup duration: 146 ms,
- Trip zone: Zone 1,
- Trip duration: 1 ms,
- Apparent fault location: 25.3 km,

Besides, the relay R2 for a phase A-phase B fault at 25 km from R1 picks up for a duration of 199 ms indicating the fault in zone 1 and sends a trip in 21 ms (refer Figure 6.6 and Figure 6.7). The calculated distance is 75.5 km (refer Figure 6.5). Correspondingly, the resistance of the fault is incremented from $R_f = 0.1\Omega$ to $R_f = 10\Omega$ and the active power supplied from the VSC-HVDC is 500 MW. The increase in the power transfer from the HVDC connection affects the distance relay scheme, as presented in Table 6.5. In addition, Table 6.5 also highlights that the relay R1 issues a trip command only for the faults at 25 km and 50 km. The relay R1 pickup for the phase A-phase B fault in zone 1 for the duration of 141 ms issuing a trip for the duration of 1 ms estimating the fault at 43.3 km.

On the contrary, the relay R1 does not operate for any other phase A-phase B faults at locations beyond 75 km, however, the relay pickup for 76 and 90 ms identifying the faults

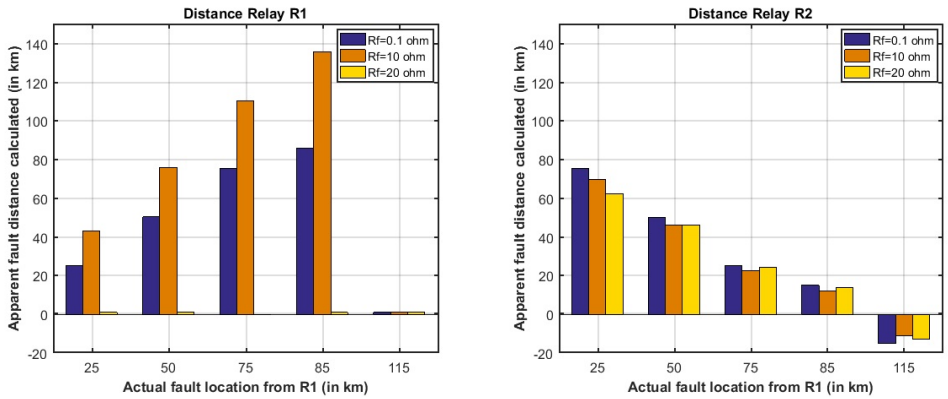


Figure 6.5: Apparent fault distance calculated by the distance relays R1 and R2 for a phase A-phase B fault with $P_{HVDC} = 0.5p.u.$

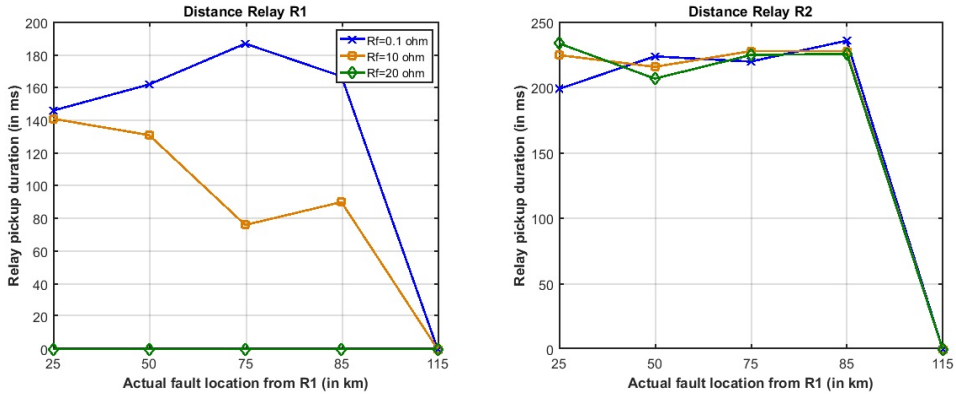


Figure 6.6: Duration of pickup by the distance relays R1 and R2 for a phase A-phase B fault with $P_{HVDC} = 0.5p.u.$

in zone 2 and zone 3, respectively (see Figure 6.6 and Figure 6.7). On the other side, the relay R2 trips for the phase A-phase B fault at 50, 75, and 85 km in 1, 4, 4 ms, respectively.

In another case, the relays R1 and R2 are investigated for the phase A-phase B at $P_{HVDC} = 500MW$ and $R_f = 20\Omega$ injecting the active power into the grid. The resistance to fault is changed from $R_f = 10\Omega$ to $R_f = 20\Omega$ from the previous case. The relay R1[44] neither operates and nor picks up for all the phase A-phase B faults at locations 25, 50, 75, 85 and 115 km, which is evident from Table 6.6, Figure 6.6 and Figure 6.7.

Likewise, Table 6.6 also dictates that the relay R2 responds to the phase A-phase B faults by issuing a trip signal (three-pole trip) when the fault is located at 25 km with $R_f = 20\Omega$. The actual estimation of the fault location is 62.4 km from Figure 6.5. Furthermore, it can be seen in Table 6.6 that the relay R2 performs at all the fault locations 25, 50, 75, and 85 km except for the fault at 115 km. The relay operates in zone 1 with operating time as 4, 16, 4, and 5 ms, respectively, (refer Figure 6.7).

[44]Operation of distance relay R1:

- Pickup zone: none,
- Pickup duration: none,
- Trip zone: none,
- Trip duration: none,
- Apparent fault location: none,

Effect of VSC-HVDC operating as a rectifier

The distance relay R1 and R2 have been observed when the VSC-HVDC operates as an inverter, injecting active power into the electrical transmission network. The distance relay is now assessed when the VSC-HVDC operates as a rectifier, drawing active power from the electrical transmission network. The active power drawn fro the grid is 500 MW and the relay is analyzed for the phase A-phase B faults at different locations. Table 6.7 presents the response of the relay R1 for a fault at 25 km where the relay pickup for for zone 2. The duration of pickup is 26 ms and the relay issues a trip signal in 1 ms. The distance calculated by the relay is 25.3 km, as shown in Figure 6.8 and Figure 6.9.

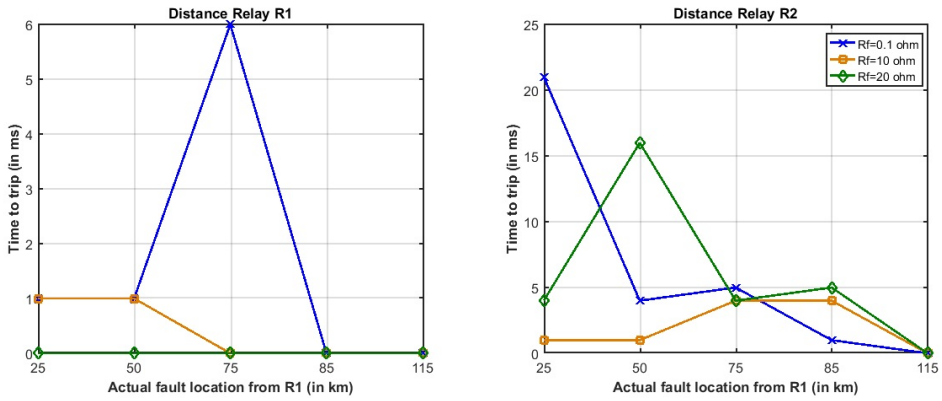


Figure 6.7: Time taken to trip by the distance relays R1 and R2 for a phase A-phase B fault with $P_{HVDC} = 0.5p.u.$

For different fault location from R1 with $P_{HVDC} = 500MW$, $R_f = 0.1\Omega$								
Relay	Location (in km)	Pickup Zone			Trip Zone			Phase loop
		Zone1	Zone2	Zone3	Zone1	Zone2	Zone3	
R1	25	X	-	-	X	-	-	ABC
	50	X	-	-	X	-	-	ABC
	75	X	-	-	X	-	-	ABC
	85	-	X	-	-	-	-	-
	115	-	-	-	-	-	-	-
R2	25	X	-	-	X	-	-	ABC
	50	X	-	-	X	-	-	ABC
	75	X	-	-	X	-	-	ABC
	85	X	-	-	X	-	-	ABC
	115	-	-	-	-	-	-	-

Table 6.4: Distance relay performance for phase A-phase B fault for different fault locations at $P_{HVDC} = 500MW$, $R_f = 0.1\Omega$.

[45]Operation of distance relay R1:
- Pickup zone: Zone 1,
- Pickup duration: 16 ms,
- Trip zone: Zone 1,
- Trip duration: 1 ms,
- Apparent fault location: 50.6 km,

In another situation, the relay R1[45] picks up for 16 ms calculating the fault lying in zone 1 and issues a trip signal by estimating the location as 50.6 km. On the other hand, the relay R1 does not operate for the fault at 85 km, however, it picks up for zone 2 and determines the fault loop as phase A-phase B. The distance located by the relay is 86.1 km, as given in Figure 6.8.

Correspondingly, the relay R2 picks up for the fault located at 25, 50, 75 and 85 km from R1 for the duration of 41, 46, 41 and 224 ms, respectively. The distance estimated are 75.4, 50.2, 25.1 and 15 km, respectively (refer Figure 6.8). The relay R2 does not respond to the fault at 115 km from R1 because it falls behind the relay R2 (see Table 6.7).

Moreover, Table 6.8 presents the relay responses for $P_{HVDC} = -500MW$ and $R_f = 10\Omega$ where the relay pickup for the fault at 25km from R1 and issues a trip for zone 1 in 10 ms (refer Figure 6.9). The calculated distance is 32.5 km for the phase A-phase-B fault at an actual distance of 25 km. In another instances, for the fault at 50 km and 75 km with $R_f = 10\Omega$, the relay R1[46] pickup for zone 2 for the duration of 115 and 12 ms, respectively. In spite of this relay pickup, the relay is unable to issue any kind of trip command to open the breakers when the VSC-HVDC is acting as a rectifier.

[46]Operation of distance relay R1:
- Pickup zone: Zone 2,
- Pickup duration: 115 ms,
- Trip zone: none,
- Trip duration: none,
- Apparent fault location: 87.9 km,

On the contrary, the relay R2 is able to open the breakers by sending the trip signals after locating the phase A-phase B faults in zone 1 at an apparent distance of 44.2 and 20.9 km for the actual fault locations of 50 km and 75 km from R1 (refer Figure 6.8 and Figure 6.9). The relay R2 issues a trip signal in 1 and 4 ms, respectively. It is also observed that the relay R2 is not able to recognize the phase A-phase B fault at a distance of 115 km from R1, which actually falls behind the relay R2 (refer Table 6.8 and Table 6.9).

For different fault location from R1 with $P_{HVDC} = 500MW$, $R_f = 10\Omega$								
Relay	Location (in km)	Pickup Zone			Trip Zone			Phase loop
		Zone1	Zone2	Zone3	Zone1	Zone2	Zone3	
R1	25	X	-	-	X	-	-	ABC
	50	X	-	-	X	-	-	ABC
	75	-	X	-	-	-	-	-
	85	-	-	X	-	-	-	-
	115	-	-	-	-	-	-	-
R2	25	X	-	-	X	-	-	ABC
	50	X	-	-	X	-	-	ABC
	75	X	-	-	X	-	-	ABC
	85	X	-	-	X	-	-	ABC
	115	-	-	-	-	-	-	-

Table 6.5: Distance Relay performance for phase A-phase B fault for different fault locations at $P_{HVDC} = 500MW$, $R_f = 10\Omega$.

For different fault locations from R1 with $P_{HVDC} = 500MW$, $R_f = 20\Omega$								
Relay	Location (in km)	Pickup Zone			Trip Zone			Phase loop
		Zone1	Zone2	Zone3	Zone1	Zone2	Zone3	
R1	25	-	-	-	-	-	-	-
	50	-	-	-	-	-	-	-
	75	-	-	-	-	-	-	-
	85	-	-	-	-	-	-	-
	115	-	-	-	-	-	-	-
R2	25	X	-	-	X	-	-	ABC
	50	X	-	-	X	-	-	ABC
	75	X	-	-	X	-	-	ABC
	85	X	-	-	X	-	-	ABC
	115	-	-	-	-	-	-	-

Table 6.6: Distance Relay performance for phase A-to-phase B fault for different fault location at $P_{HVDC} = 500MW$, $R_f = 20\Omega$.

6.4 PILOT DISTANCE RELAYING SCHEME

6.4.1 *Permissive Underreach Transfer Trip (PUTT)*

In a Permissive tripping scheme[47] [156]:

1. The local relay sends a signal if it detects the fault in its forward-looking zone;
2. Upon receipt of the signal, the remote relay checks to see if it meets the criteria for tripping in Zone 2. For a valid check, it is necessary to bypass the Zone 2 timer to trip for an internal feeder fault. Otherwise, the Zone 2 timer must operate to trip and time grade for an external fault (e.g., CB failed in the remote substation) [13].

A fault within Zone 1 causes this zone to trip immediately. Because the relay qualifies the signal before accelerating tripping, the scheme is more secure than the DTT scheme [157]. In a PUTT scheme, as the scheme name indicates, the underreaching element (Zone 1) keys or transmits the signal. Figure 6.10 is a basic representation of a PUTT scheme. One disadvantage of PUTT is the reduced arc coverage of the Zone 1 element.

[47] Salient features of PUTT scheme:

- Immediate tripping if the fault is in zone 1,
- more secure than DTT scheme,
- Reduced arc coverage of zone 1 element,

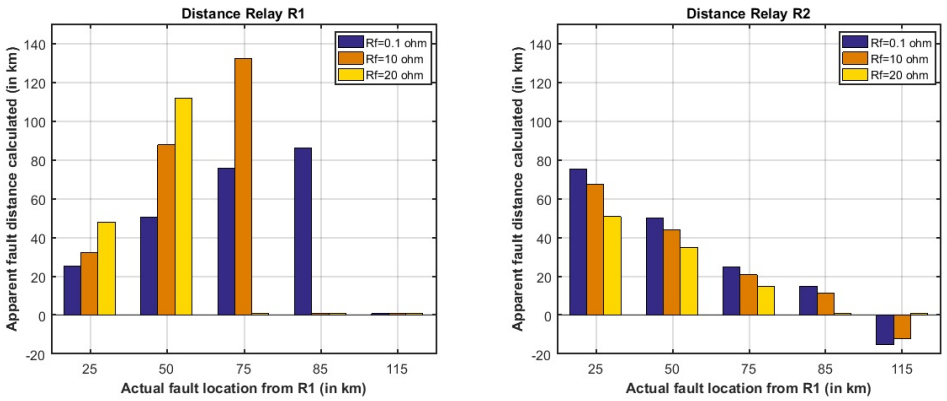


Figure 6.8: Apparent fault distance calculated by the distance relays R1 and R2 for a phase A-phase B fault with $P_{HVDC} = -0.5 p.u.$

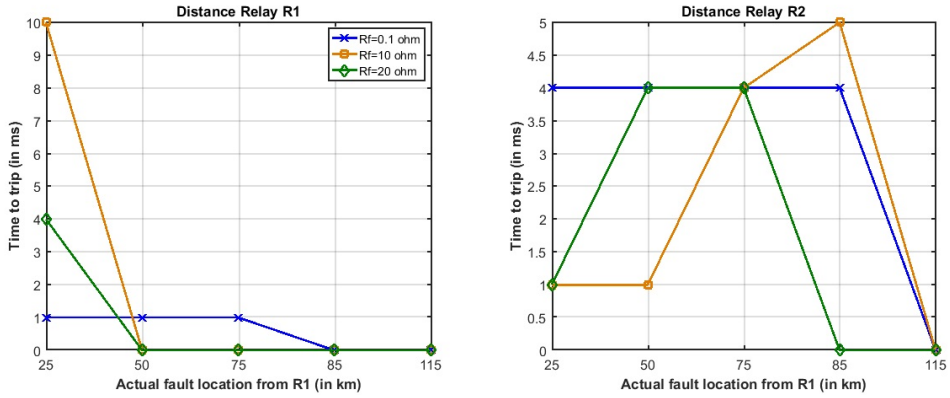


Figure 6.9: Time taken to trip by the distance relays R1 and R2 for a phase A-phase B fault with $P_{HVDC} = -0.5 p.u.$

6.4.2 *POTT*

[48] Salient features of POTT scheme:

- reverse looking zone to block the remote end from echoing a permissive signal back to the local relay for an external fault,
- more secure than DTT scheme,
- Larger arc coverage of zone 1 element,

In a POTT scheme[48], as in Figure 6.11, the overreaching element (Zone 2) has a larger arc coverage. The POTT scheme uses the overreaching element to send a permissive signal, so it must have a reverse looking zone to block the remote end from echoing a permissive signal back to the local relay for a fault external to the feeder [105]. The scheme must have a third distance zone set to look in the reverse direction. This zone is necessary to prevent the remote end from echoing the received signal back to the local end if the remote relay detects the fault behind it (i.e., the fault is external to the feeder). Permissive schemes are biased toward security of supply, rather than dependability of protection operation. This means that if the communications system is unavailable, then the remote relay will trip in Zone 2 time (delayed) for a fault close to the local relay, but it will remain stable for external faults [89].

The major disadvantage of PTT in use with communications channels associated with the protected line (Power Line Carrier (PLC) or Optical Phase ground Wire (OPGW)) is that the signal must pass through the fault. This could be difficult for analog PLC or become problematic if the line loses mechanical integrity in addition to having an electrical short circuit.

6.4.3 *DCB*

Operation of this scheme is the opposite of permissive scheme operation:

For different fault locations from R1 with $P_{HVDC} = -500MW$, $R_f = 0.1\Omega$								
Relay	Location (in km)	Pickup Zone			Trip Zone			Phase loop
		Zone1	Zone2	Zone3	Zone1	Zone2	Zone3	
R1	25	X	-	-	X	-	-	ABC
	50	X	-	-	X	-	-	ABC
	75	X	-	-	X	-	-	ABC
	85	-	X	-	-	-	-	-
	115	-	-	-	-	-	-	-
R2	25	X	-	-	X	-	-	ABC
	50	X	-	-	X	-	-	ABC
	75	X	-	-	X	-	-	ABC
	85	X	-	-	X	-	-	ABC
	115	-	-	-	-	-	-	-

Table 6.7: Distance relay performance for a phase A-phase B fault for different fault locations at $P_{HVDC} = -500MW$, $R_f = 0.1\Omega$.

For different fault locations from R1 with $P_{HVDC} = -500MW$, $R_f = 10\Omega$								
Relay	Location (in km)	Pickup Zone			Trip Zone			Phase loop
		Zone1	Zone2	Zone3	Zone1	Zone2	Zone3	
R1	25	X	-	-	X	-	-	ABC
	50	-	X	-	-	-	-	-
	75	-	-	X	-	-	-	-
	85	-	-	-	-	-	-	-
	115	-	-	-	-	-	-	-
R2	25	X	-	-	X	-	-	ABC
	50	X	-	-	X	-	-	ABC
	75	X	-	-	X	-	-	ABC
	85	X	-	-	X	-	-	ABC
	115	-	-	-	-	-	-	-

Table 6.8: Distance relay performance for phase A-phase B fault for different fault locations at $P_{HVDC} = -500MW$, $R_f = 10\Omega$.

1. The remote relay detects a fault in Zone 2. If it does not receive a signal from the local relay within a preset time, it trips instantaneously (accelerated tripping compared to a stepped distance timer).

2. The remote relay detects a fault in Zone 2. If it receives a signal from the local relay within a preset time, it delays tripping to Zone 2.The local terminal should only send a signal if it detects the fault in the reverse direction (typically Zone 3).

3. The relay trips instantaneously.

This scheme[49] differs from the permissive scheme in that it sends a signal if it detects an external fault within Zone 3. The permissive scheme, on the other hand, sends a signal if it detects the fault within a feeder's protective zone (Zone 1 or Zone 2, depending on the type of scheme selected) [63].

Figure 6.12 is a simplified sketch of a DCB communications aided tripping scheme. There will be an accelerated clearing of the fault. However, if the fault were directly behind the local relay, and the remote relay detected the fault within its protective zone (Zone 2), the remote relay would trip quickly for an external fault because the blocking signal did not reach the remote relay. Therefore, this scheme is biased toward dependability of protection operation rather than security. To improve the security of supply, DCB usually employs duplicate blocking signals and enabling through the channel OK (guard function) signal

[49] Salient features of DCB scheme:

- instantaneous tripping,
- Accelerated fault clearance,
- Priority is dependability of protection operation rather than the security,
- Duplicate blocking signals to maintain the security,
- No interference of blocking or trip signal with the fault,

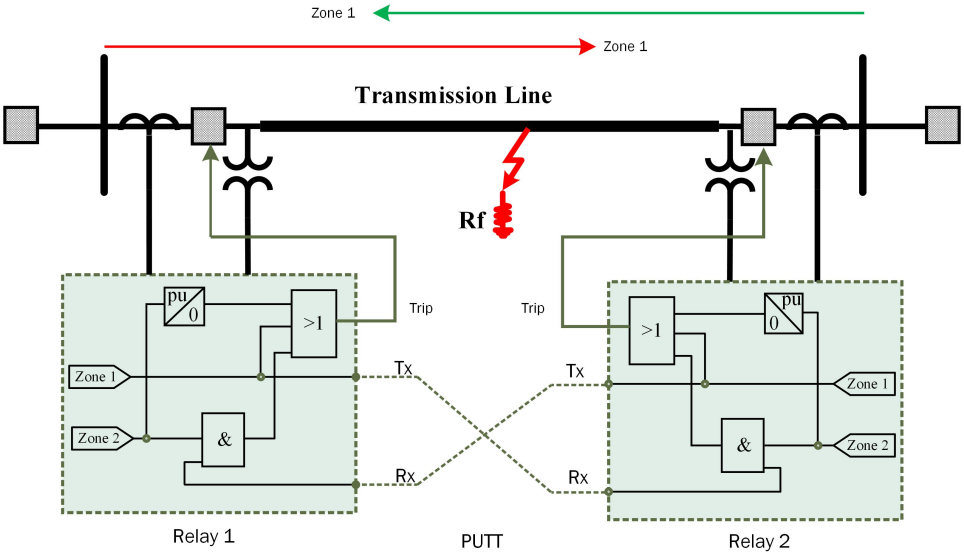


Figure 6.10: A simplified sketch of a PUTT communications assisted tripping scheme.

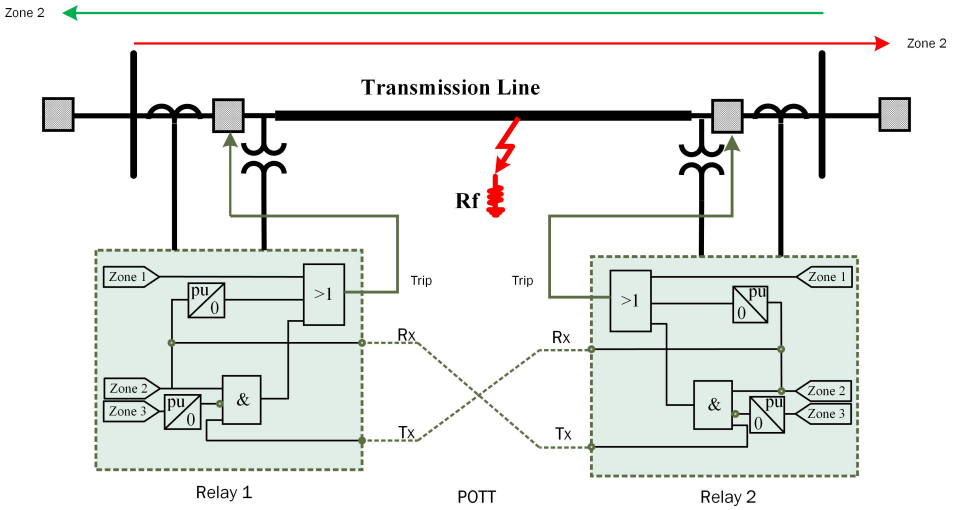


Figure 6.11: A simplified sketch of a POTT communications assisted tripping scheme.

from the communications system. The major advantage of DCB is that the signal does not pass through the fault. Its operation and speed are therefore assured.

The communication-assisted distance relays R1 and R2 are tested for the fault locations 25, 50, 75, 85 and 115 km at $P_{HVDC} = 0MW$ and $R_f = 0.1\Omega$, as presented in Figure 6.13. When a phase A-phase B fault is implemented at a distance of 25 km from the relay R1[50], the relay pickup for zone 1 and detected the fault loop as phase A-phase B for the duration of 157 ms. The relay identifies the fault in zone 1 and subsequently, issues a three-pole trip command to open the breakers. The PUTT scheme operates in 2 ms and detected the location of the fault as 25.3 km (zone 1) as the fault lies in the under reaching element of the distance relay R1, whereas, the POTT scheme operates in 3 ms, look at Table 6.9.

Likewise, another phase A-phase B fault is implemented at 50 km from the relay R1 with $R_f = 0.1\Omega$, wherein the relay R1 determines that the fault lies in zone 1 reach of the under reaching element and sends a three-pole trip to the breaker (see Table 6.9 and Figure 6.13). The PUTT and POTT functions operate by sending and receiving accelerated trip signals in 2 ms each (see Figure 6.14). The trip is accelerated and the distance to the fault is determined as 50.5 km (refer Figure 6.13). Similarly, the relay R1 detects the faults

[50]Operation of pilot-distance relay R1:

- Pickup zone: Zone 1,
- Pickup duration: 157 ms,
- Trip zone: Zone 1,
- Trip duration: 2 ms (PUTT) and 3 ms (POTT),
- Apparent fault location: 25.3 km,

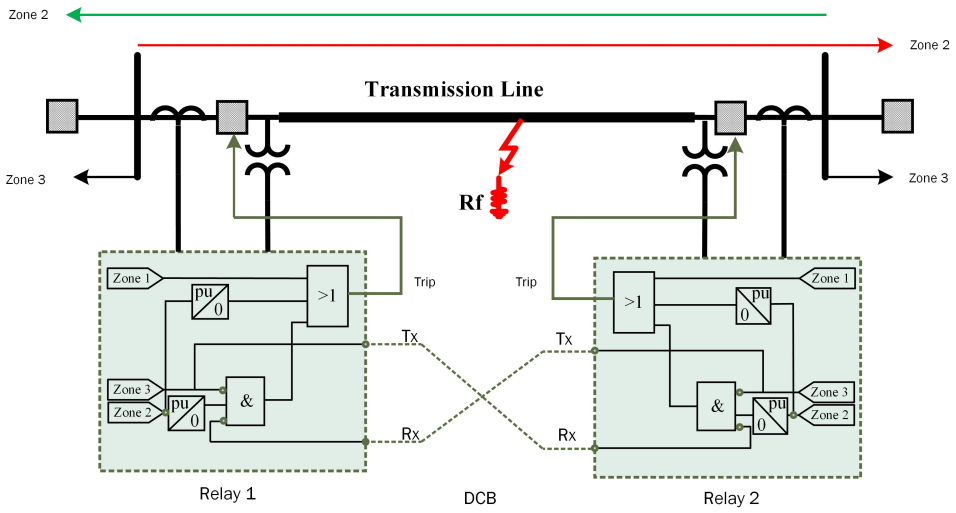


Figure 6.12: A simplified sketch of a DCB communications assisted tripping scheme.

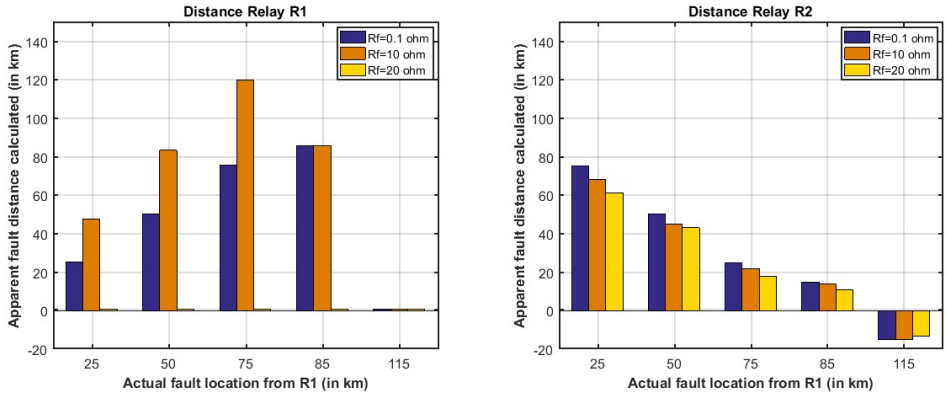


Figure 6.13: Apparent fault distance calculated by the distance relays R1 and R2 for a phase A-phase B fault with $P_{HVDC} = 0$p.u.

at 75 and 85 km to be lying in zone 1 of the relay R1. The under reaching and overreaching elements of the relay R1 identify the faults appropriately.

On the other hand, Table 6.9, Figure 6.13, Figure 6.14, and Figure 6.15 also present the operation of relay R2[51] for $R_f = 0.1\Omega$ using the tele-protection PUTT and POTT scheme. The relay R2 initiates trip signals for the phase A-phase B faults at the distance of 25, 50, 75, and 85 km from R1 in 80, 71, 72 and 3 ms, respectively, as shown in Figure 6.14 and Figure 6.15. The relay R2 operates appropriately for the low resistance fault at 25, 50, 75, and 85 km. Moreover, the relay R2 does not trip for the fault at 115 km from R1 even in the presence of POTT element of the distance function.

Table 6.10 presents the results of relays R1 and R2 for the phase A-phase B fault on the transmission line protected by communication assisted distance protection namely PUTT and POTT elements with $R_f = 10\Omega$ and $P_{HVDC} = 0MW$. The Table 6.10 shows that the relay R1 initiates the trip signals for the fault located at 75 and 85 km of distance from R1 and identifying it in zone 1 region of the relay. On the contrary, the relay R1 in the previous case of $R_f = 10\Omega$ and $P_{HVDC} = 0MW$ without pilot-distance protection performed incorrectly leading to a wrong operation, as presented in Table 6.2. The relay R1 estimates the distance to phase A-phase B faults as 120.2 and 86 km, respectively, for the faults actually located at 75 and 85 km. Subsequently, for the fault with $R_f = 20\Omega$ and $P_{HVDC} = 0MW$, the PUTT and POTT distance elements do not operate for any fault locations leading to a wrong operation of the distance relay R1 (see Table 6.11). Nonetheless, the relay R2 picks up in zone 1 and initiates a trip signal.

[51] Operation of pilot-distance relay R2:

- Pickup zone: Zone 1,
- Pickup duration: 226 ms,
- Trip zone: Zone 1,
- Trip duration: 80 ms (PUTT) and 80 ms (POTT),
- Apparent fault location: 75.3 km,

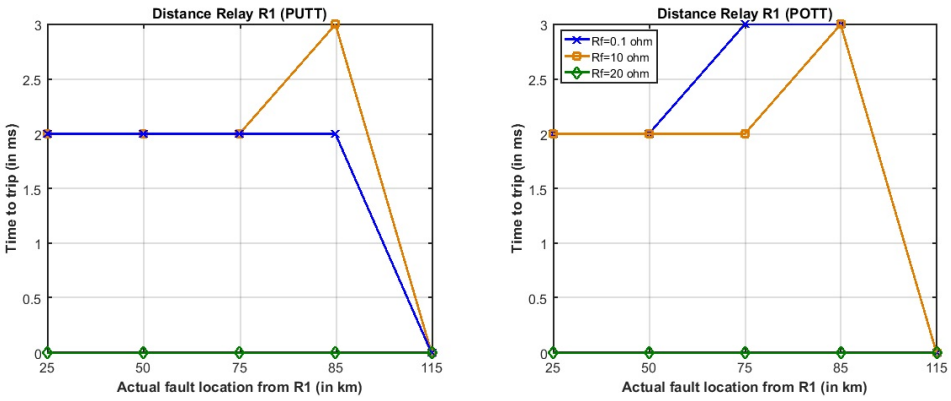


Figure 6.14: Time taken to trip by the PUTT element of distance relays R1 and R2 for a phase A-phase B fault with $P_{HVDC} = 0 p.u.$

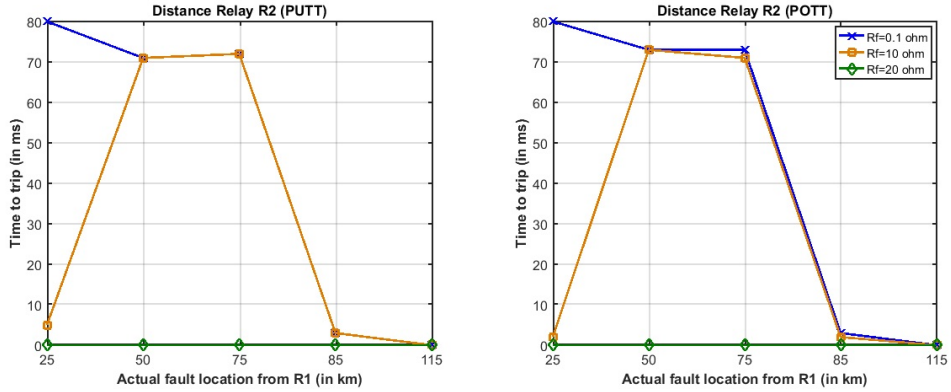


Figure 6.15: Time taken to trip by the POTT element of distance relays R1 and R2 for a phase A-phase B fault with $P_{HVDC} = 0 p.u.$

6.5 ADAPTIVE DISTANCE RELAYING SCHEME

6.5.1 *Mathematical Evaluation*

Consider a three-phase fault at the point k on the transmission line at a distance of x km from the bus p, as shown in Figure 6.16. The voltage of bus p can be given by using Z_{BUS} matrix as [85]:-

$$V_p = V_p^0 - \frac{z_{pk}}{z_{kk}}.V_k^0 \tag{6.1}$$

Where,

$$V_k^0 = x.V_p^0 + (L - x).V_n^0 \tag{6.2}$$

Where, L is the length of the line, V_p^0, V_k^0, V_n^0 are the pre-fault voltages at bus p, k, and n, Z_{pk} is the transfer impedance and Z_{kk} is the driving point impedance at the fault bus k.

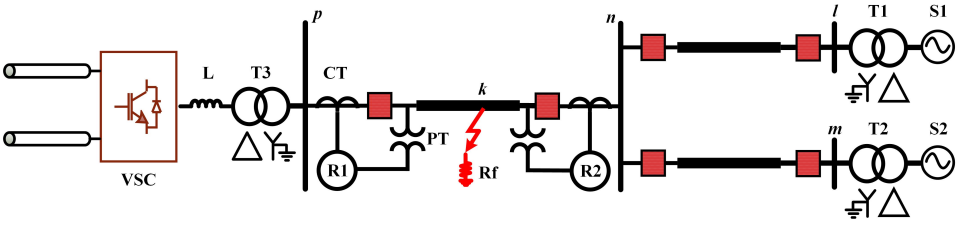


Figure 6.16: Power system with VSC-HVDC connected to transmission line.

For different fault locations from R1 with $P_{HVDC} = 0MW$, $R_f = 0.1\Omega$								
Relay	Location (in km)	Pickup Zone			Trip Zone			Phase loop
		Zone1	Zone2	Zone3	Zone1	Zone2	Zone3	
R1	25	X	-	-	X	-	-	ABC
	50	X	-	-	X	-	-	ABC
	75	X	-	-	X	-	-	ABC
	85	X	-	-	X	-	-	ABC
	115	-	X	-	-	-	-	-
R2	25	X	-	-	X	-	-	ABC
	50	X	-	-	X	-	-	ABC
	75	X	-	-	X	-	-	ABC
	85	X	-	-	X	-	-	ABC
	115	-	-	-	-	-	-	-

Table 6.9: Pilot-distance relay performance for phase A-phase B fault for different fault locations at $P_{HVDC} = 0MW$ and $R_f = 0.1\Omega$.

For different fault locations from R1 with $P_{HVDC} = 0MW$, $R_f = 10\Omega$								
Relay	Location (in km)	Pickup Zone			Trip Zone			Phase loop
		Zone1	Zone2	Zone3	Zone1	Zone2	Zone3	
R1	25	X	-	-	X	-	-	ABC
	50	X	-	-	X	-	-	ABC
	75	X	-	-	X	-	-	ABC
	85	X	-	-	X	-	-	ABC
	115	-	X	-	-	-	-	-
R2	25	X	-	-	X	-	-	ABC
	50	X	-	-	X	-	-	ABC
	75	X	-	-	X	-	-	ABC
	85	X	-	-	X	-	-	ABC
	115	-	-	-	-	-	-	-

Table 6.10: Pilot-distance relay performance for phase A-phase B fault for different fault location at $P_{HVDC} = 0MW$, $R_f = 10\Omega$.

The reactive component of converter current controls the PCC voltage or voltage at bus p. Therefore, the converter dynamics can be taken into account to calculate the post-fault PCC voltage by taking into account the reactive current injection into the network.

$$v_q^{PCC} = -L.\frac{di}{dt} - R.i_q^{'} - \omega.L.i_d^{'} + v_q \tag{6.3}$$

where

$$i_q^{'} = i_q + \Delta i_q \tag{6.4}$$

$$i_d^{'} = i_d + \Delta i_d \tag{6.5}$$

Δi_q and Δi_d are the changes in the reactive and active current after the fault. Especially, the change in reactive current has to be noticed when the converter supplies current into the network to support the network voltage.

$$\Delta i_q = k.i_q(\frac{\Delta U}{U_N}) \tag{6.6}$$

$$v_q^{PCC} = -(k_p + \frac{k_i}{s})(i_q^{ref} - i_q) - \omega.L.i_d^{'} + v_q \tag{6.7}$$

For different fault locations from R1 with $P_{HVDC} = 0MW$, $R_f = 20\Omega$								
Relay	Location (in km)	Pickup Zone			Trip Zone			Phase loop
		Zone1	Zone2	Zone3	Zone1	Zone2	Zone3	
R1	25	-	-	X	-	-	-	-
	50	-	-	-	-	-	-	-
	75	-	-	-	-	-	-	-
	85	-	-	-	-	-	-	-
	115	-	-	-	-	-	-	-
R2	25	X	-	-	X	-	-	ABC
	50	X	-	-	X	-	-	ABC
	75	X	-	-	X	-	-	ABC
	85	X	-	-	X	-	-	ABC
	115	-	-	-	-	-	-	-

Table 6.11: Pilot-distance relay performance for phase A-phase B fault for different fault location at $P_{HVDC} = 0MW$, $R_f = 20\Omega$ and active current blocked limitation strategy.

Expression (6.7) presents the inner current loop of the VSC, which can be written as:

$$v_q^{PCC} = -(k_p + \frac{k_i}{s})\Delta i_q - \omega.L.\Delta i_d + v_q \tag{6.8}$$

Therefore,

$$s.v_q^{PCC} = -(s.k_p + k_i)\Delta i_q - s.\omega.L.\Delta i_d + s.v_q \tag{6.9}$$

This can be written as:

$$s.v_q^{PCC} = -(s.k_p + k_i)\Delta i_q - s.\omega.L.\Delta i_d + s.v_q \tag{6.10}$$

$$\frac{dv_q^{PCC}}{dt} = -(\frac{dk_p}{dt} + k_i)\Delta i_q - \omega.L.\frac{d\Delta i_d}{dt} \tag{6.11}$$

Thus, the PCC voltage after taking the reactive current injection into account can be expressed as:

$$\frac{dv_q^{PCC}}{dt} = -(k_i)\Delta i_q - \omega.L.\frac{d\Delta i_d}{dt} \tag{6.12}$$

The PCC voltage is expressed in terms of d and q axis currents contribution during the fault. The limitation strategy implemented can decide the PCC voltage under the different scenarios.

1. *Active Current Blocked*

$$i_d^{lim} = 0 \tag{6.13}$$

$$i_q^{lim} = I_{max} \tag{6.14}$$

Hence, Expression can be written as (6.15):

$$\frac{dv_q^{PCC}}{dt} = -(k_i)\Delta i_q \tag{6.15}$$

$$v_q^{PCC}(t) = \Delta i_q e^{-k_i t} \tag{6.16}$$

If the reactive current injection does not hit the limit, which depends upon the PCC voltage drop, then $v_q^{PCC}(t)$ can be given by expression (6.17):

$$v_q^{PCC}(t) = k\frac{\Delta U}{U_N} i_n e^{-k_i t} \tag{6.17}$$

Otherwise, $\Delta i_q = \pm I_{max}$

$$v_q^{PCC}(t) = \pm I_{max} e^{-k_i t} \tag{6.18}$$

2. *Reactive Current Priority*

$$i_q^{lim} = i_q^{ref} \leqslant 1 \tag{6.19}$$

$$i_d^{lim} = \sqrt{(I_{max})^2 - (i_q^{lim})^2} \tag{6.20}$$

$$\frac{dv_q^{PCC}}{dt} = -(k_i) i_q^{ref} - \omega.L. \frac{d\sqrt{(I_{max})^2 - (i_q^{lim})^2}}{dt} \tag{6.21}$$

Expression (6.21) presents the PCC voltage during the reactive current priority mode; if the reactive current does not hit the limit then q axis reference current will be the reactive current.

3. *Equal Current Priority*

$$i_d^{lim} = I_{max}.\cos\alpha \tag{6.22}$$

$$i_q^{lim} = I_{max}.\sin\alpha \tag{6.23}$$

$$\frac{dv_q^{PCC}}{dt} = -(k_i) I_{max}.\sin\alpha - \omega.L. \frac{dI_{max}.\cos\alpha}{dt} \tag{6.24}$$

The PCC voltage obtained in the above conditions are utilized to calculate the apparent impedance seen by the distance relay as:

$$Z_{PCC} = \frac{V_{PCC}}{I_{PCC}} \tag{6.25}$$

The calculated impedance is then utilized as the reach setting with an additional 10% margin for a safe operation.

6.5.2 *Algorithm*

The following is the algorithm developed for the Adaptive Distance Relaying Scheme:

1. Obtain the topology of the network. Run the load flow and obtain the active and reactive power flow through the network. Acquire the voltage and current phasor at the relay bus close to the VSC-HVDC terminal.
2. Pass the voltage and current signals through the low pass filter and FFT. Compute Z_{BUS} of the network assuming VSC-HVDC as a variable voltage source.
3. Check for the faults.
4. Check for the fault types.
5. For symmetrical fault: positive sequence currents exists.
6. For Unsymmetrical faults: positive and negative sequence currents exist.
7. Check for the negative sequence current suppression or injection.
8. For the negative sequence current injection, calculate the amount of negative sequence current injected through the negative sequence network.

9. Measure the PCC voltage drop across the terminal of the VSC-HVDC and then calculate the reactive current injection discussed in Chapter 4.

$$\Delta i_q = k.i_q(\frac{\Delta U_N}{U_N}) \tag{6.26}$$

10. Check the current limitation strategy activated and then compute the limit applied.
11. Active Current Blocked limitation strategy or

$$i_d^{lim} = 0 \tag{6.27}$$

$$i_q^{lim} = I_{max} \tag{6.28}$$

12. Equal Current Priority limitation strategy or

$$i_d^{lim} = I_{max}.cos\alpha \tag{6.29}$$

$$i_q^{lim} = I_{max}.sin\alpha \tag{6.30}$$

13. Reactive Current Priority limitation strategy or

$$i_q^{lim} = i_q^{ref} \tag{6.31}$$

$$i_d^{lim} = \sqrt{(I_{max})^2 - (i_q^{lim})^2} \tag{6.32}$$

14. Compute new voltage, current and Z_{app}. Load the relay with new reach settings.

6.6 RELAY PERFORMANCE WITH ADAPTIVE SCHEME

The performance of an adaptive relaying scheme is evaluated for the different phase A-phase B fault scenarios on a transmission line connected to VSC-HVDC system. The operation of relays R1 and R2 for an adaptive distance protection are compared with the non-adaptive protection scheme, as shown in Figure 6.17 and Table 6.12.

Figure 6.17, which presents that the non-pilot distance protection with an adaptive relaying scheme for the fault at 25 km and $R_f = 10\Omega$ performed correctly by calculating the distance to fault as 25.3 km. The relay R1[52], with an adaptive scheme, picks up for zone 1 for a duration of 2 ms during a phase A-phase B fault further initiating a trip in 4 ms, which is a correct fault identification (see Figure 6.17 and Figure 6.18). On the contrary, the same relay R1 calculates the location of the fault at 47.1 km for a non-adaptive scheme and trips in 4 ms identifying the fault in zone 1.

In addition to this, the non-pilot distance relay R1 is analyzed for another asymmetrical phase A-phase B fault at a distance of 50 km from R1. As shown in Figure 6.17, the relay R1 computes this fault at a distance of 50.3 km and issues a trip signal (three-pole) trip for zone 1 in 2 ms with the adaptive protection scheme, as presented in Table 6.12. On the other hand, the relay R1 response with a non-adaptive protection scheme for the fault at a distance of 50 km is shown in Figure 6.17, Figure 6.18 and Figure 6.19. The relay picks up for 126 ms and does not initiate a trip signal to open the breaker. Thus, the adaptive scheme aids the relay R1 to operate perfectly.

Additionally, for the fault at 75 km from R1, the relay R1 responds correctly by identifying the correct fault loop and fault location with the adaptive setting. Although, Table 6.12 and Figure 6.19 presents that the relay R1 does not operate for the fault at 85 km and 115 km, which is evident from the plot Figure 6.19, nonetheless, the relay picks up for zone

[52] Operation of non-pilot distance relay R1 with adaptive protection scheme:

- Pickup zone: Zone 1,
- Pickup duration: 2 ms,
- Trip zone: Zone 1,
- Trip duration: 2 ms,
- Apparent fault location: 25.2 km,

Operation of non-pilot distance relay R1 without adaptive protection scheme:

- Pickup zone: Zone 1,
- Pickup duration: 36 ms,
- Trip zone: Zone 1,
- Trip duration: 4 ms,
- Apparent fault location: 47.1 km,

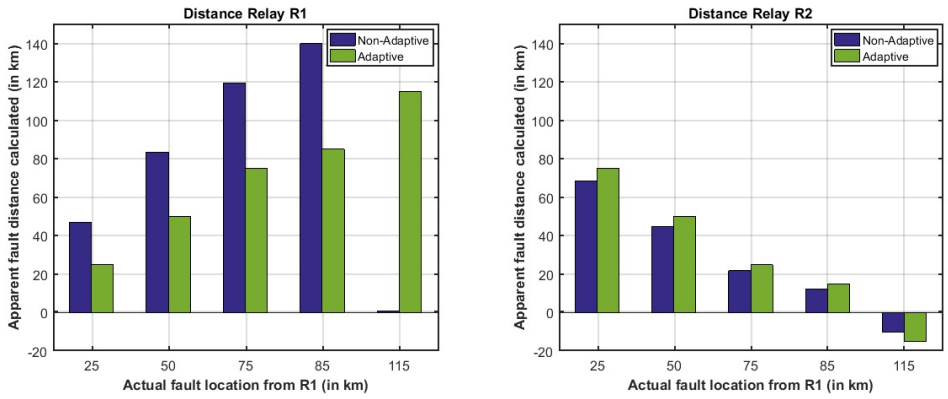


Figure 6.17: Apparent impedance calculated by the distance relays R1 and R2 for a phase A-phase B fault with $P_{HVDC} = 0 p.u.$

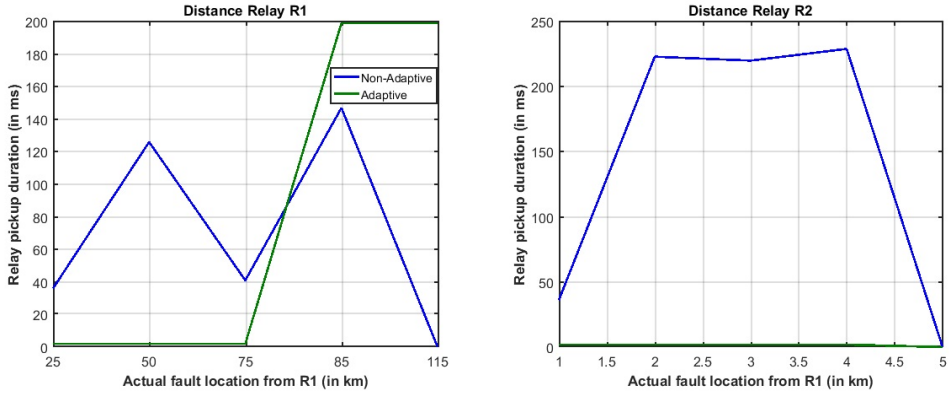


Figure 6.18: Duration of pickup by the distance relays R1 and R2 for a phase A-phase B fault with $P_{HVDC} = 0 p.u.$

2. Comparing the trip signals for the relay R1 with and without adaptive reach setting, it is observed in Figure 6.19 that the relay R1 with the adaptive setting is able to open the breaker to the fault at 80 km from R1.

In another instance, the relay R2 operates correctly for the fault at 25 km from R1 with adaptive settings, as shown in Figure 6.19. Moreover, Figure 6.17 shows the comparison of distance relay performance with and without the adaptive relay in a non-pilot distance relay scheme. It is clear from the Figure 6.19 that the conventional fixed setting scheme does not operate correctly in the presence of VSC-HVDC during the fault. The relay R2 computes the phase A-phase B fault at a distance of 75 km with adaptive reach setting. On the other hand, relay R2 computes the same fault at 61.4 km without adaptive reach settings. Furthermore, the relay picks up for the duration of 2 ms in comparison to 36 ms without adaptive reach settings, as it is evident from Figure 6.18.

Similarly, for another phase A-phase B fault located at 50 km from R1, the relay R2 estimates the distance to a fault at 44.7 km and issues a trip in 2 ms (refer Figure 6.19) with adaptive reach setting. On the contrary, the relay R2 picks up for zone 1 for the scenario without the adaptive protection. Consequently, this corresponds that the distance relay performance degrades with the increase in the fault resistance (refer Table 6.12).

A comparative analysis of a non-pilot distance relay performance with and without adaptive relay reach settings is presented in Figure 6.20. It is shown in Figure 6.20 that an increase in fault resistance decreases the relay reach without an adaptive relay scheme considerably. Moreover, the implementation of an adaptive scheme has increased the relay reach even increasing the fault resistance and VSC operation as inverter or rectifier.

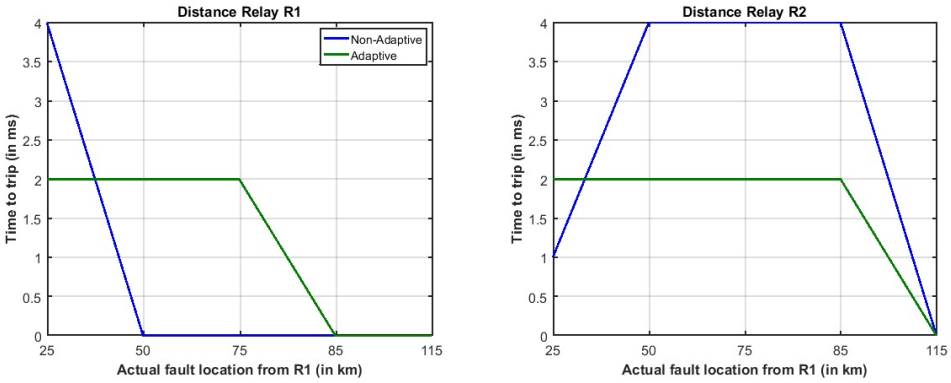


Figure 6.19: Time taken to trip by the distance relays R1 and R2 for a phase A-phase B fault with $P_{HVDC} = 0 p.u.$

For different fault locations from R1 with $P_{HVDC} = 0MW$, $R_f = 10\Omega$								
Relay	Location (in km)	Pickup Zone			Trip Zone			Phase loop
		Zone1	Zone2	Zone3	Zone1	Zone2	Zone3	
R1	25	X	-	-	X	-	-	ABC
	50	X	-	-	X	-	-	ABC
	75	X	-	-	X	-	-	ABC
	85	-	X	-	-	-	-	-
	115	-	X	-	-	-	-	-
R2	25	X	-	-	X	-	-	ABC
	50	X	-	-	X	-	-	ABC
	75	X	-	-	X	-	-	ABC
	85	X	-	-	X	-	-	ABC
	115	-	-	-	-	-	-	-

Table 6.12: Adaptive distance relay performance for phase A-phase B fault for different fault locations at $P_{HVDC} = 0MW$, $R_f = 10\Omega$.

Moreover, the distance relay performance is also evaluated for the pilot communication scheme, especially for PUTT and POTT scheme. As can be seen from Table 6.13, which presents the relay performance when VSC-HVDC acting as an inverter injecting 500 MW of active power and on the other hand acting as a rectifier drawing 500 MW of active power from the grid. With the proposed adaptive relaying scheme the relay performs correctly for a phase A-phase B fault at 75 km. Both the PUTT and POTT scheme issue a trip signal and calculates the distance to fault accurately with $R_f = 10\Omega$.

It can also be seen from Figure 6.21 that the Pilot distance protection does not provide complete coverage of the transmission line (see Figure 6.21 using the conventional distance protection. When the adaptive distance protection scheme is implemented, the relay is able to provide complete coverage of the line as shown in Figure 6.21.

Left End with $P_{HVDC} = 500MW$		Right End with $P_{HVDC} = -500MW$	
PUTT operate	3 ms	PUTT operate	0 ms
PUTT send	3 ms	PUTT operate	1 ms
POTT operate	4 ms	POTT operate	0 ms
POTT send	4 ms	POTT operate	1 ms
Distance to Fault	103.8	Distance to Fault	116.6

Table 6.13: Adaptive Distance Relay performance for phase A-to-phase B fault at 75 km and $R_f = 10\Omega$.

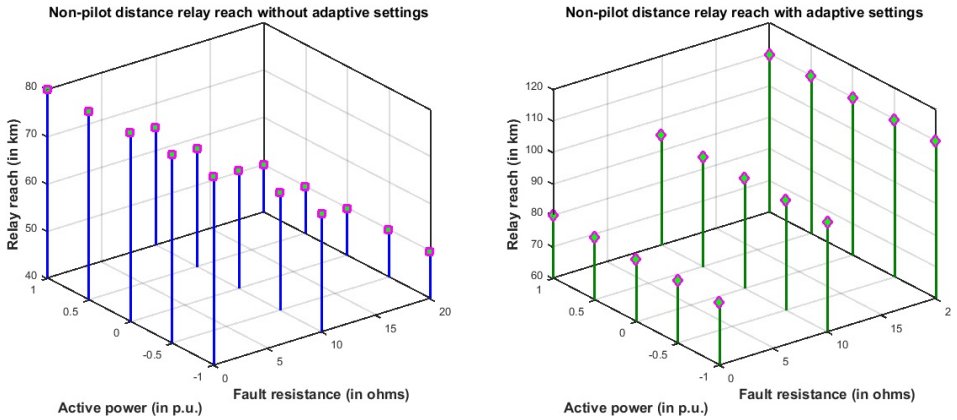


Figure 6.20: Non-Pilot distance relay performance with and without adaptive Scheme.

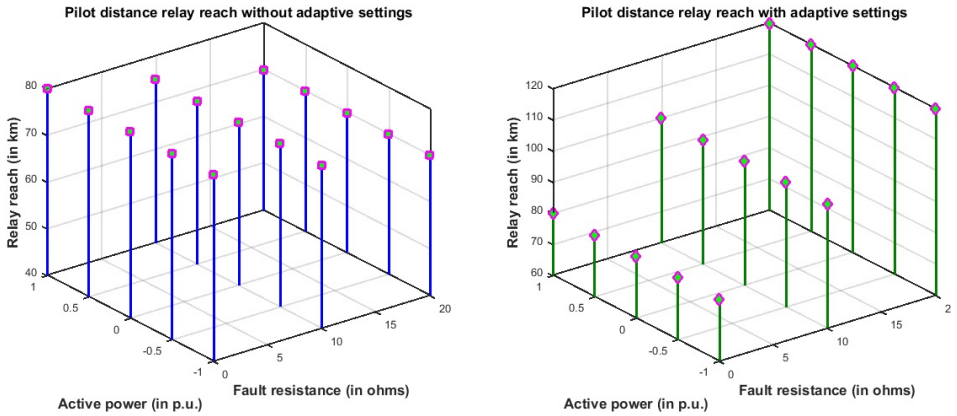


Figure 6.21: Pilot distance relay performance with and without adaptive Scheme.

6.7 FLOWCHART

Figure 6.22 presents a flowchart of an adaptive relaying scheme implemented in the distance relay for faults on the transmission line using a closed-loop test setup in RTDS. The performance of commercial distance relay with adaptive distance relaying scheme proposed here is evaluated for the different fault scenarios earlier.

6.8 CONCLUSIONS

This chapter[53] presents the performance of conventional distance protection with the fixed setting (both pilot and non-pilot) for unsymmetrical faults on the transmission lines with VSC-HVDC. The distance protection performs correctly for the fault with $R_f = 0.1\Omega$ and $P_{HVDC} = 0, 500, -500MW$. The relay performance is affected as the fault resistance increases to a high value with the increase in the distance to fault location. The non-pilot distance protection is mostly affected by the higher fault location and fault in the reverse direction.

For the case of pilot assisted distance protection, the pilot protection performs correctly for the initial fault condition of $R_f = 0.1\Omega$ and $P_{HVDC} = 0MW$. However, the fault detection efficiency of the distance protection is greatly reduced for the higher fault resistance and fault location as well as by the mode of operation of HVDC.

An adaptive distance relaying scheme is proposed in this chapter to eliminate the wrong performance of the relay in both the pilot as well as non-pilot protection scheme. The scheme takes into account the condition of power system before the fault and stores impor-

[53] Salient points:

- Relay performs correctly for the fault with $R_f = 0.1\Omega$ and $P_{HVDC} = 0, 500, -500MW$,
- Increase in fault resistance affects the relay performance,
- Non-pilot distance relay worst affected,
- Pilot distance protection also gets affected due to fault resistance and power flow in the reverse direction,
- Adaptive distance relaying scheme eliminates the error,

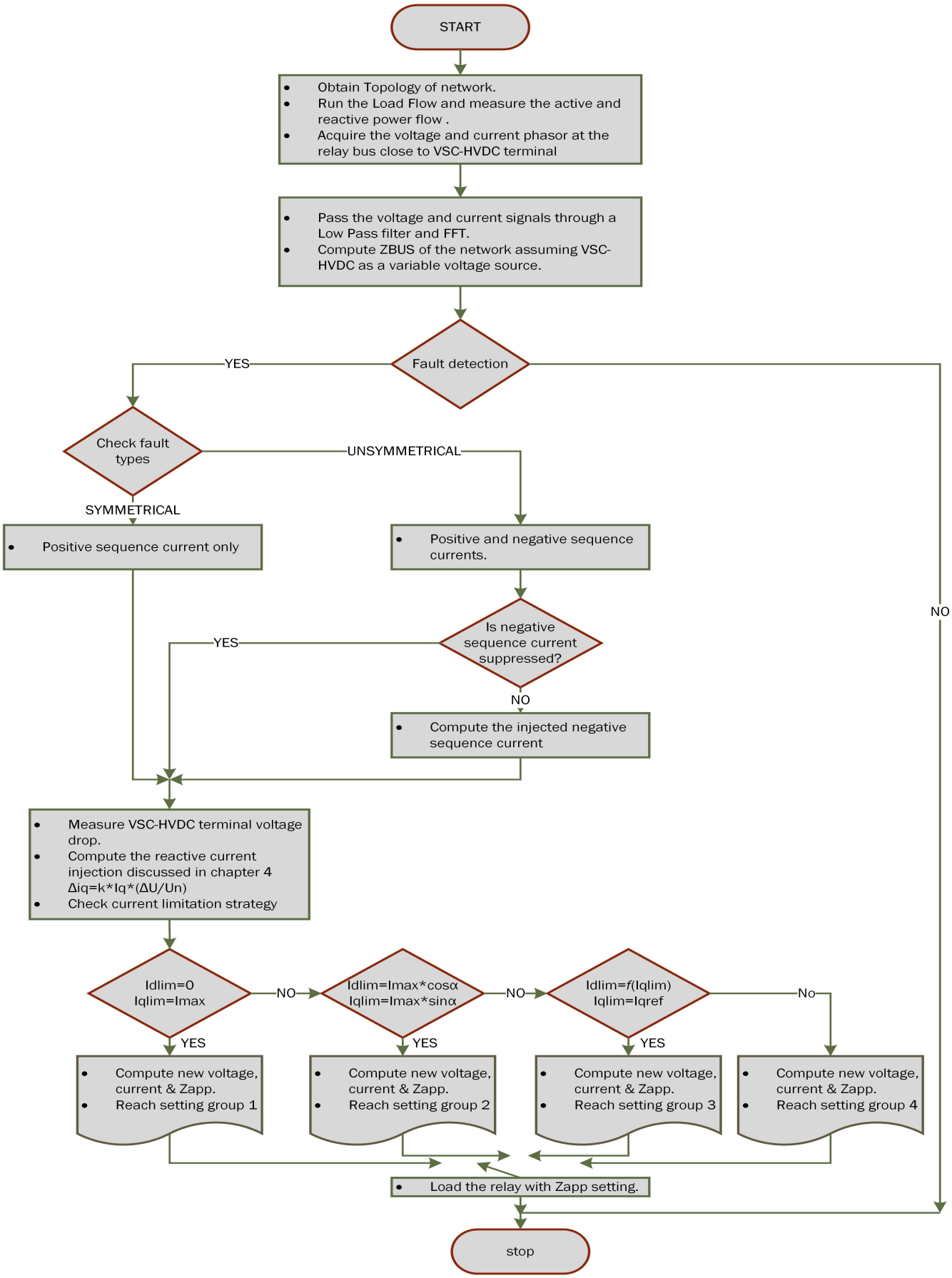


Figure 6.22: Flowchart for Adaptive Distance Relaying Scheme.

tant information of pre-fault voltage and current. Furthermore, it takes care of the current limitation strategies activated at the time of fault along with the negative sequence currents during unsymmetrical faults. The algorithm calculates the new voltage and current and then calculates the new apparent impedance as new reach setting.

7

CONCLUSIONS

Contents

7.1 Final Conclusions 130
7.2 Recommendations for Future Research 131



Luigi Aloisio Galvani (1737-1798) was an Italian physician, physicist, biologist and philosopher, who discovered animal electricity. He is recognized as the pioneer of bioelectromagnetics.

As discussed in Chapter 1, the environmental concern is leading to the maximum utilization of renewable source of energy such as wind, solar etc., which are replacing the conventional sources of energy like coal, diesel etc. In general, these renewable sources of energy are far away from the load centers that require long transmission facility to bring it to residential areas.

It has been observed that High Voltage DC technology is highly efficient for long distance transmission in comparison to its AC transmission counterpart. More recently, Voltage Source Converter based on IGBT and GTO are attracting more attention because of their numerous benefits over Thyristor based HVDC. The electrical utilities and transmission companies are adopting VSC based HVDC technology solutions to bring power from offshore wind power parks and photovoltaic plants. In this sense, integration of renewable energy technologies with the grid and the associated changes it is bringing in the grid is subject to investigation.

The main objective of the thesis was to examine the impact of VSC-HVDC on the operation of distance protection of transmission line when following the grid code requirement of reactive current support during the fault. Furthermore, the effect of negative sequence current suppression during an unbalanced fault along with the VSC current limitation strategy was also assessed, with a special focus on the connection of VSC technology to the electrical grid. Therefore, the introduction chapter (Chapter 1) presented the challenges of the distance protection of transmission lines in the presence of voltage source converter based technologies like FACTS devices, DFIG based wind turbines, IIDG together with the objectives and research questions that laid down the main motivation for the work presented in this thesis.

Chapter 2 discussed the development of High Voltage DC technology since 1888 when it was first invented by Rene Thury as "Thury system" to the present VSC based HVDC technology. Different HVDC projects installed throughout the world have also been discussed which were based on Mercury-arc valve, Thyristor based Current Source Converter and subsequently IGBT based VSC to highlight their widespread usage in transmission.

Many types of converter were also discussed under VSC technology like two-level, three-level, modular multilevel etc. out of which MMC based technology is considered the best. Furthermore, Chapter 2 also presented the behavior of VSC based HVDC during abnormal condition such as faults in order to present the difference in its fault behavior with the conventional sources.

Chapter 3 begins with the state-of-the-art of protection methodology and devices implemented to protect an electrical grid. A critical question has been raised in Chapter 3 based on the discussion in Chapter 2 about the performance of distance protection when more and more renewable energy power plants, which are low in inertia and low short circuit level, are integrated into the AC grid through VSC based HVDC connection. This question is very important for the power system operators as they are facing the challenges for grid protection with the continuous change in the power system structure. Chapter 3 actually develops this hypothesis as per the previous work about the impact of FACTS devices, DFIGs,

and IIDG on the distance protection. A list of reasons has also been pointed in Chapter 3 as why this thesis targeted the distance protection assessment.

In Chapter 4 the impact of VSC based HVDC system on the operation of distance protection of transmission line following the NC requirement of reactive current support during the fault. Furthermore, the effect of negative sequence current suppression control during an unbalanced fault along with the VSC current limitation strategies were also assessed. This assessment is done by analyzing the problem mathematically for a single line to ground and phase-to-phase faults. Later on, a study system with embedded VSC based HVDC is modeled in PSCAD/EMTDC platform to study distance protection behavior.

The models developed in PSCAD/EMTDC and discussed in Chapter 4 were later on formed the basis for the development of models in RTDS platform, which were discussed in Chapter 5 as the experimental setup and closed-loop testing of a commercial distance relay. The model developed were in detail and analog signals were fetched with proper scaling for the external device under test. The results obtained were discussed and matched with the one obtained from the simulation in Chapter 4.

As previous two chapters Chapter 4 and Chapter 5 presented the problem of mal-operation encountered by the distance protection of transmission line connected to VSC-HVDC system, the Chapter 6 presented a novel solution to counter the problem of malfunction of the distance relaying scheme by Adaptive Relaying technique, which is presented in the form of flowchart and algorithm. Many tests were performed in RTDS based closed loop test bench to validate the Adaptive relay settings.

This chapter presents the final conclusions and recommendations for the future work.

7.1 FINAL CONCLUSIONS

Till now, numerous research has been performed on the performance of the distance relay in the presence of VSC based FACTS devices, DFIG and FSC based wind generator and IIDG on the performance of the distance relay using non-real time simulation platforms like MATLAB or PSCAD/EMTDC or ATAP. However, no attention has been given towards the dynamic impact of VSC based HVDC system due to the suppression of the negative sequence current during an unbalanced condition and reactive current support based on NC along with converter current limitation strategy on the operation of the distance protection of transmission lines using either real-time or non-real simulation.

Therefore, the main objective of this thesis was to present an investigation regarding the effect of VSC based HVDC connection and its limited reactive current support during the fault (recommended by the grid code) on the performance of distance relay. Following are the main conclusions of the thesis.

VSC-HVDC System

Nowadays, ac grid, which constitutes thousands of kilometers of transmission lines also accommodates High Voltage DC technology so as to transfer bulk amount of electrical power over a very long distances offering many other benefits including interconnecting major electrical grids serving as tie-lines and supplying offshore wind energy to onshore ac grid.

Nowadays, VSC based HVDC is utilized for the grid integration of far offshore WPP and interconnection of WPPs to each other or to multiple in-feed points leading to Multi-Terminal HVDC by the efficient use of multilevel converter technologies. Modern MMC based converter are the most preferred choices for the development of HVDC because of numerous benefits.

On the other hand, the current contribution from the converter is limited in magnitude and modified in the waveform in order to protect the power electronic devices during

the fault. This eventually modifies the overall fault behaviour of VSC's compared to SG in terms of both magnitude and waveform in comparison to the synchronous generator fault current characteristics[54]. Therefore, it was prime important to analyze the performance of the distance protection because of different fault behavior of VSC-HVDC.

[54] Advantages of VSC-HVDC:
- No need of any external voltage source for commutation,
- Power reversal is easy without voltage polarity reversal,
- Black start capability,
- Best suited for an offshore wind farm,
- Can connect weak AC system, and islands

Distance Protection

The distance relays are more common for line protection, which provides high-speed primary protection and slow speed backup protection and forms the backbone of the transmission line protection due to its simple operating principle. A distance protection utilizes measured local voltage and current to compute the apparent impedance to a fault and decides whether a fault is internal or external to the protected feeder zones based on its reach settings.

However, a distance relay is associated with many challenges[55] as well. Furthermore, a recent addition to the list of problems was the impact of converter interfaced renewable energy sources on the performance of the distance relay due to their reactive current support and limited nature of fault currents.Therefore, the network operator is facing challenges in handling the grid protection systems due to these exclusive behaviours of VSC, which affect the current and voltage measured by the protective relays during the fault.

[55] Challenges of distance protection:
- Inaccurate computation of fault impedance during a high resistance fault,
- Misoperation during a large power swing,
- Effect of load encroachment,
- Best suited for an offshore wind farm,
- Can connect weak AC system, and islands

Impact of VSC-HVDC on Distance Protection

When the converter provided reactive current support to the network along with the current limitation strategy as suggested by the network guidelines for HVDC connections, the distance protection of transmission lines connected to VSC-HVDC failed to operate during symmetrical and unsymmetrical faults.

The analysis presented that the limited reactive positive sequence and suppressed negative sequence fault current from the converter, zero sequence from the transformer, grid current and fault resistance impact the distance relay heavily. The distance relay underreached due to the impact of reactive current injection to support the network voltage along with the active current blocked limitation strategy.

Th performance of the distance relay was also assessed in a closed loop using RTDS under the more realistic scenario. The results present a serious concern regarding the distance relay performance with VSC-HVDC. The relay not only shows an under reach but also unstable or oscillating trip signals behaviour.

Adaptive Relaying Scheme

The performance of distance protection with the fixed setting (both pilot and non-pilot) for unsymmetrical faults on the transmission lines with VSC-HVDC were analyzed, which were found that the relay did not perform correctly except for lower fault resistance. A novel adaptive distance relaying scheme is proposed and tested in a more realistic scenario using RTDS. The scheme eliminated the wrong performance of the relay in both the pilot as well as non-pilot protection scheme.

7.2 RECOMMENDATIONS FOR FUTURE RESEARCH

Following are the recommendations for future work that has been listed chapter-wise in bullet points:

Chapter 2: VSC-HVDC System

- The behavior of VSC-HVDC system connected to AC transmission line during a stable and unstable power swing phenomena should be assessed in detail. Its impact on the distance function should also be described.
- The fault behavior of hybrid HVDC system (both VSC and LCC) should be assessed during a permanent and temporary faults

Chapter 3: Distance Protection & its Challenges

- This chapter discussed the performance of distance protection of lines connected to VSC-HVDC. The performance of other protection schemes like over-current and differential protection should also be assessed during a fault following the grid codes.
- Effects of full bridge MMC when operating as a STATCOM should be analyzed on the operation of distance relays.

Chapter 4: Impact of VSC-HVDC on Distance Protection

- The operation of distance protection during a balanced and unbalanced fault is discussed in this chapter with negative sequence currents suppressed. The performance of distance protection should also be studied during a fault when the negative sequence currents are injected int the network.
- This chapter implemented the active current blocked limitation strategy and presented its effect on the relay. There are two more current limitation strategies, which need to be assessed namely reactive current priority and equal current priority.
- Impact of Multi-terminal DC grids on the distance protection of lines also needs to be investigated following during control schemes and grid codes.

Chapter 5: Laboratory Setup & Testing of Distance Relay Using RTDS

- The system in this chapter although in detail but only a small portion has been analyzed due to lack of processors. A big transmission system should be modeled in a full rack RTDS to obtain the complete behavior of an entire system.
- Similarly, other protection functions like load encroachment, power swing blocking should be loaded onto the commercial relay to investigate their operation during heavily loaded condition or power swing.

Chapter 6: Adaptive Distance Relaying Scheme

- A novel Adaptive Relaying Scheme is proposed and tested in this chapter in order to give correct operation of the distance protection. However, a trip logic based scheme can also be proposed or a better a design should be configured.
- As a solution to the problem of distance relays, phasor measurement based adaptive protection is also a possible solution, which should be researched.

Part IV

APPENDIX, BIBLIOGRAPHY & DECLARATION

A

STUDY SYSTEM PARAMETERS

Component	Parameters
VSC-HVDC	$S_{VSC1} = S_{VSC2} = S_{VSC3} = S_{VSC4}$ =700 MVA
	Submodules per arm = 38
	DC link voltage = 640 kV (pole-pole)
	$f_{carrier}$=150 Hz, f=50 Hz, L_{arm}=50 mH,
	C_{dc}=5100 µF per cell
Transformers	$S_{T5} = S_{T6} = S_{T7} = S_{T8}$ =700 MVA
	175/400 kV, D1/Yg winding connections
	$X_{T5} = X_{T6} = X_{T7} = X_{T8}$ =0.1 p.u.
	$S_{T1} = S_{T2} = S_{T3} = S_{T4}$ =1000 MVA
	400/400 kV, D1/Yg winding connections
	$X_{T1} = X_{T2} = X_{T3} = X_{T4}$ =0.1 p.u.
Sources	$V_{S1} = V_{S3}$=230 kV $V_{S2} = V_{S4}$=400 kV
	f=50 Hz, $\angle V_{S2} = -2.5^0$, $\angle V_{S1} = \angle V_{S3} = 0^0$, $\angle V_{S4} = -5^0$
	$Z^1 = 5.5\angle 86.2^0\Omega$, $Z^0 = 5\angle 86.2^0\Omega$
Loads	Load 1=(322+j33.3) MVA,
	Load 2= (589+j33.3) MVA
Transmission Lines	3-ph, 50 Hz, Bundled conductor=4, $K = 1.01\angle -14^0$
	Line 1=Line 2=Line 3=100 km,
	Line 4=Line 5=Line 6=50 km
	$Z_L^1 = Z_L^2 = 0.2645\angle 88.05^0\Omega/km$,
	$Z_L^0 = 1.0588\angle 77.83^0\Omega/km$
Distance Relay	Zone 1=80%, Zone 2=120%, Zone 3=200%
	Resistive reach, Zone 1=30 Ω, Zone 2=60 Ω,
	Zone 3=100 Ω, Quadrilateral characteristic,
	T_{ZONE1}=0 ms, T_{ZONE2}=250 ms, T_{ZONE3}=1000 ms

Table A.1: Study System Parameters.

B

TRANSMISSION LINE IMPEDANCE CALCULATION

Conductor arrangement type: chukar type

GMR (Geometric mean radius): 0.01628 m

Conductor DC resistance: 0.0321 ohms/km

The sequence impedances of the transmission lines has to be determined in order to decide the reach of step distance relay as well as zero sequence correction factor. There are several prerequisites before moving to the mathematical analysis of transmission line impedance calculation which can be the type of conductors, the arrangement of conductors, no. of overhead ground wires, AC and DC resistance of the conductor and ground wire etc. For a completely transposed transmission line, the impedance of the line is given by:

$$Z_{abc} = \begin{bmatrix} Z_s & Z_k & Z_k \\ Z_k & Z_s & Z_k \\ Z_k & Z_k & Z_s \end{bmatrix}$$

where Z_s is self impedance of the line and Z_k is mutual impedance of the line. The conductor chosen is "chukar", with GMR i.e. Geometric Mean Radius is 0.01628 meter[1]. The arrangement of the conductor is as shown in figure 2. The GMD i.e. Geometric Mean Distance of the conductor arrangement can be calculated as:

From the table A.3 of P. M. Anderson

$$D_{eq} = \sqrt[3]{D_{ab} D_{bc} D_{ca}}$$

$$D_{eq} = \sqrt[3]{20 * 125}$$

$$D_{eq} = 13.5721 meters$$

$$D_e = 2061 * 0.3048 * \sqrt{\frac{\rho}{f}}$$

Where ρ is ground resistivity equal to 100 $\Omega - m$ and f is frequency equal to 50 Hz. Therefore,

$$D_e = 2061 * 0.3048 * \sqrt{\frac{100}{50}} meters$$

$$D_e = 888.2646 meters$$

The GMR of 4 bundled conductors is given by:

$$GMR = 1.09 * \sqrt[4]{D_s * d^3} meters$$

$$GMR = 1.09 * \sqrt[4]{0.01628 * 0.45^3} meters$$

$$GMR = 0.214 meters$$

Where, D_s is GMR of conductor only and d is the distance between the bundled conductor equal to 0.45 meters. The DC resistance and AC resistance of the conductor also plays a very important role in the calculation of impedance of the conductor[2]. . Therefore,

These resistances can be found from the table A.3 of John J Grainger book

DC resistance of chukar conductor = 32.1 $m\Omega/km$ per conductor

AC resistance of chukar conductor = 34.1 $m\Omega/km$ at 60 Hz per conductor

1 Consult P M Anderson

2 Consult John J Grainger

As the difference of frequency between 50 Hz and 60 Hz is not so considerable therefore we will assume Ac resistance at 50 Hz is equal to resistance at 60 Hz. Also, the resistance difference is more at higher frequencies. Total resistance per conductor = 32.1+34.1 = 66.2 $m\Omega/km$ at 50 Hz per conductor. Earth resistance

$$r_d = 1.5888 * 10^{-3} * f\Omega/mile$$

$$r_d = \frac{1.5888 * 10^{-3} * 50}{1.60934}\Omega/km$$

$$r_d = 0.04936\Omega/km$$

Therefore, the self-impedance of the line can be given by:

$$Z_s = (r_a + r_d) + j\omega * 2 * 10^{-4} * \ln\frac{D_e}{D_s}\Omega/km$$

$$Z_s = (0.0662 + 0.04936) + j314 * 2 * 10^{-4} * \ln\frac{888.2646}{0.01628}\Omega/km$$

$$Z_s = 0.1156 + j0.685\Omega/km$$

While the mutual impedance is given by:

$$Z_k = r_d + j\omega * 2 * 10^{-4} * \ln\frac{D_e}{D_{eq}}\Omega/km$$

$$Z_k = 0.04936 + j314 * 2 * 10^{-4} * \ln\frac{888.2646}{13.5721}\Omega/km$$

$$Z_k = 0.04934 + j0.2626\Omega/km$$

Hence we can construct the impedance matrix of transposed line with the self-impedance and mutual impedance obtained as follows:

$$Z_{abc} = \begin{bmatrix} 0.1156 + j0.685 & 0.04934 + j0.2626 & 0.04934 + j0.2626 \\ 0.04934 + j0.2626 & 0.1156 + j0.685 & 0.04934 + j0.2626 \\ 0.04934 + j0.2626 & 0.04934 + j0.2626 & 0.1156 + j0.685 \end{bmatrix}$$

The transmission system has an overhead ground wire which has a considerable effect on the impedance of the transmission lines. It should not be neglected while calculating the impedance of the lines. Neglecting its effect will result in incorrect settings of the reach of the relay and it might lead to misoperation of the relay.

Radius of the ground wire = 0.0055245 meters

GMR of the ground wire can be given by:

$$D_{ww} = 0.7788 * 0.0055245meter$$

$$D_{ww} = 0.004302meter$$

DC resistance of the overhead ground wire $r_w = 2.8645\Omega/km$

Self-impedance of the ground wire can be given by:

$$Z_{ww} = (r_w + r_d) + j\omega * 2 * 10^{-4} * \ln\frac{D_e}{D_{ww}}\Omega/km$$

$$Z_{ww} = (2.8645 + 0.04934) + j314 * 2 * 10^{-4} * \ln\frac{888.2646}{0.004302}\Omega/km$$

$$Z_{ww} = 2.91383 + j0.7685\Omega/km$$

$$Z_{aw} = r_d + j\omega * 2 * 10^{-4} * \ln\frac{D_e}{D_{aw}}\Omega/km$$

$$Z_{aw} = 0.04934 + j314 * 2 * 10^{-4} * \ln\frac{888.2646}{14.14}\Omega/km$$

$$Z_{aw} = 0.049337 + j0.26\Omega/km$$

Similarly, for mutual impedance between the overhead ground wire and phase B can be calculated as explained just above:

$$Z_{bw} = r_d + j\omega * 2 * 10^{-4} * \ln\frac{D_e}{D_{bw}}\Omega/km$$

$$Z_{bw} = 0.04934 + j314 * 2 * 10^{-4} * \ln\frac{888.2646}{5}\Omega/km$$

$$Z_{bw} = 0.04934 + j0.3253\Omega/km$$

And for Phase C

$$Z_{cw} = r_d + j\omega * 2 * 10^{-4} * \ln\frac{D_e}{D_{aw}}\Omega/km$$

$$Z_{cw} = 0.04934 + j314 * 2 * 10^{-4} * \ln\frac{888.2646}{14.14}\Omega/km$$

$$Z_{cw} = 0.049337 + j0.26\Omega/km$$

Therefore the overall impedance of the transmission line including the effect of overhead ground wire will be a 4*4 matrix for 1 ground wire and a 5*5 matrix for 2 ground wires. By matrix reduction technique we can include its effect into a 3*3 matrix as follows:

$$Z_{abc} = \begin{bmatrix} Z_s - \frac{Z_{aw}*Z_{aw}}{Z_{ww}} & Z_k - \frac{Z_{aw}*Z_{bw}}{Z_{ww}} & Z_k - \frac{Z_{aw}*Z_{cw}}{Z_{ww}} \\ Z_k - \frac{Z_{bw}*Z_{aw}}{Z_{ww}} & Z_s - \frac{Z_{bw}*Z_{bw}}{Z_{ww}} & Z_k - \frac{Z_{bw}*Z_{cw}}{Z_{ww}} \\ Z_k - \frac{Z_{cw}*Z_{aw}}{Z_{ww}} & Z_k - \frac{Z_{cw}*Z_{bw}}{Z_{ww}} & Z_s - \frac{Z_{cw}*Z_{cw}}{Z_{ww}} \end{bmatrix}$$

But, as we know that the lines are transposed, hence the mutual impedance between the overhead ground wire and the conductors are not always same as calculated above because the conductor position changes after every fixed interval resulting in a change in the distance between the ground wire and the conductors which change mutual GMD for each conductor. Therefore, in order to add the effect of overhead ground wire, we will add its averaged impedances to the impedance of the line calculated earlier.

$$\frac{Z_{aw} * Z_{aw}}{Z_{ww}} = -0.0187 + j0.0137\Omega/km$$

$$\frac{Z_{aw} * Z_{bw}}{Z_{ww}} = -0.0239 + j0.0162\Omega/km$$

$$\frac{Z_{bw} * Z_{bw}}{Z_{ww}} = -0.0305 + j0.019\Omega/km$$

$$\frac{Z_{bw} * Z_{cw}}{Z_{ww}} = -0.0239 + j0.0162\Omega/km$$

$$Z_{abc} = \begin{bmatrix} Z_s - (-0.0226 + j0.0155) & Z_k - (-0.0204 + j0.0145) & Z_k - (-0.0204 + j0.0145) \\ Z_k - (-0.0204 + j0.0145) & Z_s - (-0.0226 + j0.0155) & Z_k - (-0.0204 + j0.0145) \\ Z_k - (-0.0204 + j0.0145) & Z_k - (-0.0204 + j0.0145) & Z_s - (-0.0226 + j0.0155) \end{bmatrix}$$

$$Z_{abc} = \begin{bmatrix} 0.1381 + j0.5077 & 0.0697 + j0.2481 & 0.0697 + j0.2481 \\ 0.0697 + j0.2481 & 0.1381 + j0.5077 & 0.0697 + j0.2481 \\ 0.0697 + j0.2481 & 0.0697 + j0.2481 & 0.1381 + j0.5077 \end{bmatrix}$$

$$Z_{012} = A^{-1} * Z_{abc} * A$$

$$A = \begin{bmatrix} 1 & 1 & 1 \\ 1 & \alpha^2 & 1 \\ 1 & 1 & \alpha \end{bmatrix}$$

$$\alpha = exp^{j120^0}$$

$$Z_{012} = \begin{bmatrix} 0.2775 + j1.1657 & 0 & 0 \\ 0 & 0.0684 + j0.4214 & 0 \\ 0 & 0 & 0.0684 + j0.4214 \end{bmatrix}$$

Zero sequence impedance can be given from the above matrix as the first diagonal element of the matrix. The positive sequence impedance is the second diagonal element while the third diagonal element is the negative sequence impedance of the line. If the sequence impedance matrix obtained above has non-zero off-diagonal elements then it shows that sequence impedance are closely coupled and it can cause under-reach and over-reach of the relay if not compensated properly.

$Z_0 = 0.2775 + j1.1657$

$Z_1 = 0.0684 + j0.4214$

$Z_2 = 0.0684 + j0.4214$

BIBLIOGRAPHY

[1] Silvanus Phillips Thompson. *Dynamo-electric Machinery: A Manual for Students of Electrotechnics*. Report. 1888.

[2] J J Messerly. *Diagram of a Thury System balancing voltage of supply with voltage of load*. Report.

[3] Web Page. URL: http://new.abb.com/systems/hvdc/references/new-zealand.

[4] Web Page. 2005. URL: http://www.ptd.siemens.de/artikel0506.html.

[5] Online Multimedia. URL: http://www.gdrectifiers.co.uk/products/category/semiconductor_components/gd_rectifiers/.

[6] Peter Meisen. "Multi-Terminal HVDC Links Distant Renewables Between Canada And The United States." In: *GENI-us Letter 2016-07* 24.06 (2016). URL: www.geni.org.

[7] Katharina Garus. "Siemens puts converter stations of HVDC link between France and Spain into operation." In: *Sun&Wind Energy* (2015). URL: http://www.sunwindenergy.com/wind-energy/siemens-puts-converter-stations-hvdc-link-france-spain-operation.

[8] Web Page. 2017. URL: http://new.abb.com/products.

[9] Web Page. URL: www.wikipedia.com.

[10] Web Page. URL: www.electrical4u.com.

[11] Web Page. URL: www.energy.siemens.com.

[12] Walter. Schossig. "Distance Protection: The Early Developments." In: *pacworld* winter (2008), pp. 70–76. URL: https://www.pacw.org/fileadmin/doc/WinterIssue08/PACWorld-Winter2008-All.pdf.

[13] I. Stevens, N. Fischer, and B. Kasztenny. "Performance issues with directional comparison blocking schemes." In: *Protective Relay Engineers, 2010 63rd Annual Conference for*, pp. 1–37. DOI: 10.1109/CPRE.2010.5469479.

[14] Allison Lantero. *The War of the Currents: AC vs. DC Power*. Report. US Department of Energy, 2014. URL: https://energy.gov/articles/war-currents-ac-vs-dc-power.

[15] ModernPowerSystems. *100 years of high voltage DC links*. Report. 2007. URL: http://www.modernpowersystems.com/features/feature100-years-of-high-voltage-dc-links/.

[16] Jos Arrillaga. *High Voltage Direct Current Transmission*. 2nd. London: The Institution of Electrical Engineers, 1998.

[17] Robert Monro Black. *The History of Electric Wires and Cables*. London: Peter Peregrinus Ltd., 1983.

[18] Lev V. Travin and Vladimir V. Khudyakov. "HVDC Advances in the Russian Federation." In: *T&D World Magazine* (2013). URL: http://www.tdworld.com/substations/hvdc-advances-russian-federation?page=3.

[19] P. Bresesti, W. L. Kling, and R. Vailati. "Transmission expansion issues for offshore wind farms integration in Europe." In: *Transmission and Distribution Conference and Exposition, 2008. T&D. IEEE/PES*, pp. 1–7. DOI: 10.1109/TDC.2008.4517316. URL: http://ieeexplore.ieee.org/ielx5/4505447/4517029/04517316.pdf?tp=&arnumber=4517316&isnumber=4517029.

[20] Du. Cuiqing. "VSC-HVDC for Industrial Power Systems." Thesis. 2007.

[21] C. Du, E. Agneholm, and G. Olsson. "Use of VSC-HVDC for Industrial Systems Having Onsite Generation With Frequency Control." In: *Power Delivery, IEEE Transactions on* 23.4 (2008), pp. 2233–2240. ISSN: 0885-8977. DOI: 10.1109/TPWRD.2008.2002650. URL: http://ieeexplore.ieee.org/ielx5/61/4626339/04626348.pdf?tp=&arnumber=4626348&isnumber=4626339.

[22] Dirk Van Hertem and Mehrdad Ghandhari. "Multi-terminal VSC HVDC for the European supergrid: Obstacles." In: *Renewable and Sustainable Energy Reviews* 14.9 (2010), pp. 3156–3163. ISSN: 1364-0321. DOI: http://dx.doi.org/10.1016/j.rser.2010.07.068. URL: http://www.sciencedirect.com/science/article/pii/S1364032110002480http://ac.els-cdn.com/S1364032110002480/1-s2.0-S1364032110002480-main.pdf?_tid=6a1e2300-551c-11e6-9bf6-00000aacb35f&acdnat=1469749301_71eadadc83571d19c7871173f759c694.

[23] C. Du, E. Agneholm, and G. Olsson. "VSC-HVDC System for Industrial Plants With Onsite Generators." In: *Power Delivery, IEEE Transactions on* 24.3 (2009), pp. 1359–1366. ISSN: 0885-8977. DOI: 10.1109/TPWRD.2009.2013384. URL: http://ieeexplore.ieee.org/ielx5/61/5109837/05109852.pdf?tp=&arnumber=5109852&isnumber=5109837.

[24] "List of IEEE Milestones." In: *IEEE Global History Network* (2012).

[25] C.C. Davidson, R.M. Preedy, J. Cao, Zhou C., and J. Fu. "Ultra-High-Power Thyristor Valves for HVDC in Developing Countries." In: *IET 9th International Conference on AC/DC Power Transmission*.

[26] Nayak R.N., Sasmal R.P., Sen S., Pelly B., and Riedel P. "Experience with blocking devices during monopolar operation of +/- 500kV, 2000MW Talcher-Kolar HVDC system in India." In: *CIGRÉ session*.

[27] S. Bernal-Perez, S. Ano-Villalba, R. Blasco-Gimenez, and J. Rodriguez-D'Derlee. "Efficiency and Fault Ride-Through Performance of a Diode-Rectifier- and VSC-Inverter-Based HVDC Link for Offshore Wind Farms." In: *Industrial Electronics, IEEE Transactions on* 60.6 (2013), pp. 2401–2409. ISSN: 0278-0046. DOI: 10.1109/TIE.2012.2222855. URL: http://ieeexplore.ieee.org/ielx5/41/6451226/06323016.pdf?tp=&arnumber=6323016&isnumber=6451226.

[28] Xu Lie, B. R. Andersen, and P. Cartwright. "VSC transmission operating under unbalanced AC conditions - analysis and control design." In: *Power Delivery, IEEE Transactions on* 20.1 (2005), pp. 427–434. ISSN: 0885-8977. DOI: 10.1109/TPWRD.2004.835032. URL: http://ieeexplore.ieee.org/ielx5/61/30033/01375123.pdf?tp=&arnumber=1375123&isnumber=30033.

[29] Liang Jun, Jing Tianjun, O. Gomis-Bellmunt, J. Ekanayake, and N. Jenkins. "Operation and Control of Multiterminal HVDC Transmission for Offshore Wind Farms." In: *Power Delivery, IEEE Transactions on* 26.4 (2011), pp. 2596–2604. ISSN: 0885-8977. DOI: 10.1109/TPWRD.2011.2152864. URL: http://ieeexplore.ieee.org/ielx5/61/6029804/05887365.pdf?tp=&arnumber=5887365&isnumber=6029804.

[30] Liang Jun, O. Gomis-Bellmunt, J. Ekanayake, and N. Jenkins. "Control of multi-terminal VSC-HVDC transmission for offshore wind power." In: *Power Electronics and Applications, 2009. EPE '09. 13th European Conference on*, pp. 1–10.

[31] Y. Liu and Z. Chen. "A Flexible Power Control Method of VSC-HVDC Link for the Enhancement of Effective Short-Circuit Ratio in a Hybrid Multi-Infeed HVDC System." In: *IEEE Transactions on Power Systems* 28.2 (2013), pp. 1568–1581. ISSN: 0885-8950. DOI: 10.1109/TPWRS.2012.2222057. URL: http://ieeexplore.ieee.org/ielx5/59/6504806/06341872.pdf?tp=&arnumber=6341872&isnumber=6504806.

[32] A. Yazdani and R. Iravani. "A generalized state-space averaged model of the three-level NPC converter for systematic DC-voltage-balancer and current-controller design." In: *Power Delivery, IEEE Transactions on* 20.2 (2005), pp. 1105–1114. ISSN: 0885-8977. DOI: 10.1109/TPWRD.2004.834307. URL: http://ieeexplore.ieee.org/ielx5/61/30624/01413358.pdf?tp=&arnumber=1413358&isnumber=30624.

[33] A. Yazdani and R. Iravani. "A unified dynamic model and control for the voltage-sourced converter under unbalanced grid conditions." In: *IEEE Transactions on Power Delivery* 21.3 (2006), pp. 1620–1629. ISSN: 0885-8977. DOI: 10.1109/TPWRD.2006.874641.

[34] A. Yazdani and R. Iravani. "A unified dynamic model and control for the voltage-sourced converter under unbalanced grid conditions." In: *Power Engineering Society General Meeting, 2006. IEEE*, 1 pp. DOI: 10.1109/PES.2006.1709332. URL: http://ieeexplore.ieee.org/ielx5/11204/36065/01709332.pdf?tp=&arnumber=1709332&isnumber=36065.

[35] A. Das, H. Nademi, and L. Norum. "A Pulse Width Modulation technique for reducing switching frequency for modular multilevel converter." In: *Power Electronics (IICPE), 2010 India International Conference on*, pp. 1–6. DOI: 10.1109/IICPE.2011.5728082. URL: http://ieeexplore.ieee.org/ielx5/5724110/5728055/05728082.pdf?tp=&arnumber=5728082&isnumber=5728055.

[36] M. Saeedifard and R. Iravani. "Dynamic Performance of a Modular Multilevel Back-to-Back HVDC System." In: *Power Delivery, IEEE Transactions on* 25.4 (2010), pp. 2903–2912. ISSN: 0885-8977. DOI: 10.1109/TPWRD.2010.2050787. URL: http://ieeexplore.ieee.org/ielx5/61/5570058/05565526.pdf?tp=&arnumber=5565526&isnumber=5570058.

[37] A. Beddard, M. Barnes, and R. Preece. "Comparison of Detailed Modeling Techniques for MMC Employed on VSC-HVDC Schemes." In: *Power Delivery, IEEE Transactions on* 30.2 (2015), pp. 579–589. ISSN: 0885-8977. DOI: 10.1109/TPWRD.2014.2325065. URL: http://ieeexplore.ieee.org/ielx7/61/7064681/06827983.pdf?tp=&arnumber=6827983&isnumber=7064681.

[38] S. Debnath, Qin Jiangchao, B. Bahrani, M. Saeedifard, and P. Barbosa. "Operation, Control, and Applications of the Modular Multilevel Converter: A Review." In: *Power Electronics, IEEE Transactions on* 30.1 (2015), pp. 37–53. ISSN: 0885-8993. DOI: 10.1109/TPEL.2014.2309937. URL: http://ieeexplore.ieee.org/ielx7/63/6883248/06757006.pdf?tp=&arnumber=6757006&isnumber=6883248.

[39] J. Peralta, H. Saad, S. Dennetiere, J. Mahseredjian, and S. Nguefeu. "Detailed and Averaged Models for a 401-Level MMC HVDC System." In: *Power Delivery, IEEE Transactions on* 27.3 (2012), pp. 1501–1508. ISSN: 0885-8977. DOI: 10.1109/TPWRD.2012.2188911. URL: http://ieeexplore.ieee.org/ielx5/61/6222050/06178298.pdf?tp=&arnumber=6178298&isnumber=6222050.

[40] M. Hagiwara and H. Akagi. "Control and Experiment of Pulsewidth-Modulated Modular Multilevel Converters." In: *Power Electronics, IEEE Transactions on* 24.7 (2009), pp. 1737–1746. ISSN: 0885-8993. DOI: 10.1109/TPEL.2009.2014236. URL: http://ieeexplore.ieee.org/ielx5/63/5075737/05170197.pdf?tp=&arnumber=5170197&isnumber=5075737.

[41] Tang Geng, Xu Zheng, and Zhou Yuzhi. "Impacts of Three MMC-HVDC Configurations on AC System Stability Under DC Line Faults." In: *Power Systems, IEEE Transactions on* 29.6 (2014), pp. 3030–3040. ISSN: 0885-8950. DOI: 10.1109/TPWRS.2014.2315666. URL: http://ieeexplore.ieee.org/ielx7/59/6926883/06802452.pdf?tp=&arnumber=6802452&isnumber=6926883.

[42] U. N. Gnanarathna, A. M. Gole, and R. P. Jayasinghe. "Efficient Modeling of Modular Multilevel HVDC Converters (MMC) on Electromagnetic Transient Simulation Programs." In: *Power Delivery, IEEE Transactions on* 26.1 (2011), pp. 316–324. ISSN: 0885-8977. DOI: 10.1109/TPWRD.2010.2060737. URL: http://ieeexplore.ieee.org/ielx5/61/5673376/05607337.pdf?tp=&arnumber=5607337&isnumber=5673376.

[43] Guan Minyuan and Xu Zheng. "Modeling and Control of a Modular Multilevel Converter-Based HVDC System Under Unbalanced Grid Conditions." In: *Power Electronics, IEEE Transactions on* 27.12 (2012), pp. 4858–4867. ISSN: 0885-8993. DOI: 10.1109/TPEL.2012.2192752. URL: http://ieeexplore.ieee.org/ielx5/63/6238385/06179545.pdf?tp=&arnumber=6179545&isnumber=6238385.

[44] H. Saad et al. "Dynamic Averaged and Simplified Models for MMC-Based HVDC Transmission Systems." In: *Power Delivery, IEEE Transactions on* 28.3 (2013), pp. 1723–1730. ISSN: 0885-8977. DOI: 10.1109/TPWRD.2013.2251912. URL: http://ieeexplore.ieee.org/ielx7/61/6544637/06504846.pdf?tp=&arnumber=6504846&isnumber=6544637.

[45] N. Flourentzou, V. G. Agelidis, and G. D. Demetriades. "VSC-Based HVDC Power Transmission Systems: An Overview." In: *Power Electronics, IEEE Transactions on* 24.3 (2009), pp. 592–602. ISSN: 0885-8993. DOI: 10.1109/TPEL.2008.2008441. URL: http://ieeexplore.ieee.org/ielx5/63/4812314/04773229.pdf?tp=&arnumber=4773229&isnumber=4812314.

[46] O. A. Giddani, G. P. Adam, O. Anaya-Lara, and K. L. Lo. "Grid integration of a large offshore wind farm using VSC-HVDC in parallel with an AC submarine cable." In: *Universities Power Engineering Conference (UPEC), 2009 Proceedings of the 44th International*, pp. 1–5.

[47] R. S. Whitehouse. "Technical challenges of realising multi-terminal networking with VSC." In: *Power Electronics and Applications (EPE 2011), Proceedings of the 2011-14th European Conference on*, pp. 1–12.

[48] S. Gordon. "Supergrid to the rescue." In: *Power Engineer* 20.5 (2006), pp. 30–33. ISSN: 1479-8344. DOI: 10.1049/pe:20060505.

[49] G. P. Adam, K. H. Ahmed, S. J. Finney, K. Bell, and B. W. Williams. "New Breed of Network Fault-Tolerant Voltage-Source-Converter HVDC Transmission System." In: *Power Systems, IEEE Transactions on* 28.1 (2013), pp. 335–346. ISSN: 0885-8950. DOI: 10.1109/TPWRS.2012.2199337. URL: http://ieeexplore.ieee.org/ielx5/59/6414672/06231708.pdf?tp=&arnumber=6231708&isnumber=6414672.

[50] A. Moawwad, M. S. El Moursi, and Xiao Weidong. "A Novel Transient Control Strategy for VSC-HVDC Connecting Offshore Wind Power Plant." In: *Sustainable Energy, IEEE Transactions on* 5.4 (2014), pp. 1056–1069. ISSN: 1949-3029. DOI: 10.1109/TSTE.2014.2325951. URL: http://ieeexplore.ieee.org/ielx7/5165391/6899716/06837516.pdf?tp=&arnumber=6837516&isnumber=6899716.

[51] A. Egea-Alvarez, S. Fekriasl, F. Hassan, and O. Gomis-Bellmunt. "Advanced Vector Control for Voltage Source Converters Connected to Weak Grids." In: *IEEE Transactions on Power Systems* 30.6 (2015), pp. 3072–3081. ISSN: 0885-8950. DOI: 10.1109/TPWRS.2014.2384596. URL: http://ieeexplore.ieee.org/ielx7/59/7175086/07006792.pdf?tp=&arnumber=7006792&isnumber=7175086.

[52] Li Guangkai, Li Gengyin, Liang Haifeng, Zhao Chengyong, and Yin Ming. "Research on dynamic characteristics of VSC-HVDC system." In: *Power Engineering Society General Meeting, 2006. IEEE*, 5 pp. DOI: 10.1109/PES.2006.1709371. URL: http://ieeexplore.ieee.org/ielx5/11204/36065/01709371.pdf?tp=&arnumber=1709371&isnumber=36065.

[53] Ferre Junyent, x, A., O. Gomis-Bellmunt, T. C. Green, and D. E. Soto-Sanchez. "Current Control Reference Calculation Issues for the Operation of Renewable Source Grid Interface VSCs Under Unbalanced Voltage Sags." In: *Power Electronics, IEEE Transactions on* 26.12 (2011), pp. 3744–3753. ISSN: 0885-8993. DOI: 10.1109/TPEL.2011.2167761. URL: http://ieeexplore.ieee.org/ielx5/63/6088512/06017130.pdf?tp=&arnumber=6017130&isnumber=6088512.

[54] S. K. Chaudhary, R. Teodorescu, P. Rodriguez, P. C. Kjaer, and A. M. Gole. "Negative Sequence Current Control in Wind Power Plants With VSC-HVDC Connection." In: *Sustainable Energy, IEEE Transactions on* 3.3 (2012), pp. 535–544. ISSN: 1949-3029. DOI: 10.1109/TSTE.2012.2191581. URL: http://ieeexplore.ieee.org/ielx5/5165391/6218808/06193197.pdf?tp=&arnumber=6193197&isnumber=6218808.

[55] C. Feltes, H. Wrede, F. W. Koch, and I. Erlich. "Enhanced Fault Ride-Through Method for Wind Farms Connected to the Grid Through VSC-Based HVDC Transmission." In: *Power Systems, IEEE Transactions on* 24.3 (2009), pp. 1537–1546. ISSN: 0885-8950. DOI: 10.1109/TPWRS.2009.2023264. URL: http://ieeexplore.ieee.org/ielx5/59/5170200/05170211.pdf?tp=&arnumber=5170211&isnumber=5170200.

[56] Tang Lianxiang and Ooi Boon-Teck. "Impact of zero sequence component on voltage-source converters." In: *Power Conversion Conference, 2002. PCC-Osaka 2002. Proceedings of the*. Vol. 1, 184–189 vol.1. DOI: 10.1109/PCC.2002.998544.

[57] Lim Sun-kyoung, Kim Jun-Ha, and Nam Kwanghee. "A DC-link voltage balancing algorithm for 3-level converter using the zero sequence current." In: *Power Electronics Specialists Conference, 1999. PESC 99. 30th Annual IEEE*. Vol. 2, 1083–1088 vol.2. ISBN: 0275-9306. DOI: 10.1109/PESC.1999.785646.

[58] A. Fuchs, M. Imhof, T. Demiray, and M. Morari. "Stabilization of Large Power Systems Using VSC-HVDC and Model Predictive Control." In: *Power Delivery, IEEE Transactions on* 29.1 (2014), pp. 480–488. ISSN: 0885-8977. DOI: 10.1109/TPWRD.2013.2280467. URL: http://ieeexplore.ieee.org/ielx7/61/6718038/06632979.pdf?tp=&arnumber=6632979&isnumber=6718038.

[59] P. Mitra, Zhang Lidong, and L. Harnefors. "Offshore Wind Integration to a Weak Grid by VSC-HVDC Links Using Power-Synchronization Control: A Case Study." In: *Power Delivery, IEEE Transactions on* 29.1 (2014), pp. 453–461. ISSN: 0885-8977. DOI: 10.1109/TPWRD.2013.2273979. URL: http://ieeexplore.ieee.org/ielx7/61/6718038/06575185.pdf?tp=&arnumber=6575185&isnumber=6718038.

[60] E. O. Schweitzer, N. Fischer, and B. Kasztenny. "A fresh look at limits to the sensitivity of line protection." In: *Protective Relay Engineers, 2011 64th Annual Conference for*, pp. 44–55. DOI: 10.1109/CPRE.2011.6035604.

[61] D. Tziouvaras. "Relay Performance During Major System Disturbances." In: *Protective Relay Engineers, 2007. 60th Annual Conference for*, pp. 251–270. DOI: 10.1109/CPRE.2007.359905.

[62] D. Novosel, G. Bartok, G. Henneberg, P. Mysore, D. Tziouvaras, and S. Ward. "IEEE PSRC Report on Performance of Relaying During Wide-Area Stressed Conditions." In: *Power Delivery, IEEE Transactions on* 25.1 (2010), pp. 3–16. ISSN: 0885-8977. DOI: 10.1109/TPWRD.2009.2035202.

[63] "IEEE Guide for Protective Relay Applications to Transmission Lines." In: *IEEE Std C37.113-1999* (2000), p. i. DOI: 10.1109/IEEESTD.2000.91147. URL: http://ieeexplore.ieee.org/xpl/articleDetails.jsp?arnumber=827748.

[64] Z. Y. Xu, S. F. Huang, L. Ran, J. F. Liu, Y. L. Qin, Q. X. Yang, and J. L. He. "A Distance Protection Relay for a 1000-kV UHV Transmission Line." In: *IEEE Transactions on Power Delivery* 23.4 (2008), pp. 1795–1804. ISSN: 0885-8977. DOI: 10.1109/TPWRD.2008.919038. URL: http://ieeexplore.ieee.org/ielx5/61/4626339/04480139.pdf?tp=&arnumber=4480139&isnumber=4626339.

[65] Z. Y. Xu, S. J. Jiang, and L. Ran. "Phase distance relaying algorithm for unbalanced interphase faults." In: *IET Generation, Transmission & Distribution* 4.12 (2010), p. 1326. ISSN: 17518687. DOI: 10.1049/iet-gtd.2009.0609.

[66] S. Jamali and H. Shateri. "Robustness of Distance Relay with Quadrilateral Characteristic against Fault Resistance." In: *2005 IEEE/PES Transmission & Distribution Conference & Exposition: Asia and Pacific*, pp. 1–6. ISBN: 2160-8636. DOI: 10.1109/TDC.2005.1547108.

[67] Juergen Hollbach. "Issues and Solutions in Setting a Quadrilateral Distance Characteristic." In: *61st Conference for Protective Relay Engineers*.

[68] James Hubertus, Joe Mooney, and George Alexander. "Application Considerations for Distance Relays on Impedance-Grounded Systems." In: *61st Annual Conference for Protective Relay Engineers*. IEEE.

[69] P. E. J. Mooney and N. Fischer. "Application guidelines for power swing detection on transmission systems." In: *59th Annual Conference for Protective Relay Engineers, 2006*. 10 pp. DOI: 10.1109/CPRE.2006.1638707. URL: http://ieeexplore.ieee.org/ielx5/10914/34361/01638707.pdf?tp=&arnumber=1638707&isnumber=34361.

[70] N. Fischer, G. Benmouyal, D. Hou, D. Tziouvaras, J. Byrne-Finley, and B. Smyth. "Do system impedances really affect power swings Applying power swing protection elements without complex system studies." In: *Protective Relay Engineers, 2012 65th Annual Conference for*, pp. 108–119. DOI: 10.1109/CPRE.2012.6201225. URL: http://ieeexplore.ieee.org/ielx5/6195237/6201216/06201225.pdf?tp=&arnumber=6201225&isnumber=6201216.

[71] L. Martuscello, E. Krizauskas, J. Holbach, and Lu Yuchen. "Tests of distance relay performance on stable and unstable power swings reported using simulated data of the August 14th 2003 system disturbance." In: *Protective Relay Engineers, 2009 62nd Annual Conference for*, pp. 236–255. DOI: 10.1109/CPRE.2009.4982516. URL: http://ieeexplore.ieee.org/ielx5/4925074/4982492/04982516.pdf?tp=&arnumber=4982516&isnumber=4982492.

[72] Z. Moravej, M. Pazoki, and M. Khederzadeh. "Impact of UPFC on Power Swing Characteristic and Distance Relay Behavior." In: *IEEE Transactions on Power Delivery* 29.1 (2014), pp. 261–8. ISSN: 0885-8977. DOI: 10.1109/TPWRD.2013.2270408. URL: http://dx.doi.org/10.1109/TPWRD.2013.2270408http://ieeexplore.ieee.org/ielx7/61/6718038/06558850.pdf?tp=&arnumber=6558850&isnumber=6718038.

[73] Web Page. 2009. URL: http://www.pes-psrc.org/Reports/D4_Application_of_Overreaching_Distance%20_Relays.pdf.

[74] A. A. van der Meer, M. Ndreko, M. Gibescu, and M. A. M. M. van der Meijden. "The Effect of FRT Behavior of VSC-HVDC-Connected Offshore Wind Power Plants on AC/DC System Dynamics." In: *IEEE Transactions on Power Delivery* 31.2 (2016), pp. 878–887. ISSN: 0885-8977. DOI: 10.1109/TPWRD.2015.2442512. URL: http://ieeexplore.ieee.org/ielx7/61/7438949/07119604.pdf?tp=&arnumber=7119604&isnumber=7438949.

[75] Pieter Tielens and Dirk Van Hertem. "The relevance of inertia in power systems." In: *Renewable and Sustainable Energy Reviews* 55 (2016), pp. 999–1009. ISSN: 1364-0321. DOI: http://dx.doi.org/10.1016/j.rser.2015.11.016. URL: http://www.sciencedirect.com/science/article/pii/S136403211501268Xhttp://ac.els-cdn.com/S136403211501268X/1-s2.0-S136403211501268X-main.pdf?_tid=69c8036c-54d1-11e6-9ca0-00000aacb360&acdnat=1469717088_895f480ece2fbce4eaf4780be81e49fa.

[76] A. A. van der Meer, M. Ndreko, J. A. Bos, M. Gibescu, M. A. M. M. van der Meijden, and W. L. Kling. "Stability assessment of VSC-HVDC connected large-scale offshore wind power: A North-Sea region case study." In: *PowerTech, 2015 IEEE Eindhoven*, pp. 1–6. DOI: 10.1109/PTC.2015.7232787. URL: http://ieeexplore.ieee.org/ielx7/7210291/7232233/07232787.pdf?tp=&arnumber=7232787&isnumber=7232233.

[77] M. Ndreko, A. M. Bucurenciu, M. Popov, and M. A. M. M. van der Meijden. "On grid code compliance of offshore mtdc grids: modeling and analysis." In: *PowerTech, 2015 IEEE Eindhoven*, pp. 1–6. DOI: 10.1109/PTC.2015.7232398. URL: http://ieeexplore.ieee.org/ielx7/7210291/7232233/07232398.pdf?tp=&arnumber=7232398&isnumber=7232233.

[78] TenneT-TSOGmbH. *Grid Code - extra high voltage*. Report. Oct. 2010. URL: http://www.tennet.eu/fileadmin/user_upload/The_Electricity_Market/German_Market/Grid_customers/tennet-NAR2015eng.pdf.

[79] ENTSO-E. *Establishing a Network Code on Requirements for Grid Connection of High Voltage Direct Current Systems and Direct Current-Connected Power Park Modules*. online. 2015, Oct. URL: https://www.entsoe.eu/Documents/Network%20codes%20documents/NC%20HVDC/HVDC_110915_Final_Provisional_Voted.pdf.

[80] I. Erlich, T. Neumann, F. Shewarega, P. Schegner, and J. Meyer. "Wind turbine negative sequence current control and its effect on power system protection." In: *2013 IEEE Power & Energy Society General Meeting*, pp. 1–5. ISBN: 1932-5517. DOI: 10.1109/PESMG.2013.

6672880. URL: http://ieeexplore.ieee.org/xpl/articleDetails.jsp?arnumber=6672880.

[81] T. Neumann, T. Wijnhoven, G. Deconinck, and I. Erlich. "Enhanced Dynamic Voltage Control of Type 4 Wind Turbines During Unbalanced Grid Faults." In: *IEEE Transactions on Energy Conversion* 30.4 (2015), pp. 1650–1659. ISSN: 0885-8969. DOI: 10.1109/TEC.2015.2470126. URL: http://ieeexplore.ieee.org/ielx7/60/7333020/07254167.pdf?tp=&arnumber=7254167&isnumber=7333020.

[82] Zhou Yuebin, Jiang Daozhuo, Guo Jie, Hu Pengfei, and Liang Yiqiao. "Analysis and Control of Modular Multilevel Converters Under Unbalanced Conditions." In: *Power Delivery, IEEE Transactions on* 28.4 (2013), pp. 1986–1995. ISSN: 0885-8977. DOI: 10.1109/TPWRD.2013.2268981. URL: http://ieeexplore.ieee.org/ielx7/61/6605682/06552229.pdf?tp=&arnumber=6552229&isnumber=6605682.

[83] BMUB. *Ordinance on System Services by Wind Energy Plants (System Service Ordinance - SDLWindV)*. Report. May 2009. URL: http://www.bmub.bund.de/fileadmin/bmu-import/files/english/pdf/application/pdf/sdl_windv_en.pdf.

[84] M. Ndreko, M. Popov, A. A. van der Meer, and M. A. M. M. van der Meijden. "The effect of the offshore VSC-HVDC connected wind power plants on the unbalanced faulted behavior of AC transmission systems." In: *2016 IEEE International Energy Conference (ENERGYCON)*, pp. 1–6. DOI: 10.1109/ENERGYCON.2016.7513950. URL: http://ieeexplore.ieee.org/ielx7/7507294/7513868/07513950.pdf?tp=&arnumber=7513950&isnumber=7513868.

[85] L. He, Liu Chen-Ching, A. Pitto, and D. Cirio. "Distance Protection of AC Grid With HVDC-Connected Offshore Wind Generators." In: *Power Delivery, IEEE Transactions on* 29.2 (2014), pp. 493–501. ISSN: 0885-8977. DOI: 10.1109/TPWRD.2013.2271761. URL: http://ieeexplore.ieee.org/ielx7/61/6776443/06563170.pdf?tp=&arnumber=6563170&isnumber=6776443.

[86] A. Hooshyar, M. A. Azzouz, and E. F. El-Saadany. "Distance Protection of Lines Emanating From Full-Scale Converter-Interfaced Renewable Energy Power Plants 2014;Part I Problem Statement." In: *Power Delivery, IEEE Transactions on* 30.4 (2015), pp. 1770–1780. ISSN: 0885-8977. DOI: 10.1109/TPWRD.2014.2369479. URL: http://ieeexplore.ieee.org/ielx7/61/7163645/06954572.pdf?tp=&arnumber=6954572&isnumber=7163645.

[87] J. V. V. N. Bapiraju, J. U. Shenoy, K. G. Sheshadri, H. P. Khincha, and D. Thukaram. "Implementation of DSP based relaying with particular reference to effect of STATCOM on transmission line protection." In: *Power System Technology, 2004. PowerCon 2004. 2004 International Conference on*. Vol. 2, 1381–1385 Vol.2. DOI: 10.1109/ICPST.2004.1460217. URL: http://ieeexplore.ieee.org/xpl/articleDetails.jsp?arnumber=1460217http://ieeexplore.ieee.org/document/1460217/.

[88] M. G. Ahsaee and J. Sadeh. "A Novel Fault-Location Algorithm for Long Transmission Lines Compensated by Series FACTS Devices." In: *Power Delivery, IEEE Transactions on* 26.4 (2011), pp. 2299–2308. ISSN: 0885-8977. DOI: 10.1109/TPWRD.2011.2166410. URL: http://ieeexplore.ieee.org/ielx5/61/6029804/06029302.pdf?tp=&arnumber=6029302&isnumber=6029804.

[89] T. S. Sidhu and M. Khederzadeh. "TCSC impact on communication-aided distance-protection schemes and its mitigation." In: *Generation, Transmission and Distribution, IEE Proceedings-* 152.5 (2005), pp. 714–728. ISSN: 1350-2360. DOI: 10.1049/ip-gtd:20045261. URL: http://ieeexplore.ieee.org/search/searchresult.jsp?searchWithin=%22Publication%20Number%22:2195&searchWithin=%22Volume%22:152&searchWithin=%22Issue%22:5&searchWithin=%22Start%20Page%22:714.

[90] F. A. Albasri, T. S. Sidhu, and R. K. Varma. "Impact of Shunt-FACTS on Distance Protection of Transmission Lines." In: *Power Systems Conference: Advanced Metering, Protection, Control, Communication, and Distributed Resources, 2006. PS '06*, pp. 249–256. DOI: 10.1109/PSAMP.2006.285397. URL: http://ieeexplore.ieee.org/ielx5/4064641/4064642/04064677.pdf?tp=&arnumber=4064677&isnumber=4064642.

[91] F. A. Albasri, T. S. Sidhu, and R. K. Varma. "Performance comparison of distance protection schemes for shunt-FACTS compensated transmission lines." In: *IEEE Transactions on Power Delivery* 22.4 (2007), pp. 2116–25. ISSN: 0885-8977. DOI: 10.1109/TPWRD.2007.900283. URL: http://dx.doi.org/10.1109/TPWRD.2007.900283http://ieeexplore.ieee.org/ielx5/61/4302501/04302504.pdf?tp=&arnumber=4302504&isnumber=4302501.

[92] S. Jamali, A. Kazemi, and H. Shateri. "Measured impedance by distance relay for inter phase faults in presence of STATCOM." In: *Power and Energy Society General Meeting - Conversion and Delivery of Electrical Energy in the 21st Century, 2008 IEEE*, pp. 1–6. ISBN: 1932-5517. DOI: 10.1109/PES.2008.4596917. URL: http://ieeexplore.ieee.org/ielx5/4584435/4595968/04596917.pdf?tp=&arnumber=4596917&isnumber=4595968.

[93] Zhang Wen-Hao, Lee Seung-Jae, Choi Myeon-Song, and S. Oda. "Considerations on distance relay setting for transmission line with STATCOM." In: *Power and Energy Society General Meeting, 2010 IEEE*, pp. 1–5. ISBN: 1944-9925. DOI: 10.1109/PES.2010.5588192. URL: http://ieeexplore.ieee.org/ielx5/5577387/5588047/05588192.pdf?tp=&arnumber=5588192&isnumber=5588047.

[94] S. Jamali, A. Kazemi, and H. Shateri. "Comparing effects of SVC and STATCOM on distance relay tripping characteristic." In: *Industrial Electronics, 2008. ISIE 2008. IEEE International Symposium on*, pp. 1568–1573. DOI: 10.1109/ISIE.2008.4676914. URL: http://ieeexplore.ieee.org/ielx5/4664822/4676877/04676914.pdf?tp=&arnumber=4676914&isnumber=4676877.

[95] M. Khederzadeh. "UPFC operating characteristics impact on transmission line distance protection." In: *2008 IEEE Power & Energy Society General Meeting, 20-24 July 2008*. 2008 IEEE Power Energy Society General Meeting. IEEE, 6 pp. DOI: 10.1109/PES.2008.4596219. URL: http://dx.doi.org/10.1109/PES.2008.4596219http://ieeexplore.ieee.org/ielx5/4584435/4595968/04596219.pdf?tp=&arnumber=4596219&isnumber=4595968.

[96] H. Shateri and S. Jamali. "Distance relay over-reaching due to UPFC presence on second circuit of a double circuit line." In: *4th IET Conference on Power Electronics, Machines and Drives. PEMD 2008, 2-4 April 2008*. 4th IET Conference on Power Electronics, Machines and Drives. PEMD 2008. IET, pp. 783–8.

[97] M. Khederzadeh and A. Ghorbani. "Impact of VSC-Based Multiline FACTS Controllers on Distance Protection of Transmission Lines." In: *Power Delivery, IEEE Transactions on* 27.1 (2012), pp. 32–39. ISSN: 0885-8977. DOI: 10.1109/TPWRD.2011.2168428. URL: http://ieeexplore.ieee.org/ielx5/61/6108459/06051507.pdf?tp=&arnumber=6051507&isnumber=6108459.

[98] P. K. Dash, A. K. Pradhan, G. Panda, and A. C. Liew. "Adaptive relay setting for flexible AC transmission systems (FACTS)." In: *IEEE Transactions on Power Delivery* 15.1 (2000), pp. 38–43. ISSN: 0885-8977. DOI: 10.1109/61.847226. URL: http://dx.doi.org/10.1109/61.847226http://ieeexplore.ieee.org/xpl/articleDetails.jsp?arnumber=847226http://ieeexplore.ieee.org/ielx5/61/18392/00847226.pdf?tp=&arnumber=847226&isnumber=18392.

[99] S. Jamali, A. Kazemi, and H. Shateri. "Effects of UPFC on measured impedance by distance relay in double-circuit lines." In: *2009 IEEE Power & Energy Society General Meeting (PES), 26-30 July 2009*. 2009 IEEE Power Energy Society General Meeting (PES). IEEE, 8 pp. DOI: 10.1109/PES.2009.5275344. URL: http://dx.doi.org/10.1109/PES.2009.5275344http://ieeexplore.ieee.org/ielx5/5230481/5260217/05275344.pdf?tp=&arnumber=5275344&isnumber=5260217.

[100] M. Khederzadeh. "Performance evaluation of fault component distance relay for protection of lines compensated by UPFC." In: *10th IET International Conference on Developments in Power System Protection (DPSP 2010). Managing the Change, 29 March-1 April 2010*. 10th IET International Conference on Developments in Power System Protection (DPSP 2010). Managing the Change. IET, 5 pp.

[101] S. M. Hashemi, M. T. Hagh, and H. Seyedi. "High-speed relaying scheme for protection of transmission lines in the presence of thyristor-controlled series capacitor." In: *Generation, Transmission & Distribution, IET* 8.12 (2014), pp. 2083–2091. ISSN: 1751-8687. DOI: 10.1049/iet-gtd.2014.0133.

[102] S. He, J. Suonan, and Z. Q. Bo. "Integrated Impedance-Based Pilot Protection Scheme for the TCSC-Compensated EHV/UHV Transmission Lines." In: *Power Delivery, IEEE Transactions on* 28.2 (2013), pp. 835–844. ISSN: 0885-8977. DOI: 10.1109/TPWRD.2012.2236849. URL: http://ieeexplore.ieee.org/ielx7/61/6484160/06480901.pdf?tp=&arnumber=6480901&isnumber=6484160.

[103] S. Jamali, A. Kazemi, and H. Shateri. "Comparing TCSC Placements on Line Ends and Mid-Point from Measured Impedance Point of View." In: *Industrial Electronics and Applications, 2007. ICIEA 2007. 2nd IEEE Conference on*, pp. 1129–1134. DOI: 10.1109/ICIEA.2007.4318584. URL: http://ieeexplore.ieee.org/ielx5/4318334/4318335/04318584.pdf?tp=&arnumber=4318584&isnumber=4318335.

[104] M. Khederzadeh and T. S. Sidhu. "Impact of TCSC on the protection of transmission lines." In: *Power Delivery, IEEE Transactions on* 21.1 (2006), pp. 80–87. ISSN: 0885-8977. DOI: 10.1109/TPWRD.2005.858798. URL: http://ieeexplore.ieee.org/ielx5/61/33198/01564184.pdf?tp=&arnumber=1564184&isnumber=33198.

[105] T. S. Sidhu and M. Khederzadeh. "Series compensated line protection enhancement by modified pilot relaying schemes." In: *Power Delivery, IEEE Transactions on* 21.3 (2006), pp. 1191–1198. ISSN: 0885-8977. DOI: 10.1109/TPWRD.2006.876982. URL: http://ieeexplore.ieee.org/ielx5/61/34480/01645155.pdf?tp=&arnumber=1645155&isnumber=34480.

[106] S. A. A. Shahriari, M. H. Abardeh, A. Y. Varjani, and M. Mohamadian. "Using Fault Current Limiter to minimize effect of Thyristor Controlled Series Capacitor on over reach problem of distance protection." In: *Power Systems Conference and Exposition, 2009. PSCE 09. IEEE/PES*, pp. 1–6. DOI: 10.1109/PSCE.2009.4840124. URL: http://ieeexplore.ieee.org/ielx5/4815087/4839920/04840124.pdf?tp=&arnumber=4840124&isnumber=4839920.

[107] P. Jena and A. K. Pradhan. "Directional Relaying in the Presence of a Thyristor-Controlled Series Capacitor." In: *Power Delivery, IEEE Transactions on* 28.2 (2013), pp. 628–636. ISSN: 0885-8977. DOI: 10.1109/TPWRD.2013.2249538. URL: http://ieeexplore.ieee.org/ielx7/61/6484160/06478858.pdf?tp=&arnumber=6478858&isnumber=6484160.

[108] M. E. Baran and I. El-Markaby. "Fault analysis on distribution feeders with distributed generators." In: *Power Systems, IEEE Transactions on* 20.4 (2005), pp. 1757–1764. ISSN: 0885-8950. DOI: 10.1109/TPWRS.2005.857940. URL: http://ieeexplore.ieee.org/ielx5/59/32618/01525104.pdf?tp=&arnumber=1525104&isnumber=32618.

[109] R. M. Tumilty, M. Brucoli, G. M. Burt, and T. C. Green. "Approaches to Network Protection for Inverter Dominated Electrical Distribution Systems." In: *Power Electronics, Machines and Drives, 2006. The 3rd IET International Conference on*, pp. 622–626.

[110] A. Sinclair, D. Finney, D. Martin, and P. Sharma. "Distance Protection in Distribution Systems: How It Assists With Integrating Distributed Resources." In: *Industry Applications, IEEE Transactions on* 50.3 (2014), pp. 2186–2196. ISSN: 0093-9994. DOI: 10.1109/TIA.2013.2288426. URL: http://ieeexplore.ieee.org/ielx7/28/6816009/06654320.pdf?tp=&arnumber=6654320&isnumber=6816009.

[111] Pan Yan, I. Voloh, and Ren Wei. "Protection issues and solutions for protecting feeder with distributed generation." In: *Protective Relay Engineers, 2013 66th Annual Conference for*, pp. 92–111. DOI: 10.1109/CPRE.2013.6822030. URL: http://ieeexplore.ieee.org/ielx7/6815117/6822016/06822030.pdf?tp=&arnumber=6822030&isnumber=6822016.

[112] He Lina and Liu Chen-Ching. "Impact of LVRT capability of wind turbines on distance protection of AC grids." In: *Innovative Smart Grid Technologies (ISGT), 2013 IEEE PES*, pp. 1–6. DOI: 10.1109/ISGT.2013.6497829. URL: http://ieeexplore.ieee.org/ielx7/6490106/6497783/06497829.pdf?tp=&arnumber=6497829&isnumber=6497783.

[113] S. De Rijcke, P. S. Peerez, and J. Driesen. "Impact of wind turbines equipped with doubly-fed induction generators on distance relaying." In: *Power and Energy Society General Meeting, 2010 IEEE*, pp. 1–6. ISBN: 1944-9925. DOI: 10.1109/PES.2010.5590164. URL: http://ieeexplore.ieee.org/ielx5/5577387/5588047/05590164.pdf?tp=&arnumber=5590164&isnumber=5588047.

[114] M. Kheshti, Kang Xiaoning, Song Guobing, and Jiao Zaibin. "Modeling and Fault Analysis of Doubly Fed Induction Generators for Gansu Wind Farm Application." In: *Electrical and Computer Engineering, Canadian Journal of* 38.1 (2015), pp. 52–64. ISSN: 0840-8688. DOI: 10.1109/CJECE.2014.2359682. URL: http://ieeexplore.ieee.org/ielx7/9754/7072586/07072632.pdf?tp=&arnumber=7072632&isnumber=7072586.

[115] Li Guanghui, Zhang Bao-Hui, Wang Jin, Bo Zhiqian, T. Yip, D. Writer, and Lei Yu-ming. "DFIG-based wind farm electromagnetic dynamic model and impact on protection relay of transmission network." In: *Advanced Power System Automation and Protection (APAP), 2011 International Conference on*. Vol. 1, pp. 694–698. DOI: 10.1109/APAP.2011.6180371.

URL: http://ieeexplore.ieee.org/ielx5/6175562/6180363/06180371.pdf?tp=&arnumber=6180371&isnumber=6180363.

[116] M. Khoddam and H. K. Karegar. "Effect of wind turbines equipped with doubly-fed induction generators on distance protection." In: *Advanced Power System Automation and Protection (APAP), 2011 International Conference on*. Vol. 2, pp. 1349–1353. DOI: 10.1109/APAP.2011.6180588. URL: http://ieeexplore.ieee.org/ielx5/6175562/6180530/06180588.pdf?tp=&arnumber=6180588&isnumber=6180530.

[117] A. Hooshyar, M. A. Azzouz, and E. F. El-Saadany. "Distance Protection of Lines Emanating From Full-Scale Converter-Interfaced Renewable Energy Power Plants 2014 Part II: Solution Description and Evaluation." In: *Power Delivery, IEEE Transactions on* 30.4 (2015), pp. 1781–1791. ISSN: 0885-8977. DOI: 10.1109/TPWRD.2014.2369480. URL: http://ieeexplore.ieee.org/ielx7/61/7163645/06954549.pdf?tp=&arnumber=6954549&isnumber=7163645.

[118] A. Hooshyar, M. A. Azzouz, and E. F. El-Saadany. "Distance Protection of Lines Connected to Induction Generator-Based Wind Farms During Balanced Faults." In: *Sustainable Energy, IEEE Transactions on* 5.4 (2014), pp. 1193–1203. ISSN: 1949-3029. DOI: 10.1109/TSTE.2014.2336773. URL: http://ieeexplore.ieee.org/ielx7/5165391/6899716/06877744.pdf?tp=&arnumber=6877744&isnumber=6899716.

[119] A. K. Pradhan and G. Joos. "Adaptive Distance Relay Setting for Lines Connecting Wind Farms." In: *Energy Conversion, IEEE Transactions on* 22.1 (2007), pp. 206–213. ISSN: 0885-8969. DOI: 10.1109/TEC.2006.889621. URL: http://ieeexplore.ieee.org/ielx5/60/4105991/04106012.pdf?tp=&arnumber=4106012&isnumber=4105991.

[120] T. S. Sidhu, D. S. Baltazar, R. M. Palomino, and M. S. Sachdev. "A new approach for calculating zone-2 setting of distance relays and its use in an adaptive protection system." In: *Power Delivery, IEEE Transactions on* 19.1 (2004), pp. 70–77. ISSN: 0885-8977. DOI: 10.1109/TPWRD.2003.820202. URL: http://ieeexplore.ieee.org/xpl/articleDetails.jsp?arnumber=1256359http://ieeexplore.ieee.org/ielx5/61/28109/01256359.pdf?tp=&arnumber=1256359&isnumber=28109.

[121] J. G. Andrichak and G. E. Alexander. "Distance relays fundamentals." In: *GE MULTILIN, GE Power Management* GER-3966 ().

[122] D. J. Spoor and J. Zhu. "Intercircuit Faults and Distance relaying of dual circuit lines." In: *IEEE Transactions on Power Delivery* 20.03 (2005), p. 7.

[123] J.L. Blackburn. *Protective Relaying Principles and Applications*. New York: Marcel Dekker, Inc., 1987. ISBN: 0-8247-7445-0.

[124] Donald D. Fentie. "Understanding the Dynamic Mho Distance Characteristic." In: *52nd Annual Minnesota Power Systems Conference*. IEEE.

[125] S. B. Wilkinson and C. A. Mathews. "Dynamic Characteristics of MHO Distance Relay." In: *GE MULTILIN, GE Power Management* GER-3742 ().

[126] Fernando Calero. "Adaptive Phase and Ground quadrilateral distance elements." In: (2009).

[127] ABB. *Line Distance Protection REL670 Application Manual*. Online. 2015, Feb. URL: https://library.e.abb.com/public/5b25d28d142a4ad0985bfe059141a566/1MRK506315-UEN_D_en_Application_manual__REL670_1.2.pdf.

[128] EFACEC. *TPU L500 Product Manual*. Report. 2013. URL: http://www.efacec.pt/PresentationLayer/ResourcesUser/Cat%C3%A1logos%202015/Automa%C3%A7%C3%A3o/500/TPU500_EN.pdf.

[129] A. P. Apostolov, D. Tholomier, and S. H. Richards. "Distance protection and dynamic loading of transmission lines." In: *Power Engineering Society General Meeting, 2004. IEEE*, 100–105 Vol.1. DOI: 10.1109/PES.2004.1372764. URL: http://ieeexplore.ieee.org/xpl/articleDetails.jsp?arnumber=1372764.

[130] Ariana Amberg, Alex Rangel, and Greg Smelich. "Validating Transmission Line Impedances Using Known Event Data." In: *Conference for Protective Relay Engineers*.

[131] Fernando Calero. "Mutual Impedance in Parallel Line - Protective Relaying and Fault Location Consideration." 2007.

[132] Kim Chul-Hwan, Heo Jeong-Yong, and R. K. Aggarwal. "An enhanced zone 3 algorithm of a distance relay using transient components and state diagram." In: *IEEE Transactions on Power Delivery* 20.1 (2005), pp. 39–46. ISSN: 0885-8977. DOI: 10.1109/TPWRD.2004.837827. URL: http://ieeexplore.ieee.org/ielx5/61/30033/01375074.pdf?tp=&arnumber=1375074&isnumber=30033.

[133] D. F. Howard, J. Liang, and R. G. Harley. "Short-Circuit Modeling of DFIGs With Uninterrupted Control." In: *IEEE Journal of Emerging and Selected Topics in Power Electronics* 2.1 (2014), pp. 47–57. ISSN: 2168-6777. DOI: 10.1109/JESTPE.2013.2293623. URL: http://ieeexplore.ieee.org/ielx7/6245517/6728629/06678192.pdf?tp=&arnumber=6678192&isnumber=6728629.

[134] IRENA. *Scaling up Variable Renewable Power: The Role of Grid Codes*. Report. 2016.

[135] B. Silva, C. L. Moreira, H. Leite, J. A. Pe, xooE, and Lopes as. "Control Strategies for AC Fault Ride Through in Multiterminal HVDC Grids." In: *IEEE Transactions on Power Delivery* 29.1 (2014), pp. 395–405. ISSN: 0885-8977. DOI: 10.1109/TPWRD.2013.2281331. URL: http://ieeexplore.ieee.org/ielx7/61/6718038/06712928.pdf?tp=&arnumber=6712928&isnumber=6718038.

[136] M. Ndreko, M. Popov, J. C. Boemer, and M. A. M. M. van der Meijden. "Sensitivity analysis on short-circuit current contribution from VSC-HVDC systems connecting far and large offshore wind power plants." In: *Innovative Smart Grid Technologies Conference Europe (ISGT-Europe), 2014 IEEE PES*, pp. 1–6. DOI: 10.1109/ISGTEurope.2014.7028961. URL: http://ieeexplore.ieee.org/ielx7/7001799/7028730/07028961.pdf?tp=&arnumber=7028961&isnumber=7028730.

[137] P. Kundur, N.J. Balu, and M.G. Lauby. *Power system stability and control*. McGraw-Hill, 1994. ISBN: 9780070359581. URL: https://books.google.pt/books?id=wOlSAAAAMAAJ.

[138] M. Guan, W. Pan, J. Zhang, Q. Hao, J. Cheng, and X. Zheng. "Synchronous Generator Emulation Control Strategy for Voltage Source Converter (VSC) Stations." In: *IEEE Transactions on Power Systems* 30.6 (2015), pp. 3093–3101. ISSN: 0885-8950. DOI: 10.1109/TPWRS.2014.2384498. URL: http://ieeexplore.ieee.org/ielx7/59/7175086/07010055.pdf?tp=&arnumber=7010055&isnumber=7175086.

[139] E. Muljadi, N. Samaan, V. Gevorgian, J. Li, and S. Pasupulati. "Different Factors Affecting Short Circuit Behavior of a Wind Power Plant." In: *IEEE Transactions on Industry Applications* 49.1 (2013), pp. 284–292. ISSN: 0093-9994. DOI: 10.1109/TIA.2012.2228831. URL: http://ieeexplore.ieee.org/ielx5/28/6413287/06355983.pdf?tp=&arnumber=6355983&isnumber=6413287.

[140] J. Martinez, P. C. Kjar, P. Rodriguez, and R. Teodorescu. "Short circuit signatures from different wind turbine generator types." In: *Power Systems Conference and Exposition (PSCE), 2011 IEEE/PES*, pp. 1–7. DOI: 10.1109/PSCE.2011.5772497. URL: http://ieeexplore.ieee.org/ielx5/5767515/5772439/05772497.pdf?tp=&arnumber=5772497&isnumber=5772439.

[141] R. A. Walling, E. Gursoy, and B. English. "Current contributions from Type 3 and Type 4 wind turbine generators during faults." In: *Transmission and Distribution Conference and Exposition (T&D), 2012 IEEE PES*, pp. 1–6. ISBN: 2160-8555. DOI: 10.1109/TDC.2012.6281623. URL: http://ieeexplore.ieee.org/ielx5/6267012/6281396/06281623.pdf?tp=&arnumber=6281623&isnumber=6281396.

[142] D. Erwin, M. Anderson, R. Pineda, D. A. Tziouvaras, and R. Turner. "PG&E 500 kV series-compensated transmission line relay replacement: Design requirements and RTDS & testing." In: *Protective Relay Engineers, 2011 64th Annual Conference for*, pp. 191–202. DOI: 10.1109/CPRE.2011.6035620. URL: http://ieeexplore.ieee.org/ielx5/6026170/6035494/06035620.pdf?tp=&arnumber=6035620&isnumber=6035494.

[143] H. W. Dommel. "Digital Computer Solution of Electromagnetic Transients in Single-and Multiphase Networks." In: *IEEE Transactions on Power Apparatus and Systems* PAS-88.4 (1969), pp. 388–399. ISSN: 0018-9510. DOI: 10.1109/TPAS.1969.292459.

[144] Web Page. 2016. URL: https://www.rtds.com/the-simulator/our-hardware/cubicles/.

[145] B. Wang, X. Dong, Z. Bo, and A. Perks. "RTDS Environment Development of Ultra-High-Voltage Power System and Relay Protection Test." In: *IEEE Transactions on Power Delivery* 23.2 (2008), pp. 618–623. ISSN: 0885-8977. DOI: 10.1109/TPWRD.2008.915818. URL: http://ieeexplore.ieee.org/ielx5/61/4476461/04472156.pdf?tp=&arnumber=4472156&isnumber=4476461.

[146] T. L. Maguire. "Real time digital electromagnetic transients simulation of power systems." In: *Power Engineering Society Summer Meeting, 2000. IEEE*. Vol. 2, 765 vol. 2. DOI: 10.1109/PESS.2000.867448. URL: http://ieeexplore.ieee.org/document/867448/?reload=true.

[147] B. Chen, A. Shrestha, F. A. Ituzaro, and N. Fischer. "Addressing protection challenges associated with Type 3 and Type 4 wind turbine generators." In: *Protective Relay Engineers, 2015 68th Annual Conference for*, pp. 335–344. DOI: 10.1109/CPRE.2015.7102177. URL: http://ieeexplore.ieee.org/ielx7/7083794/7102153/07102177.pdf?tp=&arnumber=7102177&isnumber=7102153.

[148] M. M. Alam, H. Leite, and A. S. Carvalho. "Investigating Distance Relay Behaviour on an EHV AC Lines Connected with Voltage Source Converter Based HVDC." In: *Proc. CIGRE Symp., Across Borders - HVDC Systems And Market Integration*.

[149] Mohammad Meraj Alam, Helder Leite, Jun Liang, and Adriano da Silva Carvalho. "Effects of VSC based HVDC system on distance protection of transmission lines." In: *International Journal of Electrical Power & Energy Systems* 92 (2017), pp. 245–260. ISSN: 0142-0615. DOI: https://doi.org/10.1016/j.ijepes.2017.04.012. URL: http://www.sciencedirect.com/science/article/pii/S0142061516320312https://ac.els-cdn.com/S0142061516320312/1-s2.0-S0142061516320312-main.pdf?_tid=13d0ae02-f3e8-11e7-aec5-00000aab0f26&acdnat=1515356555_5e5ac7c30cc6962f0a3f814a0750a6ff.

[150] A. Roy and B. K. Johnson. "Transmission side protection performance with Type-IV wind turbine system integration." In: *North American Power Symposium (NAPS), 2014*, pp. 1–6. DOI: 10.1109/NAPS.2014.6965429. URL: http://ieeexplore.ieee.org/ielx7/6949415/6965351/06965429.pdf?tp=&arnumber=6965429&isnumber=6965351.

[151] Mohammad Meraj Alam, Helder Leite, Nuno Silva, and Adriano da Silva Carvalho. "Performance evaluation of distance protection of transmission lines connected with VSC-HVDC system using closed-loop test in RTDS." In: *Electric Power Systems Research* 152.Supplement C (2017), pp. 168–183. ISSN: 0378-7796. DOI: https://doi.org/10.1016/j.epsr.2017.06.025. URL: http://www.sciencedirect.com/science/article/pii/S0378779617302742.

[152] V. A. Papaspiliotopoulos, G. N. Korres, V. A. Kleftakis, and N. D. Hatziargyriou. "Hardware-In-the-Loop Design and Optimal Setting of Adaptive Protection Schemes for Distribution Systems With Distributed Generation." In: *IEEE Transactions on Power Delivery* 32.1 (2017), pp. 393–400. ISSN: 0885-8977. DOI: 10.1109/TPWRD.2015.2509784. URL: http://ieeexplore.ieee.org/document/7359148/.

[153] Rahul Dubey, S. R. Samantaray, B. K. Panigrahi, and G. V. Venkoparao. "Adaptive distance relay setting for parallel transmission network connecting wind farms and UPFC." In: *International Journal of Electrical Power & Energy Systems* 65 (2015), pp. 113–123. ISSN: 0142-0615. DOI: http://dx.doi.org/10.1016/j.ijepes.2014.09.033. URL: http://www.sciencedirect.com/science/article/pii/S0142061514005845http://ac.els-cdn.com/S0142061514005845/1-s2.0-S0142061514005845-main.pdf?_tid=59ef14f0-db52-11e6-9681-00000aab0f26&acdnat=1484505922_7c393116995ebdecc6b0e9c3c5db035e.

[154] S. M. Brahma and A. A. Girgis. "Development of adaptive protection scheme for distribution systems with high penetration of distributed generation." In: *IEEE Transactions on Power Delivery* 19.1 (2004), pp. 56–63. ISSN: 0885-8977. DOI: 10.1109/TPWRD.2003.820204. URL: http://ieeexplore.ieee.org/xpl/articleDetails.jsp?arnumber=1256357http://ieeexplore.ieee.org/document/1256357/?reload=truehttp://ieeexplore.ieee.org/document/1256357/.

[155] T. S. Sidhu, D. S. Baltazar, R. M. Palomino, and M. S. Sachdev. "A new approach for calculating zone-2 setting of distance relays and its use in an adaptive protection system." In: *Power Delivery, IEEE Transactions on* 19.1 (2004), pp. 70–77. ISSN: 0885-8977. DOI: 10.1109/TPWRD.2003.820202. URL: http://ieeexplore.ieee.org/xpl/articleDetails.jsp?arnumber=1256359http://ieeexplore.ieee.org/ielx5/61/28109/01256359.pdf?tp=&arnumber=1256359&isnumber=28109.

[156] H. Shateri and S. Jamali. "Robustness of communication aided distance relay with Quadrilateral characteristic against inter phase fault resistance." In: *Power System Technology (POWERCON), 2010 International Conference on*, pp. 1–8. DOI: 10.1109/POWERCON.2010.5666018.

[157] Sifang-electric. *CSC101 Line Protection IED Technical Application Manual*. Online. Sifang Automation, 2012, Aug. URL: http://www.sifang-electric.com/index.php/en/products-solutions/distribution/22-protection-ieds/13-csc-101-line-protection-ied.

DECLARATION

I undersigned Mohammad Meraj Alam declare that no portion of the work contained in this Ph.D. thesis has been submitted in support of an application for another degree or qualification of this or any other university or other institute of learning. The work discussed in this thesis are original.

Porto, Portugal, March 2018

Mohammad Meraj Alam

COLOPHON

The research leading to these results has received funding from the People Programme (Marie Curie Actions) of the European Union's Seventh Framework Programme FP7/2007-2013/ under REA grant agreement no. 317221, project title MEDOW.

This thesis is typeset using the typographical look-and-feel `classicthesis` developed by André Miede. The style was inspired by Robert Bringhurst's seminal book on typography "*The Elements of Typographic Style*" and customized for better look and feel by Mohammad Meraj Alam.